Qualitative Adaptive Identification for Powertrain Systems

Powertrain Dynamic Modelling and Adaptive Identification Algorithms with Identifiability Analysis for Real-Time Monitoring and Detectability Assessment of Physical and Semi-Physical System Parameters

Ioannis SOUFLAS

Submitted for the degree of
Doctor of Philosophy

Faculty of Engineering and Informatics
University of Bradford

2015

Abstract

Author *Ioannis Souflas*

Title Qualitative Adaptive Identification for Powertrain Systems

Subtitle Powertrain Dynamic Modelling and Adaptive Identification Algorithms with Identifiability Analysis for Real-Time Monitoring and Detectability Assessment of Physical and Semi-Physical System Parameters

Keywords automotive powertrains, dynamic modelling, physics-based, linear, nonlinear, identifiability, sensitivity, adaptive identification, recursive filters, condition monitoring

A complete chain of analysis and synthesis system identification tools for detectability assessment and adaptive identification of parameters with physical interpretation that can be found commonly in control-oriented powertrain models is presented. This research is motivated from the fact that future powertrain control and monitoring systems will depend increasingly on physically oriented system models to reduce the complexity of existing control strategies and open the road to new environmentally friendly technologies. At the outset of this study a physics-based control-oriented dynamic model of a complete transient engine testing facility, consisting of a single cylinder engine, an alternating current dynamometer and a coupling shaft unit, is developed to investigate the functional relationships of the inputs, outputs and parameters of the system. Having understood these, algorithms for identifiability analysis and adaptive identification of

parameters with physical interpretation are proposed. The efficacy of the recommended algorithms is illustrated with three novel practical applications. These are, the development of an on-line health monitoring system for engine dynamometer coupling shafts based on recursive estimation of shaft's physical parameters, the sensitivity analysis and adaptive identification of engine friction parameters, and the non-linear recursive parameter estimation with parameter estimability analysis of physical and semi-physical cyclic engine torque model parameters. The findings of this research suggest that the combination of physics-based control-oriented models with adaptive identification algorithms can lead to the development of component-based diagnosis and control strategies. Ultimately, this work contributes in the area of on-line fault diagnosis, fault tolerant and adaptive control for vehicular systems.

Acknowledgements

I would like to express my deep gratitude to my Ph.D. supervisor, Professor Kambiz Ebrahimi, for his support and encouragement, but also for giving me the privilege to experience the opportunities and challenges of independent research.

Special thanks to Dr. Antonios Pezouvanis for the immeasurable amount of help and guidance during the period of my postgraduate studies.

Family and friends, thank you for your patience, support and encouragement. It is amazing what you can accomplish when you got nothing to lose.

And Vaggie, all this would have never been possible without you, thank you for bringing joy and happiness into my life. This work is dedicated to you...

Ioannis Souflas

November 2015

Contents

List of Figures

List of Tables

Nomenclature

Acronyms

ABTC	After Bottom Dead Centre
AC	Alternating Current
afmep	Auxiliary Friction Mean Effective Pressure
ARMA	Autoregressive Moving Average
BDC	Bottom Dead Centre
BTDC	Before Bottom Dead Centre
CAL	CAN Application Layer
CAN	Controller Area Network
cfmep	Crankshaft Friction Mean Effective Pressure
CU	Curtain
DC	Direct Current
DMA	Direct Memory Access
DOF	Degrees of Freedom
DSFC	Discrete Square Root Filtering in Covariance Form
EKF	Extended Kalman Filter
EVC	Exhaust Valve Closing
FEA	Finite Element Analysis
FIFO	First In First Out
fmep	Friction Mean Effective Pressure
FPGA	Field Programmable Gate Array
GDI	Gasoline Direct Injection

GHG	Greenhouse Gas
GRV	Gaussian Random Variable
HCCI	Homogeneous Charge Compression Ignition
HGO	High Gain Observer
IC	Internal Combustion
ID	Identification
IFOC	Indirect Field Oriented Control
IM	Induction Motor
IT	Ignition Timing
IVC	Intake Valve Closing
IVO	Intake Valve Opening
KCL	Kirchoff's Current Law
KVL	Kirchoff's Voltage Law
LM	Limit Checking
LPV	Linear Parameter Varying
LQ	Linear Quadratic
LTI	Linear Time Invariant
LVDS	Low Voltage Differential Signalling
MB	Model Based
MBC	Model Based Control
MPC	Model Predictive Control
NARMAX	Nonlinear Autoregressive Moving Average with Exogenous inputs
NMPC	Nonlinear Model Predictive Control
NMSE	Normalised Mean Square Error
OS	Operating System
PCOS	Personal Computer Operating System
pfmep	Friction Mean Effective Pressure due to Pumping losses
PID	Proportional Integral Derivative
PO	Port
PWM	Pulse Width Modulation

rfmep	Reciprocating Friction Mean Effective Pressure
RHS	Right Hand Side
RIV	Recursive Instrumental Variable
RLS	Recursive Least Squares
RLSF	Recursive Least Squares with Forgetting Factor
RLSVF	Recursive Least Squares with Vector Forgetting
RMS	Root Mean Square
RPEM	Recursive Prediction Error
RPM	Revolution Per Minute
RTOS	Real Time Operating System
SMO	Sliding Mode Observer
SS	Sum of Squares
SV	Space Vector
TDC	Top Dead Centre
TTL	Transistor Transistor Logic
UD	Upper Diagonal
UKF	Unscented Kalman Filter
UT	Unscented Transformation
vfmep	Valvetrain Friction Mean Effective Pressure
WOT	Wide Open Throttle

Symbols

Chapter 1

CO_2	kg	Carbon dioxide

Chapter 3

α	rad/s^2	Angular acceleration
α_{dy}	rad/s^2	Dynamometer angular acceleration
α_{en}	rad/s^2	Engine angular acceleration
$\bar{c}$	-	Woschni heat transfer coefficient
δ	m	Piston pin offset
$\frac{dm}{dt}$	kg/s	Mass flow
$\frac{F_t}{F_{to}}$	-	Piston ring tension ratio
γ	-	Specific heat ratio
$\hbar$	W/m^2K	Heat transfer coefficient
$\hbar$	-	Woschni heat transfer function
κ	-	Engine compression ratio
λ_r	Wb	Induction motor rotor flux linkage
λ_{rdq}	Wb	Induction motor rotor flux linkage in dq-axis
λ_{sdq}	Wb	Induction motor stator flux linkage in dq-axis
$\mathcal{L}$	m	Cylinder connecting rod length
ω_{dy}	rad/s	Dynamometer angular velocity
ω_{en}	rad/s	Engine angular velocity
ω_m	rad/s	Angular velocity of the induction motor (mechanical)
ω_r	rad/s	Angular velocity of the induction motor (electrical)
ω_{slp}	rad/s	Induction motor slip angular velocity
$\phi_{th,0}$	rad	Throttle plate minimum opening angle
ϕ_{th}	rad	Throttle plate opening angle
ϕ_V	rad	Cylinder valve seat angle
ψ	-	Engine geometric function
Ψ	-	Mass flow function

ρ_e	-	Exhaust valve diameter/bore ratio
ρ_i	-	Intake valve diameter/bore ratio
$\sqrt{\frac{\mu}{\mu_0}}$	-	Oil viscosity scaling factor
τ	Nm	Torque
τ_{dy}	Nm	Dyamometer torque
τ_{en}	Nm	Engine torque
τ_{fri}	Nm	Engine friction torque
τ_{ind}	Nm	Engine indicated torque
τ_{rec}	Nm	Engine reciprocating torque
τ_{sh}	Nm	Shaft torque
θ	rad	Angular position
θ_{dy}	rad	Dynamometer angular position
θ_{en}	rad	Engine angular position
θ_{slp}	rad	Induction motor slip angle
θ_{syn}	rad	Induction motor synchronous angle
φ	-	Engine geometric function
A	-	State matrix
a-b-c	-	Three phase electric drive quantities
A_{exh}	m^2	Exhaust manifold port area
A_o	m^2	Orifice area
A_p	m^2	Cylinder piston area
A_{th}	m^2	Throttle plate area
A_V	m^2	Cylinder valve
A_{V-CU}	m^2	Cylinder valve curtain area
A_{V-PO}	m^2	Cylinder valve port area
A_w	m^2	Cylinder wall surface area
B	-	Input matrix
b	m	Cylinder bore diameter
B_{sh}	Nms/rad	Shaft damping coefficient
C	-	Output matrix

C_1	-	Woschni heat transfer coefficient
C_2	-	Woschni heat transfer coefficient
C_d	-	Mass flow discharge coefficient
C_h	-	Woschni heat transfer coefficient
C_{oh}	-	Valvetrain friction coefficient
C_r	-	Valvetrain friction coefficient
C_{rf}	-	Valvetrain friction coefficient
$c_{v,cyl}$	J/kgK	Cylinder heat at constant volume
$c_{v,exh}$	J/kgK	Exhaust manifold heat at constant volume
$c_{v,int}$	J/kgK	Intake manifold heat at constant volume
D	m	Cylinder valve head diameter
d-q	-	Direct-quadrature quantities
$d\theta_{en}$	rad	Crank angle step
D_{th}	m	Throttle plate diameter
d_{th}	m	Throttle plate shaft diameter
D_b	m	Diameter of crankshaft bearings
D_i	m	Cylinder valve port diameter
f	Hz	Frequency
G	-	Engine geometric function
G_1	-	Engine geometric function
G_2	-	Engine geometric function
H_{bl}	J	Cylinder blow-by enthalpy
h_{ehx}	J/kg	Exhaust manifold specific enthalpy
H_{ehx}	J	Exhaust manifold enthalpy
h_{ev}	J/kg	Exhaust valve specific enthalpy
H_{ev}	J	Cylinder exhaust valve enthalpy
H_f	J	Cylinder fuel enthalpy
h_{int}	J/kg	Intake manifold specific enthalpy
H_{int}	J	Intake manifold enthalpy
h_{iv}	J/kg	Intake valve Specific enthalpy

H_{iv}	J	Cylinder intake valve enthalpy
H_{man}	J	Manifold enthalpy
i_{rdq}	A	Induction motor rotor current in dq-axis
i_{sdq}	A	Induction motor stator current in dq-axis
J	kgm^2	Inertia
J_{dy}	kgm^2	Dynamometer inertia
J_{en}	kgm^2	Engine inertia
K_{sh}	Nm/rad	Shaft stiffness coefficient
l	m	Cylinder valve lift
L_b	m	Length of crankshaft bearings
L_m	H	Induction motor mutual inductance
L_r	H	Induction motor rotor inductance
L_s	H	Induction motor stator inductance
l_V	m	Cylinder valve lift threshold
m_{cyl}	kg	Cylinder working medium mass
m_{ev}	kg	Exhaust valve working medium mass
m_{exh}	kg	Exhaust manifold working medium mass
m_{int}	kg	Intake manifold working medium mass
m_{iv}	kg	Intake valve working medium mass
N_{en}	RPM	Engine speed
n_b	-	Number of crankshaft bearings
n_c	-	Number of cylinders
n_v	-	Number of valves
p	-	Induction motor number of poles
P_0	Pa	Upstream pressure
P_1	Pa	Downstream pressure
P_{atm}	Pa	Atmospheric pressure
P_{crn}	Pa	Engine crankcase pressure
P_{cyl}	Pa	In cylinder pressure
P_{exh}	Pa	Exhaust manifold pressure

P_{int}	Pa	Intake manifold pressure
P_{ivc}	Pa	In cylinder pressure at IVC
Q_c	J	Heat release due to combustion
Q_{cyl}	J	Cylinder heat
Q_{man}	J	Manifold heat
Q_w	J	Heat transfer from the cylinder gases to the walls
R	J/kgK	Gas constant
r	m	Crank arm length
R_{cyl}	J/kgK	Cylinder working medium gas constant
R_{exh}	J/kgK	Exhaust manifold working medium gas constant
R_{int}	J/kgK	Intake manifold working medium gas constant
R_r	Ω	Induction motor rotor resistance
R_s	Ω	Induction motor stator resistance
S	m	Cylinder stroke
T_0	K	Upstream temperature
T_{cyl}	K	In cylinder temperature
T_{exh}	K	Exhaust manifold temperature
T_{int}	K	Intake manifold temperature
T_{ivc}	K	In cylinder temperature at IVC
T_w	K	Cylinder wall temperature
u	-	Input vector
u_{cyl}	J/kg	Cylinder specific internal energy
U_{cyl}	J	Cylinder internal energy
u_{exh}	J/kg	Exhaust manifold specific internal energy
u_{int}	J/kg	Intake manifold specific internal energy
U_{man}	J	Manifold internal energy
V_{cyl}	m^3	Cylinder displacement with respect to crank angle
V_{exh}	m^3	Exhaust manifold volume
V_{int}	m^3	Intake manifold volume
V_{ivc}	m^3	Cylinder displacement at IVC

v_{rdq}	V	Induction motor rotor voltage in dq-axis
v_{sdq}	V	Induction motor stator voltage in dq-axis
V_a	V	Induction motor voltage supply, phase a
V_b	V	Induction motor voltage supply, phase b
V_c	V	Induction motor voltage supply, phase c
V_d	m^3	Total cylinder displacement
v_p	m/s	Mean piston speed
W_{cyl}	J	Cylinder work
x	-	State vector
y	-	Output vector

Chapter 4

α	rad/s^2	Angular acceleration
α_{dy}	rad/s^2	Dynamometer angular acceleration
α_{en}	rad/s^2	Engine angular acceleration
d_{cyc}	-	Duration of a complete engine cycle
ω	rad/s	Angular velocity
ω_{dy}	rad/s	Dynamometer angular velocity
ω_{en}	rad/s	Engine angular velocity
τ_{dy}	Nm	Dyamometer torque
τ_{en}	Nm	Engine torque
τ_{sh}	Nm	Shaft torque
θ_{cyc}	rad	Continuous engine position
θ_{cyc}	rad	Cyclic engine position
θ_{dy}	rad	Dynamometer angular position
θ_{en}	rad	Engine angular position
$\theta_{thr,act}$	rad	Engine throttle actuator feedback
$\theta_{thr,dem}$	rad	Engine throttle actuator demand
c_{nyq}	-	Nyquist criterion constant
dt	s	Sampling time interval
enc_ppr	-	Encoder pulses per revolution

enc_pul	-	Encoder pulses
f_s	Hz	Sampling frequency
I_a	A	Induction motor current supply, phase a
I_b	A	Induction motor current supply, phase b
I_c	A	Induction motor current supply, phase c
P_{cyl}	Pa	In cylinder pressure
P_{exh}	Pa	Exhaust manifold pressure
P_{int}	Pa	Intake manifold pressure
T_{cyl}	K	In cylinder temperature
T_{exh}	K	Exhaust manifold temperature
T_{int}	K	Intake manifold temperature
T_{oil}	K	Oil temperature
V_a	V	Induction motor voltage supply, phase a
V_b	V	Induction motor voltage supply, phase b
V_c	V	Induction motor voltage supply, phase c

Chapter 5

α	-	UKF scaling factor
β	-	UKF scaling factor
ϵ	-	Observation noise
$\hat{\vartheta}_t$	-	Parameter estimate
$\hat{J}_L$	-	Least squares prediction of the sensitivity matrix
Λ	-	Forgetting factor matrix
λ	-	Forgetting factor
$\mathcal{D}$	-	Sigma points propagation through the model
$\mathcal{S}$	-	Sigma vector
$\mathcal{Y}$	-	Mean predicted output
ϕ	-	Vector of observation variables
Σ	-	Variance-covariance matrix
I	A	Current
P	W	Power

R	Ω	Resistance
V	V	Volt
$\vartheta_{\#}$	-	System parameter(s)
ζ	-	UKF scaling factor
A	-	State matrix
B	-	Input matrix
c	-	Initial estimate confidence constant
C	-	Output matrix
e	-	Prediction error
I	-	Identity matrix
I_F	-	Fisher information matrix
J	-	Jacobian or sensitivity matrix
K	-	Kalman gain
l	-	Dimension
L	-	Iteration number
$\mathcal{L}$	-	Number of estimated parameters
κ	-	UKF tertiary scaling factor
n	-	Number of samples
P	-	Covariance matrix
p	-	Parameter
p_t	-	Number of parameter
R_L	-	Residual matrix
R_L	-	Residual matrix
R_1	-	Observation covariance matrix
R_2	-	Parameter covariance matrix
S	-	Square root
$SS_{J_{\#}}$	-	Sum of squares of the sensitivity matrix
t	s	Time
$u_{\#}$	-	System input(s)
w	-	Parameter noise term

$W_0^{(c)}$	-	Weight for covariance
$W_0^{(m)}$	-	Weight for mean
$x_\#$	-	System state(s)
X_L	-	Ranking matrix
$y_\#$	-	System output(s)

Chapter 6

$\delta\theta$	rad/s	Angular velocity difference
$\delta\theta$	rad	Angular position difference
ϵ	-	Observation noise
ω_{dy}	rad/s	Dynamometer angular velocity
ω_{en}	rad/s	Engine angular velocity
ϕ	-	Vector of observation variables
τ_{sh}	Nm	Shaft torque
θ_{dy}	rad	Dynamometer angular position
θ_{en}	rad	Engine angular position
$\vartheta_\#$	-	System parameter(s)
B_{sh}	Nms/rad	Shaft damping coefficient
e	-	Prediction error
K_{sh}	Nm/rad	Shaft stiffness coefficient
n	-	Number of samples
$y_\#$	-	System output(s)
Y_m	-	Measured response/parameter
Y_p	-	Predicted response/parameter

Chapter 7

α_{en}	rad/s^2	Engine angular acceleration
ϵ	-	Observation noise
κ	m	Compression ratio
ω_{en}	rad/s	Engine angular velocity
ϕ	-	Vector of observation variables

$\sqrt{\frac{\mu}{\mu_0}}$	-	Oil viscosity scaling factor
τ_{en}	Nm	Engine torque
τ_{fri}	Nm	Engine friction torque
$\mathbf{c_{\#}}$	-	Friction regression coefficients
θ_{en}	rad	Engine angular position
$\theta_{thr,dem}$	rad	Engine throttle actuator demand
$\vartheta_{\#}$	-	System parameter(s)
b	m	Cylinder bore diameter
D_b	m	Crankshaft bearings diameter
D_e	m	Exhaust valve diameter
D_i	m	Intake valve diameter
J	-	Jacobian matrix
$j_{\#}$	-	Jacobian matrix coefficient(s)
L_b	m	Crankshaft bearings length
L_v	m	Maximum length of valve lift
n	-	Number of samples
N_{en}	RPM	Engine speed
n_b	-	Number of crankshaft bearings
n_c	-	Number of cylinders
n_v	-	Number of valves per cylinder
P_{atm}	Pa	Atmospheric pressure
P_{int}	Pa	Intake manifold pressure
r	m	Crank arm length
S	m	Cylinder stroke
t	s	Time
T_{oil}	K	Oil temperature
v_p	m/s	Mean piston speed
$y_{\#}$	-	System output(s)
Z	-	Sensitivity matrix
$z_{\#}$	-	Sensitivity coefficients

Chapter 8

α_{en}	rad/s^2	Engine angular acceleration
δ	m	Piston pin offset
$\mathcal{L}$	m	Cylinder connecting rod length
ω_{en}	rad/s	Engine angular velocity
ϕ	-	Vector of observation variables
τ_{eng}	Nm	Engine torque
τ_{fri}	Nm	Engine friction torque
τ_{ind}	Nm	Engine indicated torque
τ_{rec}	Nm	Engine reciprocating torque
θ_{en}	rad	Engine angular position
$\vartheta_{\#}$	-	Vector of estimated parameters
A_p	m^2	Piston surface area
b	m	Cylinder bore diameter
$c_{\#}$	-	Friction regression coefficients
G	-	Engine geometric function
G_1	-	Engine geometric function
G_2	-	Engine geometric function
J	-	Jacobian matrix
M_{rec}	kg	Engine reciprocating mass
n	-	Number of samples
N_{en}	RPM	Engine speed
P_{crn}	Pa	Engine crankcase pressure
P_{cyl}	Pa	In cylinder pressure
r	m	Crank arm length
t	s	Time
T_{oil}	K	Oil temperature
$y_{\#}$	-	System output(s)
Z	-	Sensitivity matrix
$z_{\#}$	-	Sensitivity coefficients

Chapter 1

Introduction

The chapter introduces the principal cause and the ultimate purpose for conducting a research on system identification theory as applied to automotive powertrains. Besides, the contributions of this study and the layout of the thesis are presented.

1.1 Motivation

It has been highlighted numerous times that, climate change, caused by greenhouse gas (GHG) emissions, risks severe impacts on growth and development. One of the main contributors to the level of GHG emissions is road transportation. More specifically, according to official figures published by European Environment Agency [1], in 2012 road transportation was accounting for approximately 20 percent of GHG emissions in Europe (Fig. 1.1a). Based on the same source, road transport was the sector with the highest increased in CO_2 emissions between 1990 and 2012 (Fig. 1.1b). In particular, transport emissions were increase by 14.1 percent compared to 1990. Furthermore, emissions from aviation and maritime transport increased by 278 Mt CO_2 eq. between 1990 and 2012. Consequently, these data are the most solid evidences that indicate the need for improving the efficiency of vehicle powertrains with the purpose of reducing the level of GHG emissions in transportation related sectors.

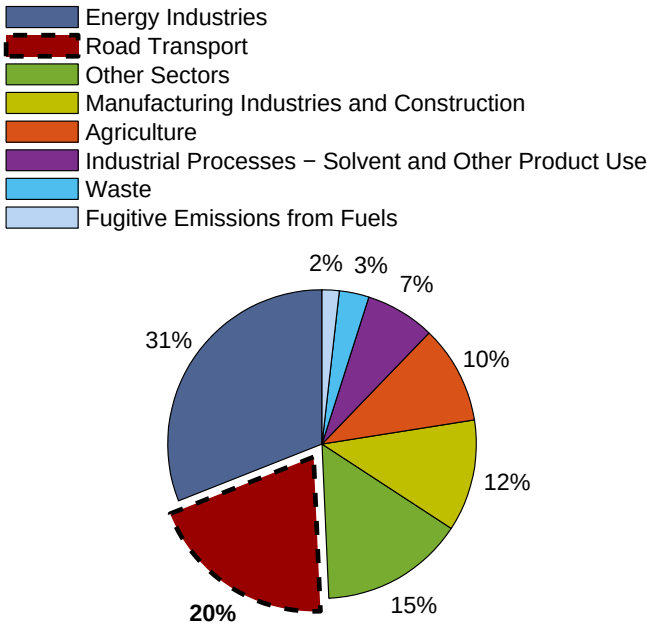

(a) GHG emissions share per sectors in 2012

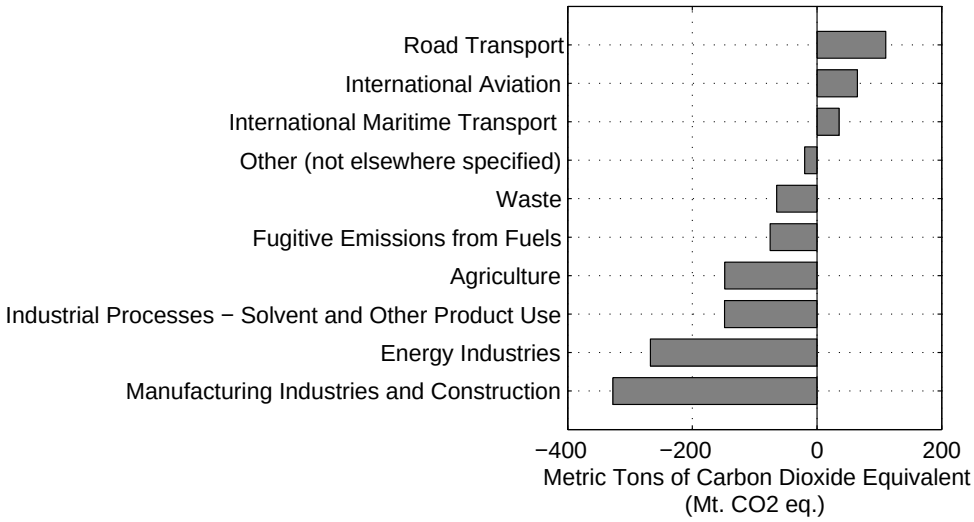

(b) Absolute difference of GHG emissions per sector from 1990 to 2012

Figure 1.1: Total GHG emissions trends per sector in Europe during 2012. The contribution of road transport accounts for approximately 20 percent of the main categories. Additionally road transport was the sector with the highest increase in GHG emission between 1990 and 2012. Data provided by European Environment Agency [1].

Over the years several potential technological concepts have been recommended to increase the efficiency of automotive powertrains. According to King [2], the efficiency of conventional propulsion systems could benefit from numerous add-on technologies, some of the most dominant are tabulated in Table 1.1.

Table 1.1: Potential technologies that could increase the efficiency of conventional powertrain systems; adapted from [2].

Technology	**Efficiency savings**
Downsizing engine capacity with supercharging	10-15%
Direct injection and lean burn	10-13%
Variable valve actuation	5-7%
Stop-start with regenerative braking	7%
Electric motor assist	7%
Reduced mechanical friction components	3-5%
Stop-start	3-4%

One practical problem associated with the inclusion of the aforementioned technologies is the increased complexity in the powertrain control and monitoring software. According to an official European Union publication [3], a typical engine control software consists of up to 500,000 lines of programme code, and will continue to grow as a result of the addition of new features to improve fuel economy and lower exhaust emissions. This will result inevitably in additional hardware resources for control and monitoring purposes.

Table 1.2: Evolution of powertrain control hardware; adapted from [3].

Feature	**Period**			
	pre 2000	*2001-2010*	*2011-2015*	*2016-2020*
Controllers per Vehicle	3-5	5-10	3-5	2-3
Sensors per Vehicle	10-35	30-40	36-45	40-50
Microprocessor Type	16-bit	32-bit	32-bit	32-bit/Multi-core

As a result of this increased complexity in the engine management system, the powertrain control community has started questioning the efficacy of existing control and monitoring software architectures and started focusing the research and development efforts towards model based control and diagnosis solutions. More specifically, according to Atkinson et al. [4] “one solution to the dilemma of rapidly increasing calibration burden is to transfer the majority of the calibration effort out of the transient engine test cell and onto the engineer’s desktop, using a systematic model-based approach". Similarly, as stated by Vint [5], “increased complexity of future engine technologies necessitate using Model Based Control (MBC) development approach".

In general model-based design provides an efficient method for developing complex control and fault diagnosis systems. However, a major disadvantage of model-based control approach is that it relies upon the existence and validity of mathematical models [5]. With this in mind, a complete chain of system identification tools that can be employed for the development of advanced model based control and condition monitoring applications in vehicle powertrains is presented.

1.2 Aims & Objectives

The aims this research is to address the gaps and contribute to the field of system identification as applied to automotive powertrain systems. The objectives of this research are listed below:

- Review recent advancements in system identification theory as applied to powertrain systems and address areas that require further investigation.
- Development and cyclic validation of a multi-domain physics-based dynamic model of a modern transient powertrain testing facility for the establishment of the appropriate system identification techniques needed in such applications.

- Design and construction of a novel engine test cell control and instrumentation platform that will enable the cyclic validation of the physics-based models and the practical implementation of the system identification tools.

- Determine the most adequate system identification algorithms for physical and semi-physical control-oriented powertrain models, and prove their efficacy with novel practical applications.

Based on the outcome of this research, some recommendations for future work in the area of automotive powertrain control and condition monitoring systems are provided.

1.3 Thesis Contribution

The major contributions of this work are enumerated below in respect of their significance and applicability across other disciplines:

1. *Qualitative Adaptive Identification*, the first and most important contribution is the establishment of a complete chain of system identification tools that can be used for real-time identification and detectability/sensitivity assessment of physical and semi-physical parameters (parameters associated directly or indirectly with design characteristics of powertrain systems e.g. diameter, length, stiffness, damping, mass, etc.) that can be found generally in physically-based powertrain control-oriented models. The efficacy of the proposed identification algorithms is presented in Chapters 6, 7 and 8, with three novel practical applications, those are: the development of a real-time health monitoring system for engine dynamometer shafts (Chapter 6), the parameter ranking and adaptive characterisation of engine friction (Chapter 7), and finally the identifiability analysis and adaptive identification of cyclic engine torque physical parameters (e.g. diameter, length, mass, etc. of related engine components), (Chapter 8). Lastly, it is useful to highlight that

the suggested framework finds direct applications in other disciplines such as biology and finance.

2. *Multi-Domain Control-Oriented System Modelling*, the second contribution is associated with the development of the first multi-domain physics-based model of a complete transient powertrain testing facility consisting of an electric drive, an internal combustion engine and a coupling shaft unit. This model provides an ideal virtual environment for model-based design studies. Additionally the model can be used for parametric simulation studies that are particularly useful in component design and selection applications. As powertrain control community focuses towards model-based solutions such multi-domain powertrain models will become more common in the future. Throughout the course of this thesis, simplified versions of this model were used for the development and implementation of the proposed system identification algorithms.

3. *Open-Architecture High-Speed Global Test Cell Controller*, last but equality important, is the design and development of a unique global test cell control and instrumentation system. The term “global" implies that the control and monitoring systems of each individual component of the test cell i.e. transient dynamometer, internal combustion engine and coupling shaft, is done by the same supervisory controller. This eliminates several practical issues such as synchronisation and data loss. Besides, this control and instrumentation system supports high-speed measurements and controls which is a “must have" feature for future cyclic control and identification applications. Lastly, the architecture of the hardware and software was kept intentionally open for reconfiguring and expanding the control and instrumentation system depending on the needs of the application. Without the creation of this system it would be impossible to develop, implement and prove the functionality of the proposed system identification tools.

Before closing, it is important to mention that the originality and novelty of this work is supported by five peer reviewed conference and journal publications. Appendix A gives the list of publications.

1.4 Scope & Limitations

Within the scope of this research, the theoretical and practical challenges related to the implementation of sophisticated system identification tools in real-world automotive powertrain applications are brought forward. In general, the main limitations of this work are enlisted below:

- The first limitation is related to the fact that the qualitative adaptive identification framework rely upon the existence of a physics-based control-oriented system model. This means that the presented tools cannot be deployed if a physical or semi-physical system model cannot be derived.
- The second limitation of this work is related to the suggested system identification algorithms. As it can be expected, it would be impossible to examine the applicability of all available system identification tools. Nevertheless, some of most adequate identifiability and adaptive identification algorithms for automotive powertrain applications are discussed.

1.5 Thesis Outline

The thesis consists of nine chapters and is organised into four consecutive parts: the first is the *"Introduction & Literature"*, the second is the *"Theoretical & Experimental Preliminaries"*, the third is the *"Practical Applications"* and fourth is the *"Conclusions & Open Problems"*. A schematic diagram that depicts the top level structure of the thesis is presented in Fig. 1.2. A laconic description of each individual chapter follows next.

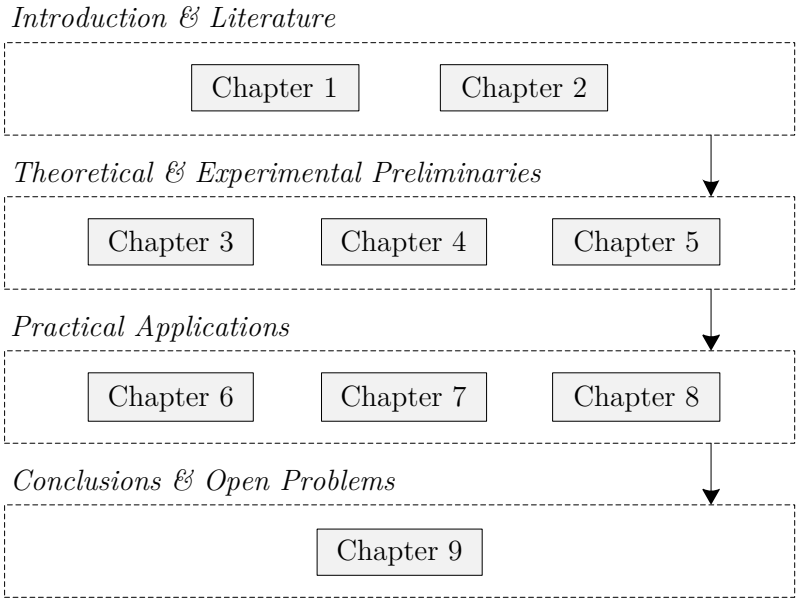

Figure 1.2: Schematic diagram showing the thesis layout.

Chapter 2

Presents the evolution of powetrain control and monitoring systems and reviews the current trends in automotive powertrain control and monitoring applications while inclining towards model-based approaches. Based on the review of the literature, future challenges and open problems are addressed.

Chapter 3

The theoretical analysis of the dynamics involved in a modern powertrain engine testing facility consisting of an electric transient dynamometer, a single cylinder, internal combustion, spark-ignited engine and a coupling shaft unit are discussed in this chapter. Based on this analysis a high fidelity multi-domain powertrain dynamic model is formed and typical simulation studies are conducted in order to examine the functionality and validity of the model. The model represents a transient engine testing facility that is presented later in Chapter 4.

Chapter 4

The features of the experimental apparatus that was used in this research are addressed in Chapter 4. This test rig was developed from scratch for the needs of this research. All the practical issues associated with the development of the

test rig are discussed. Some typical observation data are provided in order to realise the type of measurements that can be taken from this prototype test cell.

Chapter 5

The principles and background theory of the qualitative adaptive identification framework are introduced in this chapter. Recursive algorithms for the adaptive identification of physical and semi-physical parameters that can be found in powertrain models are presented and categorised in respect of the nature of the system i.e. linear or non-linear. Additionally a practical algorithm for assessing the identifiability of the parameters prior to any identification study is proposed. Some benchmark examples for understanding the implementation procedures and the practical differences of the suggested algorithms are presented. The real-world implementation of the discussed system identification mechanisms is reported in Chapters 6, 7, and 8.

Chapter 6

Shows the establishment of an on-line health monitoring system for engine dynamometer shafts. The methodology is based on the recursive identification of the physical characteristics of a coupling such as stiffness and damping coefficients. This piece of work is particularly useful in applications were the continues conditions monitoring of rotating shafts is vital such as automotive and marine propulsions, machine tools and large-scale drilling devices. This chapter is linked to Chapters 3, 4, and 5.

Chapter 7

Illustrates the application of some system identification tools that were presented in Chapter 5 for the problem of engine friction parameters ranking and adaptive identification. The material that is presented in this chapter is valuable for engine design and component selection purposes, and in applications that required adaptive estimation of engine friction such as control and fault diagnosis. Parts of this chapter came form Chapters 3, 4, and 5.

Chapter 8

A practical application of non-linear recursive parameter estimation algorithms with parameter estimability analysis for physical and semi-physical cyclic engine model parameters is reported in this chapter. The presented work contributes in the area of qualitative adaptive identification of engine parameters with physical and semi-physical interpretation which is valuable for engine adaptive control, on-line engine calibration, and on-line fault detection and isolation techniques.

Chapter 9

The final chapter summarises the work that was presented in the main body of the thesis. Based on the faced challenges and the results of this research, conclusions are drawn and some potential future directions are outlined.

The Appendices provide additional material which support the discussions that were made at the main part of the thesis.

Chapter 2

Background & Literature Review

Recent advancements and historical publications on automotive powertrain control, monitoring, modelling and identification techniques are reviewed in this chapter. Future challenges and open problems are also established. Ultimately the presented material adds more details behind the reasons that motivated us to conduct a research on this subject.

2.1 Advanced Powertrain Control & Monitoring Systems

2.1.1 Technology Evolution

Ever since the creation of the first automotive engine, one of the major problems that faced engineers and scientists was the establishment of suitable control and monitoring systems for managing the power output and energy consumption of vehicle's propulsion systems. Several milestones have been reached in respect of powertrain control and monitoring systems. Starting from the first proportional governors to control the speed of rotating machines [6], all the way down to advance mechatronic systems for control of power and emissions [7], the developments in automotive powertrain systems is closely linked with humans' ingenuity and ability to control and monitor the systems.

Probably the most important reason that drove powertrain control and monitoring technology to current standards was the enforcement of automotive emission regulation in 1965 by USA and 1970s by Europe and Japan [8]. As a result of these regulatory developments, 1970s was the decade that saw the introduction of electronic engine control with fuel injection and the development of key components for emissions control such as catalytic converter and exhaust gas recirculation systems, while establishing the first on-board diagnosis for condition monitoring purposes. The next milestone that allowed the tighter control and monitoring of engine emissions was the invention of the heated exhaust gas oxygen sensor and the three way catalytic converter. The appearance of control theory and modelling in 1980s had significant contribution in the development of automotive powertrain systems. In 1990s, the introduction of system-based solutions such as variable valvetrains, direct injection and continuously variable automatic transmissions allowed the further reduction in energy and emissions while maintaining the power output of the engine at acceptable levels. Additionally in 1990s international on-board fault diagnosis protocols contributed in eliminating the possibilities of air pollution in cases of engine faults and malfunctions. After the twenty-first century, the emission regulations were became even more stringent than before. This led engineers and scientists in the development of advanced propulsion technologies such powertrain hybridization, electrification, propulsions powered by alternative fuels, variable displacement and compression engines, and downsized and downsped turbocharged engines [8]. Not to mention that nowadays on-board fault diagnosis systems have more than five thousand fault codes for condition monitoring purposes.

As a matter of fact, this technology growth is linked with an exponential increase in the complexity of powertrain control and monitoring functionalities. For this reason the powertrain control community has grown and more people are now involved in the subject. As measure of knowledge growth, over the last decade more than ten books related to control, modelling and identification of powertrain systems have been published, some of them are listed here [9–18].

2.1.2 Research Trends

Generally speaking, current trends in the research of automotive powertrain control and fault diagnosis incline towards model-based solutions. The main reason for that is because suitable mathematical models allow the development of advanced control and condition monitoring strategies which eventually result in improvements in efficiency and robustness of propulsion systems.

The first paper that presented the application of dynamic models and advanced control theory to the design of electronic automotive engine controls was published by Cassidy et al. at the begging of 1980s [19]. The authors showed the implementation of a multivariable optimal controller with four inputs and ten outputs that was based on linear quadratic (LQ) control theory. As it can be expected one of the main problems of this control approach was related to the non-linear physical effects of the real engine. Thus for the implementation of the LQ control strategy, throughout the entire operating range of the engine, several linearised models valid around nominal operating points were developed using input/output experimental data.

A decade later Moskwa and Hedrick [20] discussed the application of non-linear multivariable automotive engine control methods. In particular the authors argued the implementation of a non-linear sliding-mode control method that was developed using a mean value physically based engine model. One of the main disadvantages of this method though was associated with chattering phenomena that accompany standard sliding mode controllers.

More recent publications address the design and development of engine controllers based on gain scheduled and Linear Parameter Varying (LPV) models. In particular, Jung and Glover [21] presented for the first time the application LPV for the development of a robust gain scheduled controller for the control of a turbocharged diesel engine. Since then, the design of diesel engine control functionalities based on LPV models has also been presented by Wei and del Re [22], by Wang et al. [23], and by Lee and Sunwoo [24]. Furthermore, the development of a switching LPV model-based controller for the regulation of air-fuel ratio in

spark-ignited engines has been published by Postma and Nagamune [25].

The development of a Model Predictive Controller (MPC) for the closed-loop control of 1-D engine simulation models was demonstrated recently by Cielsar et al. [26]. The authors made use of a non-linear mean value engine model which was then linearised on-line at each operating point to allow the formulation of an optimal quadratic controller. One of the issues of this approach is associated with the validity of the mean value engine model, in particular if the mean value model will not be valid then the linearised model will have errors which in turns will cause problems in the development of the optimal control. After all an optimal controller is as optimal as the mathematical model that describes the system. Other application of MPC strategies can be found in stratified charge engines [27], in diesel engines [28] and in hybrid electric vehicles [29]. A very recent publication by Huber et al. [30] showed how the problems related to the non-linear behaviour of internal combustion engines could be handled using a Non-linear MPC (NMPC) algorithm. The main weakness of this approach is that it relies on the validity of a physics based control oriented model, meaning that if the model is not valid throughout the entire operating range of the engine then the controller will be inevitably wrong.

Several researchers have argued the use of adaptive techniques in order to eliminate possible model inaccuracies which in turns result in control error. The application of a linear adaptive Kalman filter for re-compression four-cylinder homogeneous charge compression ignition engines (HCCI) was published by Lamirore et al. [31]. The development of a linear adaptive Kalman fitler-based load compensator for improved idle speed control of spark ignited engine was also demonstrated by Pavković et al. [32]. Idle speed control of spark ignited engines based on adaptive control theory was also studied by Yildiz et al. [33]. Adaptive control schemes were also used for regulation of air-fuel ratio for spark-ignited engines [34] and control of a pneumatic valve actuator for an internal combustion engine [35]. Finally, the combination of recursive subspace identification and MPC framework has been demonstrated recently by Ba et al. [36].

Turning to fault detection and diagnosis, one of the first model-based fault detection solutions was proposed by Sood et al. [37] in the middle of 1980s. The authors described the limitation of signal-based techniques e.g. Fourier series and autocorrelation, to localise faults and malfunctions, and demonstrated a model-based approach for identifying faulty cylinder(s) based on off-line estimation of model's parameters. Similar approach were followed later by Nyberg and Stutte [38] in order to detect and isolate faults that might occur on the air-path of a turbocharged diesel engine with exhaust gas recirculation; the faults that were encountered were the air-mass flow sensor, intake-manifold pressure sensor, air leakage, and faults associated with the exhaust gas recirculation valve. Kimmich et al. [39] also showed the application of model-based and signal-based techniques for fault detection of modern Diesel engines. The model based monitoring of large diesel engine, based on analysis of crankshaft angular speed variation was presented by Desbazeille et al. [40]. The real-time diagnosis of exhaust gas recirculation in diesel engines using recursive total least squares methods implemented successfully by Mohammadpour et al. [41]. Other state of art fault detection and isolation approaches for automotive powertrains make use of sliding mode observers [42,43], fuzzy logic techniques [44] and artificial neural networks [45].

In brief, according to the trends that were observed in literature, it turns out that the foundation behind the development of advanced control and monitoring strategies is the existence of an accurate model capable of predicting system responses throughout the entire operating range of the powertrain system. In the next section follows a background study on control-oriented modelling approaches and system identification tools suitable for automotive powertrains.

2.2 Control-Oriented Engine Modelling

Throughout the years, significant research efforts have been put in the establishment of engine powertrain models suitable for control design and model-based

condition monitoring applications. However, the complex nature that characterise the operation of internal combustion engines makes the development of representative mathematical models a rather challenging task. A number of different approaches have been proposed for the development of control-oriented engine models, these can be summarised into three independent categories (Fig. 2.1).

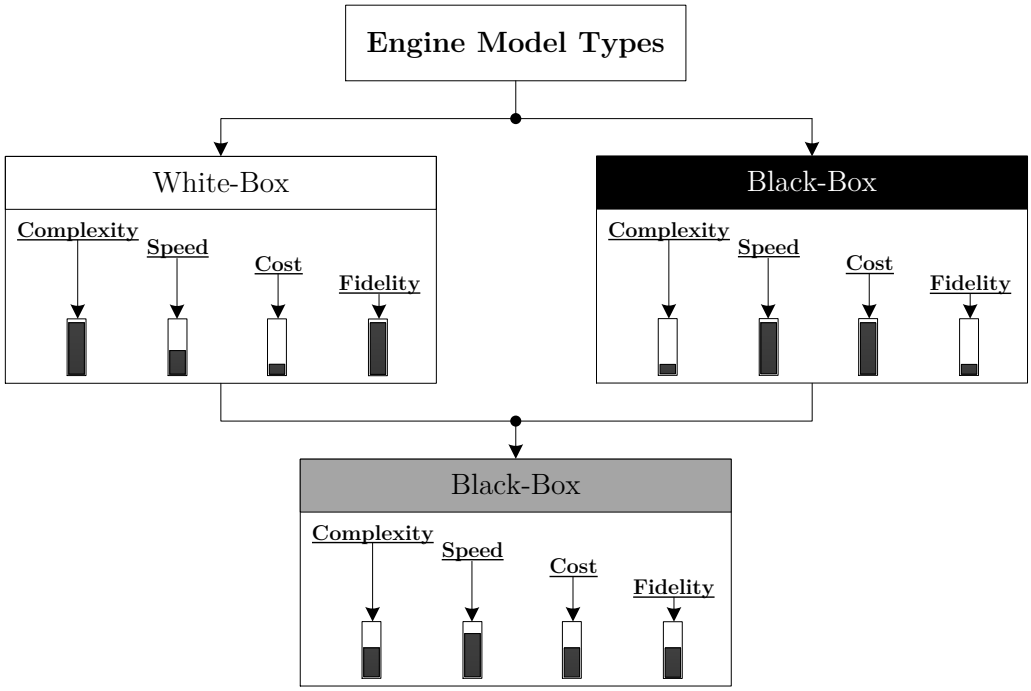

Figure 2.1: Different kinds and comparison of control-oriented engine models.

As it is observed in Fig. 2.1, the types of engine models can be distinguished into “white-box", “black-box" and “grey-box" models. In short, black-box models are developed purely based on experimental data, white-box models are formed using physics principles, whilst grey-box models are a combination of experimental and physics based models. Furthermore, Fig. 2.1 depicts the main practical differences between the various types in terms of model complexity, running speed, and development cost. As it can be seen, black-box models are more expensive compared to white-box and grey-box models since they require a large amount of experimental data in order to be developed. On the other hand black-box models are much faster and less complex compared to the white-box approach. Grey-box modelling provide an intermediate solution as opposed to white-box and black-box

techniques. At this point it should be highlighted that the above description supplies only a general guide to the reader and should not be taken for granted as the performance criteria i.e. complexity, speed and cost, can vary considerably depending on the very specific application. Further details on each individual approach are discussed bellow.

2.2.1 White-Box Models

The term “white-box" indicates the fact that the actual processes of the engine are described purely based on physics principles, these models are also known as “physics-based", “knowledge-based". White-box engine models can be categorized into two types, namely, the “total process", such that describe the operating principles of the entire engine, and the “actual process", which describe the individual working processes e.g. combustion, flow dynamics, kinematics etc. [46]. By summarizing all the actual process models, one can form total process models that ultimately describe the engine as a system. In fact the multi-physics nature of engine powertrains requires a system’s approach in order to develop a complete functional model [9].

Out of all the physics principles, thermodynamics is the most dominant subject that is required in order to develop physics-based engine models. Chow and Wyszynski [47] published an informative review article about the thermodynamic modelling methods of complete engine systems. In their work they divided the engine into elements, models, governing equations and governing sub-models (Fig. 2.2). Based on Fig. 2.2 the engine is divided into cylinders, manifolds, intercooler, catalyst, pipes, junctions and turbochargers. A review of the modelling approaches of each individual element will now follow:

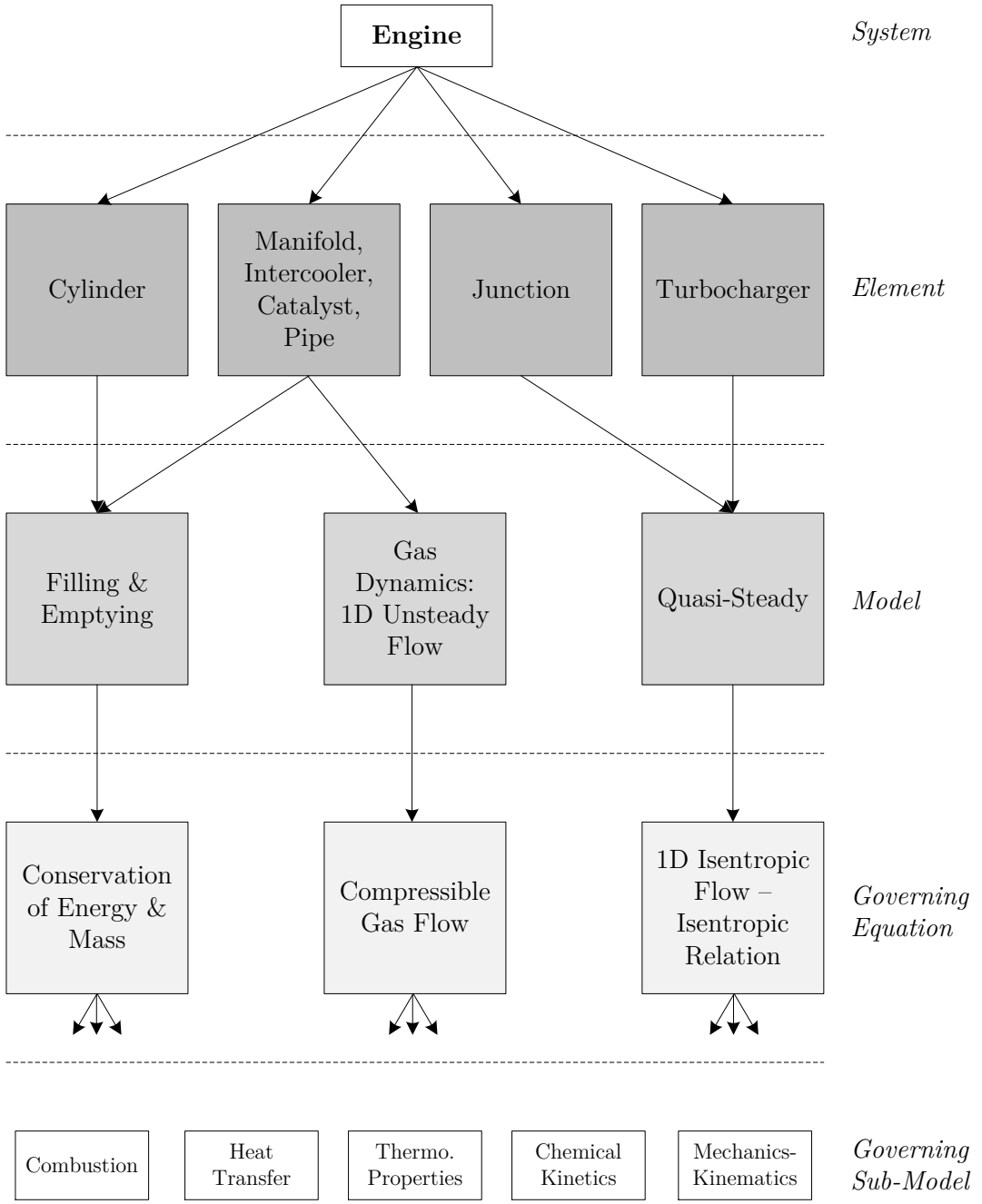

Figure 2.2: Top level structure of engine system models; adapted from [47].

- *Cylinder*: A cylinder element is usually modelled using the filling & emptying approach which is derived from the First Law of Thermodynamics by applying conservation of energy and mass principles [48–50]. The submodels that are needed for the construction of a cylinder model are combustion [46, 50–55], heat transfer [46, 49, 50, 56, 57], thermodynamic prop-

erties [49, 50, 58], chemical kinetics (optional) [46], and cylinder kinematics and mechanics [49, 50, 59, 60]. Although the majority of cylinder models, for control and monitoring purposes, are based on First Law of Thermodynamics, several works have been conducted in which Second Law of Thermodynamics was used mainly for analysis purposes [61, 62].

- *Manifold, Intercooler, Catalyst, Pipe*: Filling & empting approach is also used to model these elements. However, one drawback of using filling & emptying method is that wave effects in manifolds pipes and plenum cannot be captured [63]. Consequently one dimensional gas dynamics models have been developed to describe wave phenomena [46, 48, 63, 64]. Nevertheless, filling & empting approach is preferred for control and monitoring applications. Sub-models needed for the development of these models are heat transfer, thermodynamic properties, kinematics and mechanics (in cases where some of the elements have variable geometry mechanisms).

- *Junction*: With the term “junction" is meant the valves-orifices of the engine i.e. throttle plate and cylinder valves. The flow through these elements is evaluated using “quasi-steady" models which are based on one dimensional isentropic flow analysis [49]. Major sub-models which are needed are the thermodynamic properties, kinematics and mechanics.

- *Turbocharger*: The highly non-linear nature of turbocharger devices makes the pure physics-based modelling approaches impractical for control purposes. Consequently these models are usually developed based on experimental measurements and maps that are provided by the supplier [65]. A good overview of turbocharger modelling approaches for automotive applications was published by Moraal and Kolmanovsky [66]. Turbocharger models could classified as grey-box models, more details are given in Section 2.2.3.

The mathematical formulation of white-box models usually yields a set of ordinary differential equation in either crank angle [67] or the time [68] domain. The

selection of the domain depends on the needs of the application, a very interesting paper on the advantages and disadvantages of crank-angle based and time-based engine models was published in late 1980s by Chin and Coats [69]. The authors investigated the nature of engine dynamics to enhance the knowledge of engine control designers about the physical response of the system; they argued that all engine dynamics, apart form fuel dynamics, are less varying in crank-angle domain than in time domain. On the other hand time resolved models are preferred when the engine model is part of a complete multi-domain system e.g. powertrain system of hybrid electric vehicle [70].

White-box engine models could be used for predicting steady-state as well as transient phenomena, provided that the models have been validated. Mathematically speaking, the main difference between steady-state and transient operation is that the solution of the ordinary differential equations, that describe the engine model, does not change over time or angle depending on the selected domain. The majority of thermodynamic-based engine models that were found in literature were formulated for steady state kinematic conditions (engine speed is an input to the model) but transient thermodynamic conditions [50, 71–73]. Nevertheless, a number of completely transient models are also available [60, 74, 75]; a comprehensive literature review on transient engine modelling was published by Rakopoulos and Giakoumis [76].

Regarding the parametrisation of white-box models, this can be done without any experimental data, provided that the parameters of the model represent physical characteristics of the engine. This is the main reason that the development cost of these models is usually much less than black-box models. However, many researchers have argued that the parametrisation of physically oriented models can be quite challenging as the direct measurement and determination of the parameters might be impractical [9]. In addition to that, researchers have questioned the validity of white-box models as opposed to real experimental data [46]. According to Merker et al. [46] "*every model represents but an approximation of the real system under observation*". These reported problems arises questions

regarding parameter identification methodologies for such models. This thesis contributes in the area of identification of physical and semi-physical parameters that can be found in white and grey box models.

2.2.2 Black-Box Models

Also known as “experimental" or “empirical" models since they depend on the availability of experimental measurements. From control and monitoring point of view, the main benefit of black-box models in comparison to white-box models is related to the significantly lower computational demands. In fact, the first control-oriented engine models were developed based the black-box approach as they were relatively simpler and considerably faster [19, 77]. On the other hand, probably the most important disadvantage of black-box models is that they are not easily reconfigurable after they being developed.

Prior to any further discussions, we should clarify that in our research there was no application of the black-box modelling approach, thus the background information and literature will be limited to the absolute minimum essential to form a general idea of this modelling technique.

The development procedure of black-box engine models can be divide into three consecutive steps [78]:

1. *Design of Experiment & Data Collection*

   The first step is the definition of the model inputs/outputs and the operating conditions of the engine that the model will have to be identified and validated. The inputs and outputs of the model are usually defined according to the needs of the application, for instance if someone would like to relate the spark timing to the exhaust temperature throughout the entire operating range of the engine then the model inputs would have to be the spark timing, the engine speed and the engine load (or torque), while the exhaust temperature would have to be the output of the model. After the definition of the inputs and outputs, it is possible to specify the operating conditions that the

model will have to be developed and validated. Although this might sound simple and straightforward, it requires sophisticated mathematical tools in order to eliminate the testing time required for testing the engine throughout the desired operating range. Röpke and von Essen [79] have published an informative paper with current methods and trends on experimental design in engine development. Finally, after the design of the experimental procedure follows the actual test of engine and data collection processes.

2. *Data Modelling*

   Once the observation data have been collected, the next step is to develop a mathematical model which describes the functional relationship between the inputs and outputs. There is indeed a vast number of model structures that can be employed for describing the behaviour of the engine, simple static look-up tables, spline models, linear and non-linear regression models, artificial neural networks, Hammerstein models, Wieners models, and Volterra series, are some of the most famous black-box model structures in automotive applications. As soon as the structure of the model has been defined, it follows the model fitting process. This in most cases happens on an off-line basis based on either indirect (parametric models) or direct (non-parametric models) parameter optimisation algorithms, nonetheless it should be noted that on-line techniques have also been reported. A detailed description of black-box data modelling approaches for engine applications can be found in [9].

3. *Validation & Verification*

   The final step is the verification of the validity of the model as opposed to a set of validation data. This is usually done by computing suitable quantitative statistics that are used as a measure of prediction success. If the level of correctness of the model is not within some acceptable limits then the data modelling process is usually repeated until the model will provide the desired results [78]. Finally, it should be highlighted that the black-box

models might be quite accurate within the predefined range of model inputs but they are usually completely inaccurate for input conditions outside the operating range of the experimental design.

2.2.3 Grey-Box Models

The combination of white-box and black-box models results in the so called grey-box models. White-box models include all the functional relationships among the physical variables and parameters of the engine. On the other hand empirical models contain the parameters as mathematical values where functional description with physical processes remain unknown. Consequently, grey-box models are particularly useful in cases where the physical laws underlying the operation of the examined system are known “a-priori", but the parameters remain unknown. Such models are also known as “semi-physical" models due to the fact that their parameters have pure mathematical meaning but their structure has some physical interpretation. Grey-box engine models are preferred in control and monitoring applications as they offer better computational performance compared to white-box models. Another positive feature in comparison to black-box models is that they can be reconfigured more easily for other applications. On the other hand their dependence on experimental data availability increase the cost of the development. Something that has to be mentioned is that grey-box models cannot be operational without firstly identifying the unknown parameters of the model, this implies the importance of developing and using suitable system identification tools for such occasions.

Semi-physical models can exist either as “total-process" models or as “actual-process" models. Probably the most well-known application of grey-box models is related to the prediction of mean-value engine quantities. Moskwa and Hedrick [80] were from the first researchers that made use of the grey-box modelling technique for real-time control applications. In particular they showed the development of a non-linear port fuel injected automotive engine model (total process model) that consisted of five sub-models (actual process models) i.e. throttle body, intake

manifold, fuel injection, combustion and torque production, and rotational dynamics. Even thought the structure of this model was based on physics principles (e.g. first law of thermodynamics, one-dimensional isentropic flow, kinematics etc.), black-box models for the volumetric efficiency, indicated and friction torque, and various transport delays had to be developed by using observation data that were obtained experimentally. Another useful application of the grey-box modelling technique is the friction modelling of spark-ignited engines. In particular Patton et al. [81] developed a convenient and compact semi-physical engine friction model that was consisting of a number of physical and semi-physical parameters that could be tuned accordingly depending on engine's physical characteristics. This model has been improved recently by Sandoval and Heywood [82] to represent the mean engine friction of modern more adequately. There is indeed a rich literature in the area of grey-box engine modelling, some key references are provided here [63, 83–88].

2.3 Identification of Powertrain Systems

According to the literature (Section 2.1.2), modern automotive control and monitoring applications rely directly or indirectly on the quality of mathematical models. The validation of engine powertrain models is by no means a simple task. The complexity involved in the direct measurement of the physical characteristics of the engine, for the parametrisation of white-box or grey-box models, and the problems associated with the testing procedure of the engine, for the development of black-box or grey-box models, contribute negatively in the validity and overall predicting capability of the models. For this reason intuitive system identification tools have to be employed to ensure the efficacy of powertrain models. Although this might sound natural and trivial, the reality is that "a large gap seems to exist: neither these methods are sufficiently well known in the automotive community, nor enough attention is paid by the system identification community to the needs of the automotive industry" [13]. For general reading on recent advancements and

open problems in system identification as applied to automotive systems refer to [9, 13]. In the next paragraphs will follow a brief review of the applications of system identification theory in the automotive powertrain sector.

The most common use of identification theory in powertrain systems is related to the development of black-box engine models. Cassidy et al. [19] presented one of the first applications of system identification theory for the development of a black-box linear time invariant state-space model of a spark ignited engine for the design of an optimal multivariable linear quadratic controller. In particular the authors determined the dynamic characteristics of the engine by postulating low-order dynamics with time delays and then establishing parameter values by using least squares matching of the observed and the estimated frequency response. Melgaard et al. [89] showed the black-box identification of a four-stroke spark ignited engine using a linear state-space model and maximum likelihood estimation theory in combination with Kalman filtering in order to fit the model to experimental results. The identification of a turbocharged diesel engine based on subspace identification of a state-space model has been published by Nikzadfar and Shamekhi [90]. Salcedo and Martínez [91] presented the identification of a linear parameter varying model of a turbocharged engine by identifying several local linear models that were connected globally by means of least squares fitting using the Levenberg and Marquardt algorithm. Luh and Rizzoni [92] used NARMAX (Nonlinear Autoregressive Moving Average with Exogenous input) model structure for the identification of a multiple-input-multiple-output internal combustion engine model. More recently Togun et al. [93] presented the non-linear identification of a spark ignition engine torque output based on Hammerstein model structure. The identification of a black-box non-parametric non-linear model of a homogeneous charge compression ignition engine based on neural network and principal component analysis was presented recently by Janakiraman et al. [94]. Furthermore the implementation of adaptive identification tools for black-box models has been present by several authors. More specifically, Stosky [95] presented the adaptive estimation of engine friction torque by fitting recursively the

regression coefficients of a representative polynomial function. Similar work was presented by Jones and Muske [96] for the automatic calibration of one and two dimensional look up tables based on recursive identification techniques. Adaptive identification of look up tables was also the main subject of interest of Guardiola et al. [97], the authors showed the use of Kalman filters for updating on-line look-up tables for modelling emissions. Another very interesting application of adaptive identification tools was presented recently by Helm et al. [98], more specifically the authors used a linear Kalman filter for identifying in real-time the parameters of a cyclic parametric model that was used to model the instantaneous engine torque of a spark ignited engine.

As in the case of black-box models, system identification tools have been used several times for the development of grey-box models. A classical example of grey-box identification is this of the mean value engine model that was developed by Moskwa and Hedrick [80], in particular the experimental identification of the volumetric efficiency, indicated and friction torque were necessary in order to make the model functional. Later, Gangopadhyay and Meckl [99, 100] showed the used of a recursive least squares algorithm for the identification of semi-physical coefficients related to the volumetric efficiency. The need for a systematic method for identifying combustion heat-release model parameters was discussed by Eriksson [101]. In particular the author showed how to implement classical non-linear least squares approach to heat-release models for the purpose of increasing their validity as opposed to experimental data. Similar work was presented by Brahma et al. [102] and Yeliana et al. [103]. The modelling and identification of throttle body effective area based on grey-box approach was presented by Cary et al. [104], the authors showed the use of one dimensional isentropic flow equation in combination with a black-box two-stage model of the discharge coefficient of the throttle for modelling the effective throttle area. Analogous work was conducted more recently by Neve et al. [105], where the air flow of the engine was modelled using one dimensional isentropic flow equation and mass balance in combination with a radial basis function network.

Applications of system identification theory in white-box powertrain models have also been reported in literature. Such applications were involved in the estimation of physical model parameters, for condition monitoring purposes, and for the estimation of unmeasured system states, for control and monitoring purposes. The estimation of physical model parameters has been investigated by several researchers, Rezeka and Henein [106] showed for the first time the use of linear least squares analysis to identify the physical parameters of an instantaneous engine friction model. A year later Sood et al. [37] presented the engine fault analysis based on the identification of physical model parameters. Similarly, Constantinescu [107] presented the identification of engine's inertia and other physical parameters related to the rotational dynamics of the engine based on standard linear least squares estimation. The use of non-linear least squares and Newton-Raphson optimisation was presented by Zweiri et al. [74] for the identification of engine physical parameters from the data of crankshaft angular velocity, indicated torque, dynamometer angular velocity and load torque. Mrosek et al. [108] discussed the identification process of air path models of turbocharged engines based on least squares matching. Peragón et al. [109] argued the on-line identification of instantaneous mechanical losses in internal combustion engines, however inside their paper they use standard linear regression technique to estimate the model parameters which contradicts their argument that the instantaneous mechanical losses were identified on an on-line basis. Belaidi et al. [110] worked on the detection and localisation of diesel engine faults based on non-linear least squares estimation and Newton-Raphson optimisation of physical model parameters. The parameter estimation of powertrain torsional vibration models based on non-linear least squares has been presented by Nickmehr et al. [111]. Furthermore, recently Nickmehr [112] showed the identification of the parameters of a crankshaft model based on prediction error approach. Another new publication by Kebairi et al. [113] shows the identification of an engine air path electromechanical actuator by deploying mainly non-linear parameter optimisation tools.

Now, one common characteristic of all the above approaches is that the physical parameters of the models were identified on an off-line basis. This indicates that non of the aforementioned methodologies could be used for the identification of model physical parameters in real-time conditions. As a matter of fact, on-line identification tools were employed mostly for the estimation of unmeasured states of powertrain dynamic models, some examples are mentioned here. Shiao and Moskwa [114] presented the cylinder pressure and combustion heat release estimation based on non-linear sliding mode observers. The prediction of the port air mass flow of spark ignited engines by using an extended Kalman filter (EKF) to estimate the unmeasured states of the model was discussed by Chevalier et al. [63]. Kolmanovsky et al. [115] worked on the same practical problem and proposed the use of an input observer for the simultaneous estimation of state and parameters; here it must be clarified that the parameters were not representing some physical design characteristic of the engine but tuning coefficients (grey-box) that were used to increase the predictive capability of the observer. The use of recursive identification for dynamic compensation of an thermocouple for instantaneous exhaust temperature measurements was presented by Kar et al. [116]. Pavković et al. [32] implemented a Kalman filter for estimating the load torque of a spark ignited engine for applications in idle speed control. The estimation engine torque was also studied by Ortner et al. [117], the authors compared the estimation results form three different observers i.e. extended Kalman filter (EKF), High Gain Observer (HGO), and Sliding Mode Observer (SMO). The estimation of instantaneous states of a spark ignited engine based on extended Kalman filter (EKF) and unscented Kalman filter (UKF) was investigated by Sengupta et al. [118]. The use of a HGO for the estimation of the effective compression ratio for engines utilizing flexible intake valve actuation was presented by Stricker et al. [119]. Daroogheh et al. [120] published recently a particle filtering approach for the state and parameter estimation in gas turbine engine fault diagnostics; here the parameters were not representing some physical characteristics design but tuning coefficients (grey-box). Most recently, Baur et al. [121] worked on the estimation

of fuel properties in a common rail injection system by employing an UKF.

According to the literature on white-box powertrain identification application, it could be said that even thought there have been numerous examples on the use of adaptive identification tools for state estimation of white-box models, the on-line estimation of physical powertrain model parameters is still an immature area. Therefore extra effort is required in order to come up with suitable adaptive identification solutions that could be used to evaluate the physical parameters of white-box powertrain models, hence unlock future technologies associated with on-line model-based engine condition monitoring. Before closing, it would be useful to note that adaptive parameter identification tools are also becoming very valuable in vehicle stability and handling applications [122–124].

2.3.1 Parameter Identifiability

One concept that the automotive powertrain identification community has not investigated widely is this of the identifiability of parameters with physical and semi-physical interpretation that can be found commonly in white and grey box models. In contrast to pure identification problems were there is a vast amount of literature, the available literature related to the identifiability of white-box and grey-box powertrain model parameters is very limited. More specifically previous studies were mainly involved with optimum sensor selection for engine fault diagnosis application based on the observability principles [125, 126], which is not necessarely the same problem with the identifiability of physical and semi-physical model parameters. As a matter of fact, only few publications were found in literature discussing the concept of identifiability of powertrain model parameters. The first paper that questioned the identifiability of turbocharged internal combustion engine models was published by Sokolov and Glad [127]. More specifically the authors examined the global identifiability of the model, however they highlighted that the results of the global identifiability analysis will not mean that the identifiable parameters will be always identifiable in real world experiments. This is originated from the fact that the global identifiability examines only the structural identifiability i.e. inverta-

bility, of the model without considering the quality and information content of real world experimental measurements. Similarly, Alasty and Ramezani [128], examined the structural identifiability of a full vehicle ride model by evaluating the rank of the Jacobian of Markov parameters of the system model, this provides information related to the invertability of the model but not any indication for the quality of the parameter estimates in respect to the information content in the experimental measurements. The last and most recent document was a Licentiate Thesis authored by Nickmehr [112], in this work the concept of structural identifiability of the physical parameters of a crankshaft model is presented again. As with the other publications, the latter work can be used only for assessing the structural identifiability of the model parameters but not the effect of measurement noise and information content in the detectability of the parameters. However, according to Nickmehr [112] one way that this could be done is by examining the variance of the estimated parameters in order to get some idea regarding the effect of measurement data information content on the identifiability of the model parameters. Consequently, as it can be understood there is a need for research on the problem of parameter identifiability in powertrain applications, for the purpose of providing a complete solutions that can evaluate the structural as well as the practical identifiability of physical and semi-physical parameters.

2.4 Synopsis

A summary of the key points of this chapter is given below.

- The technological evolution of powertrain control and monitoring systems was presented.
- Based on current research trends, model based solutions tend to be the main subject of interest for the majority of powertrain control and monitoring community.
- The advantages and disadvantages of the various control-oriented engine

modelling methodologies were outlined. Furthermore some open problems in the area of control-oriented powertrain modelling were mentioned.

- A literature review on the applications of system identification theory on automotive powertrains revealed some areas that require further investigation. Those are related to adaptive identification solutions for parameters with physical interpretation, and parameter identifiability analysis tools for assessing the structural as well as practical identifiability of physical model parameters.

Chapter 3

Powertrain Dynamic Modelling

A multi-domain zero dimensional dynamic model of a complete transient engine powertrain testing facility is derived in this chapter. The term "multi-domain" indicates the application of multiple physics principles such as thermodynamics, fluid dynamics, classical mechanics and electromagnetism. The model represents all the involved physical phenomena and dynamic characteristics of a single cylinder transient cyclic engine testing facility that is presented later in Chapter 4.

3.1 Test Cell System-Level Model

Even though the set-up of modern transient engine testing facilities can vary considerably depending on the purpose of the test, the basic structural principles remain always the same. The transient dynamometer is responsible for controlling the speed or the load of an IC engine through an appropriate coupling shaft. The term "system-level" here refers to the mathematical/physical formulation of a transient engine test cell while representing it as a complete system. Consequently, a system-level mathematical analysis of a transient engine test cell is presented in this section and sets the foundations for the "component-level" analysis i.e. engine and dynamometer models, that follows in the next sections of this chapter.

The schematic diagram presented in Fig. 3.1 illustrates a typical transient dynamometer, an engine and a coupling shaft. The interactions of each subsystem with the global control and monitoring system of the test cell also are depicted in Fig. 3.1. The technical details of the actual transient engine test cell that was used in the present study are described in details in Chapter 4.

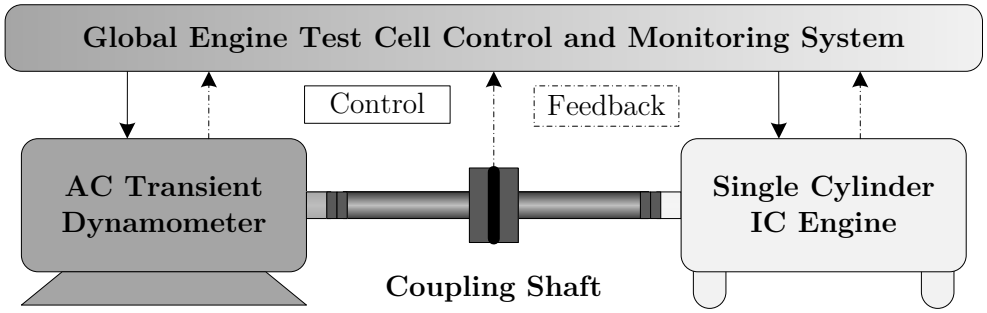

Figure 3.1: Transient engine test cell, schematic representation.

Turning to the physics-based modelling of the transient engine test cell, it is possible to derive the mathematical relationships that describe the mechanics of the system based on Newton's second law for rigid bodies in pure rotation [129]. The sum of torques $(\sum \tau)$ acting on a rotating body are proportional to the inertia (J) and acceleration (α) on the same axis (Eq. 3.1).

$$\sum \tau = J\alpha \tag{3.1}$$

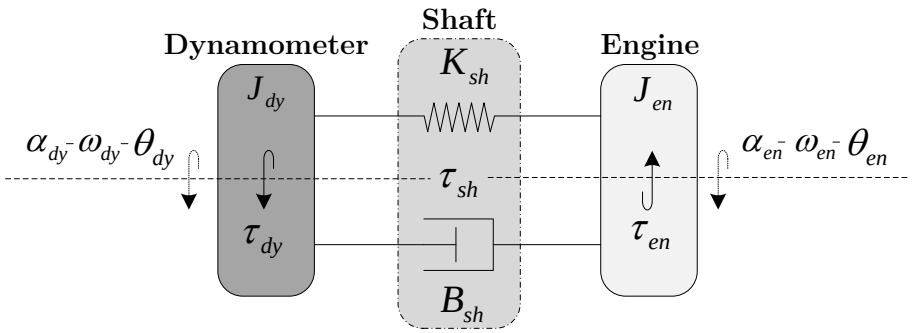

Figure 3.2: Free body diagram (2-DOF) of a transient engine test cell.

Now, considering the transient engine test cell as a two degree of freedom rotating system allows to draw the free body diagram of the system as presented

in Fig. 3.2. Assuming that the dynamometer is the primary source of the system, the principle governing equations of the system can be derived [130]:

$$\tau_{dy} - \tau_{sh} = J_{dy}\alpha_{dy} \tag{3.2}$$

$$\tau_{sh} - \tau_{en} = J_{en}\alpha_{en} \tag{3.3}$$

Where, τ_{dy}, τ_{sh} and τ_{en} represent the torque of the dynamometer, shaft and engine respectively, J_{dy} and J_{en} are the dynamometer and engine inertias, while the α_{dy} and ω_{dy} are the dynamometer and engine accelerations.

The coupling shaft torque (τ_{sh}) was modelled as a torsional spring element with a viscous damper [60]:

$$\tau_{sh} = B_{sh}(\omega_{dy} - \omega_{en}) + K_{sh}(\theta_{dy} - \theta_{en}) \tag{3.4}$$

Here, B_{sh} and K_{sh} are the internal damping coefficient and spring stiffness respectively, ω_{dy} and ω_{en} are dynamometer and engine angular velocities and finally θ_{dy} and θ_{en} are angular positions of the dynamometer and engine. At this point it would be helpful to clarify that the angular acceleration (α), velocity (ω) and position (θ) are related according to the following expressions:

$$\alpha = \frac{d\omega}{dt} = \frac{d^2\theta}{dt^2} \Leftrightarrow \theta = \int \omega\, dt = \iint \alpha\, dt^2 \tag{3.5}$$

Equivalently, since the model has a linear structure, it could be described as a Linear Time Invariant (LTI) dynamic system in a much more compact way using state-space formalism.

$$\begin{aligned} \dot{x}(t) &= Ax(t) + Bu(t) \\ y(t) &= Cx(t) + Du(t) \end{aligned} \tag{3.6}$$

Here, system's inputs (u), outputs (y) and states (x) are:

$$u = \begin{bmatrix} \tau_{dy} & \tau_{en} \end{bmatrix}, \quad y = \begin{bmatrix} \theta_{dy} \\ \omega_{dy} \\ \theta_{en} \\ \omega_{en} \end{bmatrix}, \quad x = \begin{bmatrix} \theta_{dy} \\ \omega_{dy} \\ \theta_{en} \\ \omega_{en} \end{bmatrix}$$

Whilst the parameters of the state-space coefficients are given bellow:

$$A = \begin{bmatrix} 0 & 1 & 0 & 0 \\ -\frac{K_{sh}}{J_{dy}} & 0 & \frac{K_{sh}}{J_{dy}} & \frac{B_{sh}}{J_{dy}} \\ 0 & 0 & 0 & 1 \\ \frac{K_{sh}}{J_{en}} & \frac{B_{sh}}{J_{en}} & -\frac{K_{sh}}{J_{en}} & 0 \end{bmatrix}, \quad B = \begin{bmatrix} 0 & 0 \\ \frac{1}{J_{dy}} & 0 \\ 0 & 0 \\ 0 & -\frac{1}{J_{en}} \end{bmatrix}, \quad C = \begin{bmatrix} 1 & 0 & 0 & 0 \\ 0 & 1 & 0 & 0 \\ 0 & 0 & 1 & 0 \\ 0 & 0 & 0 & 1 \end{bmatrix}$$

Note that the coefficient D in Eq. 3.6 is neglected completely as the system model does not have direct feed-through calculations.

Lastly, the system-level model block diagram is given in Fig. 3.3 with the purpose of visualising the structure but also the location and the connections among the sub-systems. Details regarding the physics underlying the operation of the IC engine and the AC dynamometer are given in the following sections.

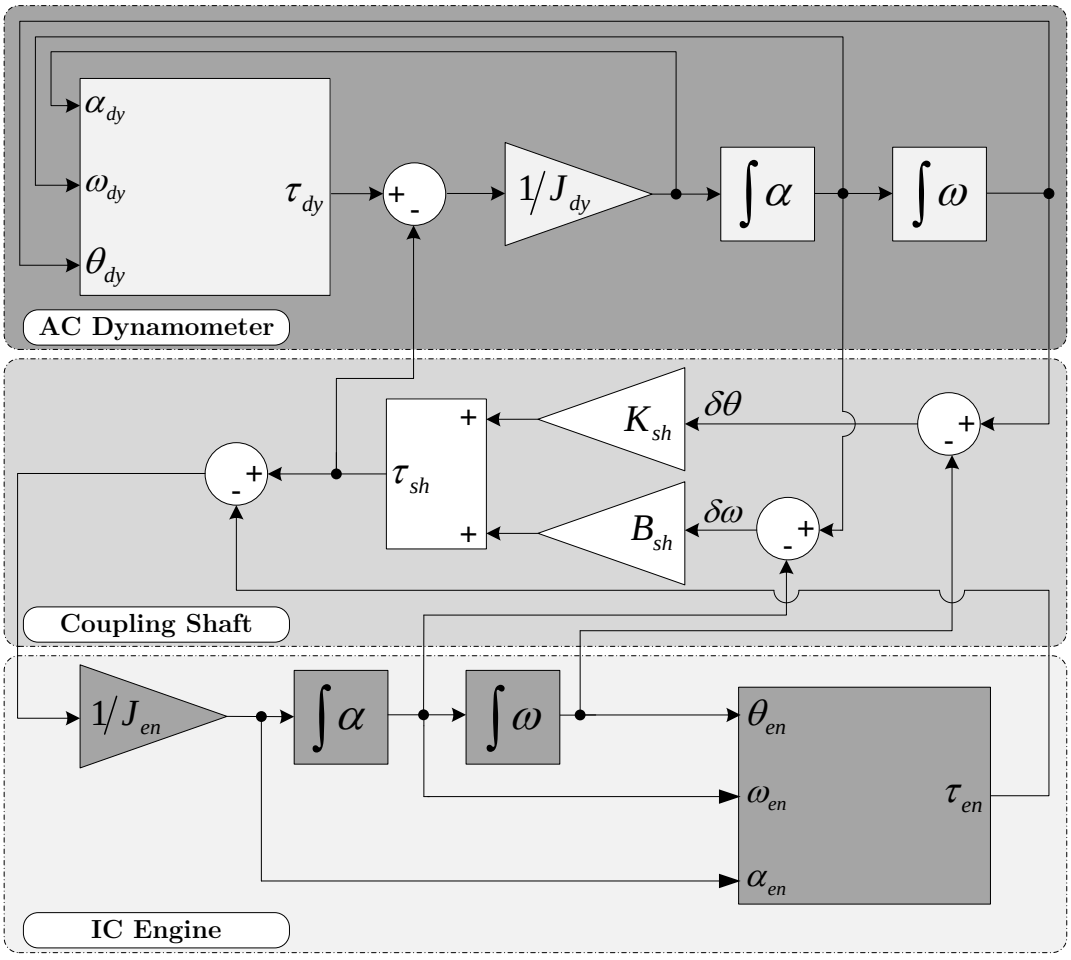

Figure 3.3: System-level engine test cell model, block diagram representation.

3.2 Single Cylinder Engine Model

The mathematical model of a single cylinder internal combustion engine is derived in this section. It reflects all the governing physical phenomena and dynamics of a real single cylinder internal combustion engine that is presented later on in Chapter 4. This model is part of the overall transient engine test cell system; according to Fig. 3.3 the IC engine model outputs the instantaneous cyclic engine torque (τ_{en}) which is one of the two inputs (the second is the electromagnetic torque of the dynamometer (τ_{dy})) of the overall system model (see Eq. 3.6). Furthermore, the inputs to the engine model are the angular acceleration (α_{en}), velocity (ω_{en}) and position (θ_{en}) whilst from system's point of view, it could be said that they are the main outputs of the system-level model that was described previously.

The model is mainly used as a tool with the purpose of proving the concept of real-time identification and estimability analysis for physical and semi-physical parameters that can be found generally in physics-based dynamic engine powertrain models. It is a zero dimensional physics-based dynamic model that was developed using thermodynamics, fluid dynamics and kinematics/mechanics principles. To explain, from thermodynamics point of view the entire engine is model based on filling and emptying approach that is the treatment of the engine as a series of interconnected control volumes (open thermodynamic systems) [48]. Energy and mass conservation principles (First Law of Thermodynamics) are applied on each control volume [49, 50, 54, 131]. The resulting model after the mathematical formulation of the system consists of a set non-linear ordinary differential equations that describe the pressure, temperature and mass of each control volume and define the dynamic and steady state operating conditions of each corresponding thermodynamic system. Coupled with the thermodynamic model, the engine kinematics/mechanics models provide the developed instantaneous cyclic engine torque perpendicular to the crankshaft. A sketch with the most important physical quantities of the engine model is presented in Fig. 3.4.

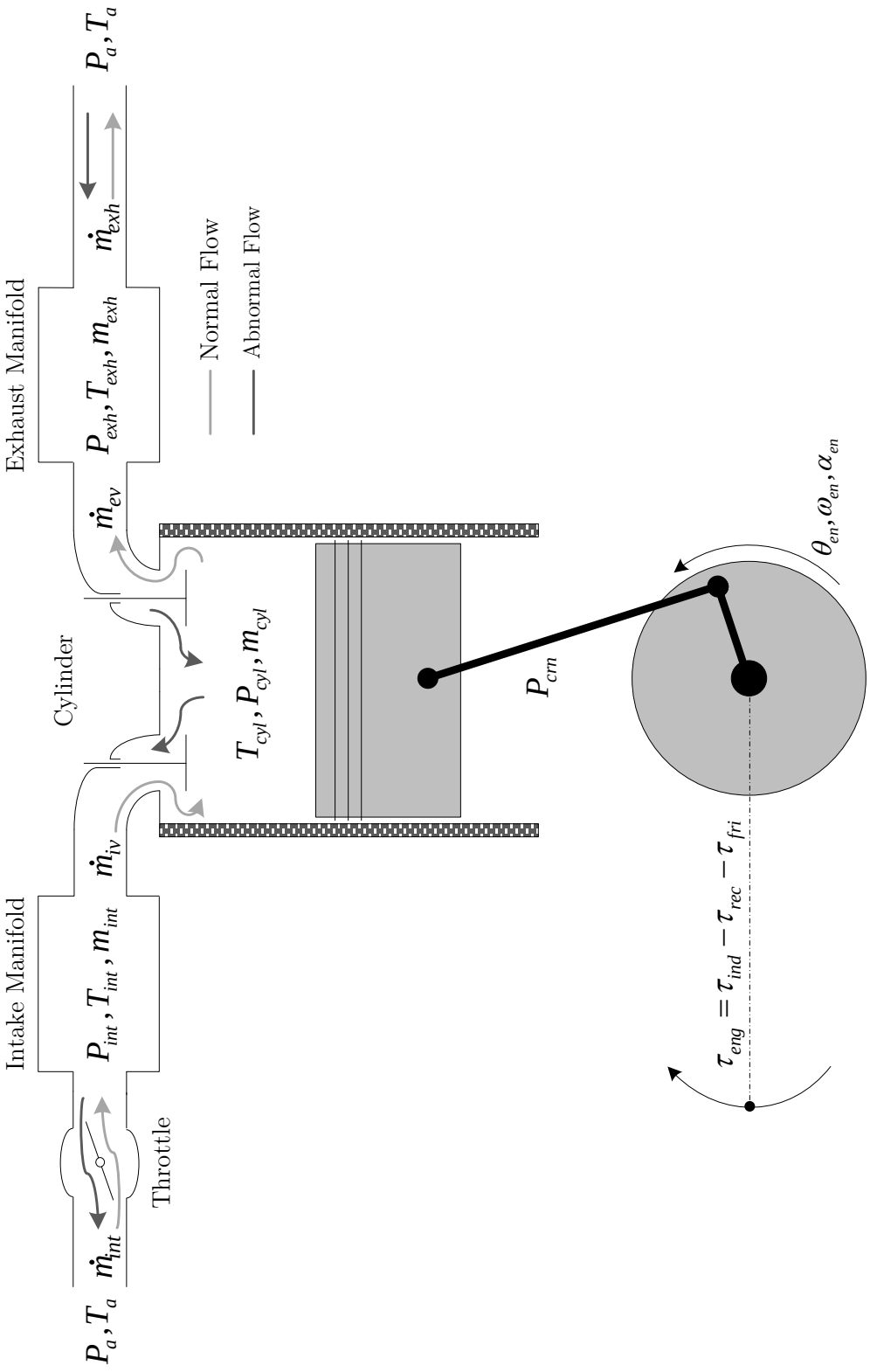

Figure 3.4: Schematic diagram of the single cylinder, internal combustion spark-ignited engine physical model.

From Fig. 3.4 the control volumes of the given single cylinder engine are assumed to be the intake/exhaust manifolds and the cylinder, while the working medium in each control volume is assumed to behave as an ideal gas. At this stage it should also be clarified that time is taken as the independent variable instead of crank angle to make the model compatible with the rest of the system components. The time step (dt) of the solver was computed with respect to the desired crank angle step $(d\theta_{en})$ and the current engine speed (ω_{en}), hence the model provided crank angle based results (Eq. 3.7) [46].

$$dt = \frac{d\theta_{en}}{\omega_{en}} \tag{3.7}$$

Finally, even though the model represents a single cylinder engine, the theoretical analysis that follows could be used for creating physical models of any type of internal combustion engines regardless the existing technology.

3.2.1 Cylinder Thermodynamics

The governing equations for the calculation of the cylinder pressure and temperature are mainly derived from the First Law of Thermodynamics. The application of the energy balance principle in the cylinder control volume is depicted schematically in Fig. 3.5. It should be noted that this figure does not illustrate the blow-by energy losses and the kinetic and potential energies of the gas exchange process as these quantities are neglected in the present analysis.

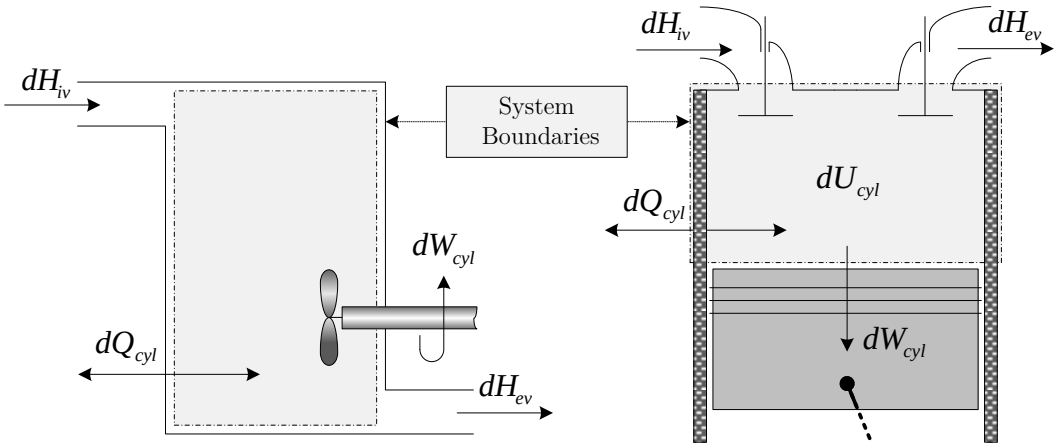

Figure 3.5: Cylinder energy balance, schematic representation.

Under these circumstances, the change in the internal energy (dU_{cyl}) of the cylinder can be written as follows (Eq. 3.8).

$$dU_{cyl} = \sum_{cyl} dQ_{cyl} - dW_{cyl} + \sum_{cyl} dH_{cyl} \tag{3.8}$$

Where, the sum of dQ_{cyl} and dH_{cyl}, is the heat and enthalpy change throughout the cylinder system boundaries, whilst the term dW_{cyl}, symbolize the work change due to the reciprocating movement of the piston.

Now, the first term on the RHS of Eq. 3.8 can be expanded in the following form:

$$\sum_{cyl} dQ_{cyl} = dQ_c - dQ_w \tag{3.9}$$

Where, dQ_c represents the release produced by the combustion of the air/fuel mixture. The combustion term will not be further analysed here, as the work that is presented in the following chapters does not require to model the combustion phenomena. This is because for all the experiments that were conducted in this study, the engine was running in its unfired state i.e. motoring conditions. Nevertheless, the mathematical analysis of the combustion term can be found in previous publications written by the author [132] or in well-known textbooks related to engine thermodynamics [49, 50, 54, 131] and combustion modelling [46, 133]. Next, the term dQ_w is the heat transfer from the cylinder gas to the walls. The heat transfer is assumed to be purely by convection (no conduction and radiation) and is expressed using the following equation:

$$\frac{dQ_w}{dt} = \hbar A_w (T_{cyl} - T_w) \tag{3.10}$$

Here, T_{cyl} and T_w are the in-cylinder gas temperature and the temperature of the cylinder walls respectively, A_w is the cylinder wall surface area (see Section 3.2.3), and $\hbar$ is the heat transfer coefficient. Several models are available to express the heat transfer coefficient [56], in the current work the model developed by Woschni [57] was employed.

$$\hbar = C_h b^{(\bar{c}-1)} {P_{cyl}}^{\bar{c}} {T_{cyl}}^{(0.75-1.62\bar{c})} \bar{\hbar}^{\bar{c}} \tag{3.11}$$

And,

$$\hbar = C_1 S \frac{\omega_{en}}{\pi} + C_2 \frac{V_d T_{ivc}}{P_{ivc} V_{ivc}} \left[P_{cyl} - P_{ivc} \left(\frac{V_{ivc}}{V_{cyl}} \right)^{\gamma} \right] \tag{3.12}$$

Where, b, P_{cyl} and T_{cyl} are the cylinder bore, pressure and temperature correspondingly, and S, V_d, V_{ivc}, V_{cyl}, T_{ivc}, P_{ivc}, and γ, are the cylinder stroke, total cylinder displacement, cylinder volume at IVC, cylinder volume with respect to crank angle, gas temperature and pressure at IVC, and specific heat ratio of the working medium repetitively. Lastly the Woschni coefficients C_h, C_1, C_2 and $\bar{c}$ are tabulated in Table 3.1.

Table 3.1: Woschni heat transfer coefficients.

Coefficient	**Process**		
	Gas Exchange	*Compression*	*Expansion*
C_h	3.26		
C_1	6.18	2.28	2.28
C_2	0	0	$3.24 * 10^{-3}$
$\bar{c}$	0.8		

The second term on the RHS of Eq. 3.8 can also be written as a function of cylinder pressure (P_{cyl}) and change of volume (dV_{cyl}) (for the computation of the change of volume see Section 3.2.3).

$$dW_{cyl} = P_{cyl} dV_{cyl} \tag{3.13}$$

The third term on the RHS of Eq. 3.8 represents the enthalpy change of the cylinder control volume caused by the inflow and the outflow of the working medium. The general form of this term is shown in Eq. 3.14.

$$\sum_{cyl} dH_{cyl} = dH_{iv} + dH_f - dH_{ev} - dH_{bl} \tag{3.14}$$

Where, the dH_f and dH_{bl} are neglected as they refer to the enthalpy due to fuel and blow-by losses, while the terms dH_{iv} and dH_{ev} are the enthalpy changes caused by the inflow and the outflow of the working medium. As a matter of fact

enthalpy change can also be express in terms of mass changes considering the mass conservation principle. Therefore, in Fig. 3.6 the schematic diagram of the mass balance principle of cylinder control volume is given.

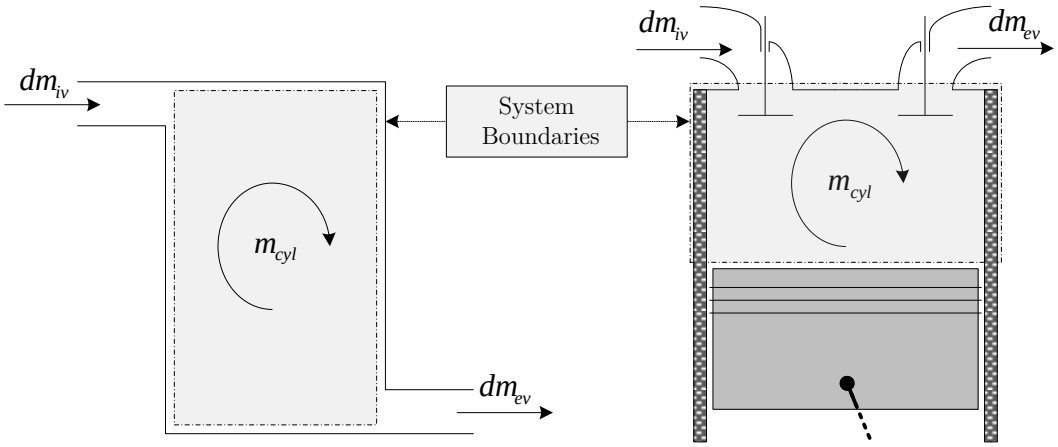

Figure 3.6: Cylinder mass balance, schematic representation.

In particular, the mass balance theorem states that for an open thermodynamic system in steady state conditions the incoming flow is equal to the flow leave the control volume [134]. In engine cylinder term this can be written as follows:

$$\sum_{cyl} dH_{cyl} = dH_{iv} - dH_{ev} \equiv dm_{iv}h_{iv} - dm_{ev}h_{ev} \tag{3.15}$$

Where, the subscripts iv and ev indicate the intake and and exhaust valves respectively, h is the specific enthalpy of the gas, and dm is the mass flow quantity that represents the gas exchange process. The mass flow through the intake and exhaust valves is described by the equation for compressible flow through a flow restriction [49], thus assuming isentropic flow the resulting expression is:

$$\frac{dm}{dt} = \frac{C_d A_o P_0}{\sqrt{RT_0}} \Psi \left(\frac{P_1}{P_0} \right) \tag{3.16}$$

And, C_d is the discharge coefficient that corresponds to the opening area (A_o) of the valve (Section 3.2.3 for geometrical analysis), R is the gas constant of the working medium, whilst P_0, T_0 and P_1 are the upstream pressure, temperature and downstream pressure conditions respectively. Finally, Ψ is a piecewise function that depends on the pressure ratio between the upstream (P_0) and down-

stream (P_1) pressure conditions (see Appendix B for the computation of γ, a typical value is 1.4):

$$\Psi\left(\frac{P_1}{P_0}\right) = \begin{cases} \left(\frac{P_1}{P_0}\right)^{\frac{1}{\gamma}} \sqrt{\frac{2\gamma}{\gamma-1}\left[1-\left(\frac{P_1}{P_0}\right)^{\frac{\gamma-1}{\gamma}}\right]} & : \frac{P_1}{P_0} < \left(\frac{2}{\gamma+1}\right)^{\frac{\gamma}{\gamma-1}} \\ \sqrt{\gamma}\left(\frac{2}{\gamma+1}\right)^{\frac{\gamma}{2(\gamma+1)}} & : \frac{P_1}{P_0} \geq \left(\frac{2}{\gamma+1}\right)^{\frac{\gamma}{\gamma-1}} \end{cases}$$

To sum up the analysis up to that point, Eq. 3.8 can now be re-written including all the assumption and derivation described above (Eq. 3.17).

$$dU_{cyl} = -dQ_w - P_{cyl}dV_{cyl} + dm_{iv}h_{iv} - dm_{ev}h_{ev} \tag{3.17}$$

At this instant it is possible to derive the expressions for computing the in-cylinder temperature and pressure. The cylinder temperature can be derived from the internal energy of the cylinder according to Eq. 3.18.

$$dU_{cyl} = m_{cyl}du_{cyl} + u_{cyl}dm_{cyl} \equiv m_{cyl}c_{v,cyl}dT_{cyl} + u_{cyl}dm_{cyl} \tag{3.18}$$

Where, subscript cyl dictates the cylinder control volume, u and du are the specific internal energy and the change of specific internal energy, m and dm are the mass and the change of mass, while $c_{v,cyl}$ is the specific heat at constant volume of the working medium inside the cylinder. Then, combining Eq. 3.17 and Eq. 3.18 results in the temperature change expression (Eq. 3.19).

$$\begin{aligned} dT_{cyl} = \frac{1}{m_{cyl}c_{v,cyl}} [&-dQ_w - P_{cyl}dV_{cyl} \\ &+ dm_{iv}(h_{iv} - u_{cyl}) - dm_{ev}(h_{ev} - u_{cyl})] \end{aligned} \tag{3.19}$$

In the same fashion the cylinder temperature over a specific time interval can be identified by differentiating Eq. 3.19 with respect to a predefined time interval (dt):

$$\begin{aligned} \frac{dT_{cyl}}{dt} = \frac{1}{m_{cyl}c_{v,cyl}} \Bigg[&-\frac{dQ_w}{dt} - P_{cyl}\frac{dV_{cyl}}{dt} \\ &+ \frac{dm_{iv}}{dt}(h_{iv} - u_{cyl}) - \frac{dm_{ev}}{dt}(h_{ev} - u_{cyl})\Bigg] \end{aligned} \tag{3.20}$$

As far as the cylinder pressure is concerned, under the assumption that all gases are treated as ideal gases, the equation of state is employed (Eq. 3.21).

$$P_{cyl} = \frac{m_{cyl} R_{cyl} T_{cyl}}{V_{cyl}} \tag{3.21}$$

3.2.2 Intake & Exhaust Systems

The mathematical model of the intake and exhaust manifold share the same physics principles with some minor differences related to the actual structure of each system. Each manifold is treated as a single volume with uniform pressure, temperature and working medium composition [135]. For both the intake and exhaust manifolds the pressure and temperature of the control volumes are derived from the First Law of Thermodynamics, as in the case of the cylinder control volume. The application of the energy and mass balance principles in the intake and exhaust systems of the discussed engine is illustrated in Fig. 3.7.

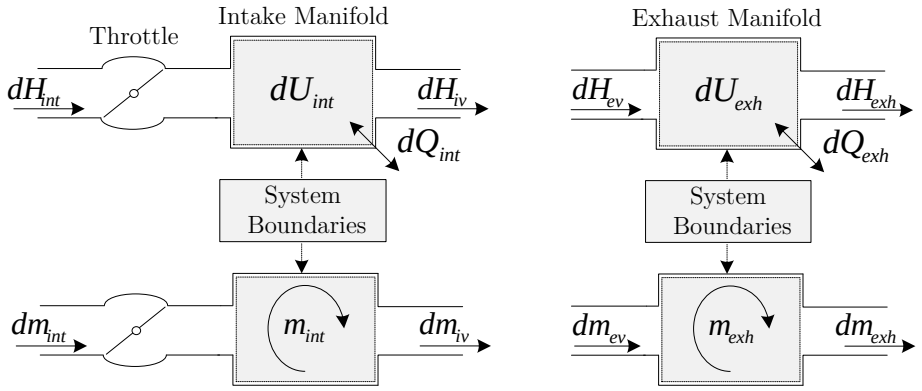

(a) Intake system **(b)** Exhaust system

Figure 3.7: Schematic representation from the application of the energy and mass balance in the intake and exhaust systems of the single cylinder engine.

The main assumptions that were considered in the manifold models are: the potential and kinetic energies due to the gas exchange processes are neglected, both manifolds are modelled as adiabatic control volumes [136, 137]. Now, the change in the internal energy of (dU) of the intake and exhaust manifolds is:

$$dU_{man} = \sum_{man} dH_{man} - dQ_{man} \tag{3.22}$$

Here, the subscript man represents both intake (int) and exhaust (exh) manifolds. Additionally, as it was mentioned earlier the term dQ_{man} is completely neglected as the manifolds are model as adiabatic open thermodynamic systems, this is a reasonable assumption for both intake and exhaust manifolds since in this research the engine was mainly operated under motoring conditions thus the heat transfer in the intake and exhaust systems was minimal [138].

As far as the enthalpy change of the manifold is concerned, the modelling philosophy is identical to the cylinder control volume. In particular for the intake manifold the sum of the enthalpy change can be derived form Fig. 3.7a (Eq. 3.23), while for the exhaust manifold form Fig. 3.7b (Eq. 3.24)

$$\sum_{int} dH = dH_{int} - dH_{iv} \equiv dm_{int}h_{int} - dm_{iv}h_{iv} \tag{3.23}$$

$$\sum_{exh} dH = dH_{ev} - dH_{exh} \equiv dm_{ev}h_{ev} - dm_{exh}h_{exh} \tag{3.24}$$

Nonetheless, one of the main differences between the intake and exhaust manifold models is located in the computation of the intake (dm_{int}) and exhaust (dm_{exh}) mass flows of the intake and exhaust manifolds respectively. To be more specific, for the calculation of the intake mass flow (dm_{int}), the throttle cross-section area (A_{th}) needs to be calculated in order to implement the compressible flow equation (Eq. 3.16) that was submitted earlier. On the other hand for the calculation of the exhaust mass flow (dm_{exh}), the orifice area (A_{exh}) of the exhaust manifold should be used instead. The calculation of these quantities is discussed in Section 3.2.3. Lastly it should be noted that besides the different geometrical characteristics of each manifold, particular importance should be given in the selection of the upstream and downstream conditions of each manifold. In the case of the intake manifold ambient conditions are taken as upstream and cylinder as downstream while in the case of the exhaust manifold cylinder conditions are taken as upstream and ambient conditions as downstream [52].

Bearing in mind the above points it is possible to write the temperature (T_{int}) (Eq. 3.25) and pressure (P_{int}) (Eq. 3.26) equations for the intake manifold:

$$\frac{dT_{int}}{dt} = \frac{1}{m_{int}c_{v,int}}\left[\frac{dm_{int}}{dt}(h_{int} - u_{int}) - \frac{dm_{iv}}{dt}(h_{iv} - u_{int})\right] \tag{3.25}$$

$$P_{int} = \frac{m_{int}R_{int}T_{int}}{V_{int}} \tag{3.26}$$

And the temperature (T_{exh}) (Eq. 3.27) and pressure (P_{exh}) (Eq. 3.28) equations for the exhaust manifold:

$$\frac{dT_{exh}}{dt} = \frac{1}{m_{exh}c_{v,exh}}\left[\frac{dm_{ev}}{dt}(h_{ev} - u_{exh}) - \frac{dm_{exh}}{dt}(h_{exh} - u_{exh})\right] \tag{3.27}$$

$$P_{exh} = \frac{m_{exh}R_{exh}T_{exh}}{V_{exh}} \tag{3.28}$$

Here the subscripts int and exh represent the intake and exhaust manifold accordingly while the rest of the notation is identical to the cylinder thermodynamic analysis (see Section 3.2.1).

3.2.3 Geometrical Analysis

Up until now the modelling discussion was limited mainly in the analysis of engine thermodynamics. However, by now the reader should have realized that the thermodynamic analysis depends on the calculation of numerous engine geometrical quantities. This section is dedicated in the geometrical analysis of all the quantities that were discussed in the previous sections such as cylinder volume, and its rate of change, cylinder wall surface area, the area of the intake and exhaust valves of the cylinder and the area of the throttle plate.

For understanding the location of the discussed physical dimensions and quantities, a schematic diagram of the cylinder and valve geometrical characteristics is given in Fig. 3.8. This sketch includes all the physical dimensions that are needed in order to develop the mathematical expressions for the cylinder volume, the cylinder wall surface area and the area of the valves. Therefore, the cylinder volume (V_{cyl}) is express according to Eq. 3.29 and its rate of change $\left(\frac{dV_{cyl}}{dt}\right)$ i.e. time derivative, using Eq. 3.30 [139].

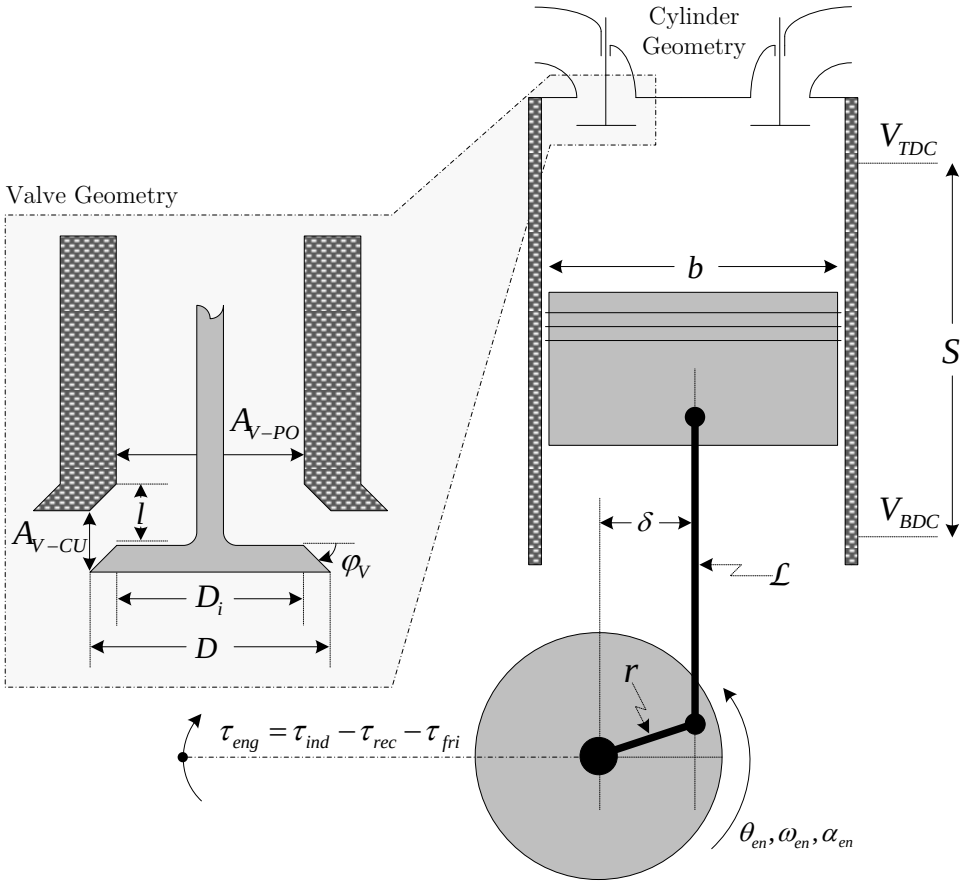

Figure 3.8: Cylinder geometrical quantities, schematic representation.

$$V_{cyl} = \frac{V_d}{\kappa - 1} + \frac{\pi b^2}{4}\left\{\sqrt{(r+\mathcal{L})^2 - \delta^2} - \left[\sqrt{\mathcal{L}^2 - (\delta + r\sin(\theta_{en} - \varphi))^2}\right] + r\cos(\theta_{en} - \varphi)\right\} \tag{3.29}$$

$$\frac{dV_{cyl}}{dt} = \omega_{en}\left\{\frac{\pi b^2}{4} r\left[\sin(\theta_{en} - \varphi) + \frac{\cos(\theta_{en} - \varphi)(\delta + r\sin(\theta_{en} - \varphi))}{\sqrt{\mathcal{L}^2 - (\delta + r\sin(\theta_{en} - \varphi))^2}}\right]\right\} \tag{3.30}$$

Where, κ, r, $\mathcal{L}$ and δ are the compression ratio, the crank arm length, the connecting rod length and the piston pin offset respectively while the variable φ is a geometric constant that can calculated according to Eq. 3.31.

$$\varphi = \sin^{-1}\left(\frac{\delta}{r + \mathcal{L}}\right) \tag{3.31}$$

Similarly, the area of the cylinder wall (A_w) with respect to crank angle (θ_{en}) can be calculated as follows:

$$A_w = \frac{\pi b^2}{2} + \pi b \left\{ \sqrt{(r+\mathcal{L})^2 - \delta^2} - \left[\sqrt{\mathcal{L}^2 - (\delta + r\sin(\theta_{en} - \varphi))^2} \right] + r\cos(\theta_{en} - \varphi) \right\} \tag{3.32}$$

Next, for the determination of the cylinder valve area, a piecewise function that depends on the lift level of the valves is used. More specifically, according to Pezouvanis [59] the valve area (A_V) is equivalent to the curtain valve area (A_{V-CU}), (Eq. 3.34) when the lift (l) is larger than a predefined lift threshold (l_V), (Eq. 3.33) while elsewhere the area is calculated using the port valve area expression (A_{V-PO}), (Eq. 3.35).

$$A_V = \begin{cases} A_{V-CU} & \text{if } l > l_V \\ A_{V-PO} & \text{if } l \leq l_V \end{cases}$$

And,

$$l_V = \frac{D}{4} \frac{\left(\frac{D_i}{D}\right)^2}{\cos(\phi_V)\frac{1+\frac{D_i}{D}}{2}} \tag{3.33}$$

$$A_{V-CU} = \frac{D + D_i}{2} \pi l \cos(\phi_V) \tag{3.34}$$

$$A_{V-PO} = \frac{\pi D_i^2}{4} \tag{3.35}$$

Where, D, D_i and ϕ_V are the valve head diameter, port diameter and seat angle accordingly.

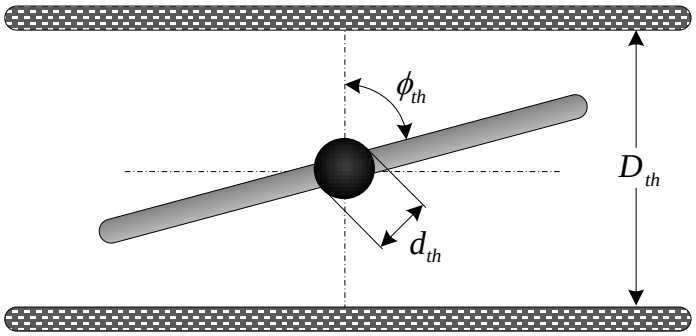

Figure 3.9: Throttle plate geometrical characteristics.

Finally, for the throttle plate area (A_{th}), (see Section 3.2.2), a well cited model that was presented initially by Moskwa [140] is used (Eq. 3.36).

$$
\begin{aligned}
A_{th} = & -\frac{d_{th}D_{th}}{2}\sqrt{1-\left(\frac{d_{th}}{D_{th}}\right)^2} \\
& + \frac{d_{th}D_{th}}{2}\sqrt{1-\left[\frac{d_{th}\cos(\phi_{th,0})}{D_{th}\cos(\phi_{th,0}+\phi_{th})}\right]} \\
& + \frac{{D_{th}}^2}{2}\sin^{-1}\left[\sqrt{1-\left(\frac{d_{th}}{D_{th}}\right)^2}\right] - \frac{{D_{th}}^2\cos(\phi_{th,0}+\phi_{th})}{2\phi_{th,0}} \\
& * \sin^{-1}\left\{\sqrt{1-\left[\frac{d_{th}\cos(\phi_{th,0})}{D_{th}\cos(\phi_{th,0}+\phi_{th})}\right]}\right\}
\end{aligned} \tag{3.36}
$$

Where, d_{th}, is the throttle shaft diameter, D_{th} is the throttle plate diameter, $\varphi_{th,0}$ is the minimum throttle opening angle, and φ_{th} the throttle angle (see Fig. 3.9 for visualising these dimensions).

3.2.4 Engine Torque

The last part in the analysis of the physics underlying the operation of the single cylinder engine is the resulting torque. This is the main output of the engine model as it is also one of the main inputs of the system model that was discussed earlier in Section 3.1. Consequently, the overall engine torque can be express using Eq. 3.37 [74, 75]. Here it can be understood that the engine torque (τ_{eng}) is proportional to the indicated torque (τ_{ind}) (Eq. 3.38), which is generated due to the cylinder gas pressure, minus the reciprocating torque (τ_{rec}) (Eq. 3.41), caused by the movement of the cylinder reciprocating components, and the friction torque (τ_{fri}) (Eq. 3.44), that is a result of the mechanical losses of the engine.

$$\tau_{eng} = \tau_{ind} - \tau_{rec} - \tau_{fri} \tag{3.37}$$

The indicated torque (τ_{ind}) is computed using Eq. 3.38. Here, P_{crn} is the pressure in the crank case, A_p is the piston area i.e $\frac{\pi b^2}{4}$, and G is a geometric function with respect to crank angle (Eq. 3.39).

$$\tau_{ind} = (P_{cyl} - P_{crn})A_p r G \tag{3.38}$$

$$G = \sin(\theta_{en}) + \sqrt{\frac{1-\psi}{\psi}}\cos(\theta_{en}) \tag{3.39}$$

Where, ψ is also a function of crank angle position and is calculate as follows:

$$\psi = 1 - \left(\frac{\delta + r\sin(\theta_{en} - \varphi)}{\mathcal{L}}\right)^2 \tag{3.40}$$

The mathematical expressions for modelling the contribution of the reciprocating torque to the final engine torque, perpendicular to the crank shaft is given bellow:

$$\tau_{rec} = M_{rec} r G \left(G_1 {\omega_{en}}^2 + G_2 \alpha_{en}\right) \tag{3.41}$$

Here, M_{rec} is the mass of the reciprocating components of the engine, α_{en} is the acceleration of the engine, whilst G_1 (Eq. 3.42) and G_2 (Eq. 3.43) are geometrical function of crank angle.

$$G_1 = r\left\{\cos(\theta_{en} - \varphi)\left[1 + \frac{\left(\frac{r}{\mathcal{L}}\right)\cos(\theta_{en} - \varphi)}{\psi^{\frac{3}{2}}}\right] - \sqrt{\frac{1-\psi}{\psi}}\sin(\theta_{en} - \varphi)\right\} \tag{3.42}$$

$$G_2 = r\left[\sin(\theta_{en} - \varphi) + \sqrt{\frac{1-\psi}{\psi}}\cos(\theta_{en} - \varphi)\right] \tag{3.43}$$

In contrast to the indicated and reciprocating torque models which were described on a crank angle basis, the friction torque was model using a mean value time-based model as it was suggested by Rakopoulos and Giakoumis [141]. As a result, the average engine friction is calculated based on Eq. 3.44,

$$\tau_{fri} = \frac{\text{fmep}}{2\pi} A_p r \tag{3.44}$$

Here, the fmep term is the friction mean effective pressure. This term was modelled based on a semi-physical model (Eq. 3.45) that was initially developed by Patton et al. [81] and recently updated by Sandoval and Heywood [82] for applications in modern spark ignition engines.

$$\text{fmep} = \text{cfmep} + \text{rfmep} + \text{vfmep} + \text{afmep} + \text{pmep} \tag{3.45}$$

Where, cfmep is the crankshaft fmep (Eq. 3.46), rfmep is the reciprocating fmep (Eq. 3.47), vfmep is the valvetrain fmep (Eq. 3.48), afmep is an auxiliary fmep (Eq. 3.49), and pmep is the fmep due to the pumping losses of the engine (Eq. 3.50).

$$\begin{aligned}\text{cfmep} = 1.22 * 10^{5} \left(\frac{D_b}{b^2 S n_c}\right) + 3.03 * 10^{-4} \sqrt{\frac{\mu}{\mu_0}} \left(\frac{N_{en} {D_b}^3 L_b n_b}{b^2 S n_c}\right) \\ + 1.35 * 10^{-10} \left(\frac{{D_b}^2 {N_{en}}^2 n_b}{n_c}\right)\end{aligned} \tag{3.46}$$

$$\begin{aligned}\text{rfmep} = 2.94 * 10^{2} \sqrt{\frac{\mu}{\mu_0}} \left(\frac{v_p}{b}\right) + 4.06 * 10^{4} \left(\frac{F_t}{F_{to}} C_r\right) \left(1 + \frac{500}{N_{en}}\right) \\ * \left(\frac{1}{b^2}\right) + 3.03 * 10^{-4} \sqrt{\frac{\mu}{\mu_0}} \left(\frac{N_{en} {D_b}^3 L_b n_b}{b^2 S n_c}\right) + 6.89 \\ * \frac{P_{int}}{P_{atm}} \left[0.088 \sqrt{\frac{\mu}{\mu_0}} \kappa + 0.182 \left(\frac{F_t}{F_{to}}\right) \kappa^{(1.33 - 0.112 v_p)}\right] + 4.12\end{aligned} \tag{3.47}$$

$$\begin{aligned}\text{vfmep} = 244 \sqrt{\frac{\mu}{\mu_0}} \frac{N_{en} n_b}{b^2 S n_c} + C_{ff} \left(1 + \frac{500}{N_{en}}\right) \frac{n_v}{S n_c} \\ + C_{rf} \left(\frac{N_{en} n_v}{S n_c}\right) + C_{oh} \sqrt{\frac{\mu}{\mu_0}} \frac{{L_v}^{1.5} {N_{en}}^{0.5} n_v}{b S n_c} \\ + C_{om} \left(1 + \frac{500}{N_{en}}\right) \frac{L_v n_v}{S n_c}\end{aligned} \tag{3.48}$$

$$\text{afmep} = 8.32 + 1.86 * 10^{-3} N_{en} + 7.45 * 10^{-7} {N_{en}}^2 \tag{3.49}$$

$$\begin{aligned}\text{pfmep} = (P_{atm} - P_{int}) + 3.0 * 10^{-3} \left(\frac{P_{int}}{P_{atm}}\right)^2 \left(\frac{{v_p}^2}{{n_v}^2 {\rho_i}^4}\right) \\ + 0.178 \left(\frac{P_{int}}{P_{atm}} v_p\right)^2 + 3.0 * 10^{-3} \left(\frac{P_{int}}{P_{atm}}\right)^2 \left(\frac{{v_p}^2}{{n_v}^2 {\rho_e}^4}\right)\end{aligned} \tag{3.50}$$

Where, P_{atm} is the atmospheric air pressure, D_b, L_b and n_b are the diameter, length and number of crankshaft bearings respectively, n_c is the number of cylinders, N_{en} and v_p are the engine speed and mean piston speed, κ, ρ_i, ρ_e, and n_v are the compression ratio, the intake and exhaust valves diameter bore ratio, and the number of valves correspondingly, additionally the term $\sqrt{\frac{\mu}{\mu_0}}$ is the oil viscosity scaling factor, $\frac{F_t}{F_{to}}$ is the piston ring tension ratio, and finally the constants C_r, C_{rf}, C_{oh} and C_{om} are constants based on the valvetrain mechanism and can be found in [82].

3.3 Transient Dynamometer Model

The analysis of the overall transient engine test cell model closes with the description of the transient dynamometer model. In this work the dynamometer was actually a four quadrant AC electric drive consisted of a three phase squirrel cage type induction machine and its controller. The technical specification of the actual dynamometer can be found in Chapter 4. Similar to the IC engine model, the main output of the dynamometer model is the electromagnetic torque (τ_{dy}) that is also one of the inputs of the overall engine test cell model (see Eq. 3.6). Additionally the major inputs to the dynamometer model are the rotational kinematic quantities of the dynamometer i.e. acceleration (α_{dy}), velocity (ω_{dy}), and position (θ_{dy}). Besides the above mentioned inputs, the dynamometer has one extra control input which is the speed demand; this reflects the functionality of the real transient engine test cell in which the test cell operator has control of the system speed (see Chapter 4).

The dynamometer model was developed with the purpose of reflecting the physics and the functionality of the actual transient engine powertrain testing facility that was used in this work. Having a complete physics-based dynamic model of the overall test cell contributed in understanding the mathematical and physical structure of the overall engine powertrain system which is a necessary requirement when the physical parameters of the system model are subject to be assessed; and this was the aim in this study. As far as the modelling methodology of the transient dynamometer is concerned, it is divided into two main parts, the model of the three phase squirrel cage type induction machine and the model of its controller. The model of the induction machine is a zero-dimensional physics-based lumped parameter dynamic model that was developed based on a well defined electric machinery modelling approach known as direct-quadrature (dq) analysis [142]. According to this methodology the principal governing equations of the model are extracted from the dq-axis equivalent circuit induction machine by applying Kirchhoff's Voltage Law (KVL) in the loops of the circuit. Concurrently

the controller of the induction motor was responsible for controlling the speed of the three phase induction motor. In this very application the speed of the dynamometer was controller based on vector control strategy. The reason for using this control strategy instead of a scalar control scheme (which is the another dominant motor control strategy) [143], was because the actual controller of the dynamometer was using also the same control principle (see technical specification of the transient dynamometer in Chapter 4).

Before presenting the theoretical analysis of the AC transient dynamometer model it is important to clarify the main assumptions that were taken into account for the development of this model. Firstly time is taken as the independent variable of the model, secondly the three phase quantities i.e. voltages, currents, fluxes, are always balanced, thirdly the variation of the induction motor parameters during steady state and transient conditions is neglected, and finally the dynamometer is either acting as a motor or as a brake while regenerative braking characteristics are not included.

3.3.1 Dynamic Model of Induction Motor

The dynamic modelling of induction motors has received great attention from engineers and researchers over the past decades, hence a wide variety of modelling approaches has been established throughout the years. Nevertheless, when someone is interested in the dynamic characteristics of the induction motor two common approaches are usually employed, known as "space vector" and "dq-axis" methods [144, 145]. The space vector model is more complicated compared to dq-axis model mainly because of complex mathematical expressions (vectors). Traditionally space vector analysis is based on the "per-phase" equivalent circuit of the machine. The application of KVL in the loops of the equivalent circuit allows the extraction of the static equation of the electric machine. The differentiation of the extracted equations with respect to time forms a set of differential equation which permits the simulation the AC electric machine to examine the dynamic but also the steady state characteristics of the machine [146]. On the other hand, the

dq-axis approach results in a more compact and simpler mathematical formulation that allows the deployment of more effiecient control strategies i.e. vector control (see Section 3.3.2). This is achieved due to the transformation of the three phase quantities (a, b, c) into equivalent two axis i.e. dq-axes as it was presented initially by Park [147, 148], (Eq. 3.51).

$$\begin{bmatrix} x_d \\ x_q \end{bmatrix} = \sqrt{\frac{2}{3}} \begin{bmatrix} \cos(\theta) & \cos\left(\theta - \frac{2\pi}{3}\right) & \cos\left(\theta - \frac{4\pi}{3}\right) \\ -\sin(\theta) & -\sin\left(\theta - \frac{2\pi}{3}\right) & -\sin\left(\theta - \frac{4\pi}{3}\right) \end{bmatrix} \begin{bmatrix} x_a \\ x_b \\ x_c \end{bmatrix} \tag{3.51}$$

Additionally, the inverse of this transformation can be achieved using Eq. 3.52.

$$\begin{bmatrix} x_a \\ x_b \\ x_c \end{bmatrix} = \sqrt{\frac{2}{3}} \begin{bmatrix} \cos(\theta) & -\sin(\theta) \\ \cos\left(\theta + \frac{4\pi}{3}\right) & -\sin\left(\theta + \frac{4\pi}{3}\right) \\ \cos\left(\theta + \frac{2\pi}{3}\right) & -\sin\left(\theta + \frac{2\pi}{3}\right) \end{bmatrix} \begin{bmatrix} x_d \\ x_q \end{bmatrix} \tag{3.52}$$

Here, x represents either voltage, current or flux linkage quantities and θ can be either the position between a_s-axis and d-axis (for stator quantities θ_{syn}) or a_r-axis and d-axis (for rotor quantities θ_{slp}) (Fig. 3.10).

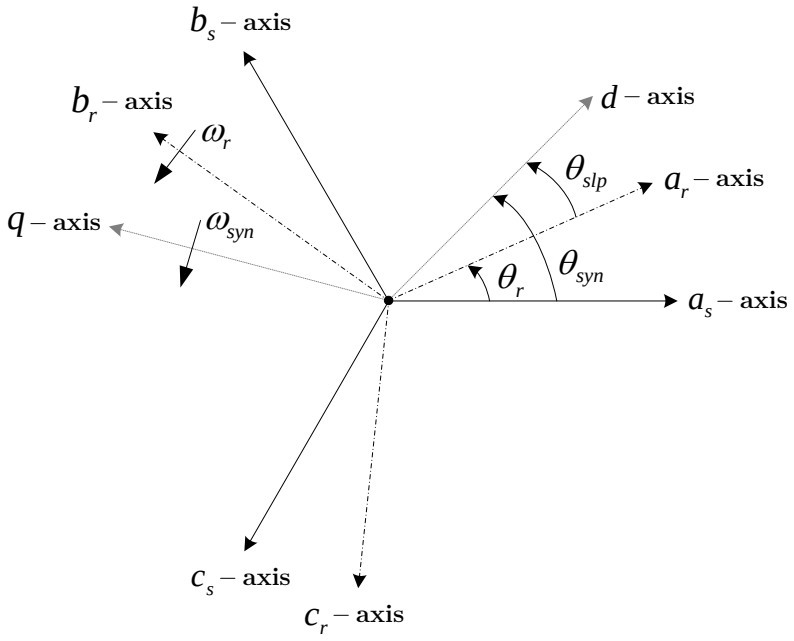

Figure 3.10: Stator (abc_s) and rotor (abc_r) representation by dq-axes.

The three phase stator quantities (abc_s) are in stationary reference frame which does not rotate in space, while the dq quantities are in the synchronous

reference frame (syn) and rotate in space at synchronous speed (ω_{syn}). The synchronous speed is defined as the speed of stator's magnetic field and can be calculated using the following expression [149]:

$$\omega_{syn} = \frac{4\pi}{p} f \tag{3.53}$$

Where, p is the number of motor poles, and f is the frequency of the magnetic field i.e. the frequency of the alternating current.

Regarding the rotor quantities (abc_r) of the motor, they rotate in space at the electrical speed of the rotor which is related with the mechanical speed (ω_m) based on Eq. 3.54 [149].

$$\omega_r = \frac{\pi}{2} \omega_m \tag{3.54}$$

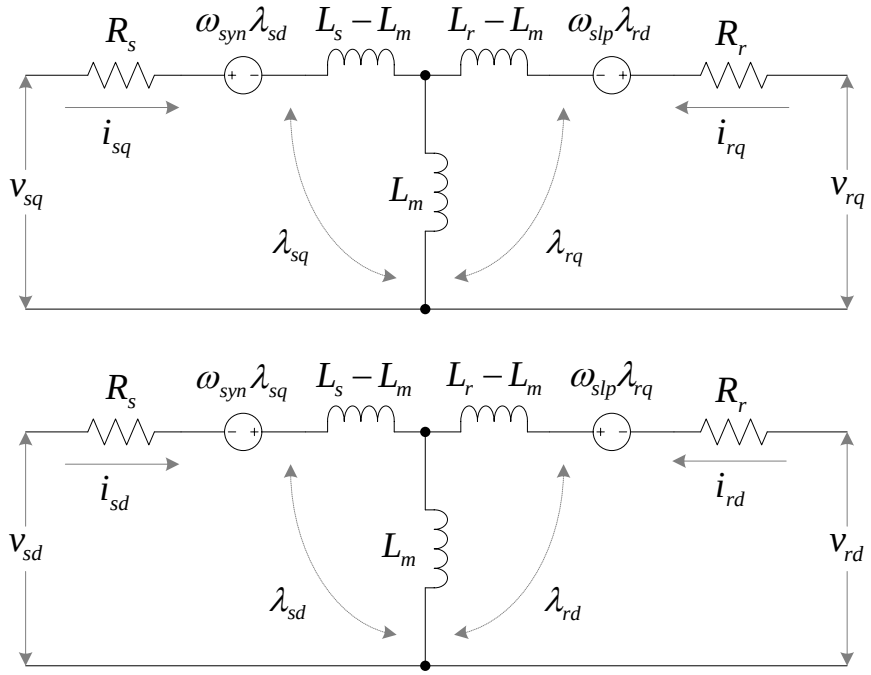

Figure 3.11: Induction machine dq-axis equivalent circuit in synchronous reference frame.

As aforementioned the dq-axis transformation serve us with a dq-axis equivalent circuit (Fig. 3.11) that can be used in order to extract the governing equations of the induction motor model. In particular the application of KVL in the loop of

the direct and quadrature equivalent circuits results in a set of linear differential equations that capture the dynamic as well as the steady state characteristics of the induction machine (Eq. 3.55) [150].

$$\frac{d}{dt}\begin{bmatrix}\lambda_{sd}\\ \lambda_{sq}\\ \lambda_{rd}\\ \lambda_{rq}\end{bmatrix} = \begin{bmatrix}v_{sd}\\ v_{sq}\\ v_{rd}\\ v_{rq}\end{bmatrix} - \begin{bmatrix}i_{sd}R_s\\ i_{sq}R_s\\ i_{rd}R_r\\ i_{rq}R_r\end{bmatrix} + \begin{bmatrix}\omega_{syn}\lambda_{sd}\\ -\omega_{syn}\lambda_{sq}\\ \omega_{slp}\lambda_{rd}\\ -\omega_{slp}\lambda_{rq}\end{bmatrix} \tag{3.55}$$

Where, λ_{sdq} and λ_{rdq} are the stator and rotor flux linkages in dq-axis respectively, v_{sdq} are the stator voltages in dq-axis, v_{rdq} are the rotor voltages in dq-axis and they are assumed to be zero because the type of the rotor is squirrel cage, R_s and R_r are the stator and rotor winding resistances, ω_{syn} and ω_{slp} are the synchronous and slip angular velocities, and the terms i_{sdq} and i_{rdq} are the stator and rotor currents in dq-axis and they are evaluated using to following expression:

$$\begin{bmatrix}i_{sd}\\ i_{sq}\\ i_{rd}\\ i_{rq}\end{bmatrix} = \begin{bmatrix}L_s & 0 & L_m & 0\\ 0 & L_s & 0 & L_m\\ L_m & 0 & L_r & 0\\ 0 & L_m & 0 & L_r\end{bmatrix}^{-1}\begin{bmatrix}\lambda_{sd}\\ \lambda_{sq}\\ \lambda_{rd}\\ \lambda_{rq}\end{bmatrix} \tag{3.56}$$

The parameters L_s, L_m and L_r are the stator, mutual, and rotor inductances respectively.

Last part of the dynamic model of the induction machine is the expression for the calculation of the electromagnetic torque which is assumed to be identical with the mechanical torque output of the dynamometer (τ_{dy}). As a result, knowning the dq-axis currents and flux linkage allows the evaluation of the dynamometer torque according to Eq. 3.57.

$$\tau_{dy} = \frac{p}{2}\left(\lambda_{rq}i_{rd} - \lambda_{rd}i_{rq}\right) \tag{3.57}$$

3.3.2 Induction Motor Vector Control Strategy

After the development of the electric machine model it is now possible to concentrate in the modelling of its controller. Main task of the controller is to constantly adjust the electrical supply to the electric machine in accordance to the demands of the user. In general electric drives are used to control either the torque or speed or position of a process. Particularly in engine testing applications usually speed and torque are the two control variables that interest the operator of the test cell. In all the experiments of this project the dynamometer was responsible for controlling the speed of the engine, hence the controller of the dynamometer was set to speed control mode instead of torque.

The control of AC electric machines is a subject that has received great attention from the research community with the purpose of improving the operation and the efficiency of electric machines. Several control methodologies have been proposed throughout the years, however after the invention of the voltage and current fed inverters the so called "scalar" and "vector" strategies dominate the control of electric motor [151].

Scalar control methodology involves controlling only the magnitude and the frequency of the control variables. Two sub-categories can be found in scalar control method, the open and closed loop control. In the open loop control the speed of the motor is mainly controlled by adjusting the frequency of the supplied voltages but also the amplitude of these voltages should vary in accordance to frequency to maintain the flux constant [152]; this method is also called "constant Volt/Hertz method" and is fairly simple to be applied, however the simplicity of the method penalise the control of the motor during transient operation. On the other hand, in closed loop control a speed feedback is included in the Volt/Hertz method which improves the dynamic response of the drive [153]; this method is also known as "Slip Regulation" method and is an upgrade of the open loop control, however the main drawback of this method is that the motor flux is controlled still using open loop scheme [151].

The drawbacks of scalar control approach were solved using vector control

strategies, in vector control the induction motor is controlled just like a separately excited DC motor where the torque and the flux are controlled by two independent vectors. This is achieved by transforming the three phase stator quantities into equivalent dq quantities where the d-axis is responsible for controlling the flux linkage and the q-axis the electromagnetic torque of the motor; in principle this method involves controlling the magnitude and the phase of the vector quantities. Vector control compared to scalar control allows more sophisticated control during steady and transient operation since both torque (or speed or position) and flux linkage quantities are controlled based closed loop tradition [154].

In this very application the dynamometer speed is controlled using vector control approach (see Chapter 4 for technical features of the dynamometer controller). As a result in the next paragraphs follows the analysis of the vector control strategy that will be used for controlling the speed of the dynamometer. At this point it should be clarified that the level of the presented analysis is elementary for an expert in vector control of electric machine, nevertheless the controller that is presented serves the functionality that is required for controlling the speed of the transient dynamometer. Additionally, considering that the average reader of this thesis will have a generic knowledge of control theory, instead of expertise in of control of electric machines, the discussion is kept as simple as possible and as complex as necessary. In any case, for individuals that are interested in learning more about the vector control strategy, a informative literature review can be found in [143].

Under vector control induction motor drives can emulate the performance of a DC motor; DC motors are controlled more precisely because of the decoupled control of stator magnetic field and the electromagnetic torque of the motor [155]. The decoupling of these two quantities is achieved by aligning (field orientation) the d-axis of the synchronous reference frame (see Fig. 3.10 for further discussion) with the rotor flux linkage vector $(\vec{\lambda}_r)$. This is depicted in Fig. 3.12.

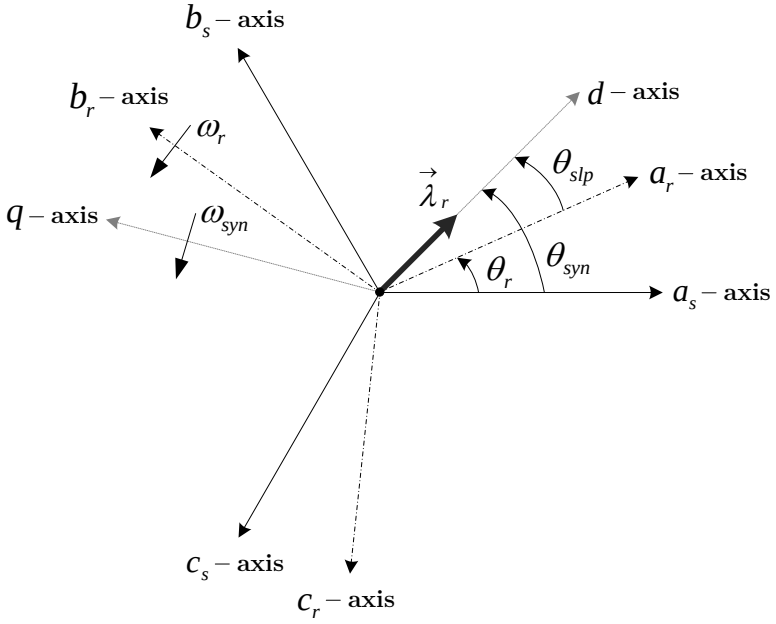

Figure 3.12: Rotor flux linkage field orientation.

The resulting flux linkage components are [150]:

$$\lambda_{rq} = 0 \text{ and } \lambda_{rd} = \lambda_r \tag{3.58}$$

$\therefore$

$$\tau_{dy} = -\frac{p}{2}\lambda_{rd} i_{rq} \tag{3.59}$$

As it can be understood based on this theory the expression for the calculation of the dynamometer torque τ_{dy} is reduced since the rotor flux linkage in q-axis turns to zero. Additionally in Eq. 3.59 the rotor current in q-axis (i_{rq}) can be related to the stator current (i_{sq}) by applying Kirchoff's Current Law (KCL) in the equivalent circuit of the induction machine (Fig 3.11) (Eq. 3.60).

$$i_{rq} = -\frac{L_m}{L_r} i_{sq} \tag{3.60}$$

$\therefore$

$$\tau_{dy} = \frac{p}{2}\lambda_{rd}\frac{L_m}{L_r} i_{sq} \tag{3.61}$$

Where the flux linkage component λ_{rd} is calculated dynamically by using the the following equation (see Eq. 3.55):

$$\frac{d}{dt}\lambda_{rd} = \frac{L_m}{\left(\frac{L_r}{R_r}\right)} i_{rd} - \frac{\lambda_{rd}}{\left(\frac{L_r}{R_r}\right)} \tag{3.62}$$

Given these points, it can be said that the dynamometer torque (Eq. 3.61) and the flux linkage (Eq. 3.62) are controlled independently via the stator current (i_{sq}) in q-axis and the rotor current (i_{sd}) in d-axis respectively. This principle is the basis of the vector control strategy that was implemented in this study.

The vector-based approach namely Indirect Field Oriented Control (IFOC) presented by Mohan [150] was adapted and used (Fig. 3.13). The core of the IFOC scheme is two control loops, one for the control of the flux linkage (Flux Controller) and the other for the control of the speed of the motor (Speed Controller). Here, the flux linkage is controlled using a PI controller where the error of the demanded and actual flux linkage (calculated via Eq. 3.62) is amplified in order to produce the stator current in d-axis (i_{sd}) which is proportional to rotor flux linkage (Eq. 3.62).

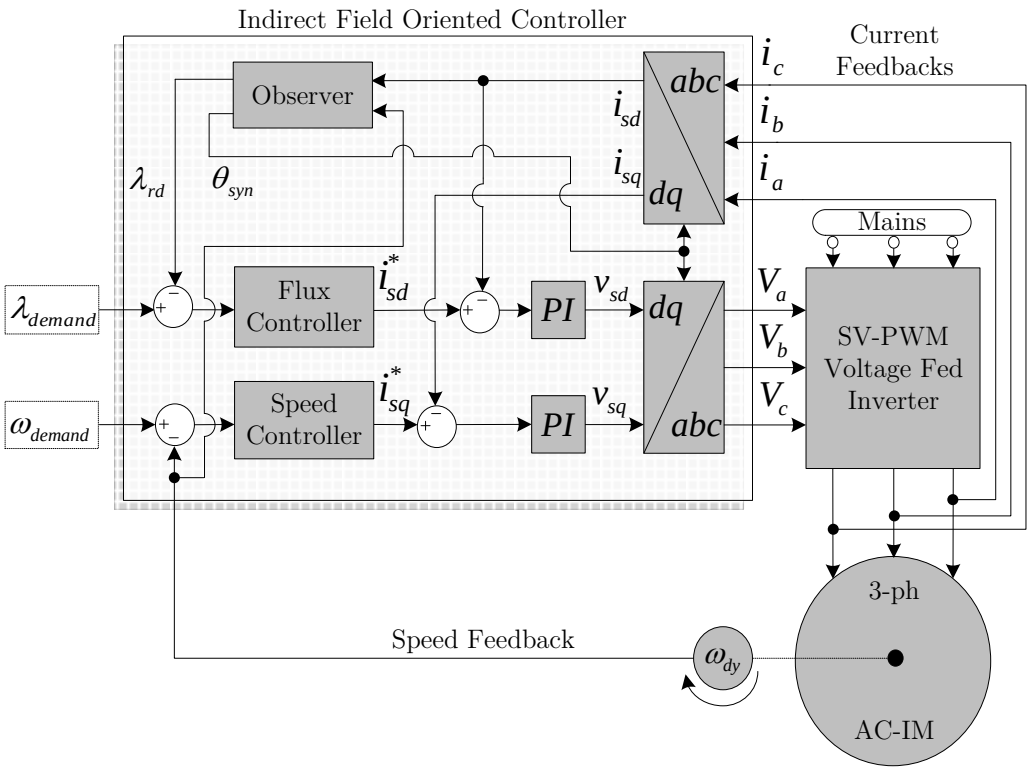

Figure 3.13: Vector control strategy of the induction machine.

The dynamometer torque is controlled indirectly via the speed control loop where the error between the demanded and the actual speed (measured with an encoder) passes through a PI controller and the output of the PI controller is

the stator current in q-axis (i_{sq}) which is proportional to the dynamometer torque (Eq. 3.61). The block named "Observer" evaluates dynamically the actual rotor flux linkage using Eq. 3.62 but also the rotor-field angle θ_{syn} which is aligned in synchronous reference frame and is calculated as follows:

$$\theta_{syn} = \int (\omega_r + \omega_{slp})\, dt \tag{3.63}$$

Where, ω_r is the electrical angular velocity of the rotor (see Eq. 3.54), and ω_{slp} is the slip angular velocity and is evaluated continuously using Eq. 3.64.

$$\omega_{slp} = \frac{L_m}{\left(\frac{L_r}{R_r}\right)\lambda_{rd}} i_{sq} \tag{3.64}$$

Moreover as it is shown in Fig. 3.13, two additional PI controllers are included for adjusting the supply voltage to stator windings in dq-axis. Next, takes place the transformation of the dq quantities into the equivalent three phase quantities abc (Eq. 3.52). The three phase voltages i.e. V_a, V_b, V_c, are then used by the voltage fed inverter in order to amplify the power supply to the actual motor. It should be highlighted that the switching sequence of the voltage fed inverter is adapted using space vector pulse width modulation method, which according to Mohan [150], is assumed to be ideal in order to simplify the overall electric drive model and improve the simulation time. This assumption do not allows examining inverterâĂŹs characteristics however, since in the present work there is no interest on this particular area, further work is avoided. In addition the electric drive model without an actual inverter model severs all the logical trends of a transient dynamometer with respect to the dynamics of the system. For an individual that interest in the characteristics of the inverter it is possible to restate the present assumption and include a proper inverter model easily as the electric drive model was developed in a modular and reconfigurable basis.

3.4 Model Functionality & Preliminary Results

The appropriate use of the preceding theoretical principles led to the realisation of the transient engine powertrain test cell dynamic model. The different parts of the overall system model were formulated by continuous-time continuous-state sets of dynamic equations. The model was developed from scratch in MATLAB-Simulink[1] in a modular way so that it would be user friendly and easily reconfigurable. The actual Simulink model and the corresponding MATLAB scripts are given in Appendix B.1.

The global inputs of the model are the dynamometer speed demand and the engine throttle position. These are also the global inputs of the actual transient engine powertrain experimental facility that was used for validating and proving the concepts of the present research (see Chapter 4). Other model inputs are associated with the ambient conditions of the test cell and internal inputs of the engine and dynamometer models (which are maintained constant in this study) such as valve timing and commanded motor flux. Similarly the outputs of the model can be directly related to the actual experimental facility, some the outputs are the cylinder, intake and exhaust pressures, dynamometer currents and voltages, engine and dynamometer torques, engine and dynamometer speeds, etc. Nevertheless, the model outputs can be customised accordingly depending on the needs of the modeller.

As the model was developed purely based on physics principles, this indicates that no experimental data were required for a first draft parametrisation of the model. The initial parametrisation and initialisation of the model states (e.g. pressures, temperatures, masses, flux linkages, speeds, etc.) took place by using physical dimension that were extracted from manufacturers data sheets or based on direct measurements; the actual physical parameters (e.g. diameter, length, mass, stiffness, resistance, inductance, etc.) that were need of the

[1] MATLAB Version: 8.2.0.701 (R2013b).

parametrisation of the model can be found in Chapter 4. As far as the validity of the model is concerned, the right physical trends were observed using the first draft parametrised model, however the absolute accuracy of the model was still far from true, these issues are further argued in the following chapters.

As for the computational performance, the multiphysics zero dimensional transient engine powertrain test cell model consists of 830 functional blocks and can run approximately up to $3 \times$ Real-Time in Rapid Acceleration[2] mode in Simulink using a fixed-step solver namely "ode1" (makes use of the Forward Euler approximation to integrate the state derivatives) with a time step equivalent to 1 crank angle degree at 1000 RPM. The real-time capability of the model indicates its potential to be used for control and monitoring applications.

In general the transient engine test cell model encapsulates transient, steady state, cyclic and mean value effects related to the operation of each individual sub-system i.e. engine, dynamometer and coupling shaft. Some representative simulation results are provided here with the purpose of illustrating the functionality of the model. The response of the results corresponds to the characteristics of the global inputs of the model that were predifined by the modeller (Fig. 3.14).

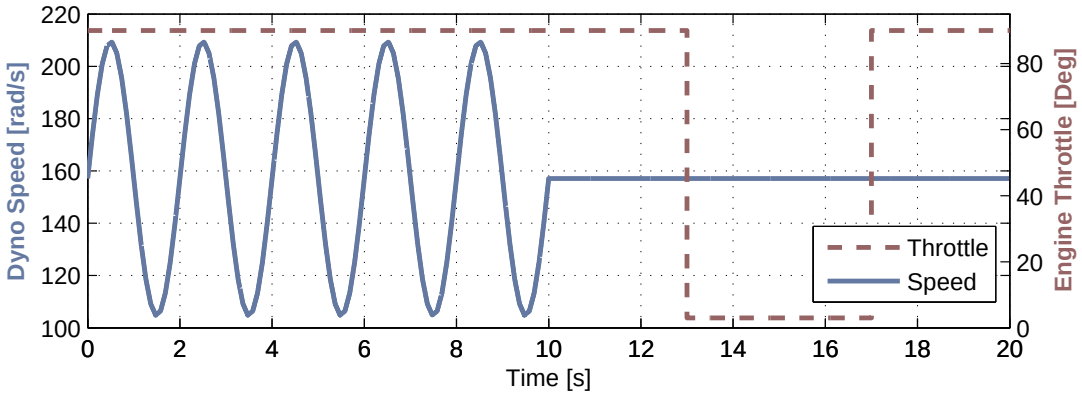

Figure 3.14: Sample settings of the model global inputs.

[2]In Rapid Accelerator mode, Simulink compiles a standalone executable for the model, which can run on a separate processing core. This executable includes the solver and model methods, but it resides outside of MATLAB and Simulink. It can only be used with those models for which C code is available for all of the blocks in the model. For more info visit: `http://mathworks.com/`.

As it can be seen from the Fig. 3.14 the speed of the dynamometer has a sinusoidal pattern for the first ten seconds and then remains constant until the end of the simulation. Concurrently, the engine throttle position has a constant value for the first thirteen seconds the simulation while then it follows a tip in and tip out manoeuvre with an overall duration of five seconds.

Some representative model responses relative to the sample settings of the model control inputs on Fig. 3.14 are presented in Fig. 3.15. For the purpose of visualising the transient as well as the cyclic responses of the system, time series representation was selected. It useful to note that theses responses are also measured in the real transient engine test cell (see Chapted 4) hence can be used for examining the validity of the model. Specifically, Fig. 3.15a shows the speed response of the engine and dynamometer, it can be seen that both the engine and the dynamometer responses follow the dynamometer speed, while the fluctuation that it observed in the zoom in version of plot is a cyclic effect that is a results of the cyclic characteristics of the reciprocating single cylinder engine. These cyclic characteristics are also present in the engine torque in Fig. 3.15b, additionally by looking at the same figure the transient characterstics of the dynamometer i.e. torque is increased and decreased inversely proportional to the speed to cope with the demanded dynamometer speed. The electical characteristics of the induction motor of the dynamometer can also be observer in Fig. 3.15c, this figure shows the three phases of the alternating current of the dynamometer. The in cylinder pressure of the engine is presented in Fig. 3.15d, the effects of the engine speed variations and throttle tip in and tip out manoeuvres are clearly visible, particularly in the zoom in section of the graph it is possible to observer the cyclic transient performance of the cylinder pressure which is caused due to the closing of the intake throttle valve. Similar effects are obtained in the intake manifold pressure (Fig. 3.15e). The intake and exhaust cylinder flows are depicted in Fig. 3.15f, here someone can observe the cylinder mass balance principles; positive values indicate cylinder inflow whilst negative values implies cylinder outflow.

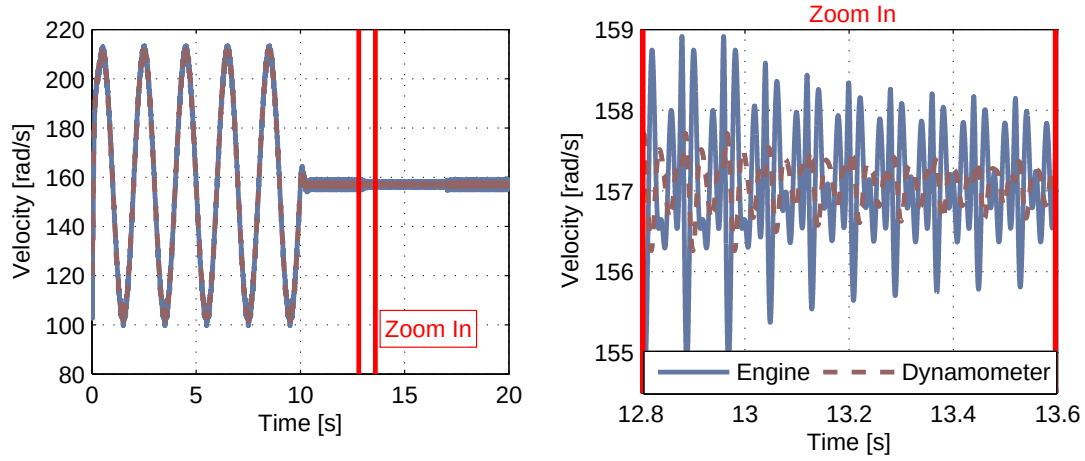

(a) Engine and dynamometer angular velocity

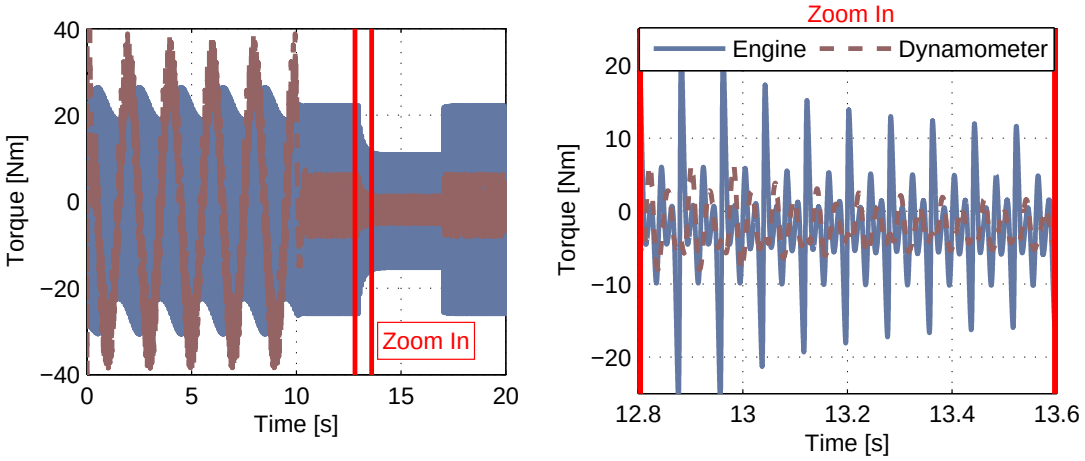

(b) Engine and dynamometer torque

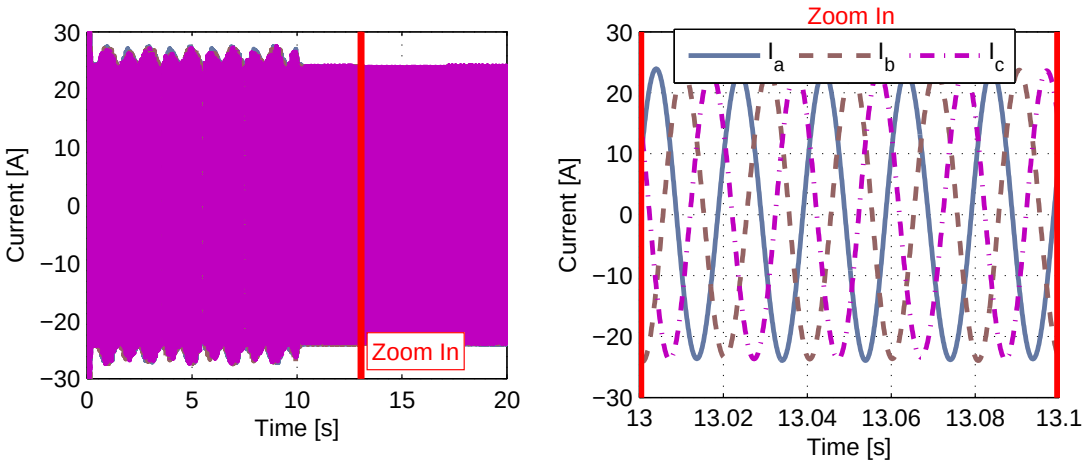

(c) Dynamometer alternating current

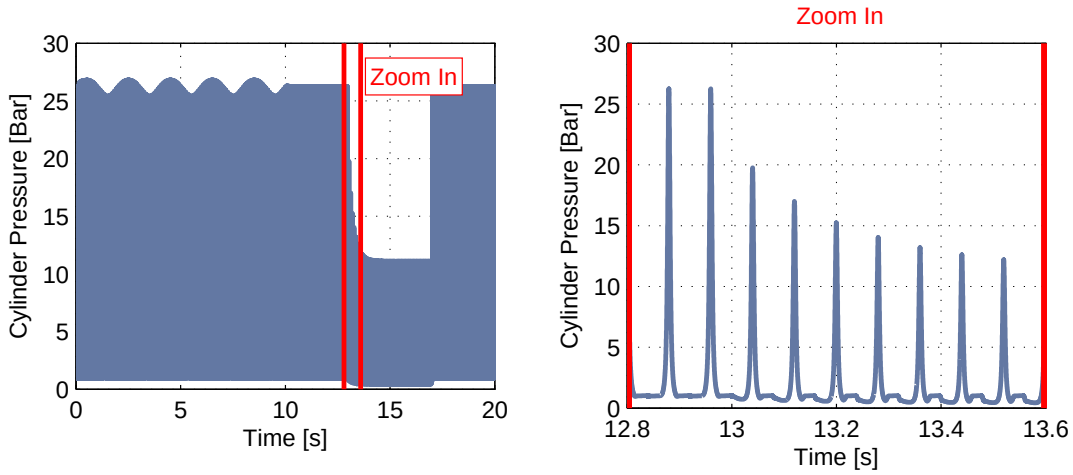

(d) Engine in cylinder pressure

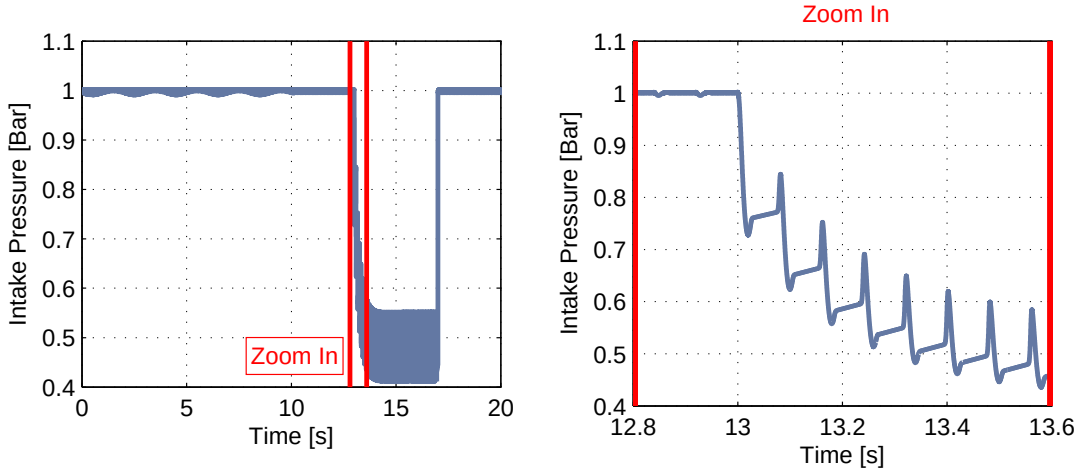

(e) Engine intake pressure

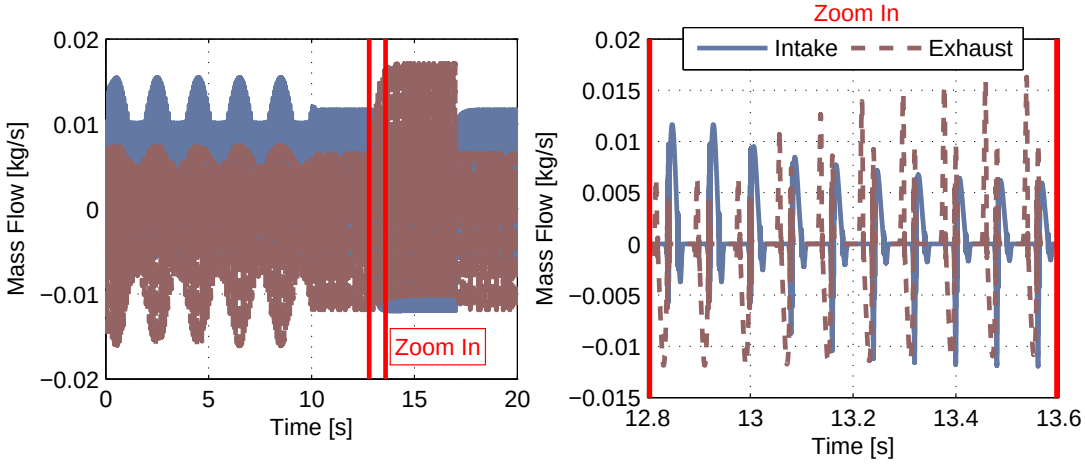

(f) Intake and exhaust flow through the engine cylinder

Figure 3.15: Model responses for the control inputs in Fig. 3.14.

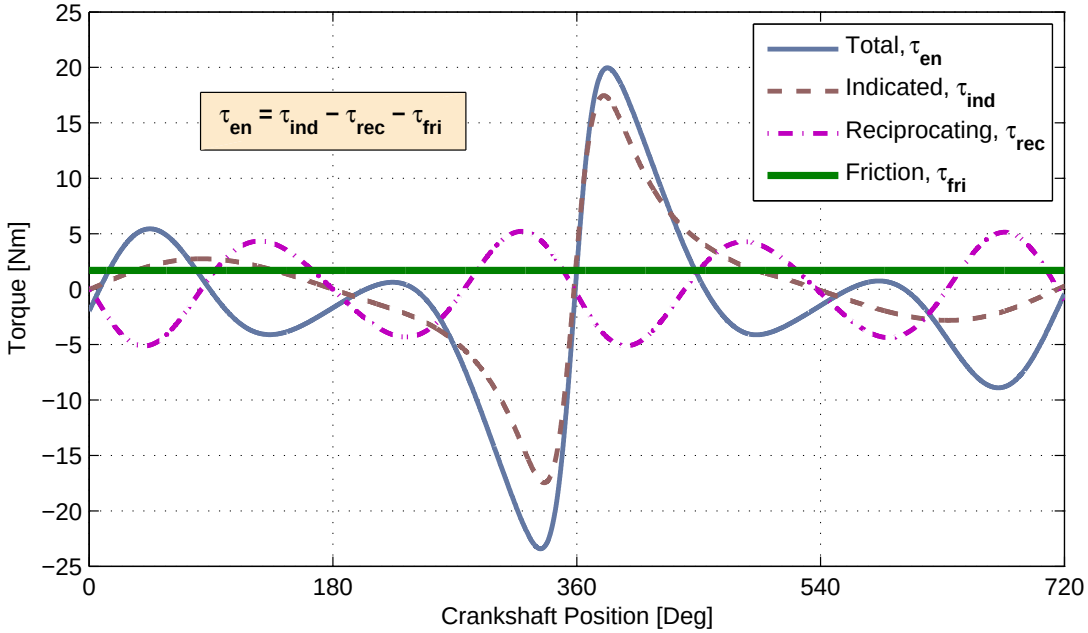

Figure 3.16: Instantaneous cyclic engine torque components, at 1000 RPM and WOT.

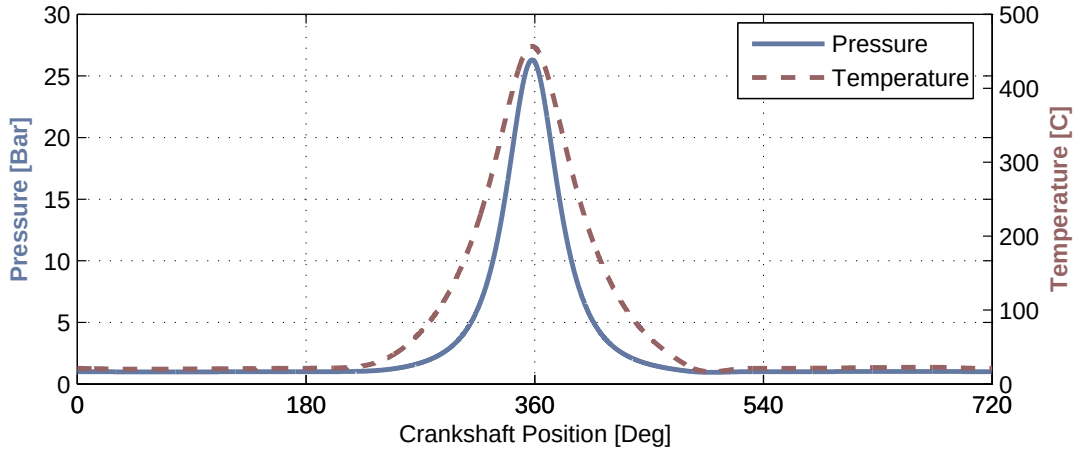

Figure 3.17: In cylinder pressure and temperature, at 1000 RPM and WOT.

The model can be used for observing the response of non-measurable physical quantities such as the engine torque components (Fig. 3.16) i.e. indicated, reciprocating and friction, or the in cylinder temperature versus the crank angle (Fig. 3.17). Another possibility would be to relate engine's geometrical and timing characteristics to engine responses such valve lift and mass flow through the intake and exhaust valves (Fig. 3.18).

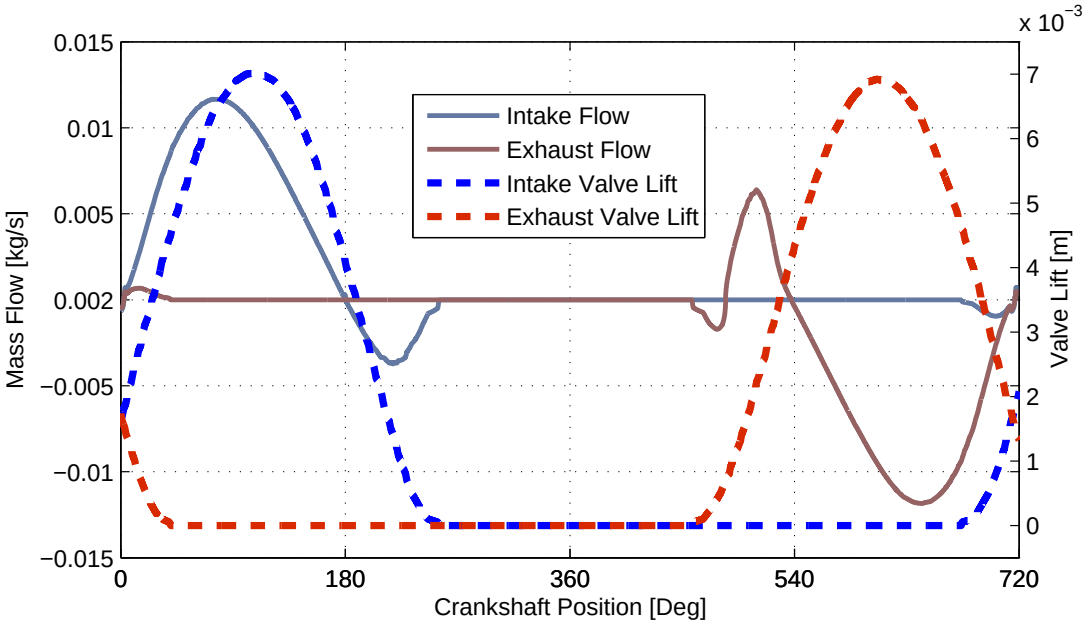

Figure 3.18: Intake and exhaust valve mass flow and lift, 1000 RPM – WOT.

3.5 Synopsis

A summary of the key points of this chapter is given below.

- The theoretical principles of a multi-domain physics-based dynamic model of a complete transient engine testing facility (see Chapter 4 for technical details) were presented. The model was developed based on a two-inertia system analysis consisting of the engine, the dynamometer and the coupling shaft.
- The single cylinder internal combustion engine was modelled based on First Law of Thermodynamics and Second Newton's Law for rotational bodies.
- The transient dynamometer was actually an AC electric drive consisting of an induction machine and a controller. The induction machine was modelled based on direct-quadrature approach and the controller was developed based on indirect field orientation scheme.
- The engine and dynamometer were coupled with a coupling shaft which was modelled as a compliant member with damping.

- The overall model consists of 830 Simulink blocks and can run up to 3 times Real-Time in rapid acceleration mode with a crank angle step of one degree at 1000 RPM. Refer to Appendix B for MATLAB codes and top-level Simulink block diagrams.
- The functionality of the model was illustrated with relative simulation results.

Chapter 4

Experimental Apparatus

The chapter covers the development process, the technical features and the functionality of a unique transient cyclic motoring engine testing facility. The experimental apparatus is an equivalent representation of the multi-domain test cell dynamic model that was derived in Chapter 3.

4.1 Test Rig Overview

The continuous research and development of vehicle powertrain systems requires continuously the development of highly sophisticated powertrain testing facilities. Nowadays, a conventional engine test cell consists of four individual sub-systems known as engine, dynamometer, coupling shaft and control system. However, significant differences can be found from test cell to test cell due to the multidisciplinary nature of modern powertrain research and development. For instance, depending on the very objective of the research e.g. emissions reduction, durability test, lubricants and fuels etc., different control and instrumentation systems might be required in order to obtain the desirable results. As a consequence of this increased demands and diversity that characterise the research of modern engine powertrains it is often rather challenging to find a readily available equipment that allows the engineers to acquire measurements from the relevant physical quantities. Under these circumstances it is common for the research en-

gineers to develop the appropriate testing equipment in order to acquire accurate and qualitative measurement data.

Similar challenges had to be overcome in this thesis for measuring properly the required physical quantities. Therefore, a novel open architect transient cyclic motoring engine testing facility was designed and developed for the purposes of this research. In particular, the main philosophy behind the developed engine powertrain experimental facility was that the control and the instrumentation system had to be able to monitor all the required engine test cell quantities i.e. from each individual sub-system (e.g. engine, dynamometer, coupling shaft), synchronously, continuously and on a crank-angle basis from a single control and monitoring platform. Usually most of the commercial engine test cell control and instrumentation solutions provide asynchronous communication between different control and monitoring platforms e.g. dynamometer controller, engine controller and instrumentation, emissions and combustion analyser, which results in an inefficient overall test cell control and instrumentation system incompetent for global real-time control and monitoring applications. On the contrary, the instrumentation system that is presented here was designed in such a way that from a single control and monitoring platform it would be possible to acquire all the required test cell physical quantities such as engine and dynamometer acceleration, speed and position, coupling shaft torque, engine torque, dynamometer currents, engine cylinder pressure etc., continuously, synchronously and on crank angle basis.

The experimental test rig developed for the project is presented in Fig. 4.1. The key sub-systems of the rig were a transient dynamometer which was actually a three phase induction motor with its drive unit, a single cylinder internal combustion engine, a rotary coupling shaft responsible for the connection of the dynamometer with the engine, and finally the control and data acquisition system. In the following sections more details are given regarding the development process, the functionality and the real world challenges that had to be overcome for the realisation of this novel transient cyclic engine testing facility.

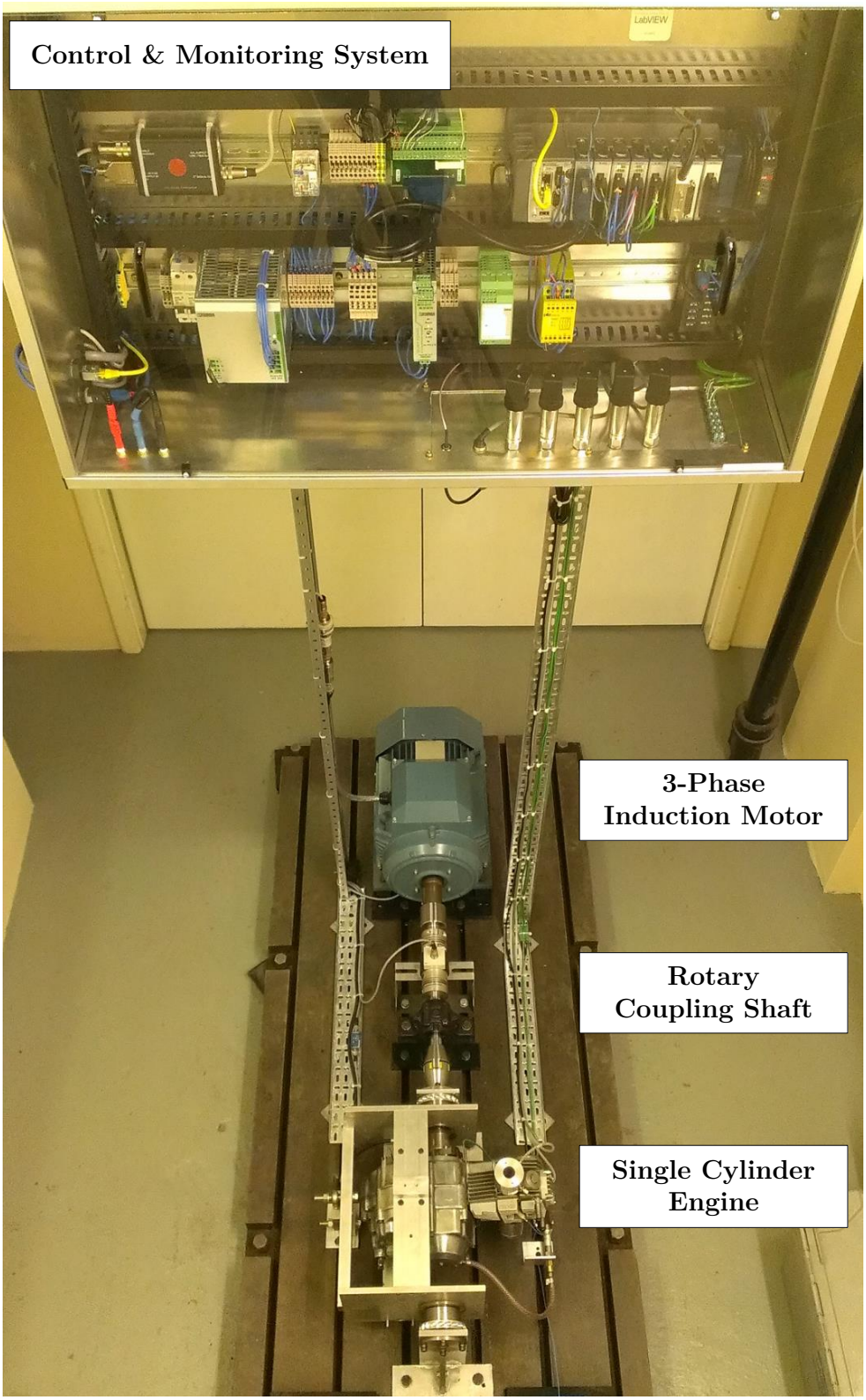

Figure 4.1: Transient cyclic motoring engine test cell.

4.2 Experimental Engine

The internal combustion engine which was used for this research was a single cylinder, naturally aspirated, spark ignited, air cooled engine, manufactured by Honda Motor Co.. Although the technology of the engine was relatively old, this was not an obstacle for proving the applicability and the potential of the proposed real-time parameter assessment framework. Prior to any experiments the engine was disassembled for measuring all the required physical/geometrical parameters for the parametrisation of the model (see Chapter 3). The main technical specifications of the test engine are submitted in Table 4.1.

Table 4.1: Engine technical specification.

Parameter	Value	Unit
Engine capacity	120	cm^3
Compression ratio	9.5	-
Number of cylinders	1	-
Cylinder bore	54	mm
Cylinder stroke	51.5	mm
Connecting rod length	88	mm
Crank arm length	25.7	mm
Reciprocating mass	0.80	kg
Number of intake valves	1	-
Intake valve head diameter	27.3	mm
Intake valve inner diameter	25.3	mm
Number of exhaust valves	1	-
Exhaust valve head diameter	23.3	mm
Exhaust valve inner diameter	20.3	mm
Intake manifold volume	12	cm^3
Throttle plate diameter	25	mm

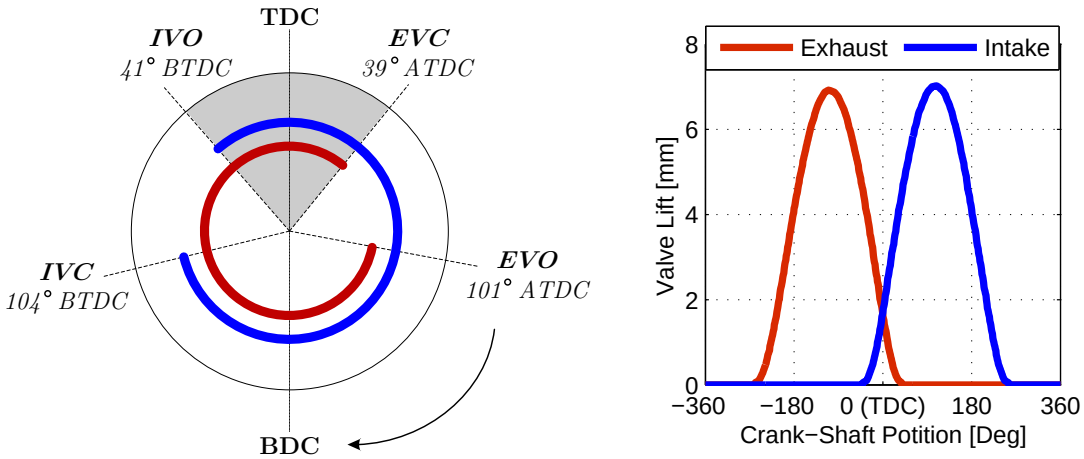

(a) Valve timing diagram

(b) Valve lift profile

Figure 4.2: Valve-train characteristics.

In addition to Table. 4.1, in Fig. 4.2 are illustrated the valve-train characteristics which were also needed for the parametrisation of the the engine model. An overlap period of 90 degrees is observed in the valve timing (shaded area in Fig. 4.2a) of the engine which as it will be shown later contributes on back-pressure phenomena on the intake manifold (see Fig. 4.8c). Additionally, it should be clarified that the valve timing (Fig. 4.2a) and valve lift (Fig. 4.2b) were fixed throughout the experiments.

The engine was mounted on a novel mounting system that enabled the accurate and direct measurement of the cyclic engine torque. Besides the measurement of the cyclic torque the engine was instrumented with the adequate sensors for acquiring signals related to the engine angular position, velocity and acceleration, and the intake port, exhaust port, cylinder and oil sump pressures and temperatures. The intake manifold pressure was independently controlled through an electronic throttle module and its controller. Informations regarding the hardware that was used refer to Section 4.2.

4.3 Transient Dynamometer

The motoring of the engine was provided by an ABB ACS800 industrial drive controlling an ABB M2AA 180 MLB4 three-phase electric motor. The main technical specifications of the electric motor and the industrial drive are tabulated in Table 4.3 and Table 4.2 respectively.

Table 4.2: Electric motor technical specifications.

Parameter	Value	Unit
Number of poles	4	-
Nominal frequency	50	Hz
Nominal speed	1465	RPM
Nominal power	22	kW
Nominal torque	143	Nm
Nominal voltage	400	V
Nominal current	41.7	A
Motor inertia	0.13	kgm^2
Nominal efficiency	91.6	%
Stator resistance	0.14	Ω
Rotor resistance	0.15	Ω
Stator reactance	0.31	Ω
Rotor reactance	0.49	Ω
Mutual reactance	13.1	Ω

An external three-phase wall outlet was providing the necessary power supply to the electric drive. The drive then was responsible for converting the AC input to DC and then controlling the AC output of the dynamometer based on vector-control scheme (similar to the one described in Chapter 3) depending on the needs of the user. It is also useful to mention that the drive was employed with a bidirectional inverter and thus under braking condition the drive was able to feed the electric power back to the grid via regenerative braking. Either dynamometer

speed or torque control mode could be selected from the test cell operator. Additionally the drive was employed with numerous operational and safety settings that were accessible to the user for improving the performance and the safety of the system. The system was designed and developed in a way that allowed the user to have complete control and monitoring of the demands and the setting of the electric driver remotely from the host computer of the test cell control and monitoring system which was located outside the rig.

Table 4.3: Electric drive technical specifications.

Parameter	**Value**	**Unit**
Input voltage	3∼380...415	V
Input current	32	A
Input frequency	48...63	Hz
Output voltage	3∼0...Input	V
Output current	34	A
Output frequency	0...300	Hz

The three-phase squirrel cage type induction machine was connected to the test engine through a custom made coupling shaft. More particularly, before the coupling shaft the motor was connected directly to an in-line torque transducer using aluminium corrugated bellows couplings. Next, the other end of the torque transducer was connected to the custom made coupling shaft that was connecting the engine with the rest of the system components via of a spider coupler.

Lastly, it is useful to mention some practical issues associated with the mounting system of the engine. In particular as soon as the entire system was coupled and running at high speeds, an intense vibration on the coupling shaft was observed which was caused by the increased vertical acceleration of the engine. This problem was solved eventually by mounting the coupling shaft on two pedestals with self-alighting bearings in order to cancel out all the undesirable vibrations.

4.4 Control & Monitoring System

The most challenging and time consuming task throughout the construction of the experimental facility was the design and development of the control and monitoring system of the test cell. The main reason behind this increased difficulty was because of the following demanding (high-level) specifications that were set prior to any design and development actions:

- *Global test cell controller*: The objective was to have a common platform for controlling and monitoring all the subsystems of the test cell i.e. dynamometer, engine, coupling shaft. Conventional test cell controllers usually consists of numerous different desks e.g. different controller for dynamometer, different data acquisition system for the engine etc. However this idea of distributed test cell control and monitoring systems usually leads to non-deterministic and asynchronous communication among the different platforms. This problem was identified and addressed in this study and the necessary actions were taken in order to prove that a different system architecture would increase the efficiency of this process. The main benefits of the proposed system structure is the deterministic, synchronous and lossless acquisition, processing and logging of the data. Additionally this type of engine test cell control and monitoring architecture promote new possibilities (or addresses new problems) in engine test cell controllers such as global test cell control and monitoring systems.

- *Cyclic monitoring system*: Cycle-by-cycle analysis of engine powertrain systems requires cyclic-based monitoring systems. More specifically, crank-angle based monitoring of internal combustion engines is the major requirement for the development and validation of physics-based models and relevant parameter estimation methodologies. Thus the data acquisition system of the test cell had to be designed in a way that would allow the monitoring of all the required physical quantities synchronously and on a crank-angle basis throughout the entire operating range of the engine.

- *High speed data processing and data logging*: The development of a high speed data processing and data logging system was a necessary need to acquire successfully all the measured signals on a crank-angle basis. Several practical issues had to be overcome for the effective completion of this high speed data processing and data logging system, some of them were the lossless and deterministic communication between the real-time computer and the host computer, on-line zero phase distortion filtering, design of the appropriate software buffers, integer calculations within real-time operating environment, calculation of engine cyclic position, cycle indexing etc. All these issues are discussed in more details in the following paragraphs.

- *Open architecture system*: Even though the transient engine testing facility was designed for the purposes of this thesis specifically, the control and monitoring system had to have a reconfigurable hardware and software architecture to ensure easy extension and configuration of the system for future research application.

For the accomplishment of the mentioned objectives, the appropriate hardware and software had to be selected and designed. The selection of the components, the construction of the necessary hardware and the design of the adequate software were developed from scratch during the period of this project.

4.4.1 Hardware Specification

Numerous sensors, actuators and controllers were included in the control and monitoring system of the transient engine test cell. The main control inputs for the test cell operator were the speed or torque demands to the electric drive of the three phase induction motor, the throttle position demand to the electronic throttle controller of the single cylinder engine and lastly fail-safe functions for emergency cases. The main outputs/measurements were system's physical quantities such as torque, pressure, temperature, position, velocity, acceleration, currents, voltages, power etc.. The architecture of the control and monitoring system hardware

is illustrated in a simplified conceptual diagram in Fig. 4.3. The diagram presents all the relevant measurements and controls that were involved in the experimental apparatus, details related to the sensors and actuators of each subsystem i.e. engine, dynamometer, coupling shaft, are listed below:

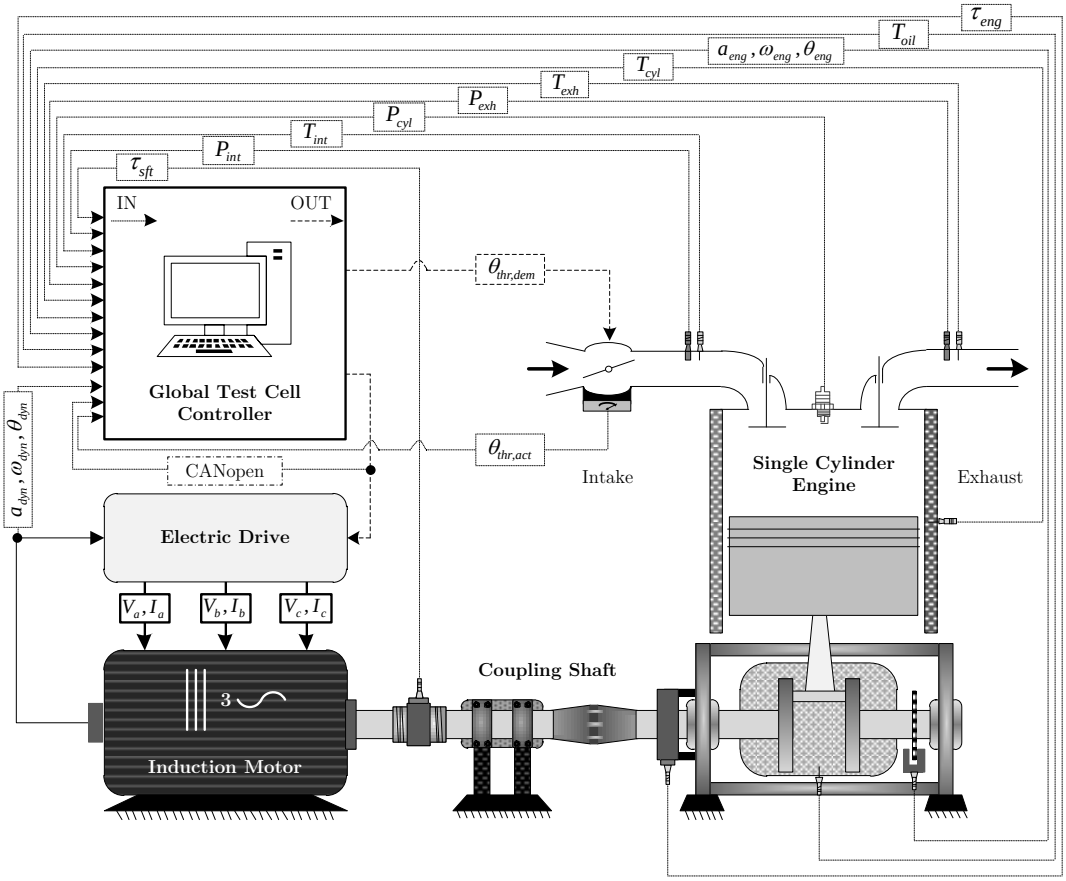

Figure 4.3: Test rig control and monitoring system hardware architecture.

- **Engine Control Inputs**

  Throttle Position: For the closed-loop control of the throttle position a PID controller was implemented in National Instruments LabVIEW using a National Instruments multifunctional data acquisition card (NI USB-6008). The output of the PID controller was then fed into a DC electric drive (Pololu 1372) which was responsible for generating the corresponding PWM for the DC electric motor of the electronic throttle body (VISTEON 2S6UFC). An encoder was providing the required throttle position feedback for the

closed-loop control of the throttle. The tuning of the PID controller was accomplished based on empirical methods.

- **Dynamometer Control Inputs**

  Speed/Torque Control: Two analogue outputs that were generated from the global test cell controller were informing the electric drive regarding the speed or torque demand for the dynamometer. Addiotnally, the selection between the speed and torque demands was achieved via a digital output from the global test cell controller. A quadrature position encoder was mounted on the electric machine for the precise control of the dynamometer speed. Furthermore, for the feedback control of the dynamometer speed a pulse encoder interface module (ABB RTAC-01) was added in the original electric drive. On the other hand, according to the control structure of the vector control scheme no feedback was required for the control of the electromagnetic torque of the motor.

  Fail-Safe Functions: Emergency stop functions were included on the electric drive with the purpose of avoiding any undesirable accident. More specifically the electric drive was programmed to brake the electric motor in 1 second as soon the test cell operator would press the emergency stop button. Lastly, additional reset button was also included in the software for resetting all the demands before the restart of the test.

- **Engine Measured Outputs**

  Position-Velocity-Acceleration: An optical contactless crankshaft encoder (AVL 365X) for high speed applications (up to 28000 RPM), was used for measuring the angular position of the engine. The encoder consisted of an optical sensor and a disk with 360 slots (360 pulses per revolution) which was fitted on the crank shaft of the single cylinder engine. For the determination of the top dead centre, one of the slots of the disk had bigger length compared to the others. The output of the optical encoder was connected to an impulse converter (AVL BG0478) which was responsible for converting

the original output of the encoder (LVDS, low-voltage-differential-signalling) to the appropriate output for the global test cell controller (TTL standard).

Cyclic Torque: A load cell (Tedea-Huntleigh Model 614) was fitted on the engine mounting system for measuring the cyclic engine force. The output of the load cell was fed into a high speed in line amplifier (Measurement Specialties Model 140) for generating the adequate analogue signal to be used by the global test cell controller. A practical issue with this measurement was an undesirable signal noise which was caused due to the problematic fitting of the sensor on the mounting system. More particularly, the load cell was fitted on the engine mounting system using ball joints that were creating vibration which was contributing in the noise of the signal. This problem was solved by developing on-line zero phase distortion filters that were implement in National Instruments LabVIEW Real-Time (more details are given in the following subsection).

Intake-Cylinder-Exhaust-Oil Pressure: The intake and exhaust cylinder pressures were measured using gauge pressure transducers (GE Measurement & Control-UNIK 5000) that were fitted on the intake and exhaust ports of the cylinder. The in-cylinder pressure was measured using the smallest available spark plug integrated with a pressure sensor (AVL ZI21). In addition the in-cylinder pressure transducer a charge amplifier (Kistler Type 5018A) was used for amplifying the signal of sensor to be used by the global test cell controller. Lastly, for the measurement of the oil pressure, a pressure transducer (KELLER PR-21S/5.5bar/81400.3) was placed appropriately on the engine.

Intake-Cylinder-Exhaust-Oil Temperature: Similarly to the engine pressure measurements, for the measurement of the intake and exhaust temperatures thermocouples (TC-Direct K Type 0.75mm x 100mm) were fitted on the intake and exhaust ports of the cylinder. The cylinder temperature was measured on the cylinder head using the appropriate thermocouple (TC-

Direct K Type 1.5mm x 100mm). Additionally, the oil temperature was measured with a thermocouple (TC-Direct 3.5mm x 150mm) on the oil sump.

- **Dynamometer Measured Outputs**

  Position-Velocity-Acceleration: A quadrature encoder was fitted on the rotor shaft (BRITISH ENCODER PRODUCTS Model 755HS, 1024 pulses per revolution) for measuring the angular position of the dynamometer. The output of the encoder was fed to the global test cell controller for converting the pulses per revolution to cyclic position, and calculating the angular velocity and angular acceleration of the dynamometer. In parallel to the global test cell controller, the encoder output was connected to the encoder module of the electric drive for the closed-loop control of the dynamometer speed.

  ABB CANopen Variables: CANopen communication protocol was used for accessing all the operating parameters of the dynamometer.[1] A CANopen adapter module (ABB RCAN 01) was placed on the ABB electric drive which gave instant access to all the operating parameters of the dynamometer. The output of the CANopen adapter module was connected to a National Instruments CANopen card (NI USB-8473) that was part of the global test cell controller. With this communication protocol the test cell operator had instant access to dynamometer quantities such as frequency, currents, voltages, torque, speed, power, temperature of the motor and the electric drive, motor run-time, kilowatt hours and total operating hours of the dynamometer.

- **Coupling Shaft Measured Outputs**

  Instantaneous Torque: For the measurement of the coupling shaft torque (dynamometer torque minus the engine torque during motoring conditions) an in-line torque transducer with an integrated amplifier (HBM T22) was

[1] CANopen is a higher layer protocol based on the CAN serial bus system and the CAL. For more information visit the following website: `http://can-cia.org/`.

placed on the shaft. Aluminium bellows couplings were used for the mounting of the sensor. The output signal of the torque transducer was fed directly to the global test cell controller.

The key element for the successful operation of the control and monitoring system was the actual controller that was used for generating the control signals and acquiring all the measurement quantities mentioned previously. Consequently a National Instruments CompactRIO real-time controller (NI cRIO-9022) was used in this application. The CompactRIO controller includes a real-time processor and a reconfigurable FPGA.[2] The real-time processor is used for network communication, data logging, control and processing with the deterministic and reliable NI LabVIEW Real-Time OS. The user-programmable FPGA provides the ability to implement custom hardware for high speed control, in-line data processing, or complex timing and triggering. These features were crucial for the successful development of the present set-up as the synchronisation of crank-angle based measurements required high speed data processing, timing and triggering functions.

Here, the maximum sampling speed was chosen based on the maximum engine speed and the sampling resolution, hence for speeds up to 9000 RPM with resolution of one degree crank-shaft angle, the sampling frequency had to be at least 108 (kHz) (Eq. 4.1). The measurement signals were all synchronised with the engine encoder data (event-based) to ensure equidistant sampling, however this required special handling of the acquisition system to avoid aliasing effects

[2]FPGA stands for Field-Programmable Gate Arrays and is actually an integrated circuit design to be configured by a customer or a designer after manufacturing. The main benefits of the FPGA chips compared to conventional processors that can be found in PCs is that programming an FPGA rewires the chip itself to implement a custom functionality rather than run a software application. As a result this provides faster response times. More information can be found in the founding company of the first commercial FPGA chip (`http://xilinx.com/`).

(see [156] for a solution to the aliasing issues).

$$f_s = \left[\frac{9000(RPM)}{60(s)} * 360\right] * c_{nyq} = 108(kHz) \tag{4.1}$$

The constant c_{nyq} is equal to 2 and is used to take into account the Nyquist criterion for sufficient sample-rate.

Furthermore, the NI CompactRIO controller was connected to an eight slot expansion chassis which had all the required input/output modules. In particular, for the needs of the present application the chassis was equipped with the following cards:

- High speed analogue input (NI-9220), this card was used for acquiring the signals of the pressure and torque transducers.
- Analogue output (NI-9263), the speed and torque demand for the dynamometer were generated from this card.
- High speed digital input (NI-9423), auxiliary signals related to the operation of the test cell i.e. start/stop and emergency stop indicators, were connected in this card.
- High speed digital output (NI-9474), this card was generating switching signal which were needed for the selection of different testing modes i.e. speed or torque mode of the dynamometer.
- Differential digital input (NI-9411), the output of the quadrature encoder of the dynamometer and the optical encoder (through the signal converter) were connected in this module.
- Thermocouple module (NI-9211), the intake, exhaust, cylinder and oil thermocouples were directly connected on the thermocouple module.

Final step in the development process of the control and monitoring system was the creation of the necessary software including a user friendly interface. Details are given below.

4.4.2 Software Specification

The software for the measurement and control system of the transient engine test cell was developed from scratch in National Instruments LabVIEW. LabVIEW is a user friendly graphical programming platform with numerous attractive features such as interfacing easily to rapid prototyping devices, parallel programming, FPGA graphical programming, dynamic simulation environment for control design, numerous custom libraries/modules, development of user friendly interfaces, etc..[3] The main reasons for using this software design platform were because it was fully compatible with the selected hardware, it had user friendly graphical environment for the development of FPGA and Real-Time applications, it was equipped with CANopen libraries that allowed the communication with the ABB electric drive relatively fast, it provided all the required tools for on-line data synchronisation, processing, streaming, visualisation and logging, and finally allowed the design of an easily reconfigurable user interfaces for controlling and monitoring all the test cell functions.

The user interface of the global test cell control and monitoring system of the transient/cyclic engine test cell is presented in Fig. 4.4. As it is observed the interface has all the necessary controls for controlling the dynamometer and the engine, and numerous graphs, gauges and indicators that visualise all the acquired quantities in real-time so that can be assessed by the test cell operator when experiments are conducted. Furthermore, it is important to highlight the cyclic phenomena of the measured quantities i.e. intake, cylinder and exhaust pressure, engine and shaft torque, engine and dynamometer speed, are clearly visible in real-time. Similar to the control and visualisation functions the user interface was equipped with a data logging dialogue which enable the test cell operator to save the data of each individual experiment.

Before to the development of the user interface it was necessary to create the firmware which contained all the low level drivers for the input/outputs of the

[3]For more details refer to: `http://ni.com/labview/`.

controller, the calibration variables and the real-time data processing, streaming and logging functions. Thus, as it can be understood the development of the entire control and monitoring software was a rather complex task. Consequently, to simplify the implementation of the required software functionalities, a software architecture was established prior to any further actions.

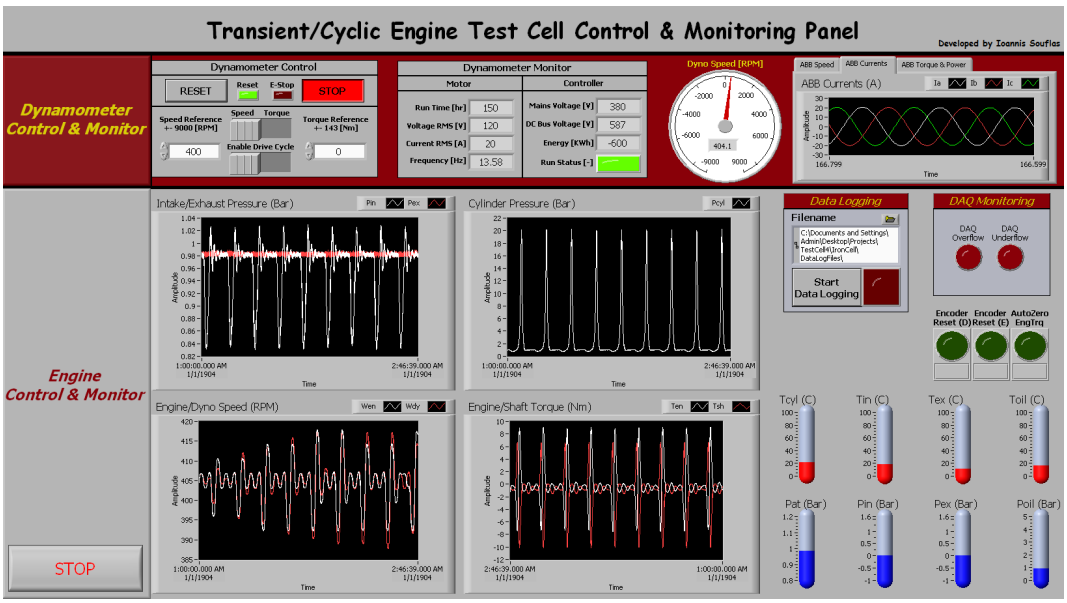

Figure 4.4: Control and monitoring system user interface.

The top-level software architecture is presented in Fig. 4.5. The entire software consists of three main application, the FPGA.vi, the RTOS.vi (Real-Time-Operating-System), and the PCOS.vi (Personal-Computer-Operating-System) (.vi stands for visual instrument and is the extension of every LabVIEW application). The first two applications were implemented in the NI CompactRIO and they talked to each other using DMA FIFO (Direct Memory Access First-In First-Out) communication. FIFO is data structure that holds elements in the order they are received and provides access to those elements using first-in-fist-out policy, while DMA does not involve the real-time processor when reading data of the FPGA chip; therefore it is the fastest method for transferring large amounts of data between the FPGA target and the real-time (local host) processor. Next, the data form or to the NI CompactRIO were transfered to or from the host PC using single process FIFO shared variables for each of the acquired signals. The communi-

cation between the host PC and the NI CompactRIO was achieved by means of Ethernet physical layer.

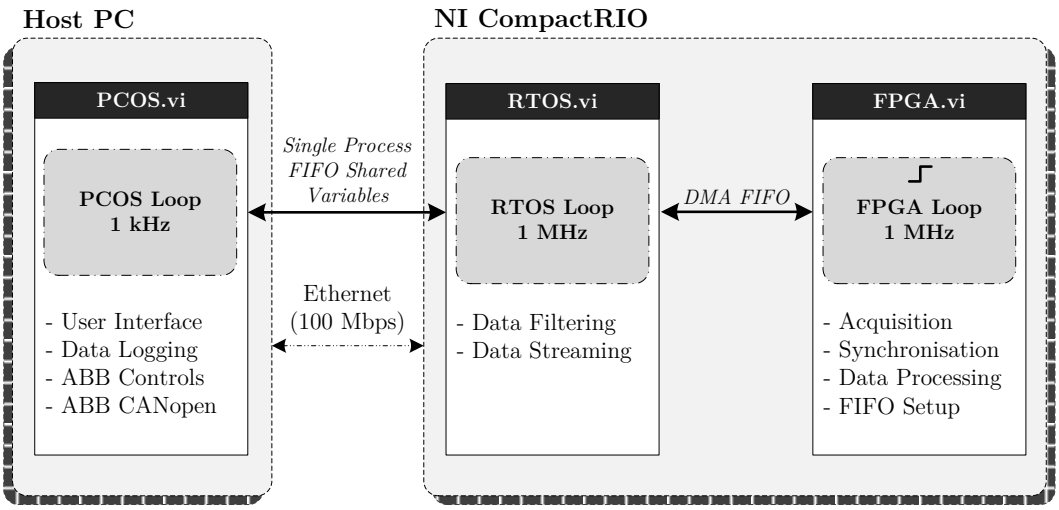

Figure 4.5: Control and monitoring system top-level software architecture.

The FPGA.vi application was running in the FPGA processor which was located in the NI CompactRIO controller. Even though the FPGA processor of the current device had maximum sampling frequency of 40 MHz, the maximum sampling frequency for this application was set to 1 MHz to reduce the processing power demand. In any case the selected sampling frequency was already ten times more than the minimum required sampling frequency of the system (see Eq. 4.1). The main reason for having this excess sampling frequency was to make sure that no data will be lost during the experiments and to avoiding any undesirable aliasing effects due to the event-based nature of the data acquisition system (see [156] for a solution to the aliasing issues). As far as the content of the FPGA application is concerned, there were four different subsections namely the acquisition, synchronisation, data processing and FIFO (DMA FIFO) set-up (see Fig. 4.5). The acquisition subsection involved the code for the set-up of the input/output channels of the controller, and the functional structure of the triggering loops that were needed for the cyclic synchronisation of the controller channels. Right after the acquisition section, started the code for the cyclic synchronisation of the data. One of the main challenges of this section was the synchronisation

of the data during the very first cycle of the operation of the engine. This problem was solved by neglecting all the acquired data up until the cylinder of the engine pass through the TDC for the first time (the optical crank shaft encoder provided a digital output every time the engine pass through the TDC). After the first cycle determination and synchronisation the measurement quantities were synchronised using the engine encoder signal. Concurrently the synchronisation section was making use of one of the functions of the data processing section which was the cyclic engine position in order to index all the data on a cyclic basis. Next, the data processing part involved the calibration parameters for the scaling of the analogue sensors i.e. pressure and torque transducer, the conversion of the continuous engine and dynamometer angular position measurements to cyclic (Eq. 4.2) and the estimation of the angular velocity (Eq. 4.3) and acceleration (Eq. 4.4) of the engine and dynamometer.

$$\theta_{cyc}(rad) = \left(\frac{\theta_{con}(rad)}{\not{d}_{cyc}(rad)} - \left\lfloor \frac{\theta_{con}(rad)}{\not{d}_{cyc}(rad)} \right\rfloor \right) * \not{d}_{cyc}(rad) \tag{4.2}$$

$$\omega(rad/s) = \frac{2\pi * enc\_pul}{dt(s) * enc\_ppr} \tag{4.3}$$

$$\alpha(rad/s^2) = \frac{2\pi * [enc\_pul_{(n)} - enc\_pul_{(n-1)}]}{dt^2(s) * enc\_ppr} \tag{4.4}$$

Where, θ_{cyc} and θ_{con} are the cyclic and continuous position respectively, $\not{d}_{cyc}$ is the duration of a complete engine cycle i.e. 720 Degrees, ω and α are the angular velocity and acceleration respectively, dt is the fixed sampling time interval, enc_pul is the encoder pulses signal and enc_ppr is pulses per revolution of the encoder.

Final section was the careful design of the DMA FIFO buffers in order to ensure lossless data transfer from the FPGA processor to the real-time processor of the NI CompactRIO controller. In particular, if the buffer size is small data would be lost, while on the other hand if buffer size is to large then it uses unnecessary processing power which can reduce the performance of the application significantly. Consequently, the size of the buffer was set appropriately, whilst functions

that indicated the loss of data or the excess buffer size where included as application diagnostics. In the end the size of the DMA FIFO buffer was set using trial and error approach.

Alongside the FPGA application, the RTOS application (RTOS.vi) was running at the same sampling frequency i.e. 1 MHz. By running both loops at the same sampling frequency provided a more deterministic communication and less DMA FIFO buffer size for transferring the data from and to the FPGA processor. The main duty of the RTOS application was to store the data of each measurement signal to a single process FIFO shared variables which were then used for streaming the data to the host computer. Similar to the FPGA application, here it was necessary to design the appropriate buffer sizes to avoid any undesirable results. Additionally in this part of the software the filtering of some of the acquired quantities took place. More particularly the measurement signals that required filtering were the shaft and engine torque transducers, and the angular velocity and acceleration estimates. The appropriate filtering of these quantities were of major importance since any filtering artifacts i.e. phase-shifts, would inevitably create problems with the crank-angle synchronisation of these measurements. In any case this problem was avoided by using two butterworth lowpass filters so that the first one was used for the forward filtering of the data while the second was filtering the data backwards to eliminate any possible signal phase distortions.

Finally, the user interface, data logging, and the communication with the ABB electric drive were implemented in the PCOS.vi application which was located at the host computer. The sampling frequency of this application (1 kHz) was much slower compared to the RTOS and FPGA loops (1 MHz) since the host computer did not have the processing power of the NI CompactRIO real-time computer. Anyway the acquired measurements were already transferred in chunks of data (FIFO buffers) which allowed the reduction of the sampling frequency. Additionally, the PCOS application included the controls and the CANopen communication protocol of the ABB electric drive as the maximum sampling speed of the electric drive was much less compared to the maximum speed of the PCOS loop (1 kHz).

The data logging system was also implemented in the host computer for storing the data in a solid state hard disk of the host computer; it is useful to mention that the data logging system could be also implemented in the NI CompactRIO controller however this would require the existence of a local hard drive which was not available at that time. In the user interface (see Fig. 4.4) were included all the essential controls and monitoring interfaces to provide a friendly environment to the test cell operator. It is worth mentioning that the user interface was completely reconfigurable and could be adapted depending on the needs of the experiment.

Last part of the developed software was a MATLAB function that was used for post-processing the experimental measurements with the purpose of making sure that there are no any inconsistencies. In particular the function was checking the synchronisation, the cycle indexing, and and the completeness i.e. no data loss throughout the experiment, of the logged data for each experiment.

4.5 Test Methodology & Experimental Results

The transient engine test cell was used for developing, proving and validating the application of the suggested real-time parameter assessment framework in physical and semi-physical engine powertrain models i.e. cyclic and mean value. Hence for the purposes of the present thesis the engine was tested under motoring condition i.e. the engine speed was controlled via the transient dynamometer, while at the same time the cylinder intake upstream conditions (pressure and temperature) were controlled by adjusting the position of the electronic throttle body. The user was able to implement either fully transient tests (transient speed and throttle), partly transient tests (constant settings for one of the two control inputs and transient for the other) and finally conventional steady state experiments (constant speed and throttle) (Fig. 4.6). In that way it was possible to physically excite all the major phenomena/dynamics that underline the operation of the given system.

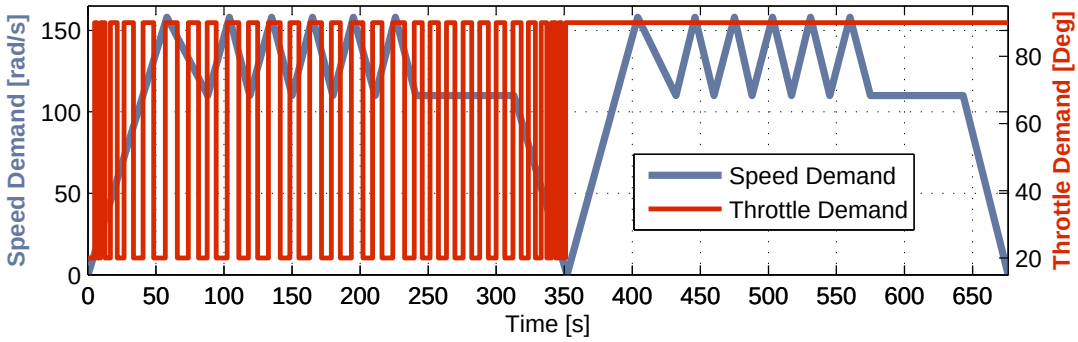

Figure 4.6: Speed and throttle control demands for a representative test case.

At this point it is also important to remind the fact that the suggested real-time parameter assessment scheme was proved and validated only for motoring engine powertrain conditions does not implies that is not valid or applicable for firing engine conditions. This is because the suggested methodology depends on the existence of a physical or semi-physical models that describe the major phenomena/dynamics underlying the operation of the system rather than the conditions that it operates.

The time series graphs in Fig. 4.6 and Fig. 4.7 provide a better inside regarding the types of the tests that were carried out and the major experimental measurements that were collected throughout a conventional experiment. Particularly, Fig. 4.6 illustrates the dynamometer speed profile and engine throttle control demands for a representative test case with a duration of approximately 10 minutes. As it is observed there are periods where the test signals are changing rapidly e.g. see speed and throttle demands for times between 50 and 200 seconds, which indicates the transient nature of the experiment, and there are also periods which allow the steady state experimentation of the system by holding the control inputs at a constant level e.g. see speed and throttle values for times between 600 and 630 seconds. In that way the experimental time was significantly reduced compared to pure steady state tests which require extensive amount of time for covering all the required operating conditions of the systems. Additionally as it is going to be shown in a following chapter the rapid change of the system's inputs contribute to the exploitation of the system dynamics which have a significant role

in the estimability of certain physical parameters of the system.

Next some of the most useful and important experimental results that were recorded during this test case are presented in Fig. 4.7. The angular velocity, acceleration and position of the dynamometer and the engine are illustrated in Fig. 4.7a, Fig. 4.7b and Fig. 4.7c respectively. The instantaneous engine torque is presented in Fig. 4.7d, the steps that are present until the 350th second of the experiment are caused due to the throttle steps, whilst the the ramp ups and downs that are clearly visible throughout the entire time series are caused due to the transient speed demand. Similar to the instantaneous torque the cylinder Fig. 4.7e and intake pressures Fig. 4.7f were affected significantly from the throttle steps while the speed ramps did not have so significant impact. On the other hand, the exhaust pressure remains almost the same throughout the experiment i.e. close to ambient conditions no matter the variation in the speed and throttle Fig. 4.7f. Interesting phenomena are also observed in the intake, exhaust and cylinder head temperature Fig. 4.7g, more particularly it was observed that the throttle steps had a direct effect on the temperature changes in the intake and the exhaust while the cylinder head temperatures did not show any relevant changes. It is important to clarify that these temperature results do not represent the instantaneous cyclic behaviour of the temperature due to the large time constants of the thermocouples that were used in the set up. For instantaneous temperature measurements, compensation of the sensor dynamics would be required (see [116]). Additionally it is observed that the temperature of the exhaust is colder compared to the intake which is opposite to exhaust temperature measurements during firing conditions. This effect is explained from the fact the engine was tested under motoring conditions while the engine block temperature was relatively low ($\approx$ 35 degrees Celsious). If the engine block temperature was higher the exhaust gas temperature would be eventually higher than the intake.

Turning to the results related to the transient dynamometer, in Fig. 4.7h, Fig. 4.7i and Fig. 4.7j are submitted the RMS current and voltage supply to the induction motor of the electric drive and the the frequency of the alternating current respec-

tively. The proportional relationship of the dynamometer voltage and frequency indicates the voltage/frequency basic control strategy of the ABB drive. Additionally the correctness of these results could be evaluated with the speed of the engine and dynamometer (Fig. 4.7a) i.e. when the frequency of the alternating current was 50 Hz then then speed of the system was approximately 1500 RPM (Speed = [Frequency*120]/Motor Poles).

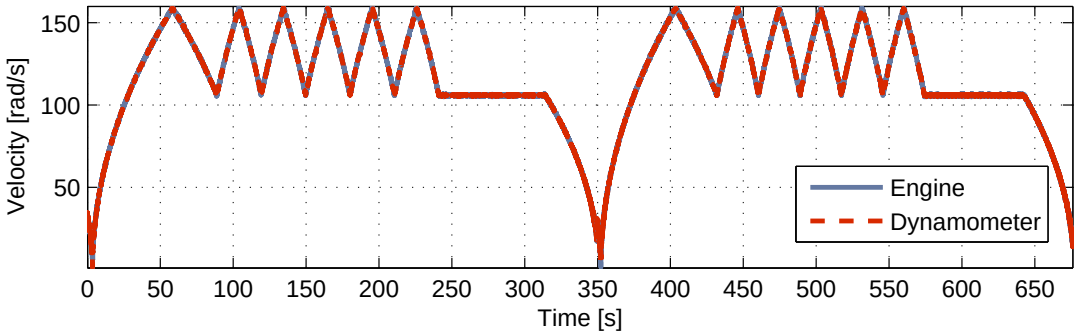

(a) Engine and dynamometer angular velocity

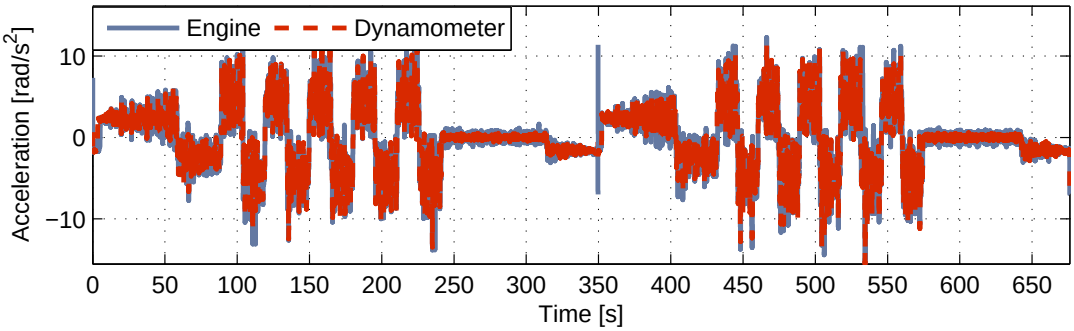

(b) Engine and dynamometer angular acceleration

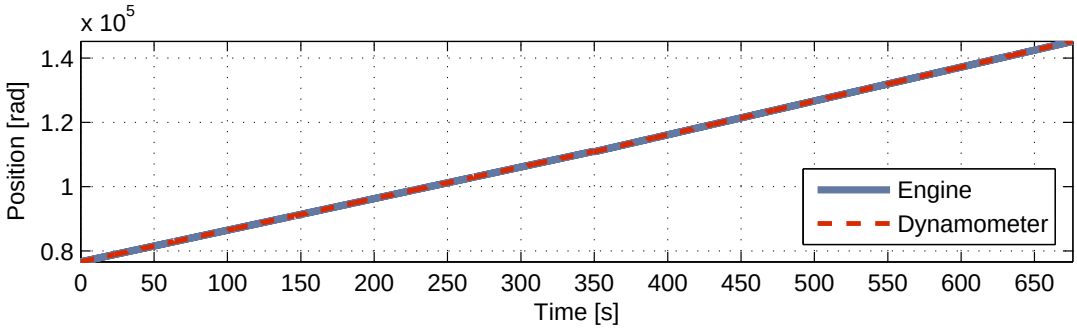

(c) Engine and dynamometer continues angular position

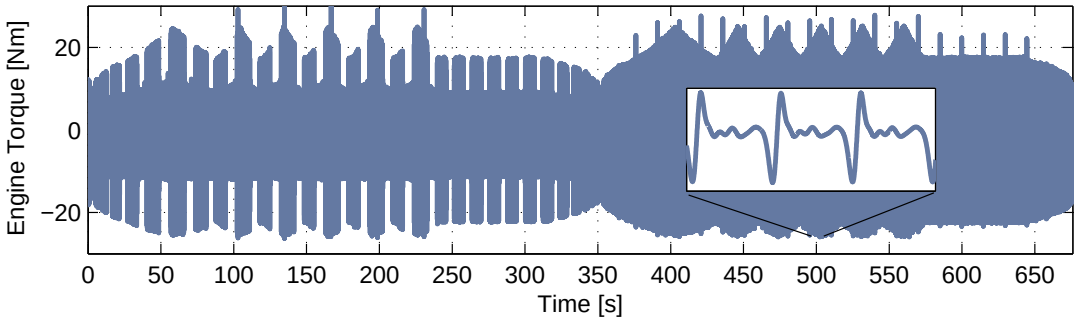

(d) Instantaneous cyclic engine torque

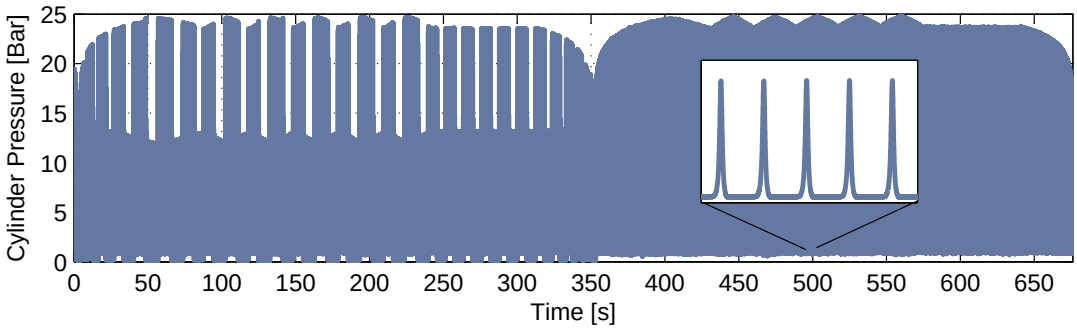

(e) In-cylinder engine pressure

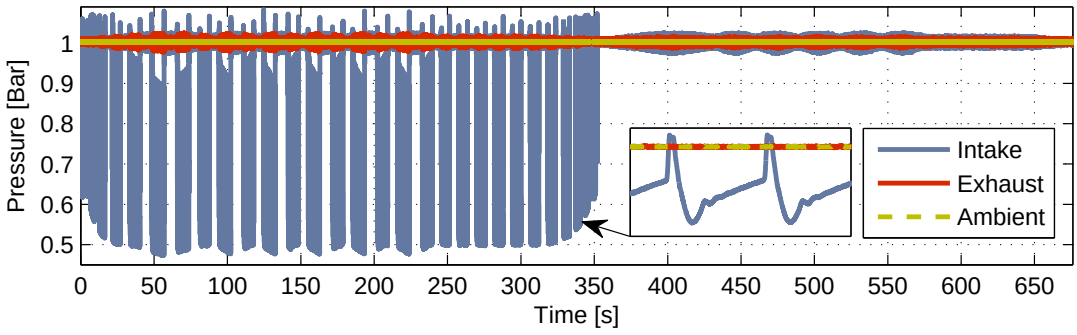

(f) Intake, exhaust and ambient pressures

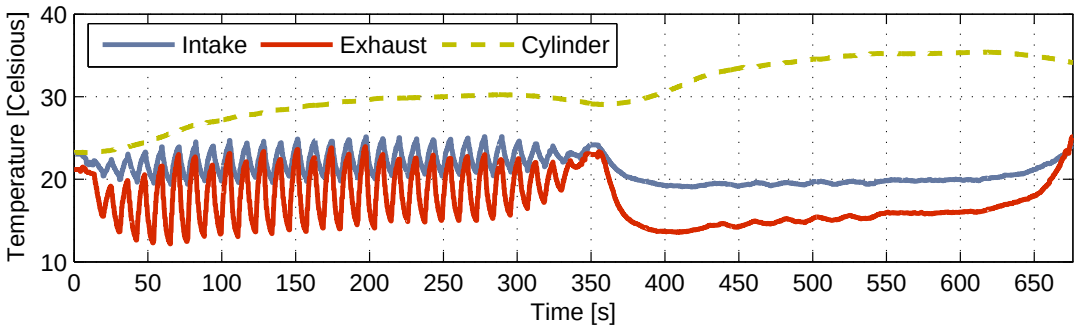

(g) Intake, exhaust and cylinder head temperatures

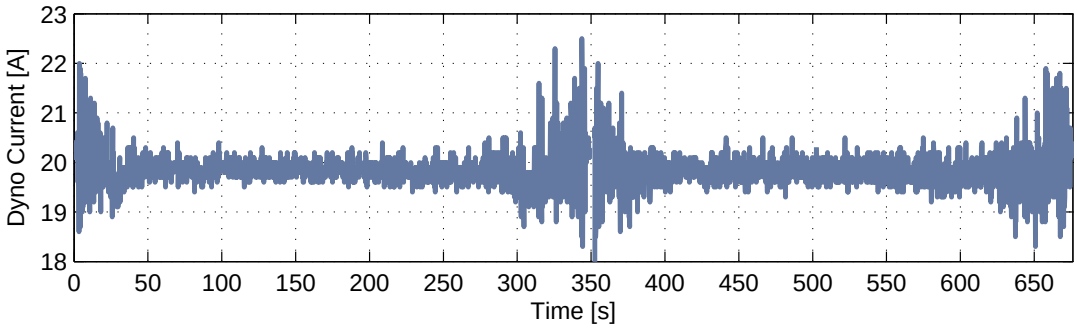

(h) RMS current output of the electric motor of the dynamometer

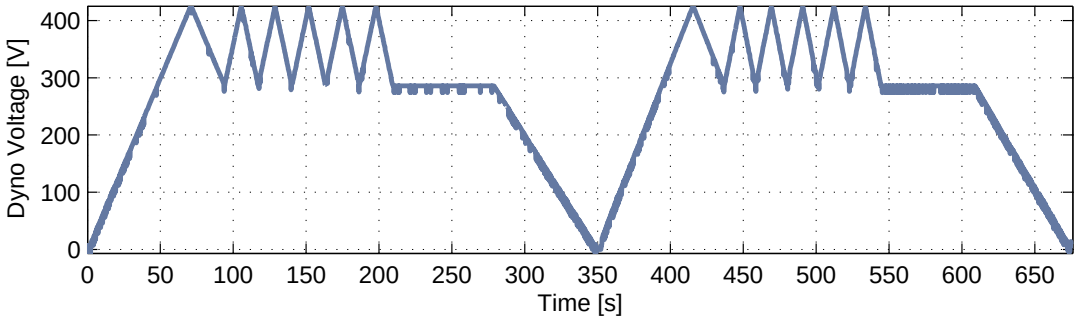

(i) RMS voltage supply to the electric motor of the dynamometer

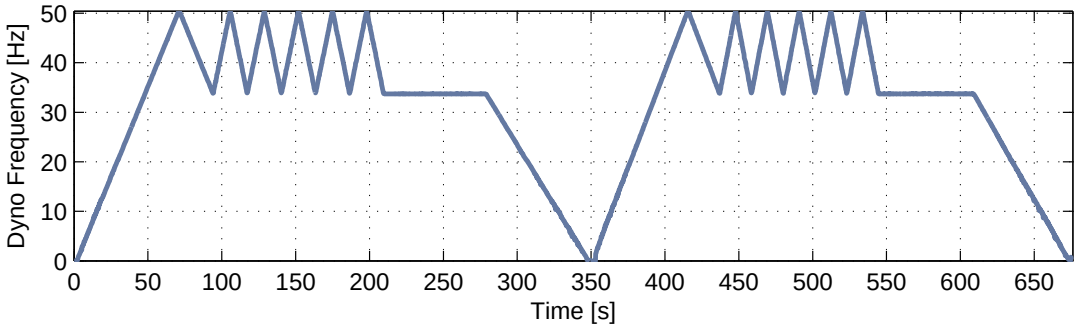

(j) Alternating current frequency

Figure 4.7: Time series experimental measurements, operating conditions defined in Fig. 4.6.

One of the main problems of crank-angle based cyclic data is the poor visibility when time series graphs are used. For example in Fig. 4.7e it is impossible for someone to see what is happening for one individual engine cycle. To increase the visualisation quality of the the data, in the next graphs some surface plots are given with respect to the engine crankshaft position and engine cycles.

The visualisation of the engine crank-angle based experimental results using the surface plots is presented in Fig. 4.8. The results illustrate crank-angle based measurements for twenty continues engine cycles. The experimental conditions for these results were constant speed at 1000 RPM while a step change in throttle angle from 20 to 90 Degrees took place approximately at the 10th cycle of the experiment (see Fig. 4.6 from 250 to 255 seconds).

Compared to the time series visualisation, the surface plot allows the reader to observed clearly the effects of the control inputs on each individual engine cycle. In particular by looking at the engine instantaneous torque (Fig. 4.8a) it is observed a step change from approximately 10 Nm to 22 Nm which is cause by the step change in the in-cylinder pressure (Fig. 4.8b). Similarly, the step in the in-cylinder pressure was caused due to the step change in the intake port pressure (Fig. 4.8c) that was created due to the step change in the throttle. Additionally the back-pressure effect from the cylinder to the intake port for closed throttle conditions it is clearly visible in the intake port pressure surface plot (see Fig. 4.8c crankshaft position 0-180 degrees and engine cycles 0-10). Lastly the exhaust port pressure does not show any significant changes throughout the given experimental condition as the pressure values remained almost steady near to ambient conditions. This is absolutely normal as the exhaust manifold and the down pipe were not connected to the engine thus the exhaust port was directly exposed to the ambient conditions.

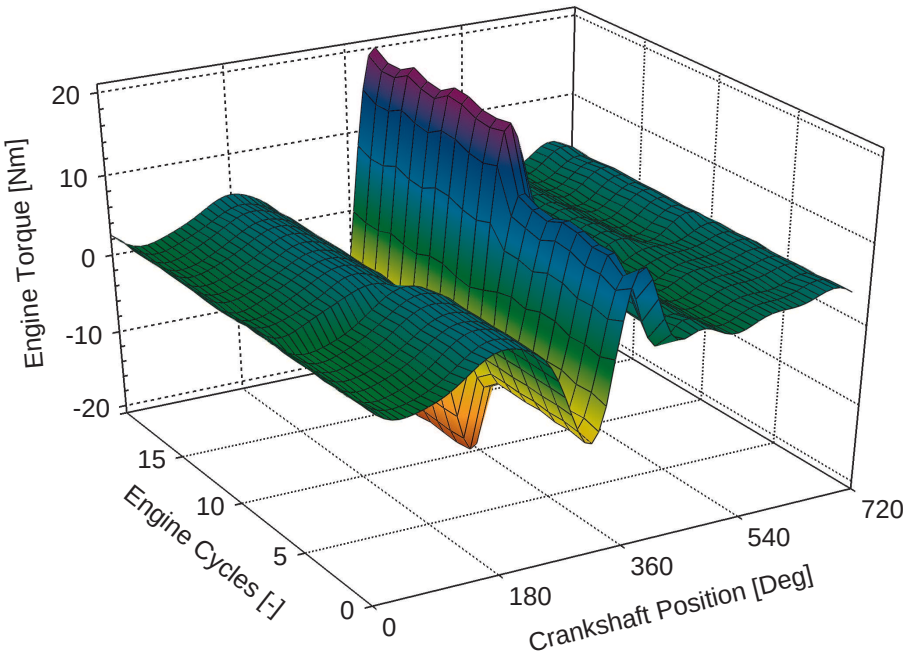

(a) Surface plot of the instantaneous cyclic engine torque

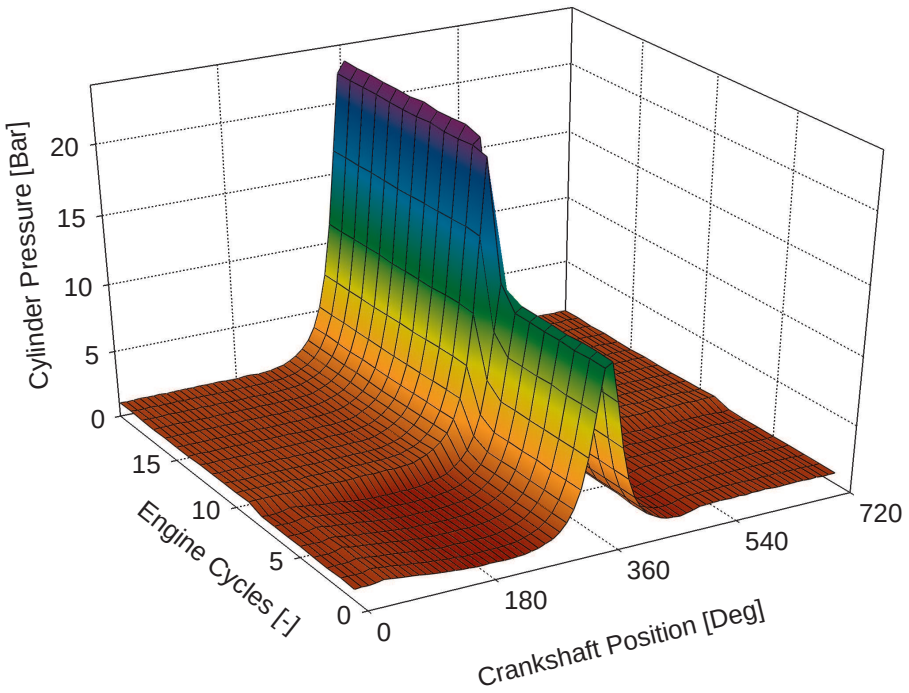

(b) Surface plot of the in cylinder pressure

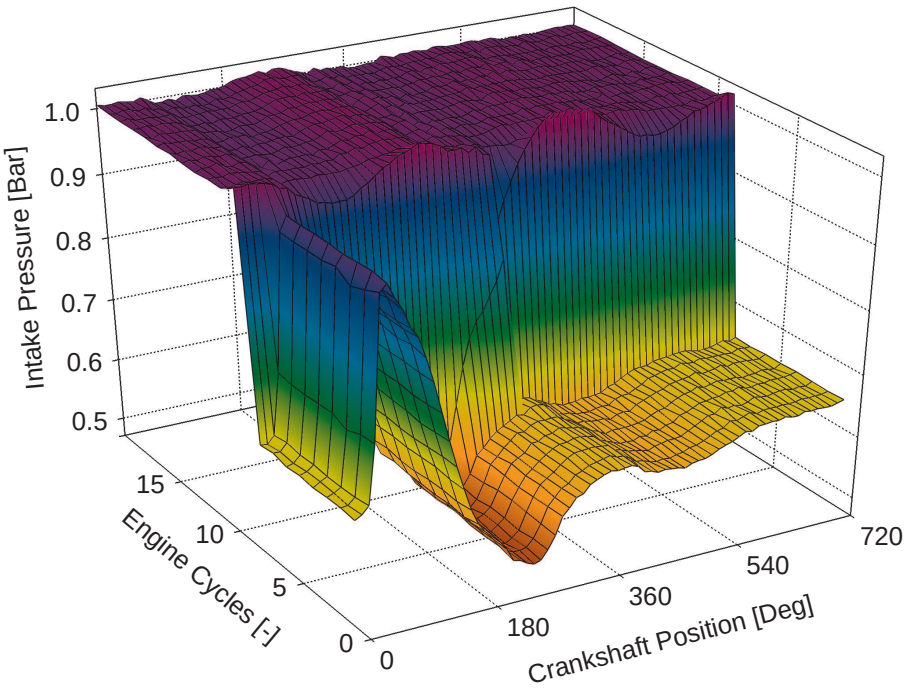

(c) Surface plot of the intake port pressure

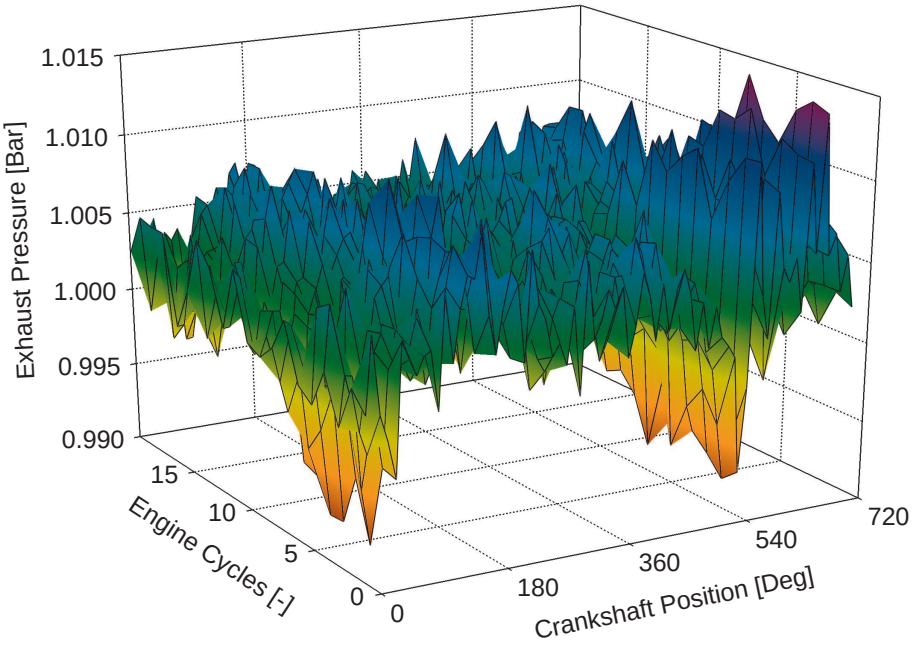

(d) Surface plot of the exhaust port pressure

Figure 4.8: Cyclic representation of the engine experimental results.

4.6 Synopsis

A summary of the key points of this chapter is given below.

- The technical features of a novel transient engine testing facility were presented. This testing facility was developed from scratch for the needs of this research.
- The main practical issues associated with the development of such experimental apparatus were highlighted.
- Some typical observation data were provided to demonstrate the capability and potential of this test rig.

Chapter 5

Parameter Identifiability & Adaptive Identification

The chapter introduces analysis and synthesis system identification tools and put them together to a complete chain for identifiability assessment and adaptive identification of parameters with physical and semi-physical interpretation that can be found generally in powertrain models. The practical implementation of the discussed system identification mechanisms is reported in Chapters 6, 7, and 8.

5.1 Overview on System Identification

The term “System Identification" was first introduced by Zadeh in 1956 [157]. According to Ljung [158], “system identification is the art and science of building mathematical models of real systems from observed input-output data". It is, indeed, a huge scientific field with a broad area of applications in engineering, biology, finance and life sciences. As a consequence of this diversity, it is beyond the bounds of possibility for an individual to be expert in all the system identification techniques that were developed throughout the years. As a measure of knowledge growth, the last two decades more than twenty books about the theory and practice of system identification have been published [159]. Some of the most

well-known and recent textbooks on the subject are those written by Ljung [160], Nelles [161] and Isermann [159]. Furthermore, the reader can refer to two informative and well cited IFAC[1] survey papers, written by Åström and Eykhoff [162], and Ljung [158], that provide common nomenclatures and a subjective view of the state of art in system identification. In the next paragraphs, a laconic overview on system identification is given and more inclined towards our specific applications.

The different identification procedures that are available can be categorised into two general classes, namely, the type of the model, and the implementation method [162].

5.1.1 Classification Based on Model Type

As it was mentioned previously, system identification is the art of building mathematical models of real systems from input-output observation data. However, prior to the actual identification of the mathematical model it is crucial to gain some understanding about the nature of the system under examination. In engineering applications there are two types of systems known as “linear", and“non-linear". A system is called linear when its output is directly proportional to its input (Fig. 5.1a). On the other hand, a non-linear system is a system which does not satisfy the superposition principle (Fig. 5.1b). This can easily be understood using Ohms law, the supplied voltage V across a resistor R is directly proportional to the generated current I, thus the relationship between current and voltage is said to be linear (Eq. 5.1); concurrently looking at the problem from another perspective the current is not directly proportional to the power P thus the relationship between power and current is non-linear (Eq. 5.2).

Now, depending on the *a priori* knowledge of the modeller about the system, there are two major modelling approaches that can be followed, these are the “parametric" and “non-parametric" methods. A model structure is called parametric (or deterministic) when the functional relationship of the model inputs,

[1] International Federation of Automatic Control.

outputs and parameters is known *a priori*; good examples of parametric models are those derived from physics principles. From identification point of view, when the model structure is already known, then the identification problem is limited to the estimation of the model parameters using the observed input/output data. The parametric models offer a number of advantages when it comes down to the identification of the parameters, however they can give results with large errors if the parametrisation is not carried out carefully [162]. On the contrary, non-parametric (or stochastic) approaches attempt to model the characteristics of partially unknown systems based on parametrised families of probability distributions. The main practical difference to parametric models is that non-parametric models do not have a fixed number of parameters, instead the number of parameters grows with the amount of the training data. Some examples of non-parametric techniques are artificial neural networks, kernel estimation and spline regression [163].

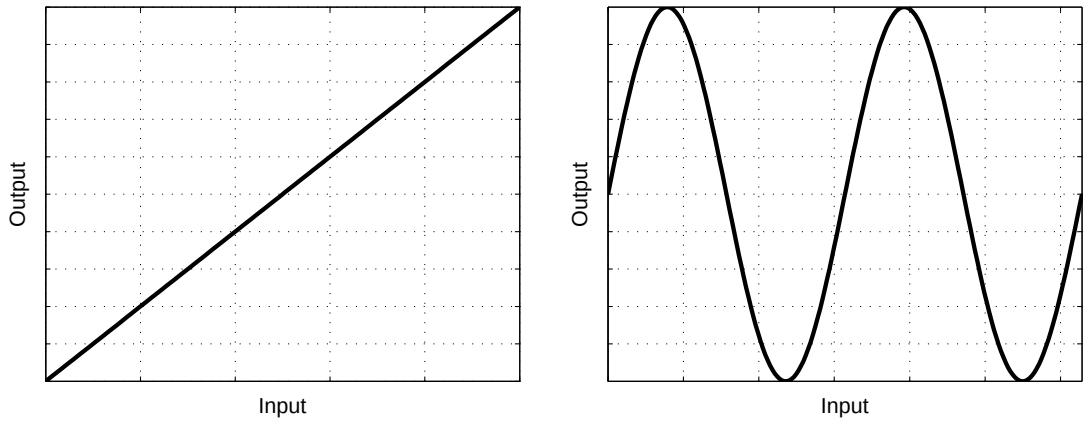

(a) Linear system **(b)** Non-linear system

Figure 5.1: Typical input/output relation of linear and non-linear systems.

$$I = \frac{V}{R} \tag{5.1}$$

$$P = I^2 R \tag{5.2}$$

At this point in time, the reader should be aware that the system identification tools that will be presented in this thesis are mainly applicable to parametric model

structures. That is because the presented work is intended for powertrain systems that can be modelled based on physics principles.

From identification point of view, when parametric models are used to describe the response of a system, two different types of models can be determined, the linear-in-the-parameter (Eq. 5.3) models and the non-linear-in-the-parameter models (Eq. 5.4). Additionally, as it is more robust and convinient to estimate linear-in-the-parameter models, it is usually the case to transform the non-linear parameter into linear, this category of models in known as “intrinsically linear" (Eq. 5.5) [162]. The above categorisation is useful especially when someone is involved in the business of assigning system identification tools for the estimation of the model parameters. The technical details regarding the parameter estimation for both types of models is the main subject of interest in the following sections of this chapter.

$$y(t) = \vartheta_1 u_1(t) + \vartheta_2 u_2(t) \tag{5.3}$$

$$y(t) = \frac{u_1(t)}{\vartheta_1} + \sin(\vartheta_2) u_2(t) \tag{5.4}$$

$$y(t) = \frac{1}{\vartheta_1} u_1(t) + \vartheta_2 u_2(t) \Leftrightarrow y(t) = \alpha u_1(t) + \vartheta_2 u_2(t) \tag{5.5}$$

Where, $y(t)$ is the model output (or dependent variable), $u_1(t)$ and $u_2(t)$ are the model inputs (or dependent variables), ϑ_1 and ϑ_2 are said to be the parameters of the model; note that the parameter $a = \frac{1}{\vartheta_1}$.

Lastly, depending on the “memory” of the system response with respect to its inputs it is possible to distinguish two types of systems, the static and the dynamic. Static systems are memoryless, meaning that the output of the system depends only on its input at that instant point in time. On the other hand, dynamic models are not affected only by the current inputs but also by the past. In general, the tools for the identification of static and dynamic parametric models share the same principles [164]. Nevertheless, when an individual is interested particularly on the identification of dynamic models from input/output observation data, it is crucial to make sure that the sampling time of the data acquisition system is significantly less than the duration of the actual dynamic phenomenon that

needs to be described. Henceforth, if the sampling time is not carefully selected, the identification of the dynamic model would be indeed inevitability wrong (see Chapter 4, Section 4.4.1 for instructions regarding the selection of an adequate sampling time).

5.1.2 Classification Based on Implementation Method

Depending on the very specific requirements of the user, it is possible to implement system identification tools either in an “off-line" or in an “on-line" fashion. The term off-line comes from the fact that in order to identify the parameters of a mathematical model, it is necessary to collect, store, evaluate and finally process a batch of experimental input/output measurements. As it can be understood, this implies that the identification of the mathematical model cannot be done at the same time with the operation of the examined system. Off-line approaches can be further separated into “direct" methods and “iterative” methods. Direct methods attempt to estimate the model parameter in one pass, while iterative methods determine the model step-wise which means that the data must be processed multiple times [158]. The main practical applications of off-line methods are model fitting and validation, system analysis, synthesis and optimisation. On the contrary, on-line mechanisms identify the parameters of the model in parallel with the operation of the actual system. More specifically, on-line identification schemes update the model as each measurement becomes available. These approaches are also known as “recursive", or “real-time", or “adaptive". Adaptive identification techniques are mainly applicable to deterministic model structures, however recent publications show the implementation of recursive algorithms in non-parametric models as well [165]. On-line identification algorithms are of great importance to practical applications that require the identification of the model parameters in real-time, such as fault detection and isolation, characterisation, input reconstruction, and adaptive control [166].

We shall restrict our attention to on-line techniques as the focus of the present study is on the application of adaptive identification algorithms to linear and non-

linear parametric physics-based powertrain models for monitoring and characterisation purposes.

5.1.3 Qualitative System Identification

According to classical system identification frameworks (e.g. see Fig. 1-10 in [160]), prior to the actual approximation of a system model it is necessary to select a model structure that can be parametrised sufficiently using a set of a given input/output observation data. This step is particularly important to non-parametric mathematical models where the modeller does not have prior knowledge about the input/output functional relationship and the parameters of the system [167]. On the other hand when someone is working with parametric models, the structure of the system is known beforehand. Especially in the case of physically oriented models, the model structure is fixed since it is derived from physics principles. At this point, the reader should be informed that methods for model structure selection are not going to be discussed in details in this thesis as we mainly work with physical and semi-physical model structures.

Nevertheless, it would be rather naive to assume that parametric or more specifically physics-based and semi-physical models can be identified for any given input/output observation data. From identification point of view, one of the biggest advantages of parametric model structures is that the mathematical relationship between inputs/outputs and parameters is known. In fact this advanced knowledge about the system allows the design of optimal experiments for the identification of the given parametric model in the minimum time [168]. What happens though when the careful design of an optimal or even a “suitable" experiment is not an option? What happens if the acquired observation data rely upon unplanned process records? As a matter of fact, according to Ljung [158] this one of the central unsolved system identification problems in industrial applications. Take as an example the monitoring of a process in a production line based on the adaptive identification of a physical model; if the quality of the process records i.e. input/output data, is not sufficient then the identified model would be inevitably

wrong leading to mistaken diagnostics.

In the following section the derivation and use of system identification tools for identifiability analysis of physics-based powertrain model parameters will be provided.

5.2 Parameter Identifiability

An important but often overlooked step in the identification of parameters with physical meaning - as well as parameter with mathematical meaning e.g. regression coefficients - is to assess their identifiability. A simple example, based on circuit theory (Fig. 5.2), could help to understand the main reason that we need to develop tools that can evaluate the identifiability of model parameters with physical interpretation. Notice then that, given measurements of $\mathrm{V}(t)$ and $\mathrm{I}(t)$ we can only identify the sum of the resistors, $\mathrm{R}_1 + \mathrm{R}_2$. Consequently, we cannot uniquely estimate each individual parameter from the data. In such cases the parameters R_1 and R_2 are called “unidentifiable".

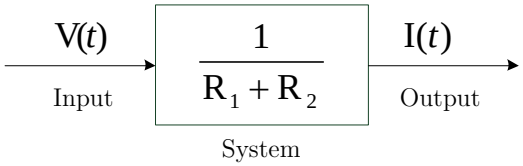

Figure 5.2: Identifiability of simple circuit model parameters.

The example in Fig. 5.2 represents a simple system that someone could easily determine whether its parameters could be identified uniquely using observation measurements or not. In fact, most of the real world systems are described according to complex models with more inputs, outputs and parameters. In that cases, the identifiability of the parameters cannot be assess based on simple observations of the user. Therefore analysis and synthesis algorithms have been developed throughout the years that allow the evaluation of the identifiability of model parameters mathematically. A formal definition of the problem areas that identifiability analysis is concerned in given bellow [160].

Definition 5.1 (Identifiability)**.** *Identifiability is concerned with two problems, the first is about the model structure ("structural identifiability") i.e. is it possible to invert the model and distinguish the desired parameters given the best possible input/output observation data? The second leg is addressing the quality of the measurements ("practical identifiability") i.e. are the data informative enough with the purpose of identifying the parameters of the model?*

Several approaches have been addressed in the past to assess the identifiability of model parameters. The structural identifiability problem is more fundamental than the practical identifiability problem, in that it represents a best-case scenario for practical identifiability analysis, and also more analytically tractable, with well defined formulations for linear and non-linear systems [169–173]. On the other hand the problem of practical identifiability considers whether experimental noise and information content of the observation will allow parameters that may be structurally identifiable to be resolved to a level of certainty. Practical identifiability could be handled by computing analytically or numerically the Fisher Information Matrix, the covariance matrix, or the Hessian of the corresponding least square function [174–177].

There is indeed a huge amount of literature in the area of identifiability analysis for linear and non-linear systems. Nevertheless, there are intuitive gaps in the underlying causes of both structural and practical identifiability. Although practical identifiability is fundamentally problem of experimental noise, understanding model sensitivity to parameter variation in most cases involves performing complex analytical and often numerical calculations. In cases of structural identifiability, many of the analytic approaches allow straight-forward computation of the binary identifiability/non-identifiability (qualitative analysis) of model parameters, however it is often the case that these approaches miss a broad intuition of what underlying mechanics of model allows or does not allow the determination of the parameters [178]. Additionally, the computational complexity of some well known methods increases exponentially with the number of model parameters which makes them impractical to be applied by the practising engineers in real

industrial problems [179, 180].

A relatively new algorithm [181] was deployed in this thesis to evaluate the structural as well as practical identifiability of model parameters. The theoretical foundation of this methodology is presented in the following section.

5.2.1 Orthogonal-Based Parameter Identifiability

The orthogonal-based parameter identifiability analysis is a simple and convenient tool, which was first introduced by Yao et al. [181], to assess the qualitative identifiability [182] of the model parameters in respect of the model structure and quality of observation data. Since then it has been applied in numerous chemical and biological applications [181, 183, 184], however applications related to vehicle powertrains have not yet been reported. As a matter of fact, this was one of the reasons that was chosen in this thesis with the purpose of investigating its applicability in the area of powertrain identification and control.

The orthogonal method for parameter identifiability is an approach based on sensitivity analysis. Sensitivity analysis is used for determining the relationship between a change in the parameters and the corresponding change to the system response. This is achieved by evaluating the partial derivatives of the model responses/states with respect to the model parameters, known as sensitivity coefficients. Sensitivity coefficients, the elements of the sensitivity matrix, are calculated analytically or numerically local at-a-point [185].

Definition 5.2 (Orthogonal-Based Parameter Identifiability)**.** *Practically, the orthogonal-based parameter identifiability method describes two things, first which of the parameters have higher sensitivity to the system output, in a prioritized list, and then which of the parameters are linearly independent for a given set of observation data.*

Having described the principle idea of the orthogonal-based parameter identifiability, it is now possible to present the formal mathematical description. Con-

sider a physical system that is described based on the following model:

$$y(t) = h(x(t), u(t), \vartheta) + \epsilon(t) \tag{5.6}$$

Where, $y(t)$ is the model output over time, $h(x(t), u(t), \vartheta)$ is the corresponding expected value of the response variable which is determined by the state variables $x(t)$, the control inputs $u(t)$, and the model parameters ϑ. Lastly, $\epsilon(t)$ is a random error term.

As it was mentioned previously, identifiability analysis is closely linked to sensitivity analysis. In fact, parameters can be estimated if and only if the sensitivity coefficients are not linearly dependent [186]. The sensitivity coefficient are the partial derivatives of the model response in respect to the model parameters and can be calculated either analytically or numerically depending on our prior knowledge about the system model:

$$\frac{\partial h(x(t), u(t), \vartheta)}{\partial \vartheta_p} \tag{5.7}$$

Here, p represents the corresponding model parameter i.e. $1, 2, ..., p_t$, where p_t is the total number of parameters.

Next, the calculation of each individual sensitivity coefficient allows the formation of the sensitivity matrix, also known as the Jacobian matrix (J):

$$J = \begin{bmatrix} \frac{\partial h(x(t_1), u(t_1), \vartheta)}{\partial \vartheta_1} & \frac{\partial h(x(t_1), u(t_1), \vartheta)}{\partial \vartheta_2} & \cdots & \frac{\partial h(x(t_1), u(t_1), \vartheta)}{\partial \vartheta_{p_t}} \\ \frac{\partial h(x(t_2), u(t_2), \vartheta)}{\partial \vartheta_1} & \frac{\partial h(x(t_2), u(t_2), \vartheta)}{\partial \vartheta_2} & \cdots & \frac{\partial h(x(t_2), u(t_2), \vartheta)}{\partial \vartheta_{p_t}} \\ \vdots & \vdots & \ddots & \vdots \\ \frac{\partial h(x(t_n), u(t_n), \vartheta)}{\partial \vartheta_1} & \frac{\partial h(x(t_n), u(t_n), \vartheta)}{\partial \vartheta_2} & \cdots & \frac{\partial h(x(t_n), u(t_n), \vartheta)}{\partial \vartheta_{p_t}} \end{bmatrix} \tag{5.8}$$

Note that the sensitivity matrix is calculated for each time step t i.e. $t_1, t_2, \ldots, t_n$, where n is the total number of samples.

Following the evaluation of the sensitivity matrix, the method iterates over the columns of the sensitivity matrix (J) to select the column with the highest sum of squared value. Since each column corresponds to a single parameter, this

corresponds to the parameter that has the highest impact on the model output. This column is added to the matrix (X_L) (L being the iteration number), in the order of the highest to the lowest sensitivity. Next, all of the original columns of J are being regressed on the column associated with the most estimable parameter (denoted $\hat{J}_L$). A residual matrix (R_L) is calculated to measure the orthogonal distance between J and the regression matrix $\hat{J}_L$. The column having the highest sum of squared value in the residual matrix R_L is chosen to be the next most estimable parameter. The steps are repeated until a specific cut-off value (related to the quality of observation data) of R_L is reached or until all the parameters have been selected as identifiable. The algorithm is as follows:

Algorithm 5.1 Orthogonal-Based Parameter Identifiability

1: Calculate the sensitivity matrix J.
2: Calculate the sum of squares (SS) of the J matrix (Eq. 5.9), i.e. the sum of square of each individual column, $SS_{J_{1\ldots p_t}} = \sum_{i=1}^{n} \left(J_{1\ldots p_t}|_{t_i} - \bar{J}_{1\ldots p_t}\right)^2$:

$$SS_J = \begin{bmatrix} SS_{J_1} & SS_{J_2} & \ldots & SS_{J_{p_t}} \end{bmatrix} \tag{5.9}$$

3: Peak the column (sensitivity coefficient), in J which has the largest sum of squared value as the first parameter. This parameter is considered to have the most effect on model predictions.
4: Mark the corresponding column as X_L ($L = 1$ for the first iteration).
5: Calculate $\hat{J}_L$, the least squares prediction of the full sensitivity matrix, J, using the matrix X_L:

$$\hat{J}_L = X_L \left({X_L}^T X_L\right)^{-1} X_L J \tag{5.10}$$

6: The residual matrix, $R_L = J - \hat{J}_L$, is calculated as measure of independence.
7: The column with the largest magnitude in R_L corresponds to the next parameter (among the remaining parameters) which has the largest effect on the response variable and which is not correlated with the effects of the parameters already selected.
8: Select the corresponding column in J and augment the matrix X_L by making the new column.
9: Repeat the last four steps iteratively until a pre-defined cut-off value of the residual matrix R_L is reached.

Example 5.1 Orthogonal-Based Parameter Identifiability

Given the following parametric model:

$$z(t) = \sin(A)x(t) + B^2 y(t)\cos(x(t)) + \sqrt{C}x(t)^2 + Dy(t)^2 + E\frac{x(t)}{y(t)} + F\frac{2x(t)}{y(t)}$$

Where, $z(t)$ is the dependent variable (output), $x(t)$ and $y(t)$ are the independent variables (inputs), and A, B, C, D, E, F are the model parameters.

Examine the identifiability of the model parameters subject to the following input conditions i.e. $x(t)$ and $y(t)$,

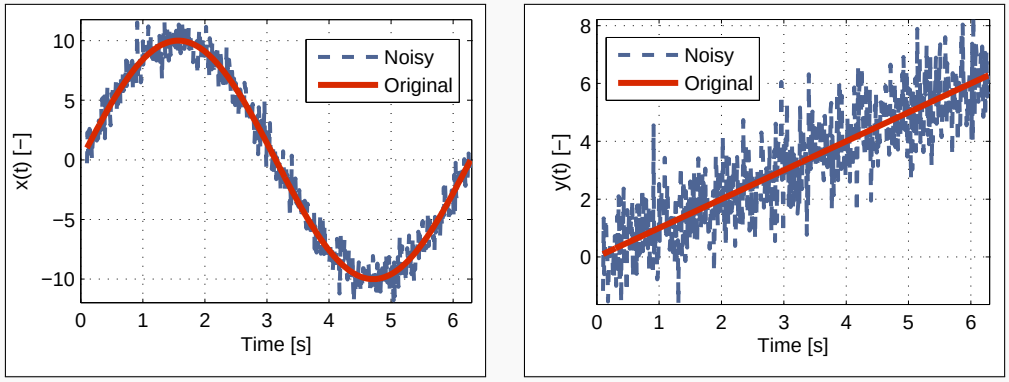

(a) $x(t)$ **(b)** $y(t)$

Figure 5.3: Input conditions.

Note that, white Gaussian noise with zero mean and unit variance was added in the original input signals to emulate real life conditions.

Solution

According to Algorithm 5.1, the first step is the calculation of the sensitivity matrix. Here it is possible to calculate the individual sensitivity coefficients analytically as we know the functional relationship of the system model. The sensitivity coefficients are given bellow:

$$\frac{\partial z(t)}{\partial A} = x(t)\cos(A), \quad \frac{\partial z(t)}{\partial B} = 2y(t)B\cos\left(x(t)\right), \quad \frac{\partial z(t)}{\partial C} = \frac{x^2(t)}{2\sqrt{C}},$$
$$\frac{\partial z(t)}{\partial D} = y^2(t), \quad \frac{\partial z(t)}{\partial E} = \frac{x(t)}{y(t)}, \quad \frac{\partial z(t)}{\partial F} = \frac{2x(t)}{y(t)}$$

The sensitivity matrix J is then formed as follows:

$$J = \begin{bmatrix} \frac{\partial z(t_1)}{\partial A} & \frac{\partial z(t_1)}{\partial B} & \frac{\partial z(t_1)}{\partial C} & \frac{\partial z(t_1)}{\partial D} & \frac{\partial z(t_1)}{\partial E} & \frac{\partial z(t_1)}{\partial F} \\ \frac{\partial z(t_2)}{\partial A} & \frac{\partial z(t_2)}{\partial B} & \frac{\partial z(t_2)}{\partial C} & \frac{\partial z(t_2)}{\partial D} & \frac{\partial z(t_2)}{\partial E} & \frac{\partial z(t_2)}{\partial F} \\ \vdots & \vdots & \vdots & \vdots & \vdots & \vdots \\ \frac{\partial z(t_n)}{\partial A} & \frac{\partial z(t_n)}{\partial B} & \frac{\partial z(t_n)}{\partial C} & \frac{\partial z(t_n)}{\partial D} & \frac{\partial z(t_n)}{\partial E} & \frac{\partial z(t_n)}{\partial F} \end{bmatrix}$$

The second step requires the calculation of sum of squares (SS) of each column (i.e. the corresponding parameter) of the J matrix. For that, we need to use the inputs $x(t)$ and $y(t)$ that were given in Fig. 5.3, additionally an initial estimate of the model parameters is needed, thus in this exercise the values of the parameters are assumed:

$$A = 1,\ B = 2,\ C = 3,\ D = 4,\ E = 5, \text{ and } F = 6.$$

Now following the rest of the steps i.e. 3 to 9, of Algorithm 5.1 allows the evaluation of the identifiable parameters in a prioritised list with respect to the parameter sensitivity to the model output:

$$\text{Identifiable Parameters} = \begin{bmatrix} D & C & B & A & F \end{bmatrix}$$

Notice that not all the parameters of the model are identifiable in the given model structure and for the given input data. In particular the unidentifiable parameter is E. This is because the sensitivity coefficient which corresponds to this parameter is linearly dependent to the sensitivity coefficient of the parameter F. This can also be seen by observing the actual sensitivity coefficients of the parameters $E\left(\frac{x(t)}{y(t)}\right)$ and $F\left(\frac{2x(t)}{y(t)}\right)$; the sensitivity coefficients are linearly linked by a factor of 2. Furthermore the parameter with the most effect on the system output for the given inputs is D while parameters C, B, A and F follow in a descending order.

Lastly, it should be mentioned that in the case of the identifiability analysis the sensitivity coefficients are normalised usually with respect to the initial conditions of the corresponding parameter. This is important because the suggested approach relies upon the calculation of the sum of squared value of each individual sensitivity coefficient, which indicates that any possible numerical issues would provide misleading results. Additionally the scaling is critical when the parameters under examinination have different physical units (Eq. 5.11).

$$\frac{\partial h(x(t_n), u(t_n), \vartheta)}{\partial \vartheta_p} * \frac{\hat{\vartheta_p}}{h(x(t_n), u(t_n), \vartheta)} \tag{5.11}$$

Where $\hat{\vartheta_p}$ is either an initial guess and $h(x(t_n), u(t_n), \vartheta)$ is the value of the response variable at time t_n.

5.2.2 Identifiability & Experimental Design

In the previous section an algorithm (Algorithm 5.1) for identifying a subset of identifiable parameters for a given model structure and observation data was given. This algorithm is particularly useful when someone wants to evaluate the quality of process records (e.g. measurements from the production line) prior to the use of the data for any identification application; this problem was also recently addressed by Ljung [158].

Another central issue in identification problems is the experimental design. In many cases it is possible to design and execute an “optimal" experiment that allows the accurate estimation of model parameters in the minimum time possible. Thankfully, identifiability analysis is also closely related to the area of optimal experimental design as the sensitivity coefficient matrix (J) is used in both types of analysis [187]. In particular, the sensitivity coefficient matrix (J) is used for the calculation of the Fisher information matrix (I_F) (Eq. 5.12). The Fisher information matrix essentially describes the amount of information data provide about an unknown parameter (ϑ) of a system e.g. Eq. 5.6 and is often utilised for describing parameter confidence region and design of experiments.

$$I_F = J^T \Sigma^{-1} J \tag{5.12}$$

Where, Σ is the variance-covariance matrix of the response variable $(y(t))$.

The information matrix forms the basis for many optimal experimental design criteria. One of the most widely used design criteria is the D-optimality design criterion [188] which aims on the minimisation of the joint confidence region size for the model parameters by maximising the absolute Fisher information matrix (Eq. 5.13), the smaller the joint confidence region, the more precisely the parameters are estimated.

$$\text{D-Optimality} = \max |I_F| \tag{5.13}$$

There are indeed numerous others criteria that can be used for the optimal design of experiments such as A-optimal, C-optimal, G-optimal, I-optimal, V-optimal etc. [188]. In engine calibration applications some of the most used criteria are the D-optimal, the V-optimal, and G-optimal [78].

5.3 Adaptive Identification

The information gained from the orthogonal-based parameter identifiability analysis allows to processed to the qualitative identification of the model parameters. Tools for the adaptive identification of parameters with physical and semi-physical interpretation that can be found generally in physics-based powertrain models will be presented in this section. As aforementioned adaptive identification allows the estimation of model parameters in parallel to the operation of the actual system. This is particularly useful for the design of adaptive controllers and system diagnostics in cases where the parameters of the system represent physical characteristics. Identification techniques that comply with this requirement are often called “recursive identification methods", since the measured input-output data are processed recursively as they become available [166].

Definition 5.3 (Recursive Identification Methods)**.** *Suppose we have an initial estimate $\hat{\vartheta}_{t-1}$ at iteration $t-1$, then recursive identification aims to compute a new estimate $\hat{\vartheta}_t$ by modifying $\hat{\vartheta}_{t-1}$ when a new observation becomes available at iteration t.*

According to the above definition (Definition 5.3) it can be understood that recursive techniques are mainly applicable to discrete systems (either dynamic or static) as their update mechanism requires the knowledge of the past as well as the present observations. Another common characteristic of recursive approaches is about the class of systems that can be implemented, in particular recursive techniques are mainly suitable for parametric model structures instead of non-parametric models. The main reason for that is because for the implementation of such methods it necessary to known the number of model parameters *a-priori*. Furthermore, depending on whether the system is linear-in-the-parameters or nonlinear-in-the-parameters the complexity and computational cost of the adaptive identification algorithms can vary significantly.

There is a substantial literature on recursive estimation techniques, for general treatments there are books [159, 164, 166, 189–191] to name few. In the following sections will be presented numerous recursive identification algorithms and will be categorised with respect to the nature of the system model parameters i.e. linear-in-the-parameter systems and nonlinear-in-the-parameter systems. Additionally, the practical application of the presented algorithms is demonstrated in Chapters 6, 7, and 8.

5.3.1 Linear-in-the-Parameter Systems

To demonstrate the principle idea of recursive identification for linear-in-the-parameter systems, let us consider the following linear regression model:

$$y(t) = \phi^T(t)\vartheta + \epsilon(t) \tag{5.14}$$

Where, $\phi(t)$ is the vector of observation variables, $y(t)$ is the system response, ϑ is the vector that contains the model parameters which are to be estimated/tracked using the recursive estimator, and $\epsilon(t)$ is a random error term.

Now, assume that there is a true and time varying value $\vartheta(t)$ for the parameters and that these parameters develop over time randomly. This indicates that the true representation of the system presented in Eq. 5.14 becomes [192]:

$$\vartheta(t) = \vartheta(t-1) + w(t) \tag{5.15a}$$

$$y(t) = \phi^T(t)\vartheta(t) + \epsilon(t) \tag{5.15b}$$

Here, $\epsilon(t)$ is the observation noise term i.e white Gaussian noise with zero mean and covariance $R_2(t)$, $(\epsilon(t) \sim N(0, R_2(t)))$, and $w(t)$ is the parameter/process noise term i.e. white Gaussian noise with zero mean and covariance matrix $R_1(t)$, $(w(t) \sim N(0, R_1(t)))$. Under those assumptions, the estimate $\hat{\vartheta}(t)$ that minimises the conditional expectation (Eq. 5.16), given past observations, is given by the Kalman filter [166].

$$\mathbb{E}\left(\hat{\vartheta}(t) - \vartheta(t)\right)\left(\hat{\vartheta}(t) - \vartheta(t)\right)^T \tag{5.16}$$

In particular the conventional Kalman filter for estimating the states of a discrete dynamic system (Eq. 5.17),

$$\begin{aligned} x(t+1) &= Ax(t) + Bu(t) + w(t) \\ y(t) &= Cx(t) + \epsilon(t) \end{aligned} \tag{5.17}$$

is given by (Eq. 5.18),

$$\hat{x}(t+1) = A\hat{x}(t) + Bu(t) + K(t)\left[y(t) - C(t)\hat{x}(t)\right] \tag{5.18a}$$

$$K(t) = AP(t)C^T\left[CP(t)C^t + R_2(t)\right]^{-1} \tag{5.18b}$$

$$P(t+1) = R_1(t) + AP(t)A^T - K(t)\left(CP(t)C^T\right)K^T(t) \tag{5.18c}$$

Where, $\hat{x}(t)$ is the state estimates, $K(t)$ is the Kalman gain, and $P(t)$ is the covariance matrix of the updated state estimates.

Now, the Kalman filter (Eq. 5.18) can be used for the estimation of the parameters of the linear regression problem (Eq. 5.14) by setting,

$$\hat{x}(t) = \hat{\vartheta}(t), \qquad A = I, \qquad B = 0, \qquad C = \phi(t)$$

This allows the formulation of a general optimal tracking recursive algorithm for linear-in-the-parameter models as follows (Eq. 5.19):

$$\hat{\vartheta}(t) = \hat{\vartheta}(t-1) + K(t)\left[y(t) - \varphi^T(t)\hat{\vartheta}(t-1)\right] \tag{5.19a}$$

$$K(t) = P(t-1)\varphi(t)\left[R_2(t) + \varphi^T(t)P(t-1)\varphi(t)\right]^{-1} \tag{5.19b}$$

$$P(t) = P(t-1) - \left[K(t)\varphi^T(t)P(t-1)\right] + R_1(t) \tag{5.19c}$$

Notice that for the execution of the above recursive algorithm it is required to have an initial estimate for the model parameters $(\hat{\vartheta}(0) = \vartheta_0)$ and the covariance matrix $(P(0) = P_0)$. Furthermore the values of the observation covariance $(R_1(t))$ and the parameter/process covariance matrix $(R_2(t))$ need to be carefully selected in order to track the parameter estimates effectively. For example the appropriate selection of these matrices would enable the identification of systems with sudden changes and time-varying parameters. However these values will rarely be known explicitly to the user, hence some ad-hoc values will have to be chosen [192]. Numerous ad-hoc alternatives can be found in literature, some of the most well known and robust methods will be presented in the following paragraphs. For more detailed derivation and convergence proof see [166].

Recursive Least Squares (RLS)

The standard recursive least squares is the most well known recursive identification algorithm. The principal idea here is the minimisation of the sum of the least squares error between the observed $(y(t))$ and calculated responses $(\phi^T(t)\hat{\vartheta}(t-1))$ by continually (recursively) adjusting the parameters of the model (Eq. 5.20),(Fig. 5.4), [193].

$$\min_{\hat{\vartheta}} \sum_{t=0}^{n} e^2(t) \equiv \min_{\hat{\vartheta}} \sum_{t=0}^{n} \left[y(t) - \phi^T(t)\hat{\vartheta}(t-1) \right]^2 \tag{5.20}$$

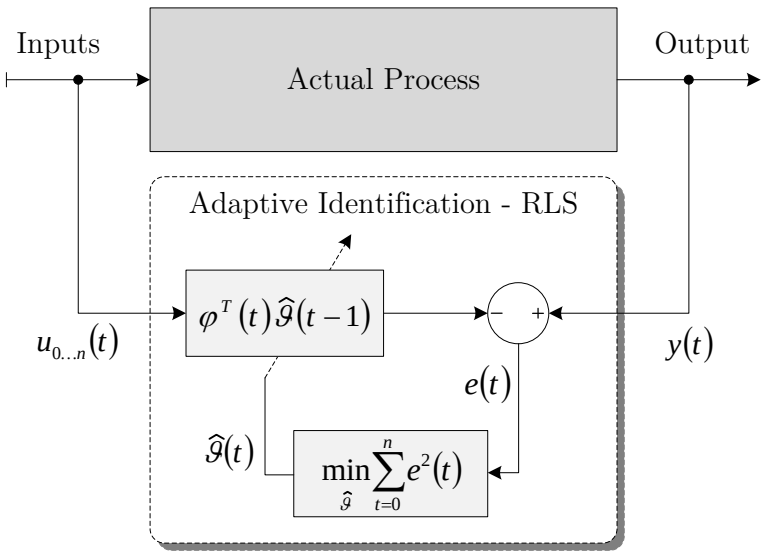

Figure 5.4: Adaptive identification using RLS algorithm, schematic diagram.

The algorithm is identical to the Kalman filtering approached (Eq. 5.19) with the main difference located on the values of the covariance $(R_1(t))$ and the variance matrix $(R_2(t))$. In particular the measurement covariance matrix is assumed to be zero $(R_1(t) = 0)$ while the parameter covariance matrix is set equal to one $(R_2(t) = 1)$. Under those circumstances the RLS algorithm is mainly applicable to systems models where the parameter are constant i.e. they don't vary overtime. Practically this means that the standard RLS would not serve us with the best tool for condition monitoring purposes as it would not track possible changes due to system malfunctions. On the other hand, in case where parameter changes are not expected, then it is indeed a very simple and convenient algorithm to use. The RLS algorithm is summarised bellow:

Algorithm 5.2 Recursive Least Squares - RLS

Require: *Initialisation*

$$\hat{\vartheta}(0) = \vartheta_0$$
$$P(0) = P_0$$

Ensure: *Implementation*

$$\hat{\vartheta}(t) = \hat{\vartheta}(t-1) + K(t)\left[y(t) - \varphi^T(t)\hat{\vartheta}(t-1)\right]$$
$$K(t) = P(t-1)\varphi(t)\left[1 + \varphi^T(t)P(t-1)\varphi(t)\right]^{-1}$$
$$P(t) = P(t-1) - \left[K(t)\varphi^T(t)P(t-1)\right]$$

As it can be seen in Algorithm 5.2 prior to the implementation of the RLS it is required to have initial estimates of the model parameters (ϑ_0) and the update covariance matrix (P_0). These initial estimates are determined based on the level of the *a-priori* knowledge of the user about the system, in cases where there is no knowledge at all, then some preliminary off-line identification exercise might be beneficial to gain some understanding. However if preliminary off-line identification cannot be conducted it is common practice to use:

$$\hat{\vartheta}(0) = 0_{1,p_t} \qquad\qquad P(0) = cI_{p_t}$$

Where the subscript p_t is the total number of parameters, $0_{1,p_t}$ is a zero matrix with one row and p_t number of columns, I_{p_t} is an identity matrix of size p_t, and the parameter c is a constant that represents our confidence in the initial parameter estimates i.e. the more accurate the initial parameter estimates the lower the value of c.

RLS with Forgetting (RLSF)

One of the main disadvantages of the standard RLS algorithm is its incapacity to track time-varying system parameters. The so call RLS with Forgetting (RLSF) factor algorithm is another version of the standard RLS that allows the tracking of slowly time-varying parameters. The main difference compared to the standard RLS is located on the least squares minimisation criterion [192]:

$$\min_{\hat{\vartheta}} \sum_{t=0}^{n} \lambda^{n-t} e^2(t) \equiv \min_{\hat{\vartheta}} \sum_{t=0}^{n} \lambda^{n-t} \left[y(t) - \phi^T(t)\hat{\vartheta}(t-1) \right]^2 \tag{5.22}$$

Where, λ is the so called forgetting factor which is exponentially proportional to the number of samples n, and $0 < \lambda \leq 1$.

Algorithm 5.3 RLS with Forgetting - RLSF

Require: *Initialisation*

$$\begin{aligned} \hat{\vartheta}(0) &= \vartheta_0 \\ P(0) &= P_0 \\ 0 &< \lambda \leq 1 \end{aligned}$$

Ensure: *Implementation*

$$\begin{aligned} \hat{\vartheta}(t) &= \hat{\vartheta}(t-1) + K(t) \left[y(t) - \varphi^T(t)\hat{\vartheta}(t-1) \right] \\ K(t) &= P(t-1)\varphi(t) \left[\lambda + \varphi^T(t)P(t-1)\varphi(t) \right]^{-1} \\ P(t) &= \lambda^{-1} \left\{ P(t-1) - \left[K(t)\varphi^T(t)P(t-1) \right] \right\} \end{aligned}$$

The parameter estimates $(\hat{\vartheta})$ can be calculated recursively by slightly modifying the classical RLS update equations (Algorithm 5.3). Practically the main difference with the classical RLS method is how the covariance matrix $(P(t))$ is

updated. In the classical RLS the covariance vanishes to zero with time, losing it capability to keep track changes in the parameter. In RLSF however, the covariance matrix is divided by $\lambda \leq 1$ at each update which slows down fading out the covariance matrix. The smaller the forgetting factor (λ) the more sensitive is the estimator to parameter changes, nevertheless the selection of the forgetting factor is always characterised by a trade-off between the tracking ability and the noise sensitivity. Typical values vary from 0.92 to 0.99 depending on the system.

The RLSF has been widely used in estimation and tracking of time-varying parameters in various applications. However during poor system excitation old information is continuously forgotten while there is very little new dynamic information coming in, this leads to a practical issues known as “wind-up" problem. When wind-up problems occur the estimator becomes extremely sensitive due to exponential growth of the covariance matrix which eventually leads to numerical and computational errors [194]. In practice, it has been found advisable to replace the constant forgetting λ with a time-varying forgetting factor $\lambda(t)$ (Eq. 5.24) which is initially smaller than λ but approaches it asymptotically. In this manner, the fading memory of the algorithm is initially small and grows gradually as time progresses and more samples are processed. This ensures the eradication of any possible wind-up effects [189]. Further discussions on convergence of RLSF can be found in [195].

$$\lambda(t) = \lambda_0 \lambda(t-1) + (1 - \lambda_0) \tag{5.24}$$

with $\lambda(0) = \lambda_0 \in \{0, 1\}$, usually between 0.92 and 0.99.

RLS with Vector Forgetting (RLSVEF)

The estimator wind-up can also occur if we are estimating multiple parameters that each vary with different rate. To deal with this sort of problems it is necessary to have multiple forgetting factors in order to be able adjust the adaptation rate for each estimate independently. Such an ad-hoc remedy has been presented in a few publications and is known as vector-type forgetting [194, 196, 197], (Algorithm 5.4). The main idea is that instead of dividing the covariance matrix $(P(t))$

by a single forgetting factor (λ), is scaled by a diagonal matrix (Λ) of forgetting factors:

$$\Lambda = \text{diag}\left[\lambda_1, \lambda_2, ..., \lambda_{p_t}\right] \tag{5.25}$$

Where, p_t is the total number of model parameters; note that λ_i is the forgetting factor reflecting the rate of change of the i^{th} parameter.

Algorithm 5.4 RLS with Vector Forgetting - RLSVEF

Require: *Initialisation*

$$\begin{aligned}\hat{\vartheta}(0) &= \vartheta_0\\ P(0) &= P_0\\ 0 < &\lambda_i \leq 1\\ \Lambda = \text{diag}&\left[\lambda_1, \lambda_2, ..., \lambda_{p_t}\right]\end{aligned}$$

Ensure: *Implementation*

$$\begin{aligned}\hat{\vartheta}(t) &= \hat{\vartheta}(t-1) + K(t)\left[y(t) - \varphi^T(t)\hat{\vartheta}(t-1)\right]\\ K(t) &= P(t-1)\varphi(t)\left[1 + \varphi^T(t)P(t-1)\varphi(t)\right]^{-1}\\ P(t) &= \Lambda^{-1}\left\{P(t-1) - \left[K(t)\varphi^T(t)P(t-1)\right]\right\}\Lambda^{-1}\end{aligned}$$

Next in order to elucidate the functional differences among the presented algorithms we provide a rather simple, yet, illustrative example that compares the tracking performance of the RLS, RLSF and RLSVEF algorithms.

Example 5.2 Linear-in-the-Parameters Recursive Identification

Given the following linear-in-the-parameter system model:

$$z(t) = A(t)\sin\left(x(t)\right) + B(t)y^2(t)$$

Where, $z(t)$, $x(t)$ and $y(t)$ are observation variables i.e. inputs and outputs, $A(t)$ is a time-varying parameter ($A(t) = 10$ for $t \leq 5$ [s], and $A(t) = 4$ for $t > 5$ [s]), and $B(t)$ is a constant parameter $(B(t) = 0.5)$.

Identify and track the parameters of the system model using RLS, RLSF and RLSVEF algorithms, given the following operating conditions:

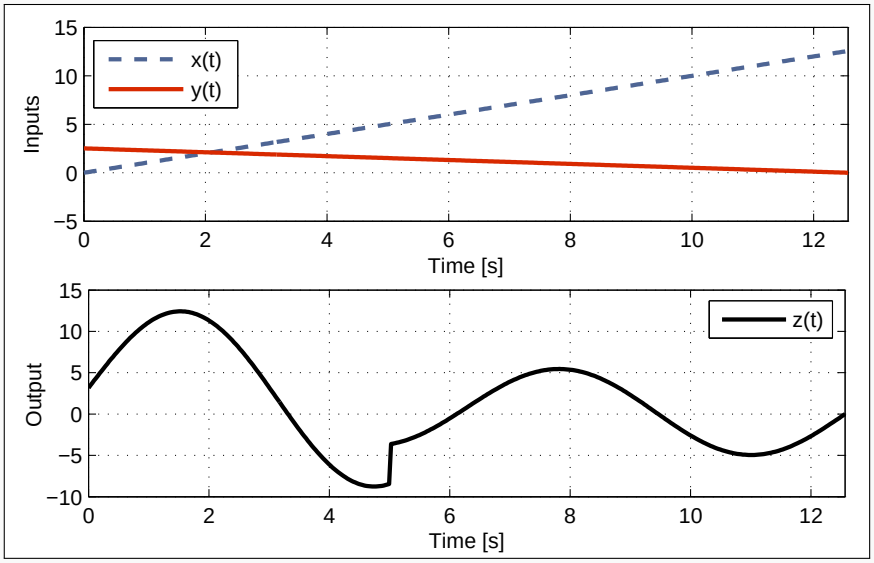

Figure 5.5: Input/output operational conditions.

Solution

First step prior to the implementation of the recursive algorithms is the formation of the vector of input variables and the system parameters.

$$\phi^T(t) = [x(t), y(t)]\,, \qquad \hat{\vartheta} = [A(t), B(t)]$$

Next for demonstration purposes we assume that we have zero knowledge about the system, thus we set the initial estimates of the parameter $(\theta(0))$ vector equal to zero. Additionally, since there is no confidence regarding the initial parameter estimates, we set the initial values of covariance matrix $(P(0))$ at relatively high values.

$$\vartheta(0) = [0, 0], \qquad P(0) = \begin{bmatrix} 10^3 & 0 \\ 0 & 10^3 \end{bmatrix}$$

Having defined the initial conditions of the parameter estimates and the covariance matrix it is now possible to implement the classical RLS algorithm. However, in order to execute the RLSF and the RLSVEF we need to define the corresponding forgetting factors. Thus in the case of the RLSF we will set the forgetting factor $\lambda = 0.97$, whilst for the RLSVEF the vector of forgetting factors will be $\Lambda = \text{diag}[0.97, 1]$. The forgetting factor of the

parameter $B(t)$ is set equal to 1 because this parameter is constant (see problem description at the begging of the example).

The results from the implementation of the recursive estimators are presented in Figure 5.6.

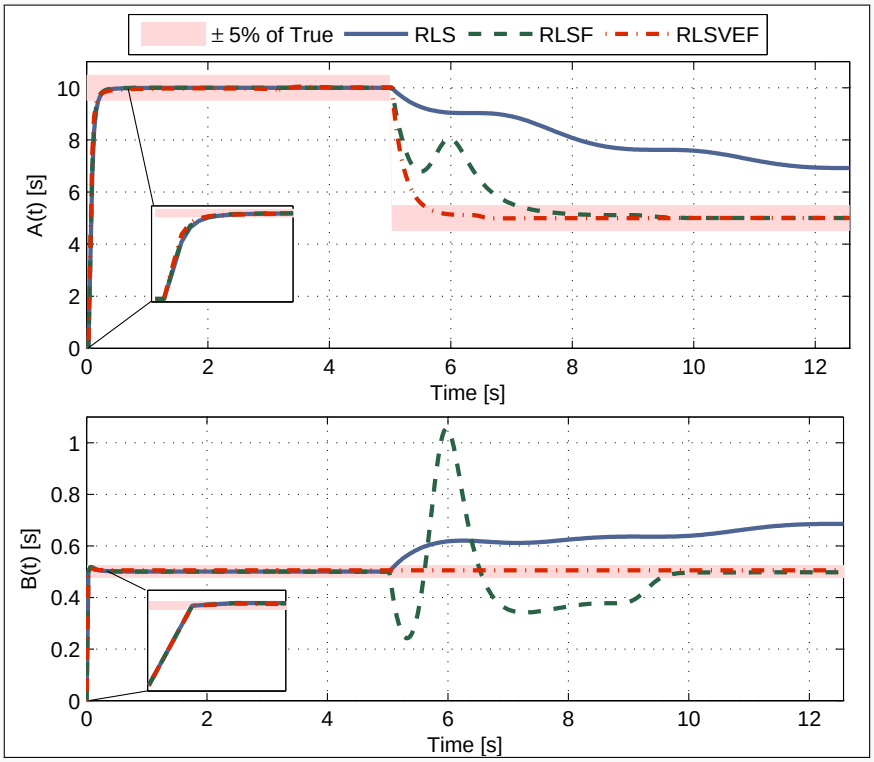

Figure 5.6: Comparison of RLS, RLSF, and RLSVEF algorithms.

The results in Figure 5.6 verify the various characteristics of each different recursive algorithm. As it observer at the 5^{th} second the parameter A changes from a value of 10 to 5 (see also the step change in the response of the system in Fig. 5.5) while the parameter B remains constant $(= 0.5)$ throughout the operation of the system. All of the recursive algorithm manage to identify the true parameters of the system within the first few seconds after the start of the simulation. However, when parameter A changes from 10 to 5 we can see that the RLS algorithm does not manage to track this parameter change (as expected) while the estimation of parameter B starts to diverge from the true value. On the other hand the RLSF algorithm shows better performance with respect to the tracking of parameter A during the

transition from one setting to the other, however a severe disturbance is observed in the estimation of parameter B during the transition of parameter A. This proves the inefficacy of this algorithm to track parameters that vary with different rate. Lastly, the RLSVEF fulfils the gaps of the algorithms RLS and RLSF with respect to tracking performance. It can be seen that the RLSVEF algorithms manages to track successfully parameter A while the estimation of parameter B is not affected. This is oriented from the fact that each parameter has its own forgetting factor.

Discrete Square Root Filtering in Covariance Form (DSFC)

A practical issue with the algorithms that have been presented up to now is related to the numerical aspects when it comes down to the implementation in real-world applications. The numerical properties are important if the word length is confined or if the changes of input signals become small, as in adaptive control or fault detection [159]. In such cases the source of problem is located in the propagation of the covariance matrix (P) by means of the Kalman filter equation (Eq. 5.18c) which results in a matrix that is not positive semidefinite. To circumvent this difficulty a method generally known as Discrete Square Root Filtering in Covariance Form (DSFC) was developed which propagates the covariance matrix (P) in a square root form. This approach can provide twice the precision of the conventional recursive estimators in ill-conditioned problems.

The main idea is to decompose the symmetric covariance matrix (P) in triangular matrices (S).

$$P = SS^T \tag{5.27}$$

Where S is known as the “square root".

This allows the rearrangement of the conventional recursive least squares formulation which leads to the DSFC algorithm (Algorithm 5.5). The starting values of the parameter estimates $(\hat{\vartheta}(0))$ obey the same rules as the previously reported algorithms. The initialisation of the square root $(S(0))$ is an identity matrix mul-

tiplied by the square root of a confidence constant i.e. $\sqrt{c}I_{p_t}$, where c is the confidence constant, and p_t is the total number of model parameters.

Algorithm 5.5 Discrete Square Root Filtering in Covariance Form - DSFC

Require: *Initialisation*

$$\begin{aligned}\hat{\vartheta}(0) &= \vartheta_0\\ S(0) &= S_0\\ 0 <&\lambda \leq 1\end{aligned}$$

Ensure: *Implementation*

$$\begin{aligned}\hat{\vartheta}(t) &= \hat{\vartheta}(t-1) + \gamma(t)\left[y(t) - \varphi^T(t)\hat{\vartheta}(t-1)\right]\\ \gamma(t) &= \alpha(t)S(t-1)f(t)\\ \alpha(t) &= \left[f^T(t)f(t) + \lambda\right]^{-1}\\ f(t) &= S^T(t-1)\phi(t)\\ S(t) &= \frac{S(t-1) - g(t)\gamma(t)f^T(t)}{\sqrt{\lambda}}\\ g(t) &= \frac{1}{1+\sqrt{\lambda a(t)}}\end{aligned}$$

Lastly it should be mentioned that apart from the DSFC algorithm there have been suggested numerous others square root filtering or factorisation approaches such as the “square root filtering in information form" or the so-called “UD factorisation". A detailed survey of the other available methods can be found in [198].

Additional Approaches & Bibliography

In the previous paragraphs there have been suggested numerous recursive algorithms that can be applied in linear-in-the-parameter system models with constant (RLS) as well as time-varying (RLSF;RLSVEF) parameters. Furthermore a recursive algorithm (DSFC) that can deal efficiently with ill-conditioned numerical problems, as in adaptive control or fault detection, were discussed. In addition to the already mentioned recursive algorithms there are still many other unmentioned alternative approaches that can be deployed in such problems. Some of

the most well known are the Recursive Instrumental Variable (RIV) method [199], the Recursive Maximum Likelihood (RML) method [200, 201], and the Recursive Prediction Error Method (RPEM) [166]. A laconic yet informative paper that summarises most of the recursive parameter estimators for linear-in-the-parameter systems can be found in [202].

At last is should be highlighted that all the above discussed algorithms can be applied equally in linear static as far as dynamic systems, as soon as the system can modelled in an analogous difference form. There is a vast number of examples in literature, some well known books [159, 166, 190] is used to enrich reader's knowledge on this particular subject.

5.3.2 Nonlinear-in-the-Parameter Systems

Linear recursive estimators were derived in Section 5.3.1. As a matter of fact many physical systems in powertrain applications are not absolutely linear. Following the considerable success enjoyed by linear estimation methods on linear-in-the-parameter problems, extensions of these methods are applied to such nonlinear systems. In this section, we investigate extension and approximation approaches for applying the methodology of optimal filtering to nonlinear-in-the-parameter system models. Prior to the presentation of the nonlinear recursive algorithms though, let us formulate the problem of nonlinear parameter estimation. For demonstration purposes consider the following nonlinear state-space regression model with possibly time-varying parameters:

$$\vartheta(t) = \vartheta(t-1) + w(t) \tag{5.29a}$$

$$y(t) = h\left(\phi(t), \vartheta(t)\right) + \epsilon(t) \tag{5.29b}$$

Where $y(t)$ is the model output over time, $h(\phi(t), \vartheta(t))$ is the corresponding expected value of the response variable which is defined by the vector of observed variables $\phi(t)$ and system's parameters (possibly time-varying) $\vartheta(t)$. Note the time varying parameters and the system response are subject to white Gaussian noise i.e. $w(t)$ and $\epsilon(t)$.

The parameter estimation problem here it to identify the non-linear model parameters given a set of input/output observation data. It should be noted that under the assumption that the model parameters are constant over the time, the aforementioned problem can be solved efficiently using off-line parameter optimisation procedures. This approach though would not allow the continues tracking of the model parameters. There is indeed a great amount of literature that describes the mathematical foundation and the practical applications of off-line non-linear parameter optimisation methods (for general guidelines see [159–161, 164]). We shall restrict our attention though to on-line techniques as the focus of the present study is on the application of adaptive identification algorithms for powertrain monitoring and characterisation purposes.

The non-linear filtering approaches for real-time parameter estimation that will be discussed in this section are based on the Kalman filtering formulation (see Section 5.3.1). Methods of linear optimal estimation theory can be applied to non-linear problems by linear approximation of the effects of small perturbation in the parameters (or states depending of the ultimate purpose of the exercise) of the non-linear systems from a “nominal" value [203]. In the following paragraphs will be presented two variants of the original Kalman filter which differ with respect to the linear approximation of the model non-linearities. These algorithms are known as Extended Kalman Filter (EKF) and Unscented Kalman Filter (UKF).

Extended Kalman Filter (EKF)

The EKF is a sub-optimal solution to the non-linear parameter (or state) estimation problem. In the EKF the update equation for the parameter estimates $(\hat{\vartheta}(t))$ is based on the true non-linear model (Eq. 5.29), whereas the update for the Kalman gain $(K(t))$ and the update covariance matrix $(P(t))$ is based on the first order Taylor series expansion of the non-linear model $h(\phi(t), \hat{\vartheta}(t-1))$ about the current best estimate of the model parameters $(\hat{\vartheta}(t-1))$ [204].

Notice that the calculation of the parameter estimates $(\hat{\vartheta}(t))$ is fully based on the non-linear relationship $h(\phi(t), \hat{\vartheta}(t-1))$ using the currently available estimates $(\hat{\vartheta}(t-1))$. The linearisation step is only needed for the calculation of the

Algorithm 5.6 Extended Kalman Filter - EKF

Require: *Initialisation*

$$\hat{\vartheta}(0) = \vartheta_0$$
$$P(0) = P_0$$

Ensure: *Implementation*

$$\hat{\vartheta}(t) = \hat{\vartheta}(t-1) + K(t)\left[y(t) - h\left(\varphi(t), \hat{\vartheta}(t-1)\right)\right]$$
$$K(t) = P(t-1)J^T(t)\left[R_2(t) + J^T(t)P(t-1)J(t)\right]^{-1}$$
$$P(t) = P(t-1) - \left[K(t)J^T(t)P(t-1)\right] + R_1(t)$$

Kalman gain $(K(t))$ and the update covariance $(P(t))$, which is in fact a first-order variance propagation step. The key component that differentiates the standard Kalman filter with the EKF is the Jacobian matrix $(J(t) = \nabla h(\hat{\vartheta}(t-1)))$. In the EKF the Jacobian matrix must be calculated at each time instant. For technical details regarding the calculation of the Jacobian matrix refer to Section 5.2.1, Eq. 5.8. The rest of the algorithm is identical to the standard Kalman filter including the initialisation of the model parameters (θ_0) and the update covariance matrix (P_0), (see Section 5.3.1).

A special note on the variables $R_1(t)$ and $R_2(t)$ which are the covariance matrices of the parameter (or process) $w(t) \sim N(0, R_1(t))$ and observation $\epsilon(t) \sim N(0, R_2(t))$ noises (similar to the standard Kalman filter, Eq. 5.18). These matrices are often look as tuning parameters, which are postulated by the user depending on the needs of the application [205]. For instance, in applications where it is expected to track slowly time-varying parameters the parameter noise covariance matrix $(R_1(t))$ has relatively larger values compared to parameters that are constant. Equivalently the observation covariance matrix $(R_2(t))$ is analogues to the noise of the measurement signals. In fact there is not a clear systematic method to choose the above covariance matrices, thus some understanding about the physical behaviour of the system with some preliminary data analysis and post processing would allow the user to develop the necessary knowledge for

the proper selection of the covariance matrices. However in cases where there is limited knowledge about the system the user needs to deploy more counter-intuitive methods for the appropriate selection of these parameters; most of these approaches rely up numerical optimisation tools that allow the self-tuning of the EKF [206].

One of the main disadvantages of the EKF in real life application is the continues evaluation of the Jacobian matrix. This is particularly problematic in applications with high signal to noise ratios as the calculation of the Jacobian matrix results inevitably in numerical issues. Additionally the need for the continues computation of the Jacobian matrix increase the computational performance that is required in order to run the algorithm - this is key characteristics that can be an obstacle in real-time applications. A Jacobian free version of the original Kalman filter for non-linear systems is presented in the following paragraphs.

Unscented Kalman Filter (UKF)

As discussed previously the EKF is a sub-optimal non-linear estimation algorithm, as it approximates the probability distribution of the parameter vector (ϑ) with a Gaussian Random Variable (GRV) by propagating it analytically through a first-order linearisation of the non-linear system which requires the calculation of the Jacobian matrix at each time step. This can introduce large numerical error and sometimes the filter might diverge from the true solution. To overcome the limitations of the EKF, Julier et al. [207] proposed the UKF. The UKF is based on the idea that “it is easier to approximate a probability distribution than to approximate an arbitrary non-linear transformation" [207].

The approximation of the probability distribution is achieved by bypassing the first-order linearisation by implementing the Unscented Transformation (UT). The UT is a method for calculating the statistics of a random variable which undergoes a non-linear transformation. The UT captures the mean and covariance of the GRV which goes through the non-linear transformation, to at least second-order accuracy (in contrast to EKF which, only achieves first order accuracy) by using a set of carefully selected sample points. That also indicates that the UKF does not

require the computation of Jacobian matrix.

The statistics of a non-linear function $g = f(x)$ are approximated for a given GRV (here x represents the parameter vector ϑ) with l dimension, $\hat{x}$ mean and P_x covariance by formatting a matrix $\mathcal{X}$ of $2l + 1$ *sigma* vectors $\mathcal{X}_i$ (Eq. 5.31):

$$\mathcal{X}_0 = \hat{x} \tag{5.31a}$$

$$\mathcal{X}_i = \hat{x} + \left[\sqrt{(l+\zeta)P_x}\right]_i \qquad i = 1, ..., l \tag{5.31b}$$

$$\mathcal{X}_i = \hat{x} - \left[\sqrt{(l+\zeta)P_x}\right]_{i-l} \qquad i = l+1, ..., 2l \tag{5.31c}$$

Where, l is practically the total number of the parameters to be estimated, and ζ is a scaling factor defined below along with the overall set up of the UT (Eq. 5.32), [207]:

$$\zeta = \alpha^2(\mathcal{L} + \kappa) - l \tag{5.32a}$$

$$W_0^{(m)} = \frac{\zeta}{l+\zeta} \tag{5.32b}$$

$$W_0^{(c)} = \frac{\zeta}{l+\zeta} + 1 - \alpha^2 + \beta \tag{5.32c}$$

$$W_i^{(m)} = W_i^{(c)} = \frac{\zeta}{2l+\zeta}, \qquad i = 1, ..., 2l \tag{5.32d}$$

$$\gamma = \sqrt{l+\zeta} \tag{5.32e}$$

Here, W are weights of the mean (m) and covariance (c) of the *sigma* points, a is indirectly a scaling parameters (typically is set to 1) since it determines the spread of the *sigma* points around (x) (i.e. the actual parameters ϑ) (typically set to 1), κ is a secondary scaling parameter and is usually set to $3 - l$, and β is used to incorporate prior knowledge of the distribution of x in the computation of the weights for covariance's $W_0^{(c)}$ (typically set to 2).

Algorithm 5.7 Unscented Kalman Filter - UKF

Require: *Initialisation*

$$\begin{aligned}
\hat{\vartheta}(0) &= \vartheta_0 \\
P(0) &= P_0 \\
\zeta &= \alpha^2(\mathcal{L}+\kappa) - l \\
W_0^{(m)} &= \frac{\zeta}{l+\zeta} \\
W_0^{(c)} &= \frac{\zeta}{l+\zeta} + 1 - \alpha^2 + \beta \\
W_i^{(m)} &= W_i^{(c)} = \frac{\zeta}{2l+\zeta}, i = 1, ..., 2l \\
\gamma &= \sqrt{l+\zeta}
\end{aligned}$$

Ensure: *Implementation*

$$\begin{aligned}
\hat{\vartheta}(t) &= \hat{\vartheta}(t-1) + K(t)\left[y(t) - \mathcal{Y}(t)\right] \\
K(t) &= P_{\hat{\vartheta}-\mathcal{Y}}(t) P_{\mathcal{Y}}^{-1}(t) \\
P_{\mathcal{Y}}(t) &= R_2(t) + \sum_{i=0}^{2l} W_i^{(c)} \left[\mathcal{D}(t) - \mathcal{Y}(t)\right]\left[\mathcal{D}(t) - \mathcal{Y}(t)\right]^T \\
P_{\hat{\vartheta}-\mathcal{Y}}(t) &= \sum_{i=0}^{2l} W_i^{(c)} \left[\mathcal{S}(t) - \hat{\vartheta}(t-1)\right]\left[\mathcal{D}(t) - \mathcal{Y}(t)\right]^T \\
\mathcal{Y}(t) &= \sum_{i=0}^{2l} W_i^{(m)} \mathcal{D}(t) \\
\mathcal{D}(t) &= h\left(\phi(t), \mathcal{S}(t)\right) \\
\mathcal{S}(t) &= \begin{bmatrix} \hat{\vartheta}(t-1) \\ \hat{\vartheta}(t-1) + \gamma\sqrt{P(t-1) + R_1(t)} \\ \hat{\vartheta}(t-1) - \gamma\sqrt{P(t-1) + R_1(t)} \end{bmatrix}^T
\end{aligned}$$

Once the UT has been set-up it is possible to proceed to the actual UKF algorithm. Hence, at each time step (t), firstly a set of *sigma* points $(\mathcal{S}(t))$ is generated from the initial parameter estimates $(\hat{\vartheta}(t-1))$ and the initial covariance matrix $(P(t-1))$. Note the process noise covariance matrix $(R_1(t))$, is also added to the initial update covariance matrix due to the additive noise assumption. Next each *sigma* point is passed through the non-linear function $(\mathcal{D}(t))$ (Eq. 5.29b).

Now that these *sigma* points have been transformed, they are used to calculate the mean of the predicted output $(\mathcal{Y}(t))$, the output covariance matrix $(P_{\mathcal{Y}}(t))$ (taking into account the measurement noise covariance matrix $(R_2(t))$), and the cross-covariance matrix $(P_{\hat{\vartheta}-\mathcal{Y}}(t))$ between the unknown parameters $(\hat{\vartheta}(t))$ and the predicted output $(\mathcal{Y}(t))$. Finally the covariance matrices are used for the computation of the Kalman gain $(K(t))$ which is then used to update the parameter $(\hat{\vartheta}(t))$ and the covariance $(P(t))$ estimates. All the required steps for the execution of the UKF are summarised in Algorithm 5.7, [204].

Regarding the initial conditions of the unknown estimable parameters $(\hat{\vartheta}(0))$ and the covariance matrix $P(0)$, and the selection procedure for the process $R_1(t)$ and measurement $R_2(t)$ noise covariance matrices, are handled as the EKF algorithm.

Additional Approaches & Bibliography

The principles of on-line non-linear parameter estimation have been discussed in the previous paragraphs with the analysis of two variants of the Kalman filter. Even though the formulation of the given algorithms i.e. EKF and UKF is mainly applicable to parameter estimation problems, it must be clarified that they can also be used for state estimation [208, 209], or even combined state and parameter (Augmented Kalman Filter) estimation [210, 211] problems. It should also be mentioned that there is huge amount of literature on different variants of the EKF and UKF but also other alternative methods that could be used instead of the ones presented here, some specific references are given here [212, 213]. In any case the presented material provides all the necessary background that is required for the applications that are going to be presented in later chapters.

5.4 Qualitative Adaptive Identification

The concept of parameter identifiability and adaptive identification for linear and non-linear parametric models were discussed in details in the the previous sections. Now, these two concepts are merged together to a common framework that has been developed for the purposes of this thesis. The proper application of the suggested scheme helps to increase the quality of adaptive identification, thus is also named “Qualitative Adaptive Identification". The process flow diagram of the framework is illustrated in Fig. 5.7.

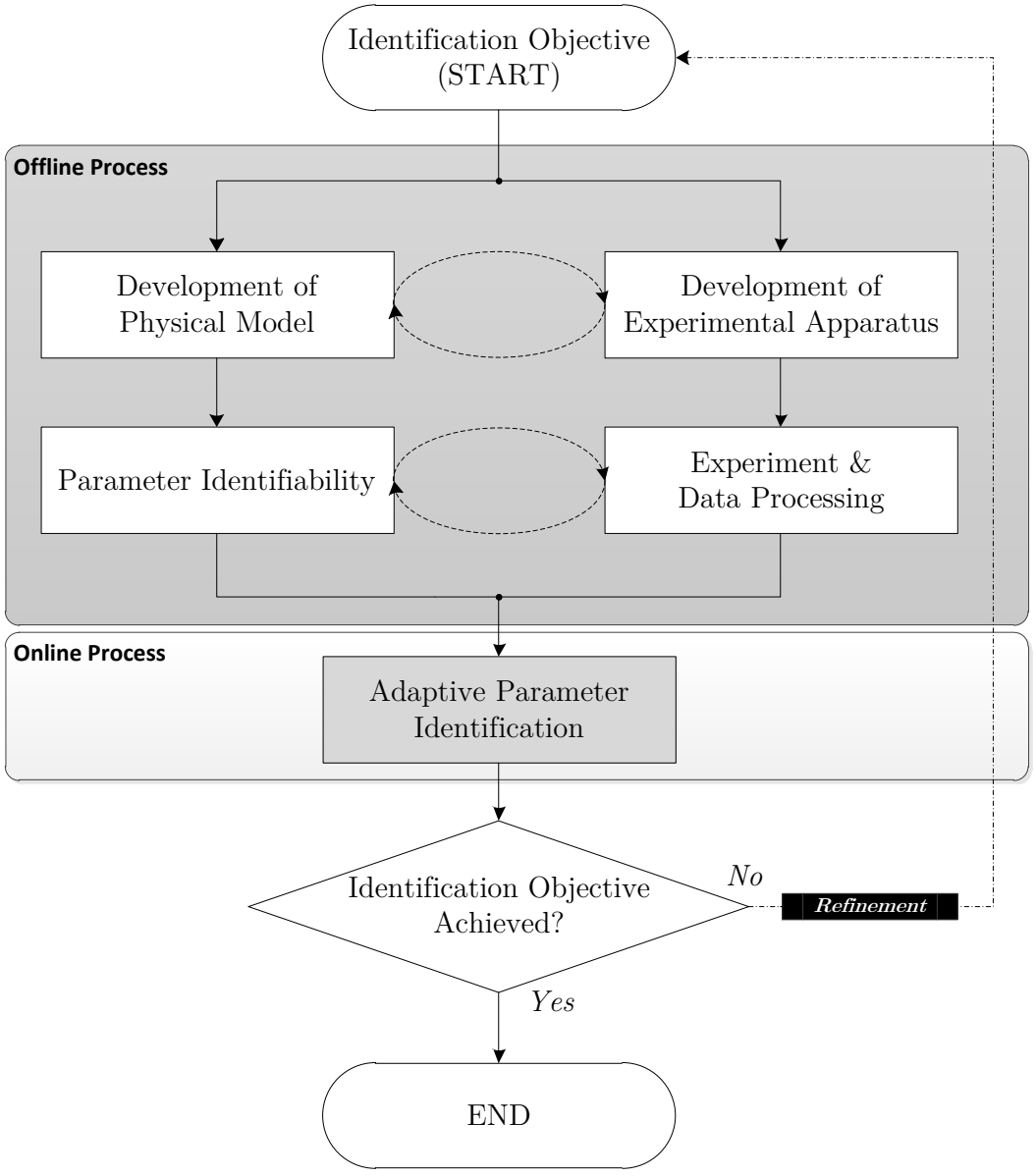

Figure 5.7: Qualitative adaptive identification, process flow diagram.

Firstly, the user should define the *Identification Objective* which could be the identification of physically based model parameters for monitoring purposes or the adaptive identification of dynamic models for real-time controller calibration.

Having defined the main goal of identification it is now possible to proceed to the *Development of Physical Model* of the system under examination. This system could either be a complete internal combustion engine or a hybrid powertrain or a subsystem such as engine friction, air-charge etc. At the same is conducted the *Development of Experimental Apparatus* in order to maximise the relevance of the model with actual system.

Next follows the *Parameter Identifiability* and *Experiment & Data Processing* tasks, these are parallel processes, since the parameter identifiability tool is used to evaluate the information content of the observation data of the experiment (as well as the structural identifiability of the model). As it has been discussed earlier the aim of the parameter identifiability process is to the provide some qualitative information about the model parameters that can or cannot be identified using the given set of observation data.

The qualitative information gained from the parameter identifiability analysis allows to proceed to the final step which is the *Adaptive Parameter Identification* using suitable techniques depending on the structure of the model e.g. linear or non-linear, and the objective of the identification e.g. parameter tracking for fault diagnosis of on-line characterisation.

Finally, the user have to evaluate whether the results of the identification process meet the requirements that where set at the start to the overall process; if not then the process must be refined. Note also that the framework is divided into the two domains namely the *Offline Process* and the *Online Process*. The main output of the offline process is the qualitative information about the model structure and the information content of the observation data. This is then taken into account during the actual application of the adaptive identification algorithm with the purpose of increasing the quality, accuracy and robustness of identification.

5.5 Synopsis

A summary of the key points of this chapter is given below.

- A classification of the available system identification tools with respect to the structure of a given model and the implementation method were presented.
- The theoretical principles of an orthogonal-based parameter identifiability algorithm were discussed. A simplistic yet representative example was also included for gaining a better understanding regarding the implementation approach and interpretation of the results.
- The theoretical background of adaptive system identification algorithms for linear-in-the-parameters and non-linear-in-the-parameters system models were discussed. Some representative examples are incorporated to gain better understanding.
- A qualitative adaptive identification framework for parameters with physical and semi-physical interpretation that can be found commonly in white-box and grey-box powertrain models was proposed.

Chapter 6

Coupling Shaft Condition Monitoring System

An on-line condition monitoring system for coupling shafts that can be found generally in testing facilities of rotating systems is presented. This chapter is linked to the physics-based test cell model that was provided in Chapter 3, the experimental apparatus of the transient engine test cell that was described in Chapter 4, and the adaptive system identification tools that were outlined in Chapter 5.

6.1 Introduction on Shaft Monitoring Systems

Rotating shafts are responsible for transferring large amounts of kinetic energy between rotating components and machines. Numerous applications can be found in different engineering areas such as power generation plants, machine tool spindles, marine, aeronautical and automotive propulsion systems. Depending on the overall purpose of the very application, coupling shafts can be designed with different characteristics in order to much the needs of the user. For instance in heavy duty industrial applications it is more probably to find coupling shafts with relatively high stiffness to be able to transfer the required power. On the other hand, in low power applications such as mechatronics and robotics more flexible and light coupling shafts are usually preferable. Furthermore, testing facilities of rotating components require carefully designed and robust coupling shaft units to

be able to experiment with the equipment under testing i.e. electric motors, internal combustion engines, reciprocating pumps, drilling systems, braking systems, transmission systems, turbines etc. into severe operating conditions to ensure the robustness of such systems [214, 215]. As a consequence of this intense operation, it is fairly common to have catastrophic shaft cracks which contributes negatively by creating down-time [216]. It is therefore of major importance to be able to continually monitor the condition of coupling shaft devices with the purpose of avoiding any fatal damages on the system components.

Several techniques can be found in literature regarding the health monitoring of engineering processes and systems. Out of these techniques, three general methodologies can be established, known as, Limit Checking (LC), Signal-Based (SB), and Model-Based (MB) [217]. LC is the simplest and most frequently used fault detection method as it is relatively easy and fast to implement. On LC techniques the measured variables of the process are monitored and checked against certain thresholds. The main challenge of the LC approach is to accurately select the threshold which usually requires some statistical analysis based on prior knowledge about the healthy condition of the system [218]. Now, many measured signals of process show oscillations that are either of harmonic or stochastic natures, or both. If changes of these signals are related to faults, then SB fault-detection methods can be applied. Especially for machine vibration, imbalance or bearing faults (turbo machines), knock (gasoline engines), chattering (metal grinding machines). SB approach is based on signal models that can be developed either using non-parametric approaches, like frequency and correlation functions, or parametric methods, like amplitude for distinct frequencies or ARMA type models [10]. Lastly, MB fault detection approaches are based on the idea of comparing measured signals with outputs from a mathematical model. MB condition monitoring systems can be found into three different forms i.e. fault detection with parameter estimation, fault detection with observer models and fault detection with parity equations [219].

Condition monitoring of coupling shafts is a well investigated area with nu-

merous publications over the last few decades. Tlaisi et al. [220] presented a technique for shaft crack detection based on a limit checking approach by using lateral and torsional vibration measurements in terms of maximum acceleration, velocity and displacement terms. Previous studies were also involved with signal based techniques by supervising the harmonics of vibration related signals and analysing their trends using spectrum and wavelet analysis [221–223]. Model-based approaches have also been reported, Sekhar [224] has presented an online model-based condition monitoring approach by developing a complex rotor-bearing system redundant model using Finite Element Analysis (FEA) and comparing it with actual measurements. Additionally Seibold and Weinert [225] have suggest the use of augmented Extended Kalman Filters (EKF) for continuous state and parameter estimation on the basis of a finite crack element approach. For a detailed survey regarding the dynamics and condition monitoring approaches of rotor shafts the reader is referred to [222].

Although numerous methods have been proposed for the condition monitoring of coupling shafts, most of those methods require either special instrumentation and off-line signal analysis, or highly complex on-line model-based solutions which might be impractical to be used in real-life applications. A simple and practically viable solution is proposed in this chapter. The method is based on the on-line identification of coupling shaft's physical parameters using measurements that can be found in most industrial testing facilities of rotary equipment. A detailed analysis of the proposed methodology follows in the next sections of the chapter. The functionality of the monitoring system is demonstrated on an engine dynamometer coupling shaft. Both simulated results based on an overall system model (Chapter 3) and experimental results using an advanced transient engine testing facility (Chapter 4) are presented showing the capabilities of the proposed on-line condition monitoring system, and the performance of the various adaptive identification algorithms which were applied.

6.2 On-line Health Monitoring Methodology

In this section information will be given about the experimental equipment, the physical models, and the adaptive system identification algorithms that are required in order to implement the suggested on-line condition monitoring system.

6.2.1 Coupling Shaft Physical Model

The principle idea of the suggested on-line condition monitoring method is based on the development and use of a simple coupling shaft physical model and the continuous tracking of its parameters i.e. damping and stiffness coefficients, using recursive identification algorithms. More specifically, the mathematical analysis of the overall transient engine test cell that was conducted in Chapter 3 (see Section 3.1 for additional details) showed that the coupling shaft unit can modelled simply as a rotational spring element with a rotational viscous damper based on the following relation (Eq. 6.1):

$$\tau_{sh}(t) = B_{sh}\left[\omega_{dy}(t) - \omega_{en}(t)\right] + K_{sh}\left[\theta_{dy}(t) - \theta_{en}(t)\right] \tag{6.1}$$

Where, B_{sh} and K_{sh} are the damping and stiffness coefficients and represent the physical characteristics of the coupling shaft, ω and α are the angular velocity and acceleration quantities respectively, whilst the subscripts dy and en indicate the dynamometer and engine devices accordingly.

Now, based on the Eq. 6.1, it can be said that the mathematical structure of the physical model of the coupling shaft is equivalent to the standard format of linear parametric static systems:

$$y(t) = \phi^T(t)\vartheta + \epsilon(t) \tag{6.2}$$

And, $\vartheta = [B_{sh}, K_{sh}]$ is the parameter's vector, $\phi^T(t) = [\theta_{dy}, \theta_{en}, \omega_{dy}, \omega_{en}]$ is the vector of independent variables, $y(t) = [\tau_{sh}(t)]$ is the dependent variable vector, and finally $\epsilon(t)$ is a random error term.

The above statement indicates that the physical parameters of the coupling shaft model could be tracked in real-time by using linear recursive identification

algorithms. Prior to that though we need to make sure that the position, velocity and torque measurements are taken properly in order to be able to implement the suggested algorithms.The next sections show the experimental equipment and the identification algorithms that were used in this application.

6.2.2 Experimental Equipment

The methodology was implemented and tested in the transient cyclic engine test cell that was described in Chapter 4. The coupling shaft was designed specifically for connecting the engine with the dynamometer via a spider coupler. The actual coupling shaft unit is presented in Fig. 6.1; as it can been seen in the middle of the shaft is placed an in-line torque transducer that measures the torque acting on the shaft. Additionally, the coupling shaft is mounted on pedestals with self-alighting bearings to eliminate any undesirable vibrations but also to provide some level of flexibility. Consequently, it is important to notice that the physical characteristics of the overall coupling shaft (from one end to the other) might be affected the components in between.

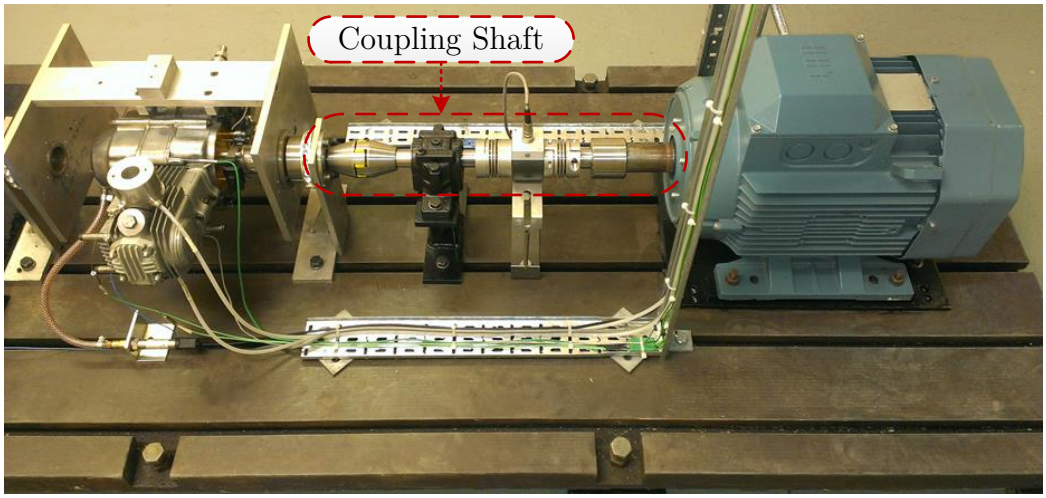

Figure 6.1: Coupling shaft.

As mentioned earlier the shaft connects the dynamometer with the engine via a spider coupler. In fact, this spider coupler can have different characteristics depending on needs of each application. Here, spiders with various characteristics

were used with the purpose of verifying that the condition monitoring system can track effectively coupling shafts with different physical parameters i.e. damping and stiffness coefficients. More specifically, three different coupling shaft spiders were used for testing the efficacy of the proposed methodology (Fig. 6.2). The various colors indicate different torque capacity characteristics i.e. the yellow (Fig. 6.2a) is for low torque systems and have high damping properties, the red (Fig. 6.2b) offers medium torque capacity and damping properties, while the green (Fig. 6.2c) offers high torque capacity and minimal damping properties.[1]

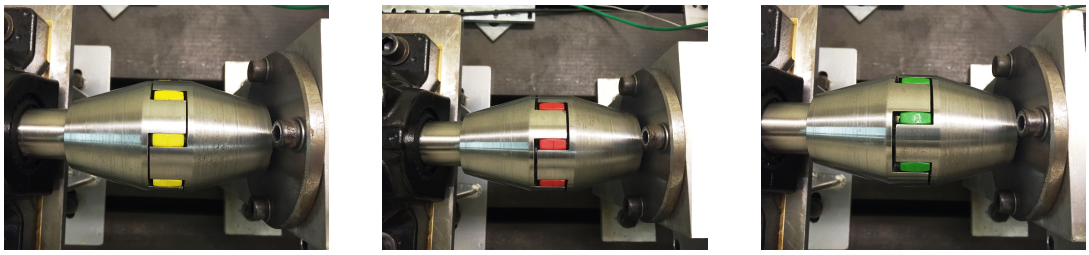

(a) Low power **(b)** Medium power **(c)** High power

Figure 6.2: Coupling shaft spiders with different characteristics.

The equipment required for the implementation of the suggested condition monitoring system is depicted in Fig. 6.3. The sensors needed are two pulse encoders at each end of the coupling shaft and an in-line torque transducer. We should highlight that depending on the exact position of the pulse encoders, the overall stiffness and damping coefficients of the system might vary. For instant if the pulse encoders are place at the back end of the dynamometer and engine then the identified coupling shaft characteristics might be slightly affected from the individual structural characteristics of the dynamometer and engine accordingly. The outputs of the sensors are then fed into the global test cell controller were are used for the on-line estimation of the coupling shaft's physical parameters. See Chapter 4 for more technical details about the hardware.

[1] For more information visit the following website: `http://abssac.co.uk/`.

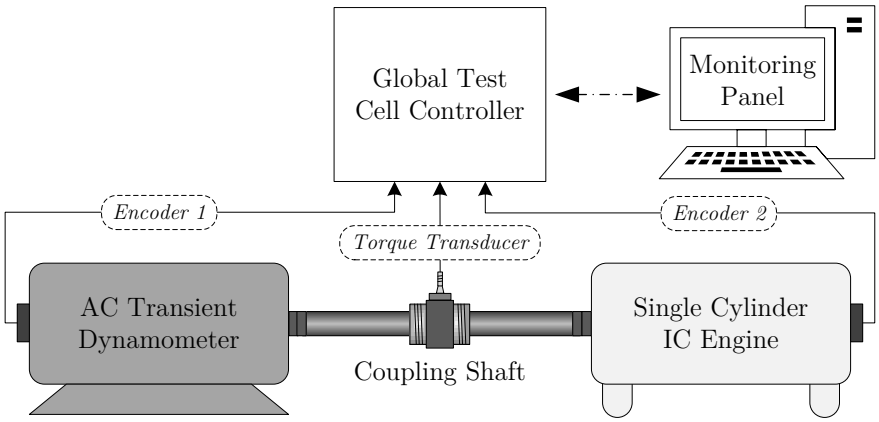

Figure 6.3: Schematic diagram of the experimental equipment.

6.2.3 Recursive Parameter Identification

The core of the on-line condition monitoring system is a linear recursive estimator that is used to track the physical parameters of the coupling shaft model (Eq. 6.1). The recursive estimator runs in parallel to the operation of the system whilst it makes use of the acquired position, velocity and torque measurements in order to compute the coupling shaft's stiffness and damping coefficients. The interaction of the on-line condition monitoring system with the actual monitored process i.e. coupling shaft, is illustrated in Fig. 6.4. As is can be seen the condition monitoring system consists of two separate modules namely the "Recursive Identification" module and the "Change Detection" module.

The inputs to the recursive identification module are the angular position $(\delta\theta(t))$ and velocity $(\delta\omega(t))$ differences and the torque of the shaft (τ_{sh}). Note however that before the signals are fed into the recursive identification module they are first filtered using zero-phase distortion filters (see Chapter 4, Section 4.4 for more technical details) to eliminate measurement noises prior the actual identification process. These information are used to estimate the parameters of the coupling shaft model i.e. stiffness $(\hat{K}_{sh}(t))$ and damping $(\hat{B}_{sh}(t))$ coefficients by using linear recursive identification algorithms. To be more specific, for this application we tested the efficacy of three linear recursive identification algorithms, the RLS (Algorithm 5.2), the RLSVEF (Algorithm 5.4), and the DSFC (Algorithm 5.5), (see Chapter 5, Section 5.3.1).

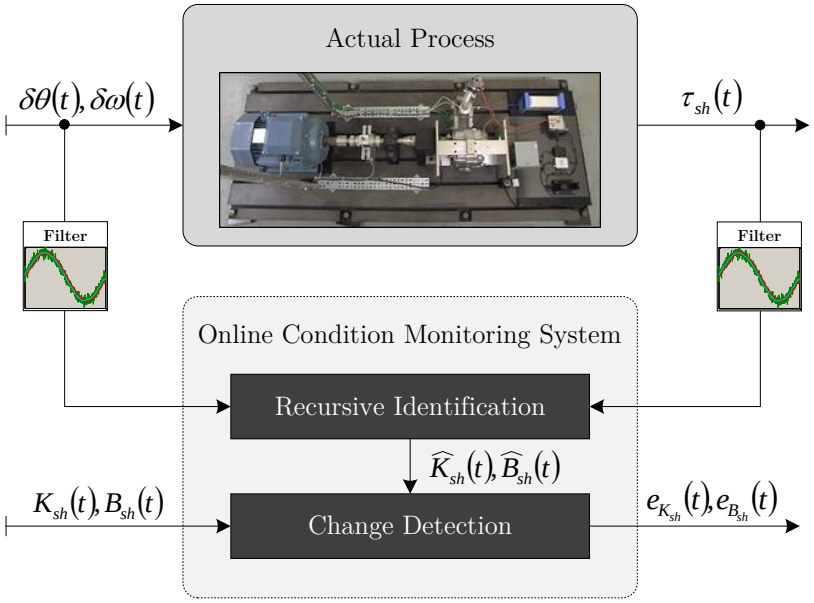

Figure 6.4: Shaft on-line condition monitoring system, schematic diagram.

Lastly, the main purpose of the change detection module is the comparison of the coupling shaft's parameter estimates with a set of healthy parameters (K_{sh}, B_{sh}) in order to be able to determine the condition of the coupling shaft. This is very simply achieved by calculating continuously the relative error $(e(t))$ between the parameter estimates $(\hat{\vartheta}(t))$ and the healthy set of parameters $(\vartheta(t))$.

$$e(t) = \frac{\vartheta(t) - \hat{\vartheta}(t)}{\vartheta(t)} \tag{6.3}$$

Note that the relative error is calculated independently for each parameter of the coupling shaft i.e. stiffness and damping coefficients. Any change larger than a prescribed error bound indicates fault in the system.

6.3 Results & Analysis

6.3.1 Experimental Results

Results from the practical implementation of the proposed on-line condition monitoring system are presented in this section. The recursive estimators were tested in several operating conditions to ensure their robustness and repeatability. Here,

for illustration purposes we present measurements for only two experiments i.e. a constant speed test (Fig. 6.5) and a speed ramp test (Fig. 6.6).

Note that the main observation data required for the implementation of the proposed coupling shaft condition monitoring system are the velocity (Fig. 6.5a and Fig. 6.6a) and position (Fig. 6.5c and Fig. 6.6c) of the engine and dynamometer and the torque of the shaft (Fig. 6.5e and Fig. 6.6e). The testing duration for both the steady-state experiment (Fig. 6.5) and the transient experiment (Fig. 6.6) was 10 seconds in total. As it will be shown later this time was more than enough for the recursive estimators to converge and start tracking effectively the physical parameters of the coupling shaft. On the other hand, one practical issue that affected the quality of the identified coupling shaft parameters was the estimation of the velocity of the engine and the dynamometer. As it can be seen in Fig. 6.5b and Fig. 6.6b the difference between the engine and dynamometer velocity does not obey a cyclic behaviour as for example the position difference (Fig. 6.5d and Fig. 6.6d). This observation implies that the velocity estimation was partly problematic and in fact the source of this problem is located in the selection of the time step (dt) the calculation of the velocity using Eq. 4.3 (see Chapter 4, Section 4.4.2 for more details). The rest of the measurements appear to be valid as the cyclic characteristics are clearly visible.

Now, prior to the implementation of the recursive estimators the actual values of the stiffness and damping coefficients were identified for each different spider characteristics (Fig. 6.2) by applying classical off-line least-squares approach (Table 6.1). These estimates were assumed to be the true parameters and they were actually used to compare the estimates of the recursive estimators.

Table 6.1: True coupling shaft parameters.

Parameter	**Spider Colour**		
	Yellow	*Red*	*Green*
Stiffness $\left[\frac{\text{Nm}}{\text{rad}}\right]$	1250	1340	1490
Damping $\left[\frac{\text{Nms}}{\text{rad}}\right]$	0.95	0.70	0.52

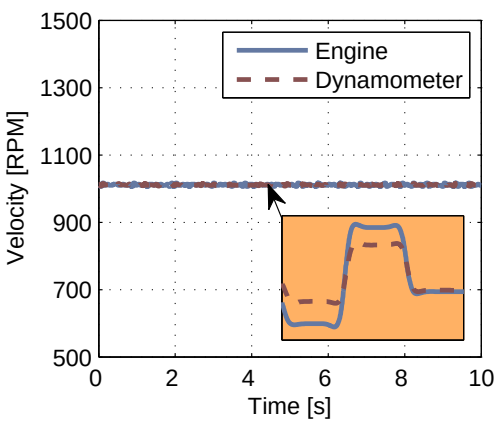

(a) Velocity

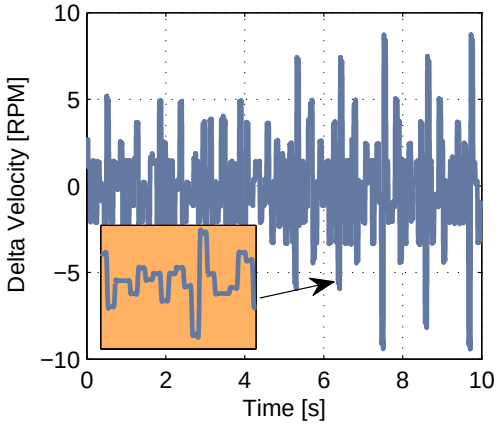

(b) Velocity difference

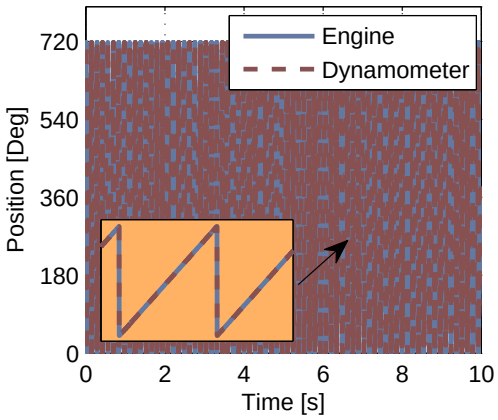

(c) Cyclic position

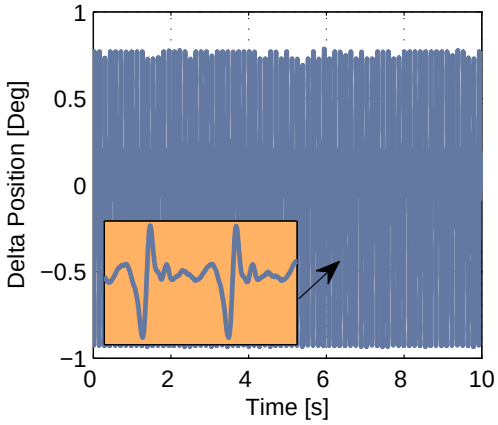

(d) Position difference

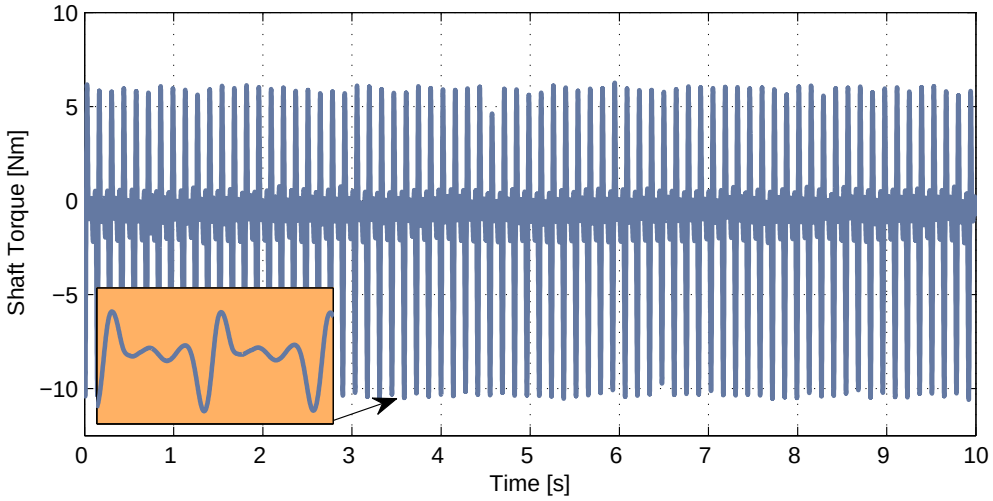

(e) Shaft torque

Figure 6.5: Constant speed experiment (Test ID: T01).

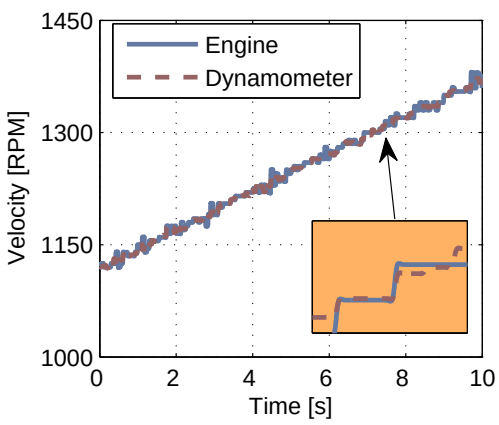

(a) Velocity

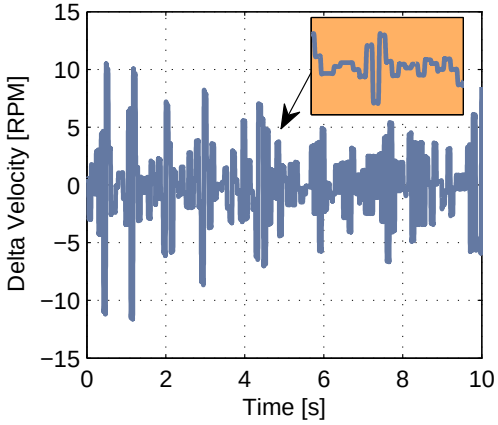

(b) Velocity difference

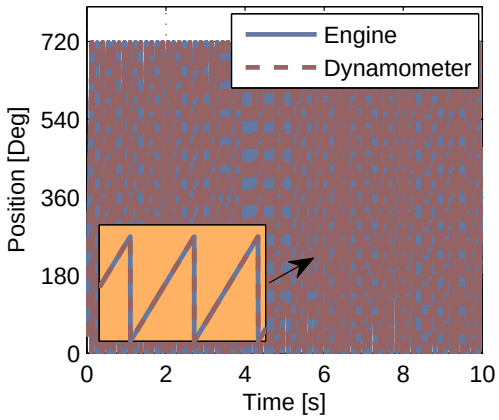

(c) Cyclic position

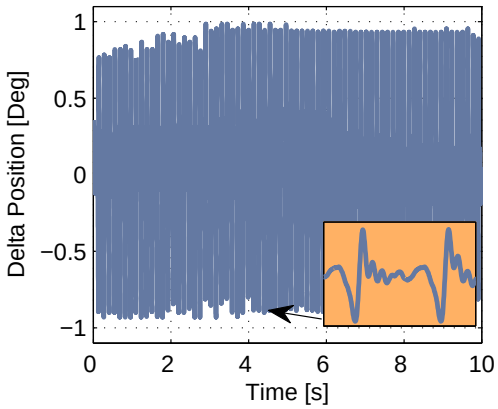

(d) Position difference

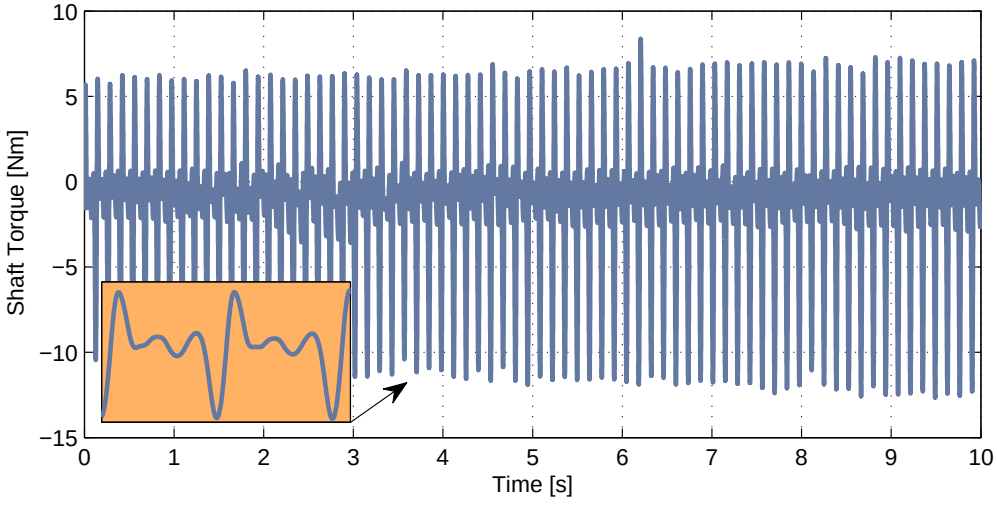

(e) Shaft torque

Figure 6.6: Speed ramp experiment (Test ID: T02).

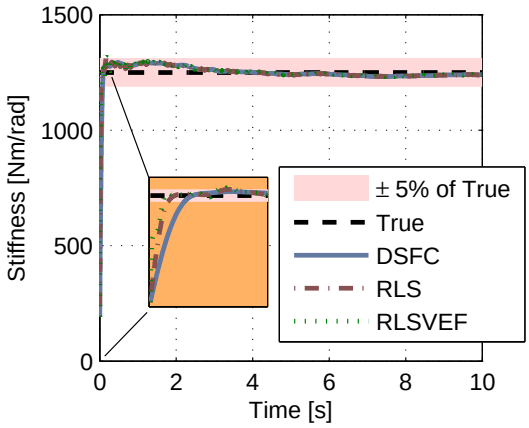

(a) Stiffness-Yellow $(\approx 1250\ [\frac{Nm}{rad}])$

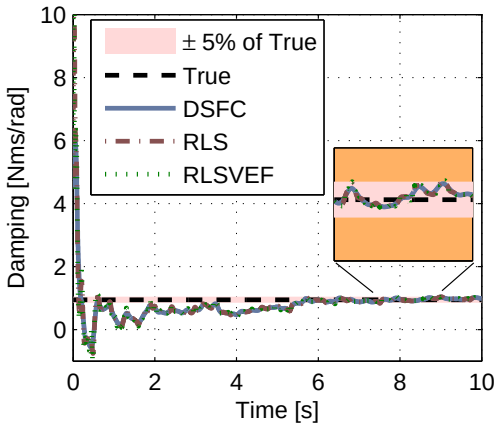

(b) Damping-Yellow $(\approx 0.95\ [\frac{Nms}{rad}])$

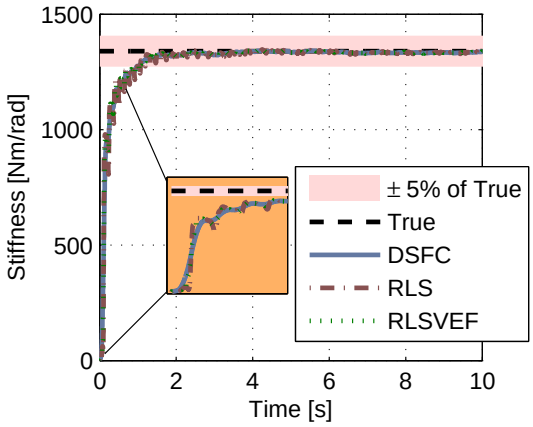

(c) Stiffness-Red $(\approx 1340\ [\frac{Nm}{rad}])$

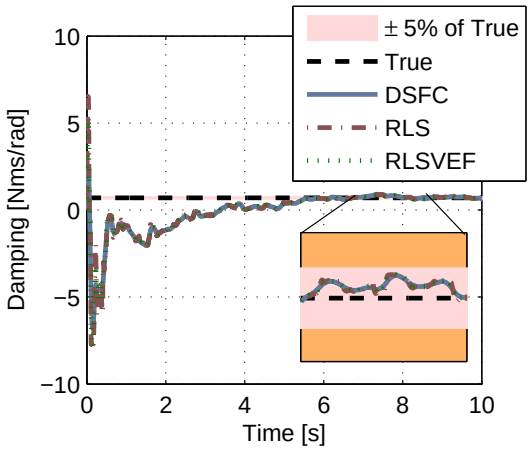

(d) Damping-Red $(\approx 0.70\ [\frac{Nms}{rad}])$

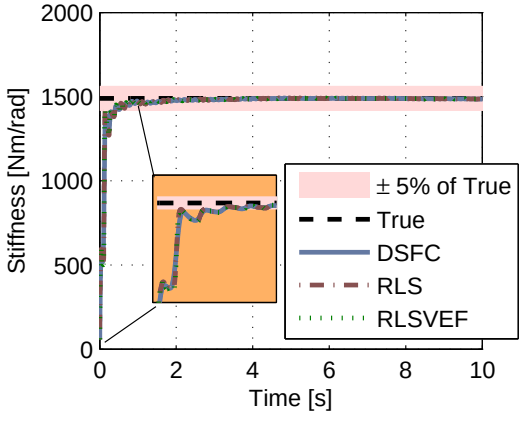

(e) Stiffness-Green $(\approx 1490\ [\frac{Nm}{rad}])$

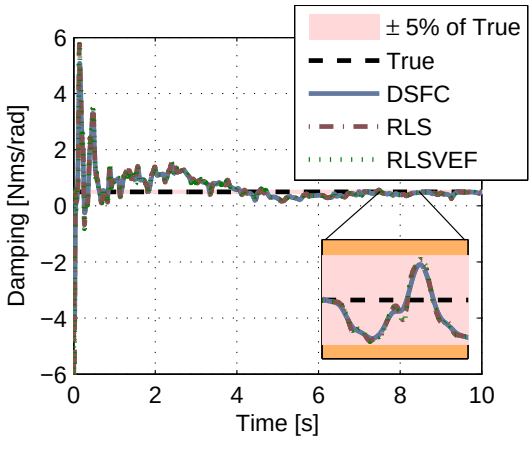

(f) Damping-Green $(\approx 0.52\ [\frac{Nms}{rad}])$

Figure 6.7: Estimation results from test T01.

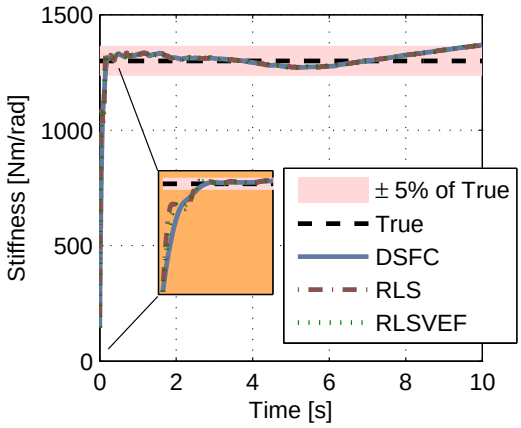

(a) Stiffness-Yellow ($\approx 1250\ [\frac{Nm}{rad}]$)

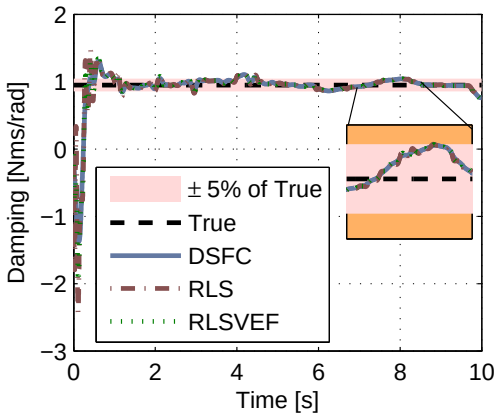

(b) Damping-Yellow ($\approx 0.95\ [\frac{Nms}{rad}]$)

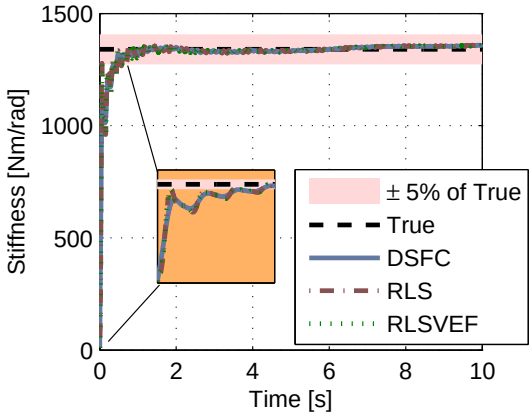

(c) Stiffness-Red ($\approx 1340\ [\frac{Nm}{rad}]$)

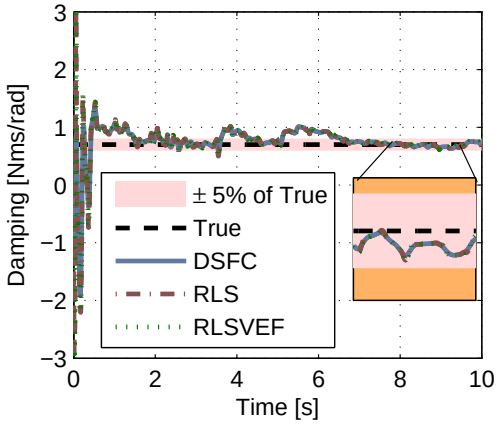

(d) Damping-Red ($\approx 0.70\ [\frac{Nms}{rad}]$)

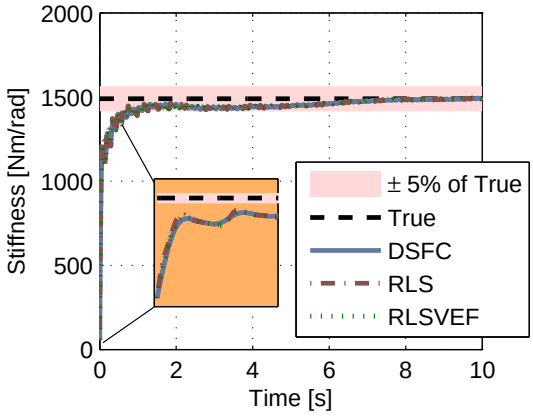

(e) Stiffness-Green ($\approx 1490\ [\frac{Nm}{rad}]$)

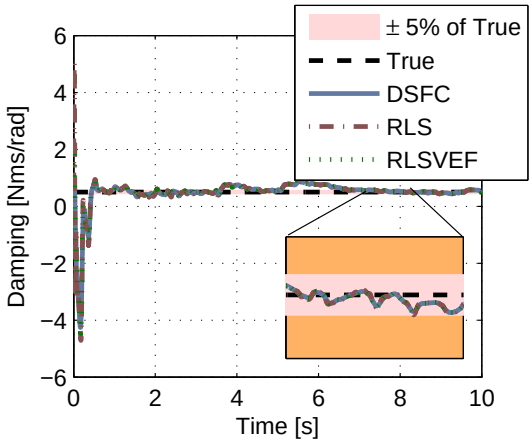

(f) Damping-Green ($\approx 0.52\ [\frac{Nms}{rad}]$)

Figure 6.8: Estimation results from test T02.

The results from the implementation of the three different linear recursive estimators i.e. DSFC, RLS, and RLSVEF, are presented in Fig. 6.7 and Fig. 6.8 for the constant speed experiment (Fig. 6.5) and the speed ramp experiment (Fig. 6.6) respectively. A first look at the results depicts that all of the applied estimators converge and identify $(\pm 5\%)$ the true parameters of the coupling shaft within the first 5 seconds of the estimation window. As far as the initialisation of the recursive algorithms is concerned, the parameter estimates were set to 0 for all different algorithms (to examine the performance of the estimators under worst case scenarios) while the confidence constant c (see Chapter 5, Section 5.3.1) of the covariance (RLS, RLSVEF) and the square root covariance (DSFC) matrices was set equal to 1000 for all different test cases. It should be mentioned that the adjustment of those values could affect the speed of convergence of the estimator. Additionally the forgetting factors was set equal to 0.98 in all algorithm as slight changes in the parameters was expected. Regarding the repeatability of the estimators with respect to the various operating conditions it can be said that they manage to identify the true parameters without any significant errors and this verifies the robustness of the proposed methodology. One general trend that was observed thought, is that the parameter estimates of the damping coefficient (Fig. 6.7b, Fig. 6.8b, Fig. 6.7d, Fig. 6.8d, Fig. 6.7f, Fig. 6.8f) seem to be more noisy compared to the parameter estimates of the stiffness coefficient (Fig. 6.7a, Fig. 6.8a, Fig. 6.7c, Fig. 6.8c, Fig. 6.7e, Fig. 6.8e). This was caused probably by the problematic estimation of engine and dynamometer velocities (damping torque is a proportional to the velocity difference while stiffness torque to the position difference, see Eq. 6.1). Lastly, as far as the actual identified parameters of the examined coupling shafts it can be said that they are in close vicinity with their true physical characteristics that were discussed in Section 6.2.2, Fig. 6.2.

A quantitative comparison among the three recursive estimators is presented in Fig. 6.9. The performance of the estimators is evaluated using a suitable descriptive statistic namely, Normalised Mean Square Error (NMSE).

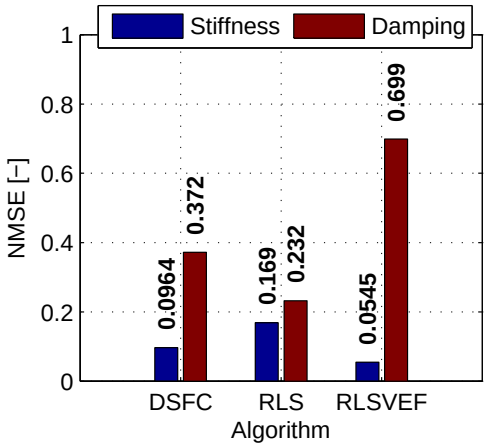

(a) Yellow spider - Test ID: T01

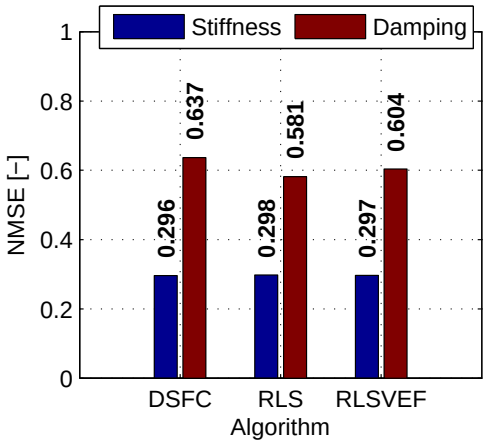

(b) Yellow spider - Test ID: T02

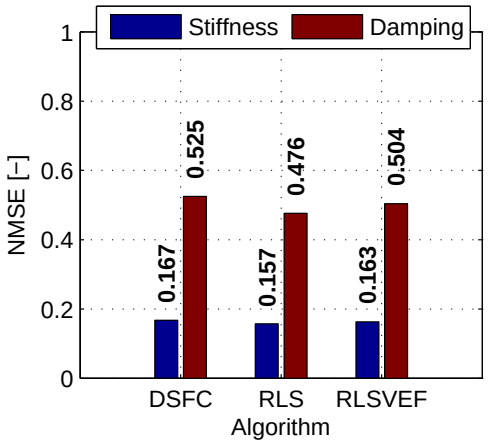

(c) Red spider - Test ID: T01

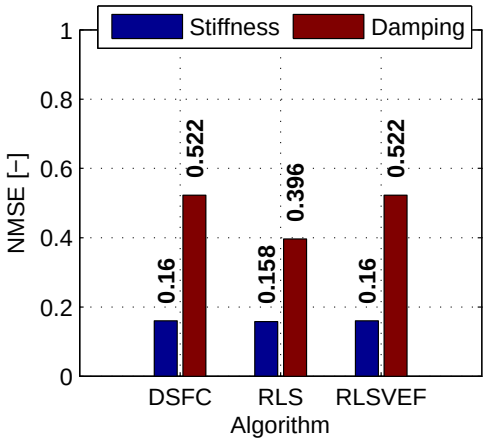

(d) Red spider - Test ID: T02

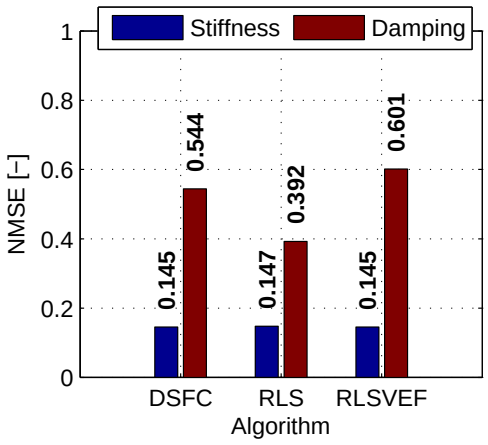

(e) Green spider - Test ID: T01

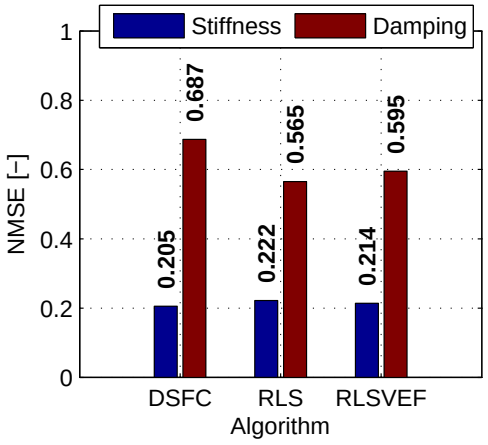

(f) Green spider - Test ID: T02

Figure 6.9: Quantitative comparison among the three different recursive estimators, and differences between stiffness estimates and damping estimates.

$$\text{NMSE} = \frac{1}{n}\sum_{i=1}^{n}\frac{(Y_m - Y_p)^2}{\left(\frac{1}{n}\sum_{i=1}^{n}Y_m\right)\left(\frac{1}{n}\sum_{i=1}^{n}Y_p\right)} \tag{6.4}$$

Where, n is the total number of samples, Y_m is the measured parameter (true) and Y_p is the predicted parameter (estimation). The higher the value of the NMSE the less accurate was the corresponding estimation.

According to the statistics presented in Fig. 6.9, the algorithms estimate the stiffness coefficient with greater accuracy compared to the damping coefficient, in every occasion i.e. operating condition and coupling shaft configuration. This is another evidence which support the statement that the problematic velocity computation affects the coupling shaft parameter estimates. Turning to the estimation accuracy among the different algorithms, there is no a clear evidence that a specific algorithm is superior to another. It is believed that more experimental data would be required in order to draw a conclusion about the actual performance of the various algorithms. In any case all algorithms manage to identify the parameter successfully which indicates their efficacy for the given problem.

6.3.2 Simulation Results

Given the successful practical implementation of the proposed algorithms, we attempt to generate some representative coupling shaft fault cases in order to evaluate the effectiveness of the on-line condition monitoring system to track and isolate possible faults and malfunctions. The faults were generated using the simulation model of the complete transient engine test cell that was discussed in Chapter 3. Two types of faults were examined namely process faults (Fig. 6.10), and sensor faults (Fig. 6.11). The process faults involved individual changes in the coupling shaft characteristics i.e. stiffness and damping coefficients, whilst the sensor fault was related to the reading of the dynamometer encoder i.e. change in the measured speed of the dynamometer.

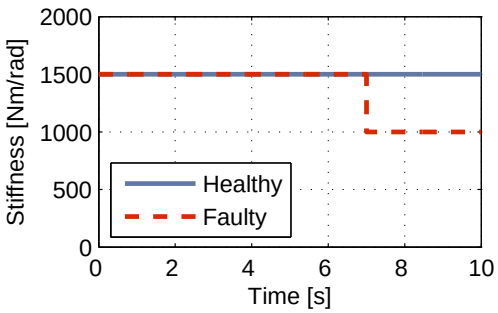

(a) Stiffness fault

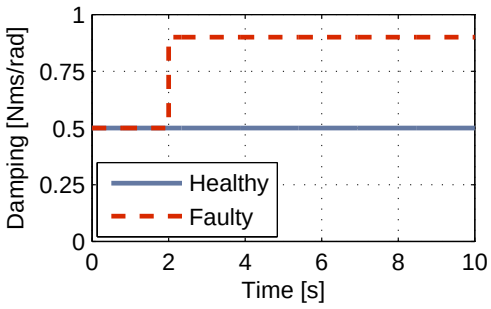

(b) Damping fault

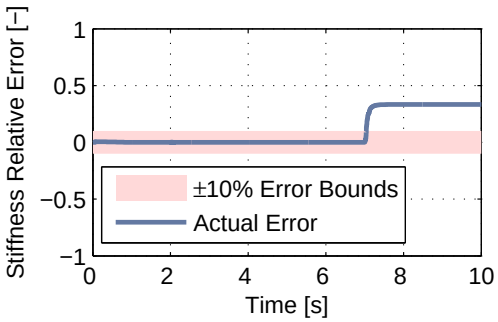

(c) Stiffness relative error

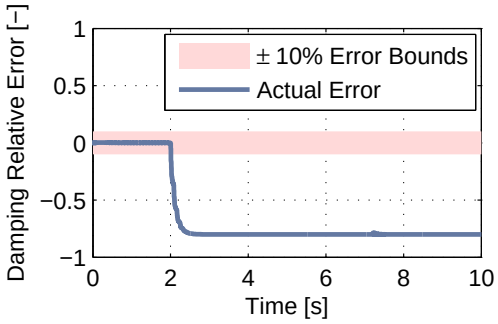

(d) Damping relative error

Figure 6.10: Process fault simulation.

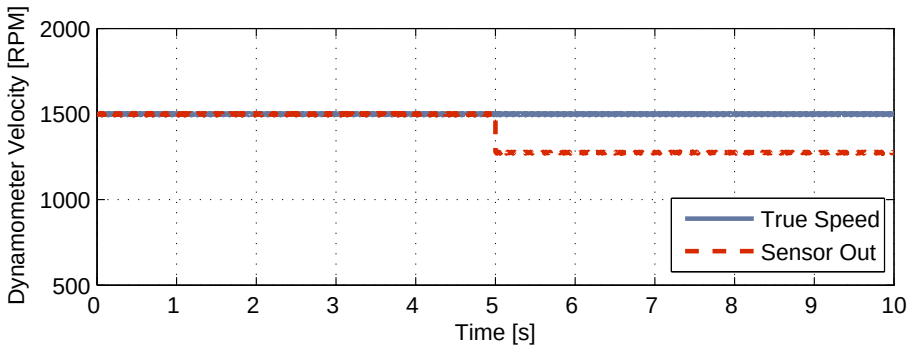

(a) Speed sensor fault

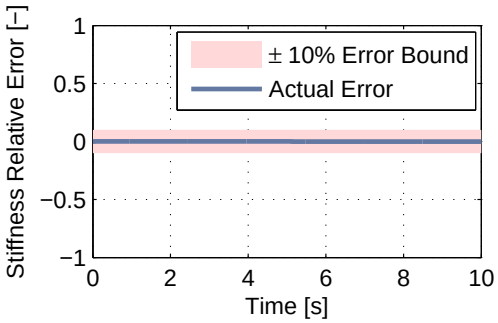

(b) Stiffness relative error

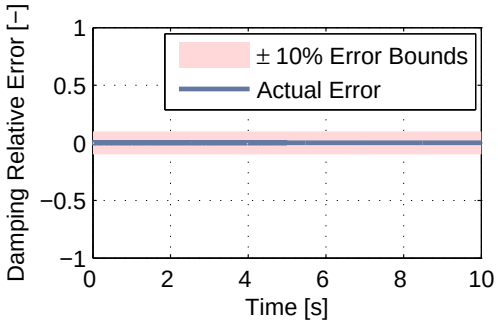

(c) Damping relative error

Figure 6.11: Sensor fault simulation.

For this study the coupling shaft model was parametrised using the estimates of the green spider i.e. $K_{sh} \approx 1490 \left[\frac{\text{Nm}}{\text{rad}}\right]$ and $B_{sh} \approx 0.52 \left[\frac{\text{Nms}}{\text{rad}}\right]$, whilst only the DSFC algorthm was implemented for tracking any changes in the parameters. For this application, the forgetting factor was set to 0.98 as changes in the parameters were expected. Furthermore the DSFC algorithm was properly initialised (parameter estimates and square root of covariance matrix) as we already knew what were the healthy conditions of the coupling shaft.

The simulation results revealed that the proposed condition monitoring system can effectively isolate different process faults, as when changes in stiffness coefficient (Fig. 6.10a and Fig. 6.10c) occur the damping coefficient (Fig. 6.10b and Fig. 6.10d) estimate is not affected and vice versa (the relative error is calculated using Eq. 6.3). Similarly in the case of the sensor fault, when the speed sensor of the dynamometer provides wrong readings, the parameters estimates of the coupling shaft are not affected. This is also what was expected as sensor faults should not result in misleading parameter estimates of the coupling shaft.

6.4 Synopsis

A summary of the key points of this chapter is given below.

- An on-line health monitoring system for engine dynamometer coupling shafts was proposed in this chapter.
- The suggested health monitoring system was based on the recursive identification of the physical characteristics of a coupling shaft, i.e. stiffness and damping coefficients.
- Three different recursive identification algorithms were employed and compared in order to determine if there is any practical difference among the algorithms.
- Three different coupling shaft configurations were tested. The results proved the efficacy of the proposed methodology.

- Simulation studies revealed that the suggested adaptive health monitoring system can effectively detect and isolate coupling shaft faults and malfunctions.

Chapter 7

Engine Friction Parameters Ranking & Characterisation

This chapter shows the application of the identifiability and adaptive identification tools, that were presented in Chapter 5, for the problem of engine friction parameters ranking and characterisation. Given the semi-physical friction model that was described in Chapter 3, firstly is presented a methodology that allows the ranking of the physical friction parameters in respect to their importance to engine friction, and secondly is shown the application of adaptive identification algorithms that can be used for the on-line monitoring and characterisation of engine friction.

7.1 Engine Friction: A Brief Review

Modern internal combustion engines consists of several moving components which contribute negatively in the mechanical losses of the engine. The greater the number of moving parts, the greater the amount of energy lost to heat by friction between the parts. In particular friction accounts for up to 15-20% of all the internal combustion engine losses [226]. A reduction in friction is seen as essential in the development of new internal combustion engines, which is driven by a number of key concerns such as fuel efficiency, the emissions levels, the noise, vibration

and harshness issues and the cost. Furthermore, according to King [2] the reduction of engine's mechanical losses is one of the main actions that would enable the increase of the overall engine efficiency by 5-7% with almost no cost. Consequently, it is important to continue working towards the reduction of frictional losses by suggesting new approaches and ideas.

7.1.1 Determination Procedures

The improvements in engine design characteristics could reduce significantly the level of frictional losses. The determination of engine friction is a rather complex process as there are numerous components and operating conditions that contribute in the overall engine losses. A possible subdivision could be made into three groups i.e. the mechanical losses, the pumping losses, and the auxiliary losses [227].

- The mechanical losses are created due to the friction of the piston rings, crankshaft bearings, connecting rod bearings, and valve-train mechanism.
- The pumping losses are caused by the resistance incurred when pistons pump intake and exhaust gases through the cylinder, and it is particularly high when the intake throttle is closed.
- The auxiliary losses are a result of various systems such as electrical devices (e.g. cooling fan and alternator), pumps such as oil, fuel, and water, gears and belts.

It is noteworthy that the above classification supplies only a guide to the reader and should not be taken as an absolute as each researcher might give a different categorisation of the engine losses.

Several different approaches have been suggested to determine the engine friction. A classification into two different groups can be made, namely, the instantaneous and the average methods.

- The instantaneous approach describes the losses of each engine component on a crank angle basis. In general for the determination of the instantaneous friction torque, analytical expression are usually derived from physics principles. This approach was first presented by Rezeka and Herein [106] where it was shown that by measuring the engine velocity and the in-cylinder pressure it was possible to determine the instantaneous frictional torque and therefore validate relevant mathematical models. A more recent publication by Zweiri et al. [74] shows similar yet a more comprehensive analysis of the instantaneous engine friction. One of the main challenges of this approach though is the proper parametrisation and validation of the models developed. This is because some of the required parameters are rather difficult to be measured/identified, but also because the measurement of the instantaneous friction is a rather challenging procedure (see [74] for further details). In fact all of the presented instantaneous friction models are relying upon the estimation of the instantaneous friction via the measurement of the engine velocity and in-cylinder pressure [228] (similar to Rezeka and Herein [106] procedure). Nevertheless, a very recent publication by Gore et al. [229] shows a methodology that can be used for measuring directly the piston fiction using floating-liner principle, this will probably provide a more accurate and reliable measurement which will contribute in the development and validation of more accurate models. Lastly, another disadvantage of these models is the relatively high computational power that is required to run in real-time conditions, thus most practical engine strategies are not making use of this approach for control and diagnosis purposes.

- The average method describes actually the mean value of the engine friction over a complete engine cycle. In order to determine the overall average friction it is necessary to conduct an appropriate experiment that will allow the accurate measurement/identification of the engine friction, some well-known techniques are the method of free deceleration curves, the Williams lines method, the Morse test, the motoring method, and the indicator diagram

method [227]. The actual determination of the engine losses can be done either globally or locally. Global approaches are based on the development of a single mathematical model of either parametric [78] or non-parametric [230] structure that relates the engine operating conditions with the actual losses. One of the problems of global approaches is that the resulting mathematical models have little physical interpretation which is a useful characteristic if someone is interested to conduct analytical component studies. On the other hand the local approach includes the evaluation of the losses for each different component (similar to the instantaneous approach) [82]. Compared to the global approach, local methods result in more detailed formulae that are composed of many terms with physical meaning. Consequently, there is a trade-off between the model complexity (global models more suitable) and physical interpretation (local models better). Overall it should be noted that mean value friction models are used more often in industrial applications compared to instantaneous based models as they are more reliable and easier to identify and validate [78].

7.1.2 Evaluation of Engine Friction Models

The determination of engine friction serves two practical purposes, the first is for improvement in the design of the engine, and the second is for the real-time control and diagnosis of the engine. The first (design) is usually achieved through extensive simulation studies that allow engineers to understand what are the key factors and operating conditions that affect the engine friction level in order to make the necessary design changes [81, 231]. The second (control/diagnosis) is based on the real-time prediction of engine torque that is used by the engine controller in order to operate the engine more efficiently and safely [232]. As can be expected, studies on this matter are numerous, however this does not necessarily implies that there is no space for additional work. For instant our literature review has shown that engine friction models with physical interpretation are quite challenging to parametrise which indicates the importance of developing appropriate

system identification tools that can do this work efficiently. Additionally the analytical assessment of parameters with physical meaning that can be found commonly in engine friction models have not been studied thoroughly until now. Instead previous studies where focused on understanding the origin of the friction in terms of engine components such as crankshaft, piston, valvetrain, pumping losses and external engine accessories i.e. alternator. Even though these studies are highly valuable for eliminating engine's frictional losses, they do not provide any direct relationship to engine design parameters that could be taken into account during the design process.

The material that is presented in this chapter provides analytical tools that can be used for engine design as well as control and diagnosis purposes. To be more specific, in the next sections will be shown how it is possible to rank -in a prioritised list- the physical parameters/characteristics of the engine that affect the frictional losses based on analytical sensitivity analysis, and secondly will be presented adaptive friction identification for on-line monitoring and characterisation purposes. It should be highlighted that even though these tools are applied to the mean value engine friction model that was presented in Chapter 3 this does not limits their application to crank-angle based friction models.

7.2 Engine Friction Parameters Ranking

A methodology for ranking the sensitivity of engine's design characteristics in respect to the frictional losses is discussed in this section. Analytical sensitivity analysis is implemented in the physical parameters of the mean value semi-physical engine friction model that was presented earlier in Chapter 3. The effect of the operating conditions such as engine speed and load on the sensitivity coefficients is also presented. The output of this study could be then used from design engineers for the purpose of improving the design of individual engine parts e.g. tightening component's mechanical tolerances, optimising components sizing etc. The mathematical formulation of the problem and the ranking of the design char-

acteristics based on analytical sensitivity analysis follows next.

7.2.1 Problem Formulation

For this study the mean value semi-physical engine friction model developed by Sandoval and Heywood [82] was used to assess the sensitivity of various design characteristics in the engine friction. It should emphasized that the presented methodology is not limited only for this particular engine models. Instead the presented mathematical tools could be implemented in different (maybe more of less detailed) engine friction model. Thus the reader should take this case study as an example in order to understand the principles of the suggested ideas.

The process starts with appropriate formulation of the engine friction model. According to the analysis conducted in Chapter 3 (see Eq. 3.44 to Eq. 3.50), the mean value semi-physical engine friction model consists of one depended variable (friction torque), several independent variables (e.g. engine speed, intake pressure, oil temperature), physical parameters (e.g. cylinder bore, stoke, compression ratio, etc.) that represent some design characteristics of the engine, and regression coefficients that are used to fit the model to real experimental data. Here the model is rearranged in such a manner so that the user would be able to assess the sensitivity of the physical parameters of the model (engine design characteristics) under different operating conditions that are defined by the model inputs (independent variables). For the sake of simplicity the model is written in the following functional form:

$$\tau_{fri}(t) = f\left(N_{en}(t), P_{int}(t), T_{oil}(t), b, S, r, D_b, D_i, D_e, L_b, L_v, \kappa\right) \tag{7.1}$$

Where, $\tau_{fri}(t)$ is the engine torque, $N_{en}(t)$, $P_{int}(t)$ and $T_{oil}(t)$ are the control inputs that define the operating conditions of the engine and represent the engine speed, intake manifold pressure, and oil temperature respectively, whilst the rest of the variables are the physical parameters of the model that represent various engine design characteristics i.e. b is the cylinder bore diameter, S is the cylinder stroke length, r is the crank arm length, D_b is the diameter of the crankshaft

bearings, D_i is the diameter of the intake valve, D_e is the diameter of the exhaust valve, L_b is the length of the crankshaft bearings, L_v is maximum valve lift, and κ is the compression ratio.[1]

At this point in time it is very important to clarify that the above formulation could be rearrange to add some additional parameters that are related to the design characteristics of the engine. For instance, here the number of crankshaft bearings or valves are fixed as we assume that these characteristics are usually predefined by the engine designers. However if someone was interested particularly to examine the level of influence of these parameters, it would be possible to included them in the overall problem. In either case, what the reader has to appreciate is that given a physical or semi-physical model it is possible to pre-select the parameters (design characteristics) that will be tested regarding their sensitivity on the engine frictional losses.

Now, knowing the functional relationship of the model inputs/output and physical parameters it is possible to proceed to the analytical sensitivity analysis.

7.2.2 Parameters Ranking based on Sensitivity Analysis

The analytical sensitivity analysis was the core of the orthogonal-based parameter identifiability analysis that was presented in Section 5.2.1. Here the same principle is implemented in order to rank the sensitivity of the engine friction parameters in respect to friction torque in a ascending order.

The ranking of the engine friction parameters requires the deployment of the three first steps of the orthogonal-based parameter identifiability algorithm (Algorithm 5.1) that was presented in Section 5.2.1. The first step involves the analytical calculation of the sensitivity or Jacobian matrix; for the present problem the

[1] Additional information on the engine friction model can be found in Chapter 3 and in Reference [82].

sensitivity matrix takes the following form:

$$Z = \begin{bmatrix} z_b|_{t_1} & z_S|_{t1} & z_r|_{t1} & z_{D_b}|_{t1} & z_{D_i}|_{t1} & z_{D_e}|_{t1} & z_{L_b}|_{t1} & z_{L_v}|_{t1} & z_\kappa|_{t1} \\ \vdots & \vdots & \vdots & \vdots & \vdots & \vdots & \vdots & \vdots & \vdots \\ z_b|_{t_n} & z_S|_{tn} & z_r|_{tn} & z_{D_b}|_{tn} & z_{D_i}|_{tn} & z_{D_e}|_{tn} & z_{L_b}|_{tn} & z_{L_v}|_{tn} & z_\kappa|_{tn} \end{bmatrix} \tag{7.2}$$

Where $z|_t$ represent the partial derivatives of the corresponding parameter e.g. b, S, r, etc., at time t (note that under steady state conditions $t = 0$); this is equivalent to the following notation:

$$z_b|_t = \frac{\partial \tau_{fri}(t)}{\partial b} * \frac{b_0}{\tau_{fri_0}}, \quad z_S|_t = \frac{\partial \tau_{fri}(t)}{\partial S} * \frac{S_0}{\tau_{fri_0}}, \quad z_r|_t = \frac{\partial \tau_{fri}(t)}{\partial r} * \frac{r_0}{\tau_{fri_0}}$$

$$z_{D_b}|_t = \frac{\partial \tau_{fri}(t)}{\partial D_b} * \frac{D_{b_0}}{\tau_{fri_0}}, \quad z_{D_i}|_t = \frac{\partial \tau_{fri}(t)}{\partial D_i} * \frac{D_{i_0}}{\tau_{fri_0}}, \quad z_{D_e}|_t = \frac{\partial \tau_{fri}(t)}{\partial D_e} * \frac{D_{e_0}}{\tau_{fri_0}}$$

$$z_{L_b}|_t = \frac{\partial \tau_{fri}(t)}{\partial L_b} * \frac{L_{b_0}}{\tau_{fri_0}}, \quad z_{L_v}|_t = \frac{\partial \tau_{fri}(t)}{\partial L_v} * \frac{L_{v_0}}{\tau_{fri_0}}, \quad z_\kappa|_t = \frac{\partial \tau_{fri}(t)}{\partial \kappa} * \frac{\kappa_0}{\tau_{fri_0}}$$

See also that the sensitivity coefficients are also normalised with respect to the initial conditions of the corresponding parameters. This is important because as it will be shown later the suggested approach relies upon the calculation of the sum of squared value of each individual sensitivity coefficient, which indicates that any possible numerical issues would provide misleading results. Additionally the scaling is critical when the parameters under examination have different physical units.

Following the successful computation of the sensitivity matrix, it is required now to calculate the sum of square of each individual column of the sensitivity matrix. To do that we need to assign an initial set of parameters and provide some representative operating conditions that the system would operate. In this particular case the operating conditions were defined by the engine speed, intake manifold pressure, and the temperature of the oil.

The last step in the process is the actual ranking of the parameters. This is achieved by peaking the column in the sensitivity matrix which has the largest sum of square value as the most influential parameter in the engine frictional

torque. The same task is undertaken in order to find the second most influential parameter in the system. This process repeats up to the point were all the friction parameters have been eliminated.

A MATLAB script was developed for the deployment of all the above steps. In fact the complexity involved in the analytical evaluation of the partial derivatives made it impractical to calculate them by hand, which was one of the main reason to use MATLAB to calculate them using the MATLAB symbolic toolbox. This MATLAB program executes automatically all the above steps and outputs the actual ranking of the parameters for the given operating conditions and initial values. The user is able to control the operating conditions of the engine i.e. engine speed, intake manifold pressure (implies engine load), engine oil temperature. Additionally the initial conditions of the physical parameters of the model can be controlled by the user. The reader can find the complete M-code in the Appendix B.2.

Coming to the results, the ranking order of the physical parameters of the engine friction model were determined for various operating conditions. In fact, a full factorial experiment with three variables and three levels (3^3) was designed, resulting in 27 different experiments. The reader must remember that this process does not require real world experiments as it is based on the analytical sensitivity analysis of the model. With that in mind, the number of experiments could be increased up the level of resolution that the user would need without any real cost; here we only present a small number of tests for demonstration purposes. The variables of the experiment were the inputs of the engine friction model i.e. the engine speed (N_{eng}) $(min = 1000[RPM] - max = 5000[RPM])$, the intake manifold pressure (P_{int}) $(min = 0.1[Bar] - max = 1.0[Bar])$, and the engine oil temperature (T_{oil}) $(min = 20[C^o] - max = 90[C^o])$. The parameter ranking results are tabulated in Table 7.1 and visualised in Fig. 7.1.

Test	Operating Point			Parameters Ranking								
	N_{en} [RPM]	P_{int} [Bar]	T_{oil} [^{o}C]	b	S	r	D_b	D_i	D_e	L_b	L_v	κ
1	1000	0.10	20	1	4	2	3	9	8	5	6	7
2	3000	0.10	20	2	5	1	3	9	8	4	6	7
3	5000	0.10	20	2	5	1	3	9	8	4	6	7
4	1000	0.55	20	1	4	2	3	9	8	6	7	5
5	3000	0.55	20	2	5	1	3	9	8	4	7	6
6	5000	0.55	20	3	5	1	2	9	8	4	7	6
7	1000	1.00	20	2	4	1	3	9	8	6	7	5
8	3000	1.00	20	3	5	1	2	9	8	4	7	6
9	5000	1.00	20	3	5	2	1	9	7	4	8	6
10	1000	0.10	55	1	4	2	3	9	8	5	6	7
11	3000	0.10	55	1	4	2	3	9	8	5	6	7
12	5000	0.10	55	1	4	2	3	9	8	5	6	7
13	1000	0.55	55	1	4	2	3	9	8	6	7	5
14	3000	0.55	55	2	4	1	3	9	8	5	7	6
15	5000	0.55	55	2	4	1	3	9	8	5	7	6
16	1000	1.00	55	2	4	1	3	9	8	6	7	5
17	3000	1.00	55	2	4	1	3	9	8	5	7	6
18	5000	1.00	55	3	5	1	2	9	7	4	8	6
19	1000	0.10	90	1	4	2	3	9	8	5	6	7
20	3000	0.10	90	1	4	2	3	9	8	5	6	7
21	5000	0.10	90	1	4	2	3	9	8	5	6	7
22	1000	0.55	90	1	4	2	3	9	8	6	7	5
23	3000	0.55	90	1	4	2	3	9	8	5	7	6
24	5000	0.55	90	1	4	2	3	9	8	5	7	6
25	1000	1.00	90	2	4	1	3	9	8	6	7	5
26	3000	1.00	90	2	4	1	3	9	8	5	7	6
27	5000	1.00	90	2	4	1	3	9	7	5	8	6

Table 7.1: Parameters ranking results for each different operating conditions.

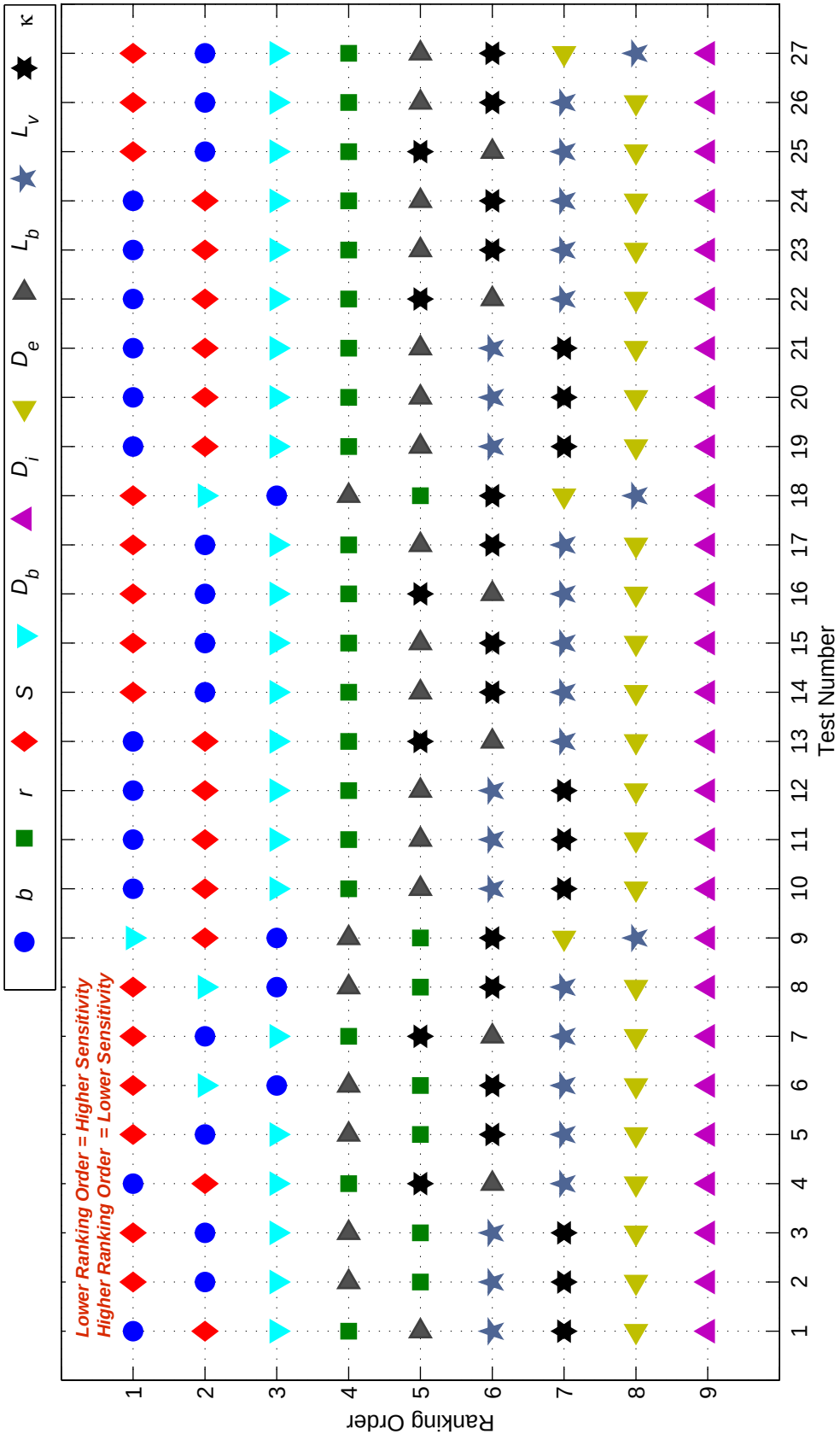

Figure 7.1: Graphical illustration of the parameters ranking results, scatter plot.

The above results show the ranking order of each individual engine friction parameter in respect to the operating conditions of the engine. We should clarify in the first place, that the higher the ranking order the lower the sensitivity of the corresponding parameter to the engine friction, e.g. a parameter with ranking order 1 is more sensitive to a parameter with ranking order 5. It should also be noted that the presented results were cross-validated by conducting a pure simulation study in which the effect of the each individual parameter was examined based on one-at-a-time approach.

One of the first conclusion that could be drawn, is that the operating conditions affect the ranking order of the parameters. For instance the ranking order of the cylinder bore diameter (b) parameter is 1 for the first test while for the second test is 2. The difference between these tests was located on the engine speed value (lower for the first test) so someone could say that the higher the engine speed the lower the sensitivity of the cylinder bore diameter in the engine friction level. Another trend is that design characteristics related to crank-piston assembly have higher sensitivity to valve-train parameters. Similar results were obtained in another study conducted by Shayler et al. [233], however this study was not providing information regarding the sensitivity of each individual physical parameter of the piston assembly e.g. bore diameter or crank-arm length, but was investigating the contribution of the different engine components such as piston, crankshaft, oil pump, valve-train etc. This information could then be used by engine designer during the engine development process.

As a matter of fact the sensitivity analysis of each parameter under different operating conditions, could be a whole different study on its own. Thus here we limit our discussion to the presentation of the principles and potential of the suggested methodology rather than making use of it, for a practical application. Nevertheless the result that are presented here can be used by the reader in order get a first impression with regards to the ranking order of each parameter under a small number of different operating conditions of the engine.

7.3 Adaptive Friction Characterisation

One of the main disadvantages of the semi-empirical model developed by Patton et al. [81] and recently updated by Sandoval and Heywood [82] (see Chapter 3, Eq. 3.44 to Eq. 3.50) is its heavy reliance on experimental data in order to accurately represent the friction losses of a given engine. This was also shown in a more recent study conducted by Shayler et al. [233]; the authors showed that Patton's model cannot accurately predict the frictional losses of engines under cold and low speed operating conditions. Consequently, Shayler et al. [233] re-parametrised Patton's model using data from cold and low speed running conditions, to enhance its validity.

Similar problems were identified during our research on the subject. In particular it was found that trend-wise the model had good agreement with the actual friction, however the absolute estimated values had significantly large errors. This problem is presented in Fig. 7.2 and Table 7.2 were the actual and predicted engine friction torques are compared during slow transient as well as steady state conditions.

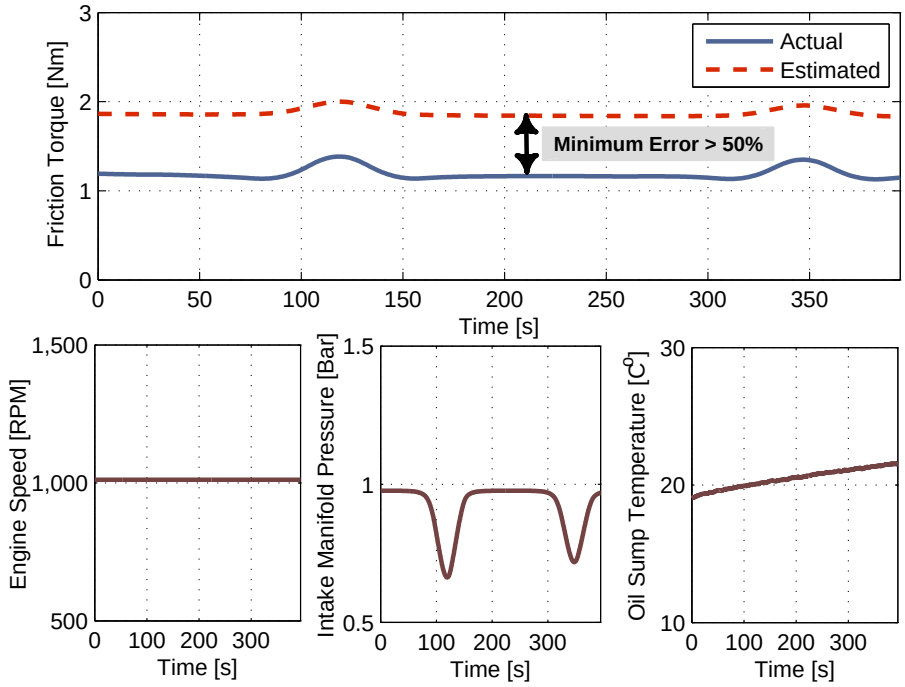

Figure 7.2: Difference between estimated and actual engine friction torque.

Table 7.2: Steady state error between actual and estimated engine friction.

Speed [RPM]/Pressure [Bar]	Actual Friction [Nm]	Estimated Friction [Nm]	Relative Error [%]
750[RPM]/1[Bar]	1.14	1.74	52.63
1000[RPM]/1[Bar]	1.16	1.81	56.03
1250[RPM]/1[Bar]	1.22	1.90	55.73
1500[RPM]/1[Bar]	1.34	2.10	56.55

Given these significant differences, it was decided to make use of the adaptive identification tools that were presented in Chapter 5 in order to fit adaptively the parameters of the engine friction model and increase its validity as opposed to real measurements. Additionally it should be emphasized that the application of adaptive identification algorithms is also very valuable particularly for engine friction condition monitoring purposes. Thus to summarise, the material that is presented bellow could be used for two different application i.e. on-line condition monitoring, and on-line engine friction characterisation

7.3.1 Problem Formulation

The main objective of this study is to refine sequentially (recursively) the parameters of the semi-empirical friction model in respect of minimising the difference between the modelled and the actual engine friction. This would allow the on-line identification of friction which is very valuable for control and diagnosis purposes. To do so the present engine friction model (see Chapter 3, Eq. 3.44 to Eq. 3.50) had to be formulated in such a way so that the application of recursive identification algorithms would be possible.

The major question to be answered is about the functional relationship of the model parameters in respect to its output e.g. linear-in-the-parameters or non-linear-in-the-parameters system. This question can be easily answered if we as-

sume that Sandoval and Heywood [82] friction model can be divided into two main parts, namely the physical part and the empirical part. To explained this argument we take as an example the equation that describes the engine frictional losses caused by the crankshaft mechanism (Eq. 7.3):

$$\text{cfmep} = \underline{1.22 * 10^{5}} \left(\frac{D_b}{b^2 S n_c}\right) + \underline{3.03 * 10^{-4}} \sqrt{\frac{\mu}{\mu_0}} \left(\frac{N_{en} {D_b}^3 L_b n_b}{b^2 S n_c}\right) + \underline{1.35 * 10^{-10}} \left(\frac{{D_b}^2 {N_{en}}^2 n_b}{n_c}\right) \tag{7.3}$$

Note that the above equation consists of a number of parameters that represent the physical characteristics of the engine e.g. b (cylinder bore diameter) and S (cylinder stroke length), and some numerical constants (underlined numbers) that are actually the regression coefficients that are used to fit the model to the real experimental results. The structure of this model can be said that is both linear-in-the-parameters and non-linear-in-the-parameters. This is because someone could isolate the dependence of the physical parameters and work only with the regression coefficients; in that case the model structure would be linear-in-the-parameters. On the other hand if someone would assume that the regression coefficients remain always constant and work with the physical parameters of the model then the structure would be non-linear-in-the-parameters.

In our case, we are interested to enhance the validity of the model by tracking only the values of the regression coefficients. Considering the above assumptions, the individual components of the friction mean effective pressure equation (Eq. 7.3) can be re-written as follows:

$$\text{cfmep} = \mathbf{c_1} \left(\frac{D_b}{b^2 S n_c}\right) + \mathbf{c_2} \sqrt{\frac{\mu}{\mu_0}} \left(\frac{N_{en} {D_b}^3 L_b n_b}{b^2 S n_c}\right) + \mathbf{c_3} \left(\frac{{D_b}^2 {N_{en}}^2 n_b}{n_c}\right) \tag{7.4}$$

$$\begin{aligned}\text{rfmep} = {} & \mathbf{c_4} \sqrt{\frac{\mu}{\mu_0}} \left(\frac{v_p}{b}\right) + \mathbf{c_5} \left(\frac{F_t}{F_{to}} C_r\right) \left(1 + \frac{500}{N_{en}}\right) \\ & * \left(\frac{1}{b^2}\right) + \mathbf{c_6} \sqrt{\frac{\mu}{\mu_0}} \left(\frac{N_{en} {D_b}^3 L_b n_b}{b^2 S n_c}\right) + \mathbf{c_7} \\ & * \frac{P_{int}}{P_{atm}} \left[0.088 \sqrt{\frac{\mu}{\mu_0}} \kappa + 0.182 \left(\frac{F_t}{F_{to}}\right) \kappa^{(1.33 - 0.112 v_p)}\right] + \mathbf{c_8}\end{aligned} \tag{7.5}$$

$$\begin{aligned}\text{vfmep} = \mathbf{c_9}\sqrt{\frac{\mu}{\mu_0}}\frac{N_{en}n_b}{b^2Sn_c} + \mathbf{c_{10}}\left(1+\frac{500}{N_{en}}\right)\frac{n_v}{Sn_c} \\ + \mathbf{c_{11}}\left(\frac{N_{en}n_v}{Sn_c}\right) + \mathbf{c_{12}}\sqrt{\frac{\mu}{\mu_0}}\frac{{L_v}^{1.5}{N_{en}}^{0.5}n_v}{bSn_c} \\ + \mathbf{c_{13}}\left(1+\frac{500}{N_{en}}\right)\frac{L_v n_v}{Sn_c}\end{aligned} \tag{7.6}$$

$$\text{afmep} = \mathbf{c_{14}} + \mathbf{c_{15}}N_{en} + \mathbf{c_{16}}{N_{en}}^2 \tag{7.7}$$

$$\begin{aligned}\text{pfmep} = \mathbf{c_{17}}(P_{atm}-P_{int}) + \mathbf{c_{18}}\left(\frac{P_{int}}{P_{atm}}\right)^2\left(\frac{{v_p}^2}{{n_v}^2{\rho_i}^4}\right) \\ + \mathbf{c_{19}}\left(\frac{P_{int}}{P_{atm}}v_p\right)^2 + \mathbf{c_{20}}\left(\frac{P_{int}}{P_{atm}}\right)^2\left(\frac{{v_p}^2}{{n_v}^2{\rho_e}^4}\right)\end{aligned} \tag{7.8}$$

Here, the symbol $\mathbf{c_\#}$ represents all the regression coefficients of the friction mean effective pressure model. For additional information regarding the rest of the symbols refer to Chapter 3, Section 3.2.4.

Based on the above formulation it is now clearly visible that the friction mean effective pressure equation is linear-in-the-parameters. Equivalently, the same could be said for the model of the engine friction torque (Eq. 3.44) as it is linearly proportional to the friction mean effective pressure (Eq. 3.45). Overall the model engine friction torque model could be expressed in the following general form of linear regression models:

$$y(t) = \phi^T(t)\vartheta + \epsilon(t) \tag{7.9}$$

And in this particular case, $y(t)$ is the dependent variable $(\tau_{fri}(t))$, $\phi^T(t)$ is the independent variables vector $[N_{en}, P_{int}, P_{amb}, T_{oil}]^T$, ϑ is the vector of unknown parameters $[\mathbf{c_1}, \mathbf{c_2}, ..., \mathbf{c_{20}}]$, and $\epsilon(t)$ is a random error term.

Consequently, it is now possible to implement linear recursive algorithms in order to adjust the unknown model parameters and thus fit the model to actual experimental measurements in real-time. Concurrently this process allows the tracking of the model parameters which provides valuable information regarding the health condition of the system.

7.3.2 Experimental Procedure

The transient cyclic motoring test cell, presented in Chapter 4, was used for implementing and testing the proposed adaptive friction identification methodology. The instrumentation equipment required for the friction identification is depicted in Fig. 7.3. As it can be seen readings from the engine torque transducer, oil sump thermocouple, engine encoder, and intake manifold pressure were needed. Ambient pressure and temperature measurements were taken during the course of the tests, however these quantities were maintained relatively constant thus were not monitored continuously. Most of these measurements (apart from the oil sump temperature) were acquired on a crank angle basis, but then were averaged for the characterisation of the mean value friction model. The control inputs of the experiment were the dynamometer speed and engine throttle.

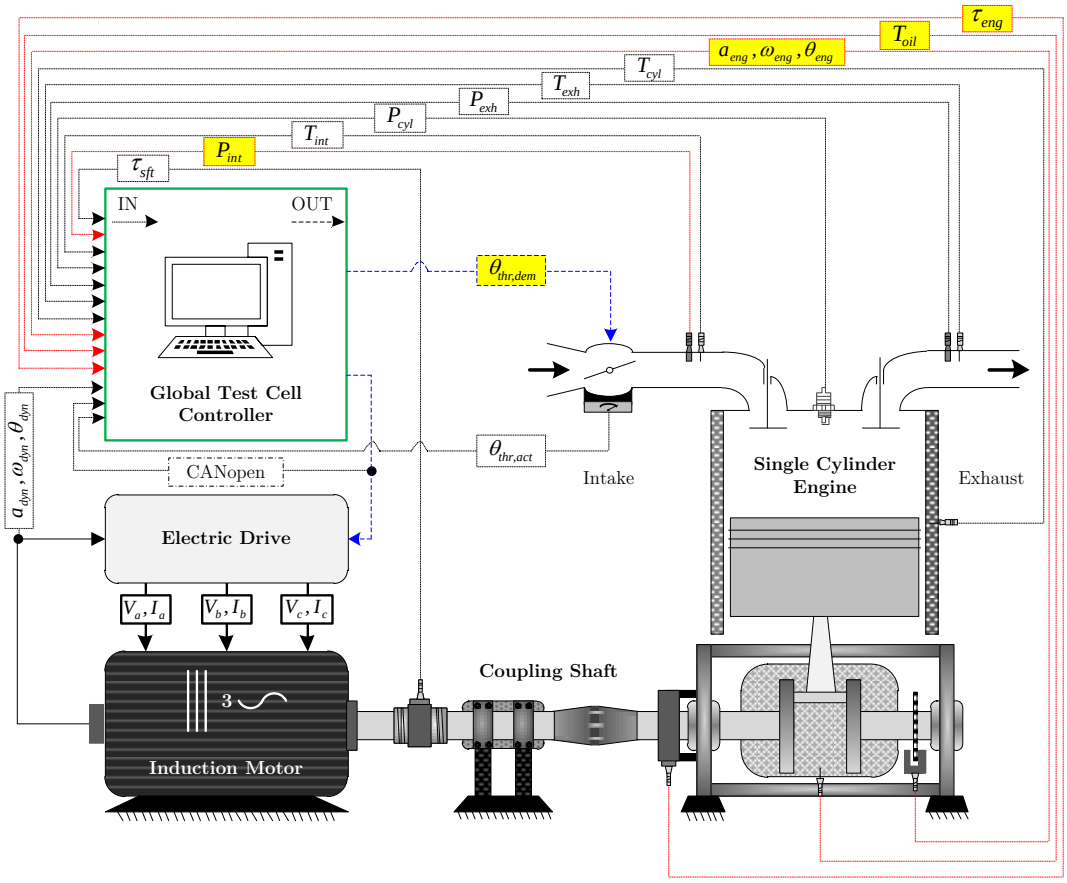

Figure 7.3: Instrumentation equipment for the adaptive friction estimation, coloured lines: red=sensors, blue=actuators, green=controller.

The engine friction torque was measured at various speed and load conditions. In particular, the dynamometer was responsible to rotate the engine at fixed speeds while the load of the engine was controlled via the intake throttle position. Here engine friction measurements were taken for 4 different engine speeds i.e. 750 (Fig. 7.4a), 1000 (Fig. 7.4b), 1250 (Fig. 7.4c), and 1500 (Fig. 7.4d) RPM. As far as the engine load conditions, intake manifold pressure was swept (slowly) from atmospheric conditions down to around 0.7 Bar by controlling throttle valve position. It should be highlighted that the present characterisation exercise was not aiming in the complete mapping of the engine (as presented in [78]), thus speed and load conditions did not cover the entire operating range of the engine. Instead the objective is to show a characterisation example so that the reader would understand the principles behind the suggested approach.

Turning to the actual experimental measurements, in Fig. 7.4 are presented the results from the 4 different tests. Each sub-figure shows the friction torque, the engine speed, the intake manifold pressure, and the oil temperature. These are also the main observation variables that are required for the characterisation of the engine friction model. By observing the results it is possible to see how friction is increased with higher engine speeds but also during non-atmospheric manifold pressure condition due to the increase of the pumping losses.

At this point in time, it is also useful to note that standard engine friction characterisation exercises require steady state speed as well as intake manifold conditions [78]. In this work we present how friction torque can characterised under slow transient intake manifold conditions in order to save testing time. Note that this process is on-line so time is also saved from the off-line characterisation process which is usually required in order to develop an engine friction torque models.

The qualitative adaptive identification of the engine friction torque for the aforementioned experiments is presented in the next section.

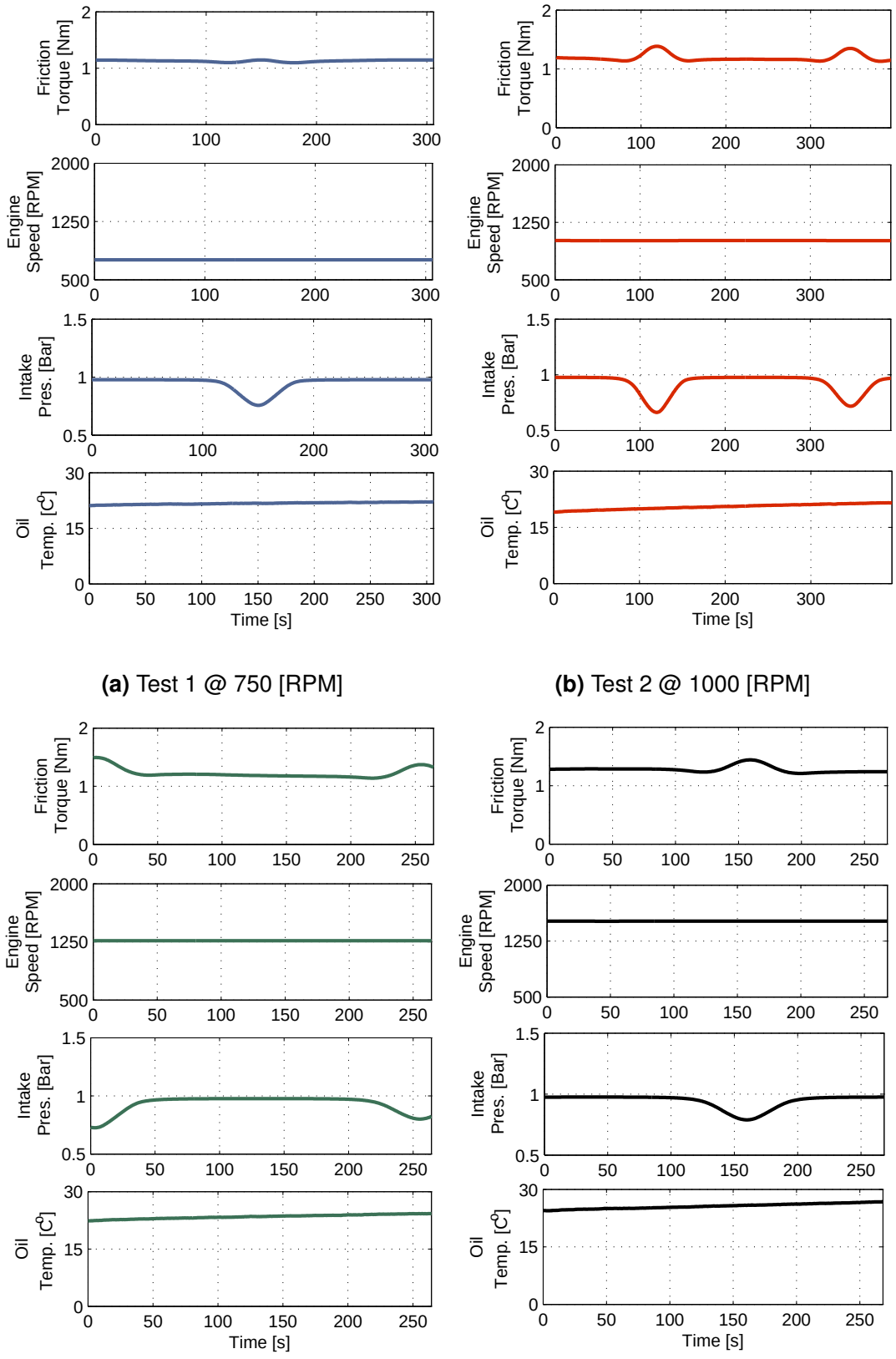

(a) Test 1 @ 750 [RPM]

(b) Test 2 @ 1000 [RPM]

(c) Test 3 @ 1250 [RPM]

(d) Test 4 @ 1500 [RPM]

Figure 7.4: Engine friction motored experiments, mean value measurements.

7.3.3 Qualitative Adaptive Friction Identification

The engine friction torque model could be categorised in the general class of linear regression system models (see Section 7.3.1). This argument indicates that the unknown or uncertain parameters of the friction model could be identified/tracked by using linear recursive identification algorithms as the ones used in Chapter 6, in the coupling shaft conditions monitoring application. Although this may be true, the complexity of the friction model arises some questions regarding the identifiability of its parameters. Consequently, prior to the application of the recursive algorithms it would be beneficial to assess the estimability of the model parameters i.e. linear regressions coefficients, under different operating conditions.

The process that was followed for the identification of the parameters is identical to the “Qualitative Adaptive Identification" framework that was presented in Chapter 5, Section 5.4, Fig. 5.7. The main idea behind this framework is that the user assesses the identifiability of the model parameters in an off-line mode, prior the actual adaptive identification step. In this manner the quality and robustness of the on-line identification results are increased while the user gets a better inside regarding the model estimability and the validity of the parameter estimates.

Under those circumstances, the identifiability of the engine friction regression coefficients was examined for the four different test cases as presented in Fig. 7.4. To do that, the orthogonal-based identifiability algorithm was deployed (Algorithm 5.1). For the implementation of the orthogonal-based identifiability algorithm the sensitivity matrix (Eq. 7.10) of the system was the main element that had to be predefined.

$$J = \begin{bmatrix} j_{\mathbf{c_1}}|_{t_1} & j_{\mathbf{c_2}}|_{t_1} & \cdots & j_{\mathbf{c_{20}}}|_{t_1} \\ \vdots & \vdots & \ddots & \vdots \\ j_{\mathbf{c_1}}|_{t_n} & j_{\mathbf{c_2}}|_{t_n} & \cdots & j_{\mathbf{c_{20}}}|_{t_n} \end{bmatrix} \tag{7.10}$$

Where $j_{\mathbf{c_\#}}|_{t_1}$ represents the partial derivatives of the corresponding regression parameter e.g. $\mathbf{c_1}$, $\mathbf{c_2}$, $\mathbf{c_{20}}$, etc., at time t. Note that the sensitivity matrix is calculated for each time step t i.e. $t_1, t_2, \ldots, t_n$, where n is the final sample time. It is important to remember that each sensitivity coefficients is normalised with respect to the initial conditions of the corresponding parameters.[2]

$$j_{\mathbf{c_\#}}|_{t_1} = \frac{\partial \tau_{fri}(t)}{\partial \mathbf{c_\#}} * \frac{\mathbf{c_{\#_0}}}{\tau_{fri_0}}$$

Having defined the sensitivity matrix of the problem it is possible to proceed to the next steps of the orthogonal-based identifiability algorithm (Algorithm 5.1). The calculation of the sensitivity matrix as well as the rest of the steps of the orthogonal-based identifiability algorithm were executed automatically in MATLAB. The reader can find the complete M-code in the Appendix B.3.

The results of the identifiability analysis are presented in Table 7.3. The table shows the effect of experimental conditions (Fig. 7.4) in the identifiability of the parameters. As it is observed only six out of twenty regression coefficient are identifiable in all different test cases (Fig. 7.4a, Fig. 7.4b, Fig. 7.4c, Fig. 7.4d). In particular the identifiable parameters are $\mathbf{c_1}$, $\mathbf{c_4}$, $\mathbf{c_5}$, $\mathbf{c_7}$, $\mathbf{c_{17}}$, and $\mathbf{c_{19}}$. As far as the rest of the parameters are concerned, those are not identifiable, meaning that they should not be taken into account during the adaptive identification process; in such cases the non-estimable parameters were fixed to some initial known values. Here the values of the non-estimable parameters are taken from the original friction model as it was presented in Chapter 3 (Eq. 3.44 to Eq. 3.50), [82].

One of the main advantages of conducting an identifiability analysis prior to actual adaptive identification is related to the computational requirements of the recursive algorithms, provided that some of the parameters will be non-identifiable thus removed from the adaptive identification process. The above statement is also true in the present application. The identifiability analysis showed that only

[2]The reader should be informed that the identifiability could also be evaluated without calculating the sensitivity matrix, provided that the system has been described based on a linear regression model structure (see [234] for an alternative approach).

six out of twenty parameter should be considered during the identification process. This implies that the adaptive identification process will be much less computationally demanding if we were to compare it with the identification of all twenty parameters.

Table 7.3: Identifiability ranking of the friction regression coefficients.

Parameter	Identifiability Ranking			
	Test 1	*Test 2*	*Test 3*	*Test 4*
$\mathbf{c_1}$	1	1	1	1
$\mathbf{c_2}$	–	–	–	–
$\mathbf{c_3}$	–	–	–	–
$\mathbf{c_4}$	2	2	2	2
$\mathbf{c_5}$	3	5	5	4
$\mathbf{c_6}$	–	–	–	–
$\mathbf{c_7}$	6	6	6	6
$\mathbf{c_8}$	–	–	–	–
$\mathbf{c_9}$	–	–	–	–
$\mathbf{c_{10}}$	–	–	–	–
$\mathbf{c_{11}}$	–	–	–	–
$\mathbf{c_{12}}$	–	–	–	–
$\mathbf{c_{13}}$	–	–	–	–
$\mathbf{c_{14}}$	–	–	–	–
$\mathbf{c_{15}}$	–	–	–	–
$\mathbf{c_{16}}$	–	–	–	–
$\mathbf{c_{17}}$	5	4	4	5
$\mathbf{c_{18}}$	–	–	–	–
$\mathbf{c_{19}}$	4	3	3	3
$\mathbf{c_{20}}$	–	–	–	–

Now that a set of estimable parameters has been determined, it is possible to proceed to the final step of the process which is the adaptive identification of engine friction torque (τ_{fri}) (Eq. 7.9). This is based on the on-line estimation of the estimable parameters i.e. $\mathbf{c_1}$, $\mathbf{c_4}$, $\mathbf{c_5}$, $\mathbf{c_7}$, $\mathbf{c_{17}}$, and $\mathbf{c_{19}}$, by using linear recursive identification algorithms. More specifically in the present application the Discrete Square Root Filtering (see Chapter 5, Algorithm 5.5) algorithm was deployed to track the estimable parameters of the friction model.

For the execution of the DSFC algorithm the depenedent variable $(y(t))$, the

vector of independent variables $(\phi(t))$, and the vector of unknown estimable parameters (ϑ) had to be defined. These are form as follows:

$$y(t) = \tau_{fri}(t)$$

$$\phi(t) = [N_{en}(t), P_{int}(t), P_{amb}(t), T_{oil}(t)]$$

$$\vartheta = [\mathbf{c_1}, \mathbf{c_4}, \mathbf{c_5}, \mathbf{c_7}, \mathbf{c_{17}}, \mathbf{c_{19}}]$$

Additionally the initial parameter and square root covariance estimates had to be provided. Here the initial friction parameter estimates (ϑ_0) were extracted from the original friction model (Eq. 3.44 to Eq. 3.50) [82].

$$\vartheta_0 = [1.22 * 10^5, 294, 4.06 * 10^4, 6.89, 1, 0.178]$$

As for the initial square covariance estimates (S_0), those were set equal to $\sqrt{100}$ provided that the initial parameter estimates were relatively close to the true expected values.

$$S_0 = \sqrt{100} * I_6$$

Where, I_6 is an identity matrix of size 6.

The results from the adaptive identification of engine friction torque are summarised in Fig. 7.5. The results show that the estimated friction torque is in close vicinity with the actual (measured) friction torque in all different test cases i.e. Fig. 7.5a, Fig. 7.5b, Fig. 7.5c, and Fig. 7.5d. Note that during the first seconds of the the identification process the estimated friction torque was larger than the actual. This is originated from the fact that the initial conditions of the estimated parameters were resulting in higher friction torque predictions (see Fig. 7.2). Nevertheless after the initialisation period the estimated friction responses were lying within $\pm 5\%$ of the actual friction in every occasion. Additionally the Normalised Mean Square Error (NMSE) (Eq. 6.4) was used as a measure of estimation success, showing that the estimated friction had meaningless difference as opposed to the actual friction measurements.

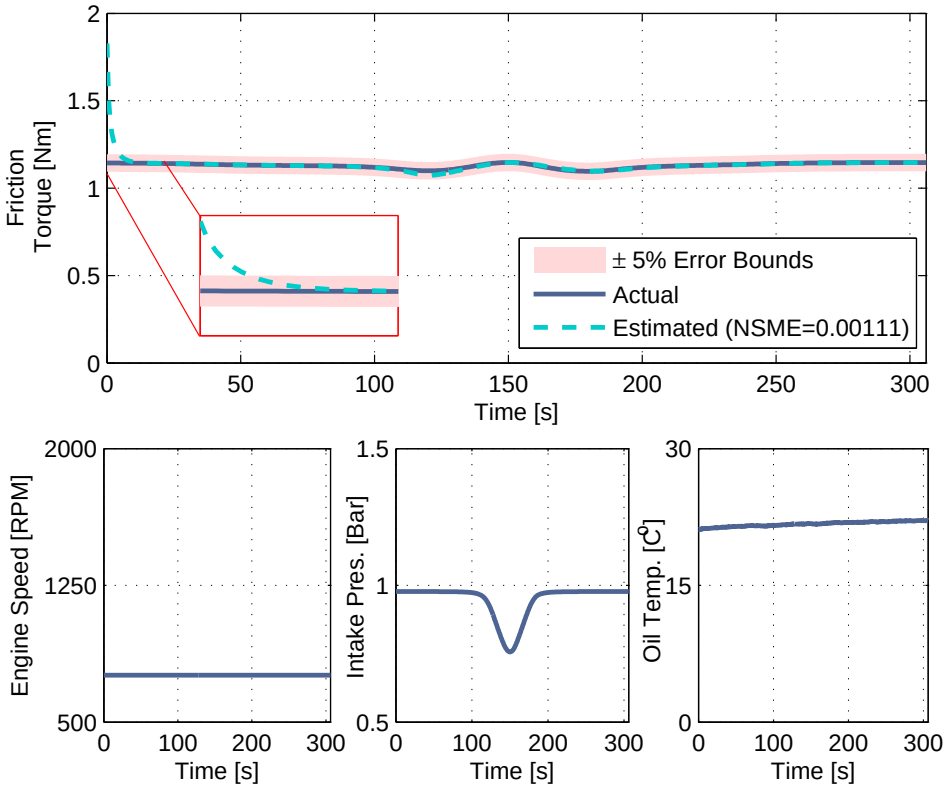

(a) Estimated friction torque @ 750 [RPM] (Test 1, Fig. 7.4a)

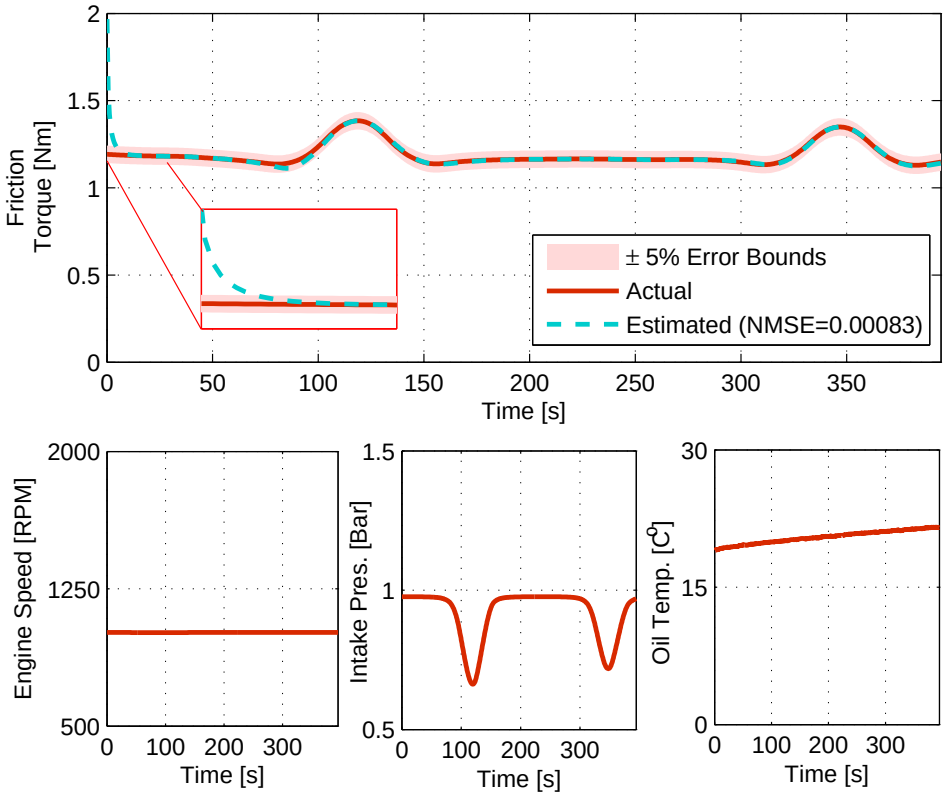

(b) Estimated friction torque @ 1000 [RPM] (Test 2, Fig. 7.4b)

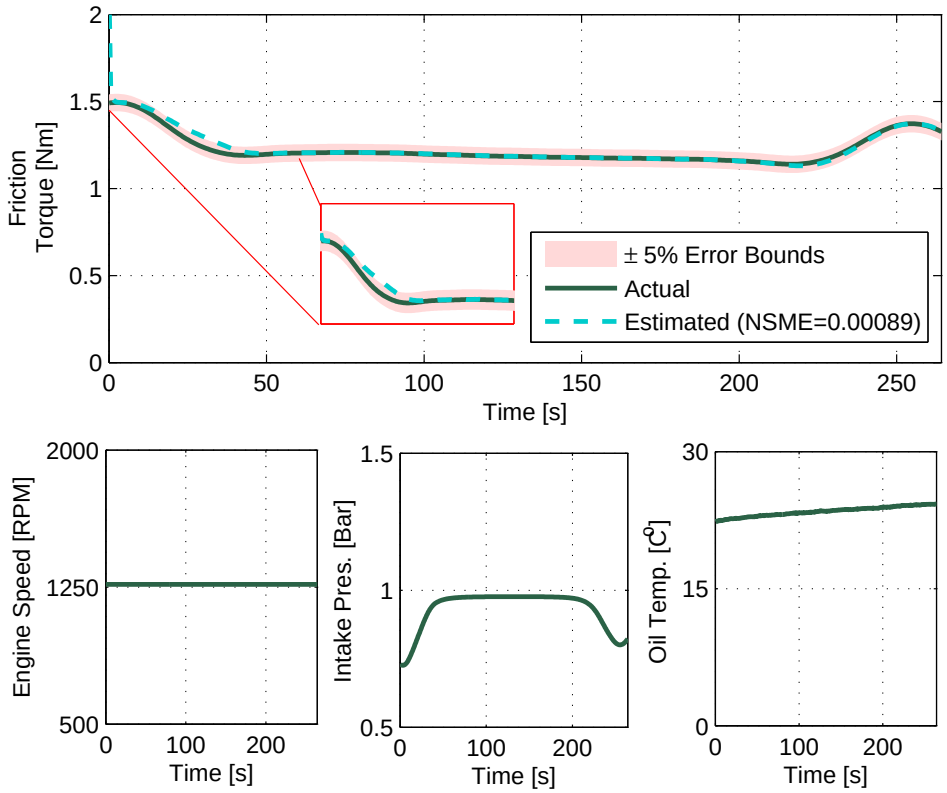

(c) Estimated friction torque @ 1250 [RPM] (Test 3, Fig. 7.4c)

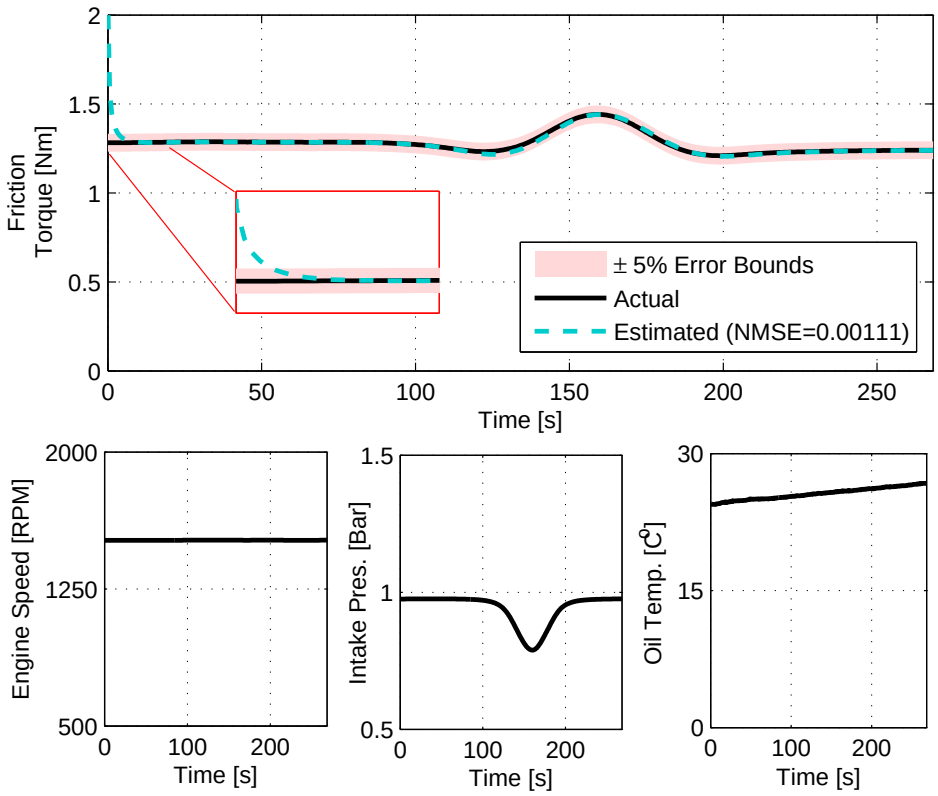

(d) Estimated friction torque @ 1500 [RPM] (Test 4, Fig. 7.4d)

Figure 7.5: Estimated friction torque under different operating conditions.

Table 7.4: Relative error between initial and final parameter estimates.

Parameter	Initial Value $[-]$	Final Value $[-]$	Relative Error $[\%]$
$\mathbf{c_1}$	$1.22 * 10^5$	$1.17 * 10^4$	90.42
$\mathbf{c_4}$	294	93.37	68.24
$\mathbf{c_5}$	$4.06 * 10^4$	$2.31 * 10^4$	42.96
$\mathbf{c_7}$	6.89	6.16	10.54
$\mathbf{c_{17}}$	1	0.89	11.22
$\mathbf{c_{19}}$	0.178	0.109	38.33

The difference between the initial friction parameters (as they were extracted from Sandoval and Heywood model [82]) and estimated (final), ones are tabulated in Table 7.4. The parameter with the greatest difference is $\mathbf{c_1}$ (90.42%) while it follows the parameters $\mathbf{c_4}$ (68.24%), $\mathbf{c_5}$ (42.96%), $\mathbf{c_{19}}$ (38.33%), $\mathbf{c_{17}}$ (11.22%), and $\mathbf{c_7}$ (10.54%). Note that the order of differences is similar to the identifiability order as presented in Table 7.3. This is because the parameter with the higher identifiability ranking, is at the same time the parameter with the higher sensitivity to the response of the system. Lastly, it should be clarified that the values presented in Table 7.4 were equally representative for all test cases, as presented in Fig. 7.5.

7.4 Synopsis

A summary of the key points of this chapter is given below.

- The application of the identifiability and adaptive identification tools, which were presented in Chapter 5, for the problem of engine friction parameters ranking and characterisation was presented.
- A methodology for sensitivity analysis ranking of engine design characteristics in respect of their contribution to the overall engine friction torque is

outlined. The results of this study reveal that the ranking order of the engine design characteristics can change depending on the operating conditions of the engine.

- The application of the qualitative adaptive identification framework for the on-line characterisation of engine friction torque was shown. This involved the identifiability analysis for selecting a set of estimable parameters for given operating conditions, and the application of linear recursive identification algorithms for the on-line identification of the estimable parameters of the semi-physical engine friction torque model. Experimental results proved the functionality of the proposed adaptive identification solution.

Chapter 8

Identifiability & Adaptive Identification of Cyclic Engine Torque Physical Parameters

The chapter starts with an introduction on the applications, modelling and identification approaches of cyclic engine torque models. Next follows the formulation of the cyclic engine torque model of a single cylinder engine and the description of the experiments that were conducted. Lastly details on and results from the implementation of the identifiability and adaptive identification algorithms are discussed. The material presented in this chapter finds applications in cold engine testing fault diagnosis.

8.1 Introduction to Cyclic Engine Torque

8.1.1 Principles & Applications

Conventional internal combustion engine crankshaft mechanisms generate cyclic torque components due to the conversion of reciprocating power to rotating power. The two main sources of the cyclic torque in engines are the inertia forces caused by the mass and geometry of the reciprocating assembly, and the gas pressure variation within the cylinder. The knowledge of the in-cylinder pressure and the

engine position-speed-acceleration quantities allow the relatively simple calculation of the instantaneous engine torque. Similarly the measurement of the cyclic engine torque allows the calculation of several in-cylinder quantities such as, instantaneous pressure, mean effective pressure, and cylinder trapped mass, which are very useful to know for engine control purposes. As a matter of fact, in modern engine control strategies driver's throttle demand is usually converted to torque demand (feed-forward maps) for the purpose of relating more easily driver's demands into in-cylinder desired quantities. Although modern feed-forward torque based engine control strategies supply much more tight engine controls, they are based on cyclic average values, which indicates their lack of controlling the engine responses on a crank angle basis. One of the main reasons for still having mean value torque based engine control strategies is because the measurements of cyclic engine torque is a rather challenging task.

The accurate measurement and estimation of the cyclic engine torque could unlock numerous technologies that could be used to control and monitor internal combustion engines more efficiently. The above argument has been proved in the past with relevant applications, some related publication are discussed bellow. Larsson and Andersson [235] presented the possibility of increasing the efficiency of spark-ignited engines relying upon instantaneous engine torque measurements for the control of the combustion phasing based on extremum-seeking algorithms. Another more recent publication by Thor et al. [236] discusses feedback control approaches for combustion phasing in diesel engines based on measurements of the instantaneous crankshaft torque. Furthermore, the cyclic combustion torque estimation for misfire detection and calibration purposes has been illustrated by Helm et al. [98]. From monitoring and diagnosis point of view, Karman et al. [237–241] presented a series of papers focusing on the fault detection and diagnosis in cold engine testing application based on instantaneous engine torque measurements and signal analysis techniques. Similarly, Wei et al. [242, 243] showed the application of physics-based engine torque models and signal-based techniques for fault detection of diesel engines in cold tests.

8.1.2 Modelling & Identification

As it was discussed earlier, prior to the development of torque-based control and monitoring applications, it is beneficial to be able to estimate accurately the instantaneous engine torque. A number of models have been developed for this purpose, some of the most interesting approaches are discussed below.

The event based estimation of the indicated torque for internal combustion engines based on crank-angle resolved indicated torque model and sliding mode observers has been published by Wang et al. [244]. Zweiri et al. [60, 74, 75] have derived physics-based equations for describing the engine torque components i.e. indicated, reciprocating and friction, in a crank-angle domain. One common problem encountered in Zweiri's approach was related to the parametrisation and validation of the model as opposed to real experimental data. With this in mind Zweiri et al. [245] conducted a parameter optimisation study based on non-linear least squares and Newton-Raphson algorithm. A more recent work by Nickmehr [112], shows the development of a physics-based lumped parameter dynamic model for the estimation of the instantaneous engine torque. The author showed the application of the prediction error approach for the identification of engine's physical parameters. Additionally Nickmehr [112] showed the assessment of the identifiability of the model parameters prior the identification exercise; this is very valuable and it is indeed the only publication that was found which shows the application of identifiability analysis for engine's physical parameters. Nevertheless, one of the limitations of the suggested identifiability analysis approach is that it cannot be used for assessing mathematically the information content of the experimental measurements; that is because it is assesses only the structural identifiability of the system model (see Chapter 5, Section 5.2.2 for further information).

Non-physics-based modelling approaches have also been suggested. One of the most interesting works has been published by Helm et al. [98]. In this work the authors showed the development of cyclic regression parametric functions that were adaptively parametrised using linear Kalman filters. The main benefit of this approach is that can be easily applied to different engine configurations

without great parametrisation effort; on the other hand the lack of physical interpretation makes the method not so popular for analysis and conditions monitoring purposes.

Even though there have been numerous publications on cyclic torque modelling and identification procedures, there are still some unsolved problems related specifically to the parameter identification of cyclic engine torque models. The first problem is associated with the identifiability of physical and semi-physical parameters that can be found generally in physics based engine torque models. More specifically no publications were found presenting the structural as well as practical identifiability of the engine torque model physical parameters, the only related document that was found literature was the one published recently by Nickmehr [112] but the author was showing only the evaluation of the structural identifiability. The second problem is related to the identification of cyclic engine torque model physical parameters. In particular most of the previous attempts to identify engine physical parameters were making use of off-line estimation algorithms which is something that limits the possible applications, i.e. adaptive monitoring and control cannot be implemented efficiently using off-line identification schemes. The only application of on-line parameter identification algorithms that was found in literature was the one published by Helm et al. [98], however this publication was not showing the adaptive identification of physical oriented parameters but mathematical regression coefficients.

Having said that, the author mixes well known analysis and synthesis system identification tools and put them together to a complete chain for adaptive parameter estimation with a practical parameter identifiability analysis scheme as applied to a cyclic engine torque model. The main contribution of this work is located on the practical application identifiability and adaptive identification of engineâĂŹs physical parameters. Ultimately the presented methodology could be used in End-of-Line cold engine testing applications as a fault detection and isolation tool based on adaptive parameter estimation approach.

8.2 Cyclic Engine Torque Model Analysis

The mathematical structure of the physics-based cyclic engine torque model that will is used to illustrate the functionality of the identifiability and adaptive identification tools is discussed in this section. The model represents the instantaneous engine torque output of the single cylinder engine that was presented in Chapter 4, Section 4.2. According to the analysis that was conducted in Chapter 3, Section 3.2.4, the overall engine torque (τ_{eng}), (Eq. 3.37) is proportional to the indicated torque (τ_{ind}), (Eq. 3.38) which is generated due to the cylinder gas pressure (P_{cyl}) that acts perpendicular to the piston minus the reciprocating torque (τ_{rec}), (Eq. 3.41) and the friction torque (τ_{fri}), (Eq. 3.44).

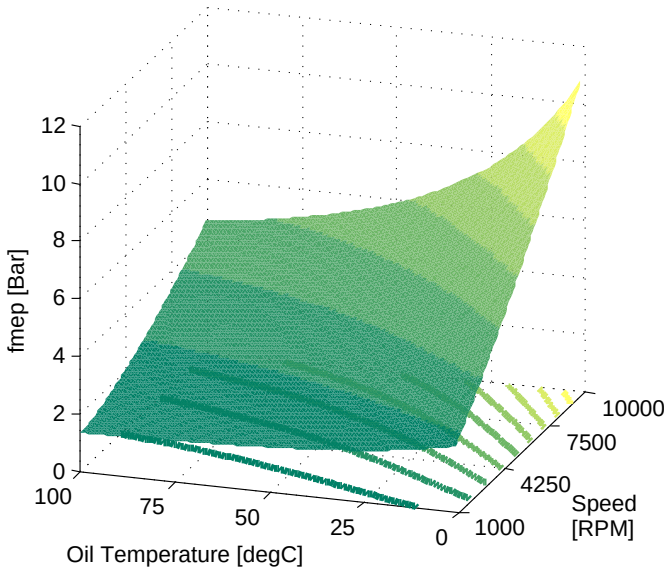

Figure 8.1: Friction mean effective pressure (fmep) map.

The only difference compared to the formulation described in Chapter 3, Section 3.2.4, is related to the modelling of the friction mean effective pressure (fmep). Here, for the sake of simplicity, fmep is modelled as a third order polynomial, as a function of the engine speed and oil temperature [246], (Eq. 8.1), (Fig. 8.1),

$$\begin{aligned}\text{fmep} = c_1 + c_2 N_{en} - c_3 T_{oil} + c_4 {N_{en}}^2 - c_5 T_{oil} N_{en} + c_6 {T_{oil}}^2 - c_7 {N_{en}}^3 \\ + c_8 T_{oil} {N_{en}}^2 + c_9 {T_{oil}}^2 - c_{10} {T_{oil}}^3\end{aligned} \tag{8.1}$$

Where, N_{en} and T_{oil} are the engine speed and oil sump temperature respectively, while c_1 to c_{10} are linear regression coefficients related to the mean effective pressure. It should also be mentioned that this simplified fmep function (Eq. 8.1) was generated using the detailed semi-physical engine friction model as presented in Chapters 3 and 7.

At last, combining Eq. 3.37 to 3.44 and 8.1, the instantaneous engine torque (τ_{eng}) can be expressed as a non-linear system as a function of the inputs variables (engine position (θ_{en}), velocity (ω_{en}), acceleration (α_{en}), cylinder (P_{cyl}) and crank case (P_{crn}) pressures and oil temperature (T_{oil})), the model physical parameters (mass of the reciprocating components (M_{rec}), cylinder bore (b), connecting rod length $(\mathcal{L})$, crank arm length (r), piston pin offset(δ)), and the regression coefficients of the friction mean effective pressure model ($c_{1...10}$), (Eq. 8.2), (Fig. 8.2).

$$\tau_{eng} = h\left(\theta_{en}, \omega_{en}, \alpha_{en}, P_{cyl}, P_{crn}, T_{oil}, M_{rec}, b, \mathcal{L}, r, \delta, c_{1...10}\right) \tag{8.2}$$

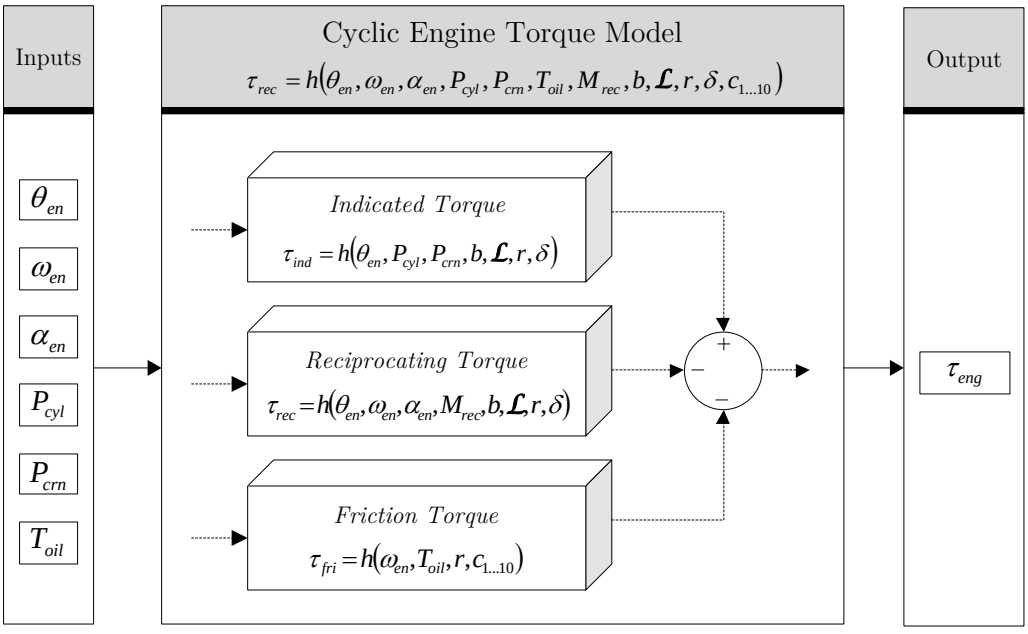

Figure 8.2: Schematic representation of the cyclic engine torque model.

8.3 Experimental Procedure

8.3.1 Test Rig

As aforementioned the cyclic engine torque model represents the instantaneous engine torque output of the single cylinder engine that was presented in Chapter 4, Section 4.2. Consequently, the transient cyclic motoring engine test cell (Fig. 4.1) was used for methodology development, implementation and testing. The control variables of the experiment were the speed demand to the transient dynamometer and the throttle demand to the electronic throttle controller of the engine (similar to Section 7.3.2, Fig. 7.3). The main acquired signals that were needed for the parameter identifiability and adaptive identification processes were the inputs (i.e. position, velocity and acceleration, cylinder and crankcase pressure and oil temperature) and the output (torque) of the cyclic engine torque model (Eq. 8.2), (Fig. 8.2).

One of the main considerations of the present experiment was the appropriate acquisition of the measurement signals. To be more specific the identification of the cyclic engine torque model physical parameters would not be possible without the development of a crank-angle-based (event-based) data acquisition system (details are given in Chapter 4). Furthermore, it should be emphasised that some practical issues associated with data filtering (forward-backward filtering) and aliasing effects (due to event-based signal acquisition [156]) had to be solved prior to the experiments, otherwise any data inconsistencies would result inevitably in wrong parameter estimates.

8.3.2 Measurement Data

Two experiments i.e. steady-state Fig. 8.3 and transient Fig. 8.4, were conducted for assessing the effect of different operating conditions on the identifiability of the model parameters. Both figures show all the inputs (engine position (θ_{en}), velocity (ω_{en}), acceleration (α_{en}), cylinder (P_{cyl}) and crankcase (P_{crn}) pressures, oil temperature (T_{oil})) and output (torque (τ_{eng})) of the cyclic torque model.

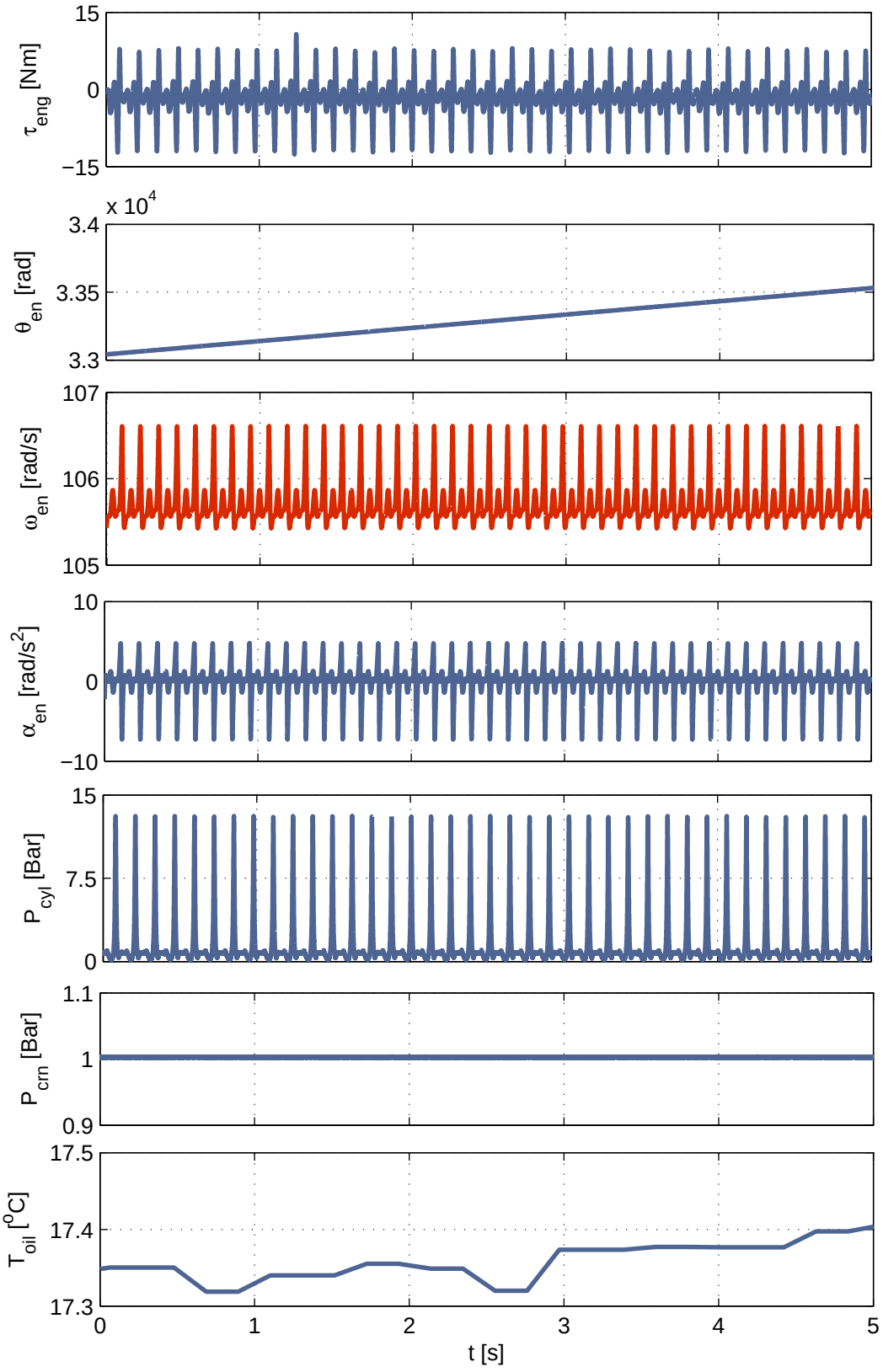

Figure 8.3: Steady-state experiment (Test ID: T1).

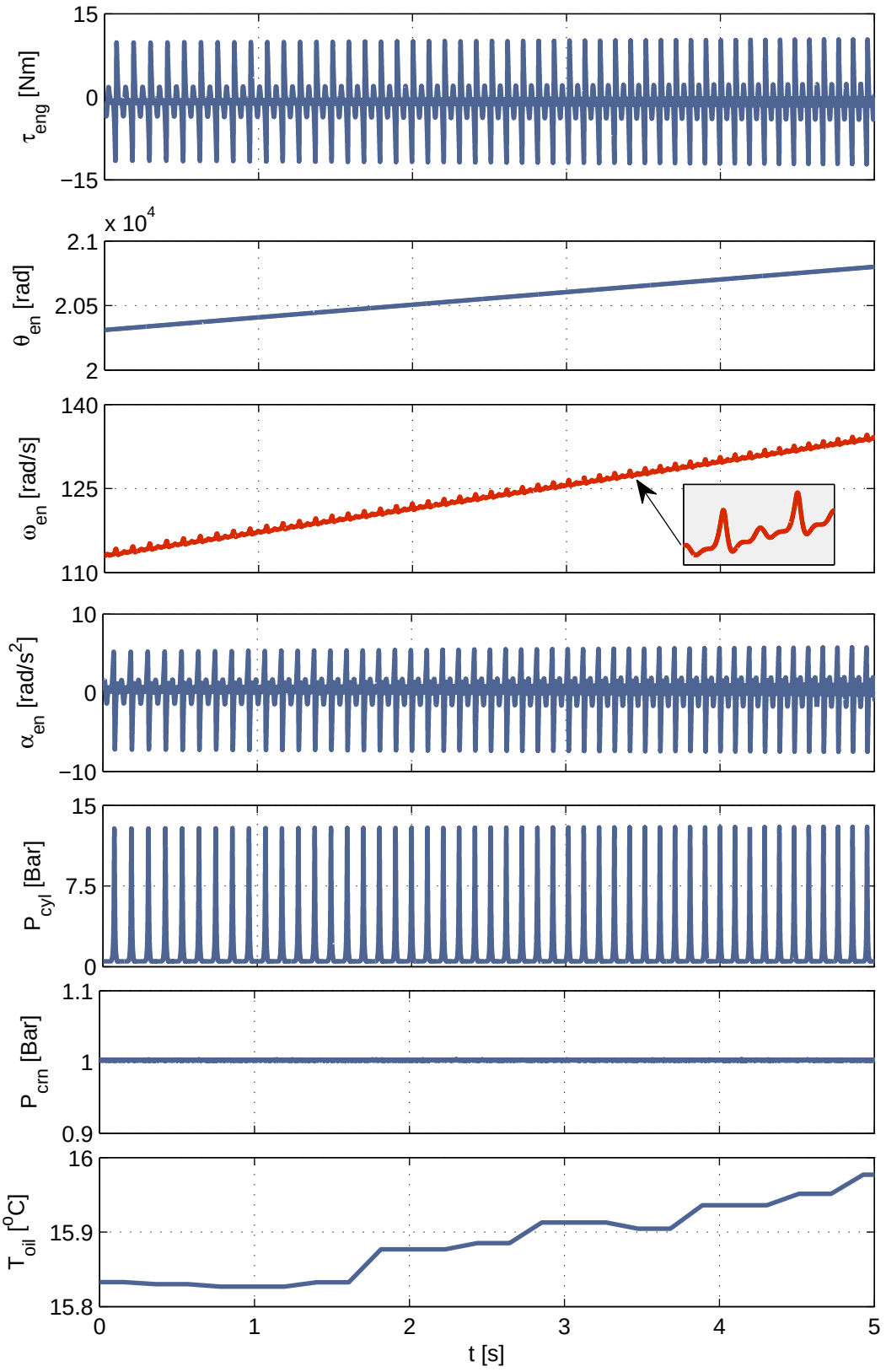

Figure 8.4: Transient experiment (Test ID: T2).

8.4 Identifiability & Adaptive Identification

This section shows the application of system identification tools for assessing the detectability and identifying adaptively the physical and semi-physical parameters of the cyclic engine torque model. The ultimate purpose of this section is to reveal how could someone use the suggested algorithms in cold engine testing fault diagnosis applications.

8.4.1 Identifiability of Cyclic Torque Model Parameters

The identifiability of the cyclic torque model physical and semi-physical parameters was evaluated for the aforementioned test cases. The main outcome of this step is the qualitative information regarding the detectability of the model parameters under different operating conditions. As a matter of fact this is an important step that is often overlooked in parameter estimation of physical and semi-physical models and as it will be revealed, it is very important to be consider prior to any parameter estimation exercise.

The identifiability of the cyclic engine torque model parameters was assessed by using the orthogonal-based identifiability algorithm (Chapter 5, Algorithm 5.1). More specifically, the orthogonal-based identifiability algorithm was deployed, provided that the cyclic engine torque model (Eq. 8.2) was expressed in the general format of non-linear parametric models:

$$y(t) = h(\phi(t), \vartheta) + \epsilon(t) \tag{8.3}$$

Where, $h(\phi(t), \vartheta)$ is a vector function relating the independent variables $\phi(t)$ with the dependent variables vector $y(t)$, ϑ contains all the unknown parameters that have to be estimated from the available data, and finally $\epsilon(t)$ is random error term. The vectors are formed as follows:

$$y(t) = \begin{bmatrix} \tau_{eng}|_{t_1} & \tau_{eng}|_{t_2} & \dots & \tau_{eng}|_{t_n} \end{bmatrix}^T$$

Dependent variable vector $y(t) \in \mathbb{R}^{n\times 1}$ (where n is the number of observations) contains the output of the cyclic engine torque model $(\tau_{eng}(t))$, (Eq. 8.2) acquired at discrete time intervals, t_1, t_2, ..., $t_n \in \mathbb{R}^+$ with time step (dt) equivalent to one crank angle degree.

$$\vartheta(t) = \begin{bmatrix} \vartheta_{en}|_{t_1} & \omega_{en}|_{t_1} & \alpha_{en}|_{t_1} & P_{cyl}|_{t_1} & P_{crn}|_{t_1} & T_{oil}|_{t_1} \\ \vartheta_{en}|_{t_2} & \omega_{en}|_{t_2} & \alpha_{en}|_{t_2} & P_{cyl}|_{t_2} & P_{crn}|_{t_2} & T_{oil}|_{t_2} \\ \vdots & \vdots & \vdots & \vdots & \vdots & \vdots \\ \vartheta_{en}|_{t_n} & \omega_{en}|_{t_n} & \alpha_{en}|_{t_n} & P_{cyl}|_{t_n} & P_{crn}|_{t_n} & T_{oil}|_{t_n} \end{bmatrix}$$

Independent variables matrix $\phi(t) \in \mathbb{R}^{n\times v}$ (where n is the number of observations and v is the number of independent variables) contains the inputs of the cyclic engine torque model.

$$\vartheta = \begin{bmatrix} M_{rec} & b & \mathcal{L} & r & \delta & c_{1\ldots10} \end{bmatrix}^T$$

And, the parameters vector $\vartheta \in \mathbb{R}^{p\times 1}$ (where p is the number of parameters).

Next, according the instructions of the orthogonal-based identifiability algorithm, the sensitivity matrix has to be formed.

$$Z = \begin{bmatrix} z_{M_{rec}}|_{t_1} & z_b|_{t_1} & z_{\mathcal{L}}|_{t_1} & z_r|_{t_1} & z_\delta|_{t_1} & z_{c_1}|_{t_1} & \ldots & z_{c_{10}}|_{t_1} \\ z_{M_{rec}}|_{t_2} & z_b|_{t_2} & z_{\mathcal{L}}|_{t_2} & z_r|_{t_2} & z_\delta|_{t_2} & z_{c_1}|_{t_2} & \ldots & z_{c_{10}}|_{t_2} \\ \vdots & \vdots & \vdots & \vdots & \vdots & \vdots & \ddots & \vdots \\ z_{M_{rec}}|_{t_n} & z_b|_{t_n} & z_{\mathcal{L}}|_{t_n} & z_r|_{t_n} & z_\delta|_{t_n} & z_{c_1}|_{t_n} & \ldots & z_{c_{10}}|_{t_n} \end{bmatrix} \tag{8.4}$$

Here, $z_{M_{rec}}$, z_b, $z_{\mathcal{L}}$, z_r, z_δ, z_{c_1}, ..., $z_{c_{10}}$, are the normalised partial derivatives of the physical and semi-physical parameters w.r.t the cyclic engine torque model output (τ_{eng}). For the calculation of the normalised partial derivatives, the initial conditions of the unknown parameters had to be defined, these initial conditions were extracted from the actual physical dimensions of the engine as the parameters represent physical and semi-physical quantities. The normalisation of the

partial derivatives should be undertaken because the suggested approach relies upon the calculation of the sum of squared value of each individual sensitivity coefficient which indicates that any possible numerical issues would provide misleading results. Additionally the normalisation is critical when the parameters under examination have different physical units. Finally it is important to notice that the sensitivity coefficients are evaluated at each time step i.e. t_1, t_2, ..., t_n, this ensures that detectability of the parameters is assessed for all different operating conditions.

The next steps of the identifiability algorithm (Algorithm 5.1) can now be undertaken provided that the sensitivity matrix has been determined. Due to the complexity involved in the execution of all the steps of the identifiability analysis, a program was written in MATLAB for the purpose evaluating the identifiability of the parameters automatically. See Appendix B.4.

Table 8.1: Identifiability ranking of the cyclic engine torque physical and semi-physical parameters.

Parameter	**Identifiability Ranking**	
	Test ID: T1	*Test ID: T2*
M_{rec}	–	8
b	3	3
$\mathcal{L}$	6	7
r	2	2
δ	4	4
c_1	–	–
c_2	–	–
c_3	–	–
c_4	5	5
c_5	–	–
c_6	–	–
c_7	8	10
c_8	1	1
c_9	7	6
c_{10}	–	9

The results of the parameter estimability study are tabulated in Table 8.1. The parameter with the most effect on the system response is ranked as the first parameter whilst the parameter with the less effect on the system is ranked at the end of the list, the parameters that are not estimable are neglected (-), i.e. are set constant to an approximate value. Based on the results of the parameter identifiability study (Table 8.1), the data of the *Test ID: T1* i.e. steady speed (Fig. 8.3), can estimate 8 parameters out of 15, while the data of *Test ID: T2* i.e. speed ramp (Fig. 8.4), allow the estimation of two more parameters, those are the engine reciprocating mass (M_{rec}) and one of the regression coefficients (c_{10}) of the friction mean effective pressure (fmep) model. The main reason for estimating these additional parameters using the observation data of *Test ID: T2* is originated from the fact that the velocity of the engine in the *Test ID: T2* was not constant as *Test ID: T1* but was varying continuously. This probably works as excitation signal for the estimation of these parameters as both parameters are exponentially proportional to the angular velocity of the engine. Regarding the non-estimable parameters of Test 2, they are fixed to an initial known value and they are not taken into account in the estimation process since these parameters have not significant effect in the response of the system.

Remark 8.1 (Unidentifiable Parameters)**.** *Practically speaking, in cases where the unidentifiable parameters have a physical meaning e.g. mass, diameter, etc., and are important to be known, then the experiment should be repeated with different input conditions (different experimental design). However if and only if, there are no any input conditions that can enable the estimation of the non-estimable parameters then the model must be reformulated accordingly.*

At last the results of the identifiability analysis reveal that the detectability of the physical parameters e.g. reciprocating mass, can be affected from the operating conditions of the engine. This supports the statement that before attempting to identify the physical parameters of the engine, is needed first to assess their identifiability in respect to the operating conditions of the engine.

8.4.2 Parameter Identification using Non-Linear Filters

Coming to the adaptive identification of the physical and semi-physical parameters of the cyclic engine torque model, it should be reminded the main practical goad of the adaptive identification study. As it was mentioned earlier, the suggested tools could be particularly useful in End-of-Line cold engine testing applications in which the engine is tested under various operating conditions to determine the health status of its mechanical assembly. Currently this is done with signal-based and limit-checking techniques [237–243], which are usually deployed on an off-line basis and provide very little information regarding the localisation of faults. Now, as it can be understood, the ultimate tool for determining the cause and location of any possible faults or malfunctions in the engine assembly, would be the on-line monitoring of the actual physical characteristics of the engine. The application of non-linear filters for the on-line monitoring of engine's physical characteristics is presented here for the first time.

However, prior to the implementation of non-linear filters, for the on-line parameter identification, it is necessary to make sure that the parameters that are to be estimated can be actually estimated; here is were the parameter identifiability analysis proves its importance and usefulness. Bearing in mind that the main practical purpose of this application is to monitor in real-time the physical characteristics of the engine, it is necessary to test the engine under operating conditions that allow the estimation of most of its physical characteristics. According to the results of the identifiability analysis in Section 8.4.1, Table 8.1, the transient test (Fig. 8.3, Test ID: T1) enabled the estimation of more physical and semi-physical system parameters than the steady test (Fig. 8.3, Test ID: T2). Therefore, in this application the engine was tested under transient conditions as more parameters could be identified compared to steady state tests. The estimable parameters (ϑ_{est}) during transient testing conditions are shown bellow:

$$\vartheta_{est} = \begin{bmatrix} c_8 & r & b & \delta & c_4 & c_9 & \mathcal{L} & M_{rec} & c_{10} & c_7 \end{bmatrix}^T$$

Note that the estimable parameters (ϑ_{est}) are listed in an ascending order in respect to their identifiability ranking. Now that a set of estimable parameters has been determined it is possible to proceed to the formulation of the adaptive parameter identification problem.

Given the non-linear-in-the-parameter structure of the cyclic engine torque model, it is possible to rewrite the model in a general state-space non-linear format while assuming that the estimable parameters (ϑ_{est}) of the model are time varying and develop over time randomly; this can be translated mathematically as follows (Eq. 8.5) (note that the variables $y(t)$ and $\phi(t)$ have identical meaning with those described previously for Eq. 8.3).

$$\vartheta_{est}(t) = \vartheta_{est}(t-1) + w(t) \tag{8.5a}$$

$$y(t) = h\left(\phi(t), \vartheta_{est}(t)\right) + \epsilon(t) \tag{8.5b}$$

The above formulation implies that the adaptive identification of the physical and semi-physical parameters of the cyclic engine torque model requires the deployment of recursive algorithms suitable for non-linear-in-the-parameter systems. Consequently for the adaptive identification of the parameters two variants of the Kalman filter i.e. the Extended Kalman Filter, EKF (Algorithm 5.6) and the Unscented Kalman Filter, UKF (Algorithm 5.7) were utilised.

The theoretical preliminaries and implementation instructions of these algorithms have been discussed in details in Chapter 5, Section 5.3.2. Based on those instructions, for the implementation of the EKF the analytical calculation of the Jacobian matrix $(J(t) = \nabla h(\hat{\vartheta}_{est}(t-1)))$ is required. The calculation procedure of the Jacobian matrix is similar to the sensitivity matrix as it was presented in Section 8.4.1, the only differences are that the partial derivatives of the Jacobian matrix should not be normalised as in the identifiability analysis, and that the Jacobian matrix should be evaluated only for the estimable parameters (ϑ_{est}). In contrast to the EKF, for the implementation of the UKF the Jacobian matrix does not have to be computed which is generally the main benefit of the UKF (see Chapter 5, Section 5.3.2).

In either algorithm though i.e. EKF (Algorithm 5.6) and UKF (Algorithm 5.7), a set of initial parameters (ϑ_{est_0}) and covariance estimates (P_0) were required. The initial values of the physical parameters i.e. crank arm length r, cylinder bore b, piston pin offset δ, connecting rod length $\mathcal{L}$, and reciprocating mass M_{rec}, were identified by direct measurements, thus these parameters represent the actual physical quantities of the components i.e. length and mass. The rest of the parameters were the friction model regression coefficients which were approximated using the friction mean effective pressure physical model (See Chapter 3, Section 3.2.4). The initial parameter estimates are tabulated in Table 8.2. The initial covariance estimates (P_0) were set equal to $100 \times I_{10}$ (where I_{10} is an identity matrix of size 10 i.e. the total number of estimable parameters), provided that the initial parameter estimates (ϑ_{est_0}) were relatively close to the true expected values.

Table 8.2: Initial parameter estimates (ϑ_{est_0}).

Parameter	Value	Unit
Friction Coefficient, c_8	1.06×10^{-9}	-
Crank arm length, r	25.7	mm
Cylinder bore, b	54	mm
Piston pin offset, δ	0.0	mm
Friction Coefficient, c_4	1.96×10^{-6}	-
Friction Coefficient, c_9	7.14×10^{-6}	-
Connecting rod length, $\mathcal{L}$	88.0	mm
Reciprocating mass, M_{rec}	0.80	kg
Friction Coefficient, c_{10}	3.13×10^{-4}	-
Friction Coefficient, c_7	1.38×10^{-4}	-

Having described the groundwork behind the implementation of the EKF and UKF for the recursive identification of the physical and semi-physical parameters of the cyclic engine torque model, it is now possible to discuss some representative results obtained from this application.

One of the first things that had to be examined was the validity of the cyclic

engine torque model as opposed to real experimental data. This was an important step as it revealed some useful information regarding the correctness of the physical and semi-physical parameters of the model. Consequently the validity of the model was inspected by parametrising the cyclic engine torque model using the initial conditions that were submitted in Table 8.2. The results are presented in Fig. 8.5. The Normalised Mean Square Error (NMSE) (Eq. 6.4) was utilised as measure of success. As it can be seen, even though the trend of the output of the cyclic engine torque model is similar to the observation data, the absolute values of the model do not agree with real response of the system. The results suggested that the parametrisation of the model does not represent absolutely the true instantaneous torque of the single cylinder engine. Models are not perfect.

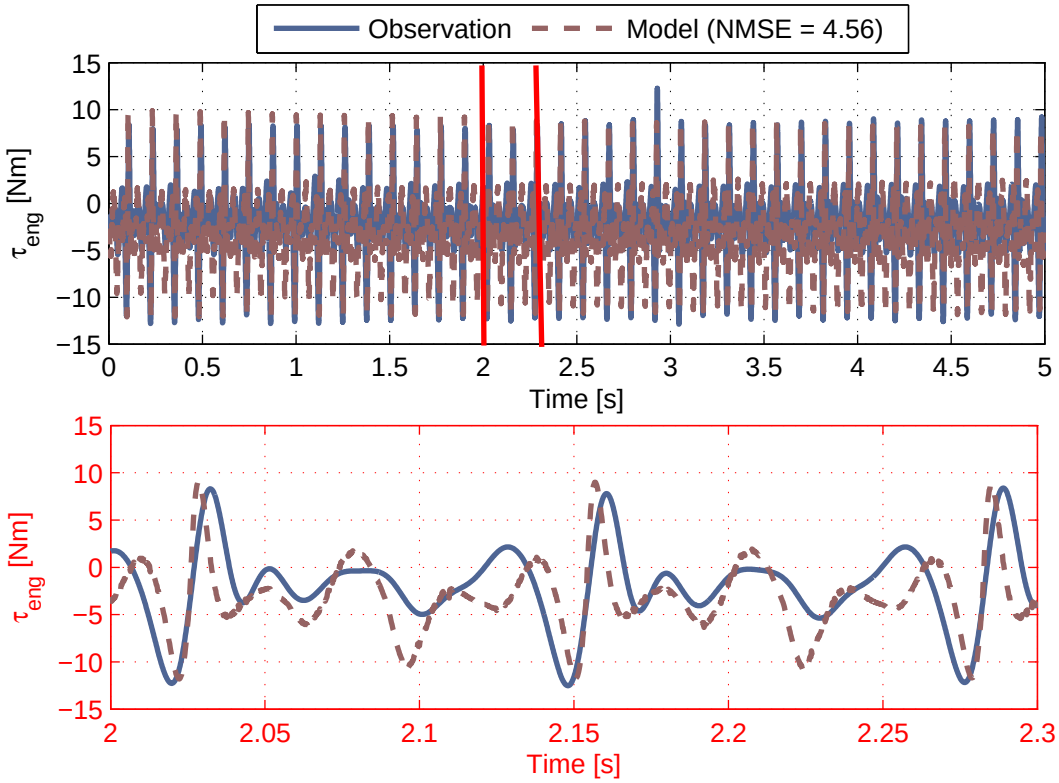

Figure 8.5: Cyclic engine torque model accuracy compared to the actual measurement (model parametrisation using the initial conditions, Table 8.2).

Therefore, as it can be expected, the recursive identification of the cyclic engine torque physical and semi-physical parameters serves two purposes, the first

is the refinement of the model parameters so that the model would be in close vicinity with the true response of the system, and the second and most importantly the on-line tracking of the physical parameters which can be used for monitoring the health status of the engine during cold engine testing applications.

The results from the recursive identification of the estimable parameters are presented in Fig. 8.6. These results were obtained while the engine was tested under transient operating conditions (Test ID: T2, see Fig. 8.4). To add some details, the parameter tracking performance of the EKF and UKF over time is visualised in Fig. 8.6. See that at the start of the identification process the parameter estimates were adjusted up until they converged to a new estimate. This was happening due to the parameter initialisation issues that were reported earlier (Fig. 8.5). Another thing that can be seen is some noise in the parameter estimates, in particular the EKF appears to be more acute to noise compared to UKF. This was probably occurred due to numerical issues associated with the analytical calculation of the Jacobian matrix. What was also observed is that in some parameters, for instance $\mathcal{L}$, the new estimates were slightly different for each algorithm i.e. EKF and UKF. To examine the level of difference between the two identification algorithms, the mean parameter estimates are tabulated in Table 8.3. Based on these results the mean parameter estimates for both of the non-linear recursive estimators are in close vicinity which indicates that both converge in a realistic estimate. Furthermore, it can be observed that the actual values of the the physical parameters i.e. crank arm length r, cylinder bore (b), piston pin offset (δ), connecting rod length $(\mathcal{L})$, and reciprocating mass (M_{rec}), were not significantly affected which is actually what was initially expected since these parameters were directly measured prior to the estimation. Nonetheless slight changes are observed which was probably necessary in order to minimise the mean square error between the measured and predicted engine torque.

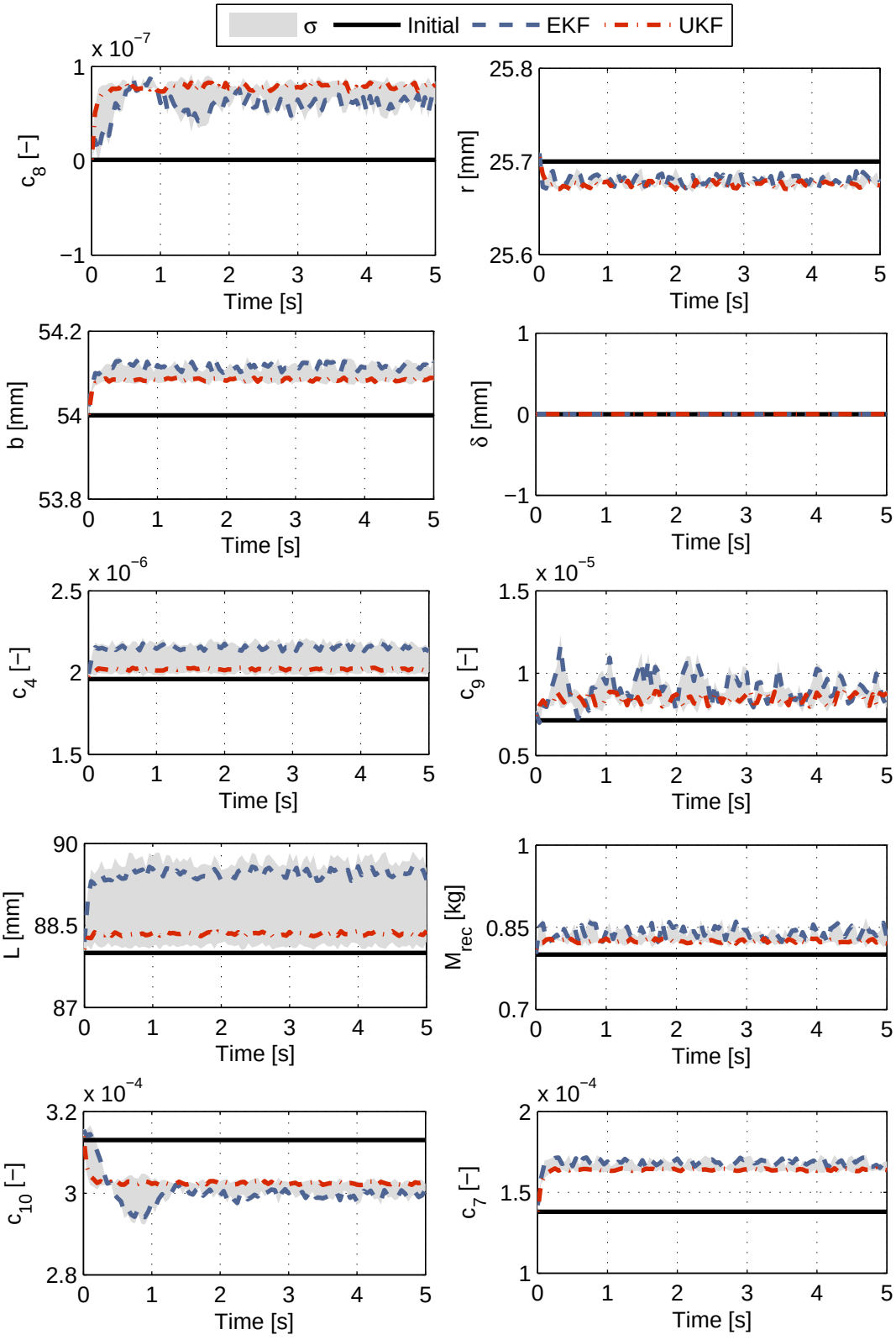

Figure 8.6: Visualisation of the performance of the non-linear recursive estimators during the estimation of the cyclic engine torque parameters.

Table 8.3: Mean parameter estimates $(\hat{\vartheta}_{est})$ and absolute relative error $(|e|\,\%)$ compared to the initial values of the parameters (Table 8.2).

Parameter	Initial Value	EKF		UKF		Unit
		$\hat{\vartheta}_{est}$	$\lvert e\rvert\,\%$	$\hat{\vartheta}_{est}$	$\lvert e\rvert\,\%$	
c_8	1.06×10^{-9}	5.08×10^{-8}	52.07	7.32×10^{-8}	30.94	-
r	25.7	25.67	0.11	25.67	0.11	mm
b	54.0	54.10	0.18	54.08	0.14	mm
δ	0	4.1×10^{-8}	≈ 0.0	2.6×10^{-8}	≈ 0.0	mm
c_4	1.96×10^{-6}	2.13×10^{-6}	8.67	2.01×10^{-6}	2.55	-
c_9	7.14×10^{-6}	8.12×10^{-6}	13.72	7.98×10^{-6}	11.76	-
$\mathcal{L}$	88.0	89.3	1.40	88.8	0.91	mm
M_{rec}	0.80	0.82	2.50	0.82	2.50	kg
c_{10}	3.13×10^{-4}	2.98×10^{-4}	4.79	3.02×10^{-4}	3.51	-
c_7	1.38×10^{-4}	1.65×10^{-4}	19.56	1.63×10^{-4}	18.11	-

The predictive capability of the cyclic engine torque model after the implementation of the EKF and UKF for the refinement and tracking of its physical and semi-physical parameter is presented in Fig. 8.7. The results reveal that the parameter estimates of both the EKF and UKF algorithms increase significantly the predictive capability of the model. More specifically, it is observed that the model lied always within $\pm 5\%$ of the observed values. This can also be understood by observing the NMSE of the model response when the parameters were identified using the EKF (0.135) and UKF (0.048), the comparison of those values with the NMSE of the model prior to the adaptive identification process (4.56) proves the functionality of the algorithms in respect of increase the predictive capability of the instantaneous engine torque model output. Additionally based on these results it could be said that the UKF is more adequate compared to EKF if someone is interested on increasing the predictive capability of the model. Nevertheless, this statement should not be generalised since in other application the UKF could be inferior to the EKF.

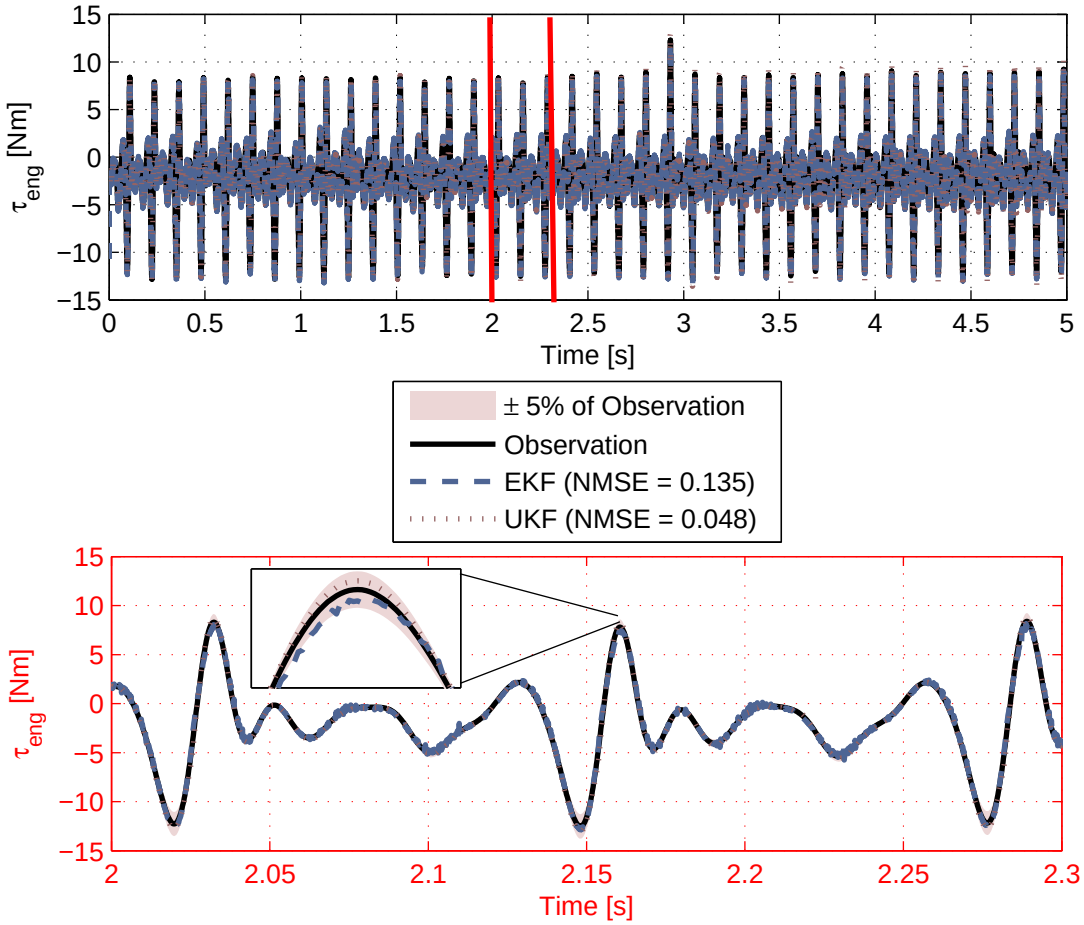

Figure 8.7: Functionality of the EKF and UKF algorithms in respect of refining the parameters of the cyclic engine torque model and increasing its predictive capability (observation data identical to Test ID: T2, Fig. 8.4).

Finally, the efficacy of the proposed methodology under different engine operating conditions is discussed. More specifically up until now it has been shown how the EKF and UKF can refine and track the estimable parameters of the cyclic engine torque model under specific operating and testing conditions i.e. five seconds transient test (speed ramp up) Test ID: T2, Fig. 8.4. Now for the propose of ensuring that the non-linear filters can identify and track effectively the physical and semi-physical parameters of the cyclic torque model under different operating conditions, a final experiment was conducted. The experimental results are presented in Fig. 8.8. This test lasted approximately two minutes while the engine speed was ramped up and down for four consecutive times.

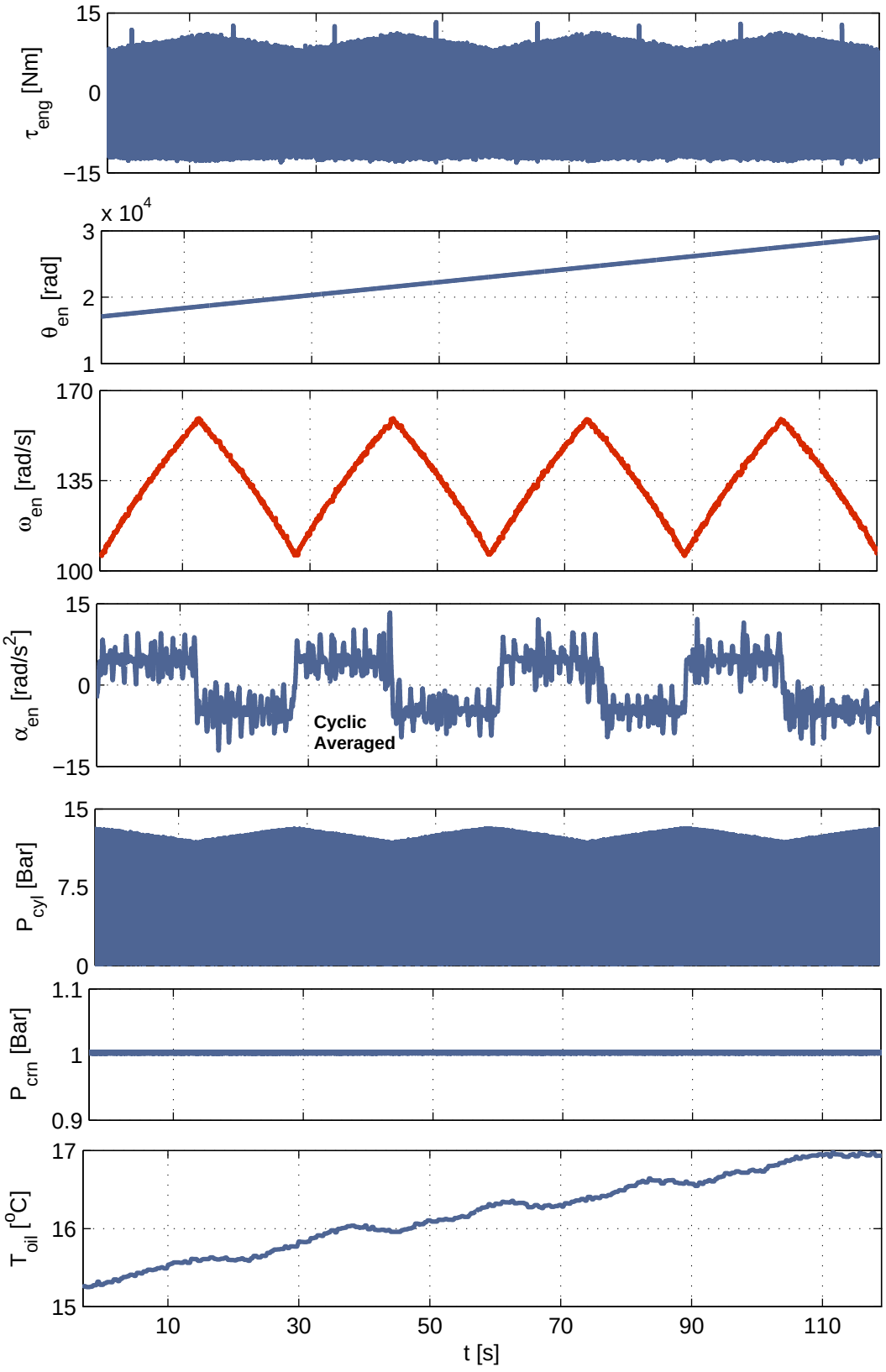

Figure 8.8: Transient experiment for methodology validation (Test ID: T3).

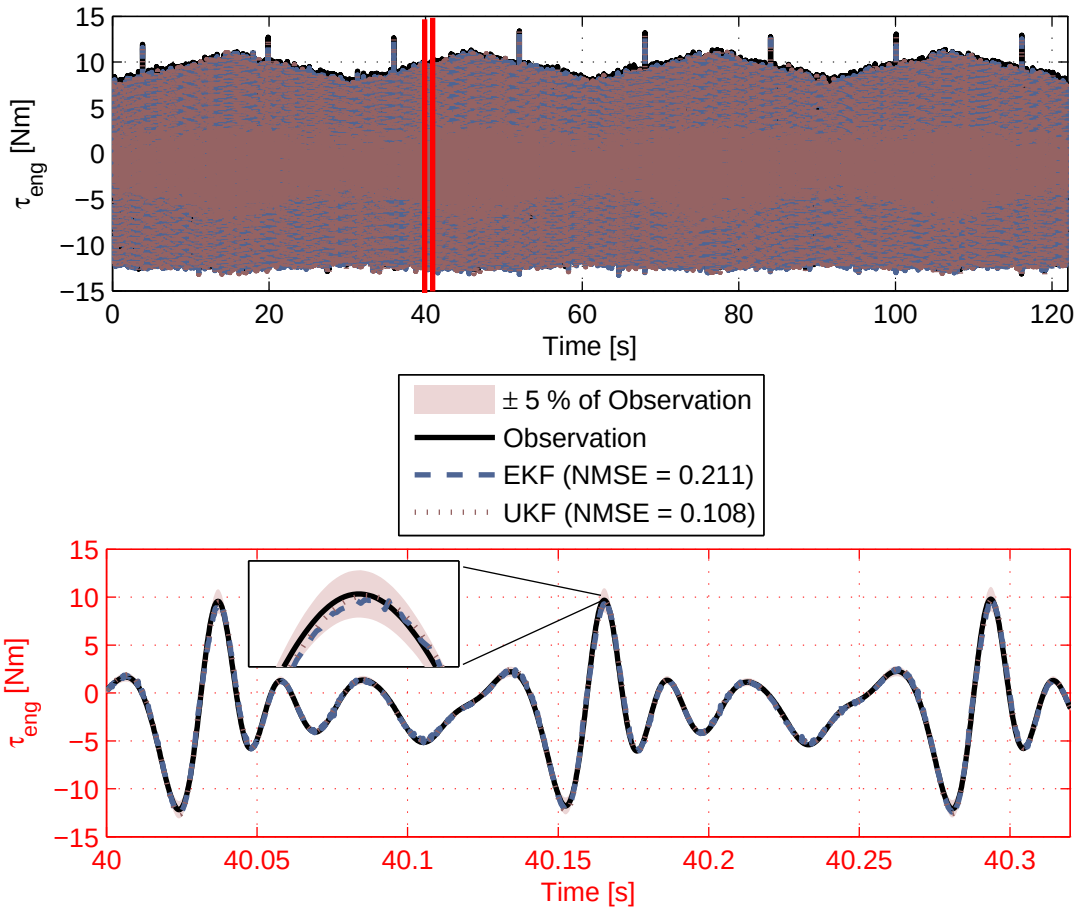

Figure 8.9: Functionality of the EKF and UKF algorithms in respect of refining the parameters of the cyclic engine torque model and increasing its predictive capability (observation data identical to Test ID: T3, Fig. 8.8).

The results in Fig. 8.9 verify that the non-linear adaptive identification algorithms estimate the true parameters of the model, provided that the responses of the cyclic engine torque model maintains roughly the same level of accuracy (EKF-NMSE = 0.211 and UKF-NMSE = 0.108) under different engine operating conditions. Overall, it is can be said that both algorithms provide successful results despite the complexity involved in the actual system, however it should be acknowledge the fact that the parameter estimates of the UKF provide better model accuracy compared to EKF estimates which proves its superior performance in this very specific application.

8.5 Synopsis

A summary of the key points of this chapter is given below.

- A methodology for non-linear recursive identification with identifiability analysis for physical and semi-physical parameters that can be found generally in cyclic engine torque models was reported.
- The identifiability analysis proved that not all the parameters of a physical engine model can be estimated directly for any given experimental conditions.
- The qualitative information gained from the identifiability analysis was then used for estimating the estimable parameters by using two well-known non-linear adaptive identification algorithms known as Extended and Unscented Kalman Filters.
- The findings of this work contribute on understanding the real-world challenges associated with the effective implementation of system identification techniques suitable for on-line non-linear estimation of parameters with physical interpretation.
- The proposed methodology could be used for assessing in real-time the mechanical integrity of engines in End-of-Line cold engine testing applications.

Chapter 9

Conclusions & Future Work

This chapter outlines the main conclusions of the thesis and recommends future research directions.

9.1 Conclusions

The work described in this thesis was focused on investigating the potential use of system identification algorithms for detectability assessment and real-time tracking of physical and semi-physical parameters that can be found generally in white-box and grey-box powertrain models. This research was conducted considering the fact that future powertrain control and monitoring strategies will rely increasingly on physically oriented system models for the ultimate purpose of improving the efficiency of modern cars, while maintaining complexity and development cost into viable levels. The key message of this thesis is that:

> *Powertrain systems can become more intelligent and safe by employing suitable adaptive identification algorithms for assessing and monitoring their condition in real-time.*

Prior to the implementation of such algorithms certain steps have to be taken. The most crucial is the development of control-oriented models that represent the physics underlying the operation a given powertrain system. In this thesis

this step was emulated with the development of a multi-domain physics-based dynamic model of a complete single cylinder transient engine testing facility. The theoretical analysis of this model was presented in Chapter 3 whilst the technical features of the actual engine testing facility were discussed in Chapter 4. The main lesson to be learned from this process is that a model can be as good as the information that can extracted from the real system. In other words the development of a high fidelity physically oriented engine powertrain model would have no meaning if the same level of accuracy could not be obtained from the control and monitoring system of the actual powertrain system. In this thesis, the aforementioned challenge was anticipated with the development of a unique high-speed global test cell controller (Chapter 4) that enabled the measurement of all the quantities of interest with the same resolution as the one obtained by the model. Consequently, it must be highlighted that high fidelity powertrain models should only be develop if high fidelity control and instrumentation systems can exist.

System identification tools for detectability assessment and real-time monitoring of physical and semi-physical model parameters were presented in Chapter 5. The concept of parameter identifiability was discussed and an algorithm for assessing the qualitative identifiability of physical and semi-physical model parameters was proposed. Concurrently adaptive identification algorithms for linear and non-linear systems were derived. The combination of the qualitative identifiability theory and adaptive identification algorithms lead us in the establishment of a general framework, named “Qualitative Adaptive Identification". Such framework could be used in adaptive identification applications were the detectability of physical and semi-physical model parameters is uncertain due problems associated with model complexity and realistic experimental conditions e.g. unplanned process records, high signal-to-noise ratio etc. The efficacy of the proposed system identification algorithms was demonstrated successfully with three novel practical applications. From the practical applications of the qualitative adaptive identification framework it can be said that it would be rather naive to assume that param-

eters with physical and semi-physical interpretation are always identifiable. Identifiability analysis must be undertaken prior to the implementation of any adaptive identification algorithm to ensure that the parameters to be estimated can be actually estimated.

Turning to the practical applications of the proposed system identification tools, the use of recursive identification algorithms for the on-line health monitoring of engine dynamometer shafts was presented in Chapter 6. The results from three different recursive identification algorithms were compared, leading to the conclusion that no practical differences were observed as far as the tracking performance is concerned. Additionally the tracking performance of the algorithms was examined for three different coupling shaft configurations, the results proved the efficacy of all three recursive identification algorithms. On the other hand it was found that the accuracy of the parameter estimates was significantly affected by noisy measurements. Simulation results revealed that the proposed on-line conditions monitoring methodology can be used for detecting and isolating faults and malfunctions.

The second application of the proposed identification tools was presented in Chapter 7 and was related to engine friction parameters ranking and estimation. The ranking order of engine design characteristics in respect to their contribution to the overall engine friction was evaluated based on analytical sensitivity analysis. Results from this study showed that the ranking order of the engine design characteristics can vary depending on the operating conditions of the engine. Analytical sensitivity analysis seams to be very convenient analysis tools as it can be employed without the need of experimental data, provided that a physical or a semi-physical model of the process exists. Additionally the qualitative adaptive identification framework was employed in order to estimate the engine friction in real-time. Experimental results revealed that the engine friction torque can be estimated under various steady-state and slow transient operating conditions verifying the effectiveness of the suggested approach.

A practical application of non-linear recursive parameter estimation algorithms with parameter identifiability analysis for physical and semi-physical engine model parameters was reported in Chapter 8. The qualitative identifiability analysis proved that not all the parameters of a physical engine model can be estimated directly for any given observation data. Thus, the use of the proposed identifiability analysis algorithm for assessing the compatibility of the model structure and the information content of the observation data prior to the actual estimation of the parameters is highly recommended. Furthermore, the formulation of two variants of the Kalman Filter, the EKF and UKF for the adaptive estimation of the cyclic engine torque model parameters was presented for the first time. It is observed that both algorithms provide successful results despite the complexity involved in the actual system. The proposed methodology could be used as a conditions monitoring tool in End-of-Line cold engine testing application.

Ultimately, the findings of this research suggest that powertrain component-based diagnosis and control strategies could be established by combining physics-based control-oriented models with adaptive identification algorithms.

9.2 Future Work

Based on the outcome of this work some recommendations for future research efforts are enlisted bellow:

- *Self Calibrated Models*, the development of an object-oriented library with self calibrated engine models would solve existing problems associated with the validity of physical and semi-physical control oriented engine models. Self calibrated models could be developed by the incorporation of adaptive identification algorithms within the original structure of the model leading to adaptable or as said self calibrated models.

- *Recursive Identifiability*, one limitation of existing parameter identifiability approaches is that they cannot be used for assessing the identifiability of

the parameters in an on-line basis. Consequently the development of on-line parameter identifiability algorithm would be a significant contribution in the area of adaptive identification and control.

- *Quantitative Adaptive Identification*, the concept of qualitative adaptive identification was discussed for the first time in this thesis. A natural extension of this idea would be the establishment of the so called “Quantitative Adaptive Identification" framework. The main difference would be related to the identifiability tools that are used to determined the detectability of the parameters. More specifically, the major advantage of the quantitative adaptive identification framework is that it could provide not only information regarding the detectability of the model parameters but also information related to the confidence interval of the estimable parameters.

- *Adaptive Learning Control*, the combination of the adaptive learning algorithms (i.e. recursive identification and iterative learning control) with optimal control theory could lead to the establishment of self calibrated optimal learning controllers. A conceptual diagram from the implementation of the adaptive learning control strategy in engine applications is presented in Fig. 9.1. Such control strategies would unlock the full potential of automotive powertrains and open the road to new technologies such as human-specific adaptive learning vehicles.

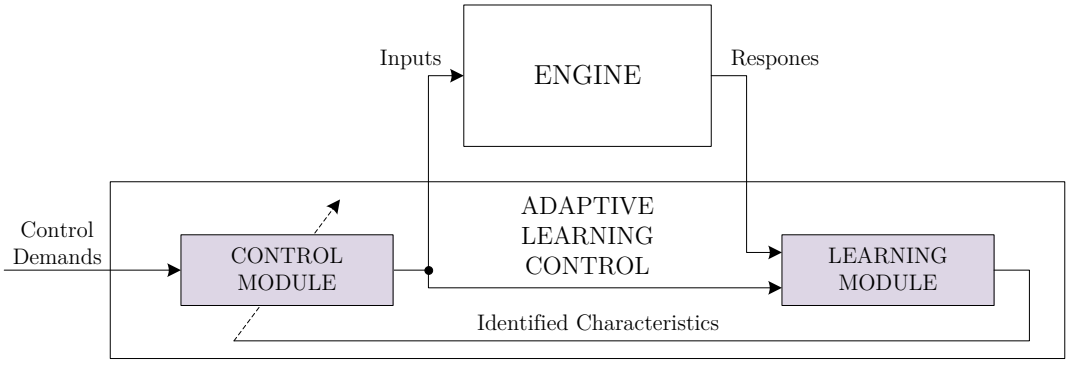

Figure 9.1: Conceptual diagram of the adaptive learning control strategy.

References

[1] European Environment Agency, “Total greenhouse gas (GHG) emission trends and projections,” 2014. [Online]. Available: http://www.eea.europa.eu/data-and-maps/indicators/greenhouse-gas-emission-trends-5/assessment-1 [Accessed: 15-August-2015].

[2] J. King, “The King Review of low-carbon cars Part I: the potential for CO2 reduction.” London: HM Treasury, 2007. ISBN 978-1-84532-335-6

[3] E. Juliussen and R. Robinshon, “Is Europe in the Driver’s Seat? The Competitiveness of the European Automotive Embedded Systems Industry.” Luxembourg: Publications Office of the European Union, 2010. ISBN 978-92-79-17658-6

[4] C. Atkinson, M. Allain, and H. Zhang, “Using Model-Based Rapid Transient Calibration to Reduce Fuel Consumption and Emissions in Diesel Engines,” apr 2008, SAE Technical Paper: 2008-01-1365. doi: 10.4271/2008-01-1365

[5] M. Vint, “Future of IC Engine Control Challenges,” in *SAE 2011 Electronic Systems for Vehicle Propulsion Symposium*. Troy MI: SAE, 2011.

[6] J. C. Maxwell, “On Governors,” *Proceedings of the Royal Society of London*, vol. 16, pp. 270–283, jan 1867. doi: 10.1098/rspl.1867.0055

[7] K. Reif, *Automotive Mechatronics: Automotive Networking, Driving Stability Systems, Electronics*, ser. Bosch Professional Automotive Informa-

tion. Wiesbaden: Springer Vieweg, 2014. ISBN 978-3-658-03974-5. doi: 10.1007/978-3-658-03975-2

[8] J. A. Cook, J. Sun, J. H. Buckl, I. V. Kolmanovsky, H. Peng, and J. W. Grizzle, "Automotive powertrain control - a survey," *Asian Journal of Control*, vol. 8, pp. 237–260, 2006.

[9] R. Isermann, *Engine Modeling and Control: Modelling and Electronic Management of Internal Combustion Engines*. Berlin Heidelberg: Springer-Verlag, 2014. ISBN 978-3-642-39933-6. doi: 10.1007/978-3-642-39934-3

[10] R. Isermann, *Fault-Diagnosis Applications Model-Based Condition Monitoring: Actuators, Drives, Machinery, Plants, Sensors, and Fault-tolerant Systems*. Berlin Heidelberg: Springer-Verlag, 2011. ISBN 978-3-642-12766-3. doi: 10.1007/978-3-642-12767-0

[11] L. Guzzella and A. Sciarretta, *Vehicle Propulsion Systems Introduction to Modeling and Optimization*, 3rd ed. Berlin Heidelberg: Springer-Verlag, 2013. ISBN 978-3-642-35912-5. doi: 10.1007/978-3-642-35913-2

[12] L. Guzzella and C. H. Onder, *Introduction to Modeling and Control of Internal Combustion Engine Systems*. Berlin Heidelberg: Springer-Verlag, 2010. ISBN 978-3-642-10774-0. doi: 10.1007/978-3-642-10775-7

[13] D. Alberer, H. Hjalmarsson, and L. Del Re, *Identification for Automotive Systems*. Berlin Heidelberg: Springer-Verlag, 2012. ISBN 978-1-4471-2220-3. doi: 10.1007/978-1-4471-2221-0

[14] W. Harald, I. Kolmanovsky, M. Steinbuch, and L. Del Re, *Optimization and Optimal Control in Automotive Systems*. Berlin Heidelberg: Springer-Verlag, 2014. ISBN 978-3-319-05370-7. doi: 10.1007/978-3-319-05371-4

[15] A. P. White, G. Zhu, and J. Choi, *Linear Parameter-Varying Control for Engineering Applications*. Berlin Heidelberg: Springer-Verlag, 2013. ISBN 978-1-4471-5039-8. doi: 10.1007/978-1-4471-5040-4

[16] J. T. Pukrushpan, A. G. Stefanopoulou, and H. Peng, *Control of Fuel Cell Power Systems: Principles, Modeling, Analysis and Feedback Design*. Berlin Heidelberg: Springer-Verlag, 2013. ISBN 978-1-85233-816-9. doi: 10.1007/978-1-4471-3792-4

[17] K. Reif, *Gasoline Engine Management: Systems and Components*, ser. Bosch Professional Automotive Information. Wiesbaden: Springer Vieweg, 2014. ISBN 978-3-658-03963-9. doi: 10.1007/978-3-658-03964-6

[18] K. Reif, *Diesel Engine Management: Systems and Components*, ser. Bosch Professional Automotive Information. Wiesbaden: Springer Vieweg, 2014. ISBN 978-3-658-03980-6. doi: 10.1007/978-3-658-03981-3

[19] J. Cassidy Jr, M. Athans, and W. Lee, "On the design of electronic automotive engine controls using linear quadratic control theory," *Automatic Control, IEEE Transactions on*, vol. 25, no. 5, pp. 901–912, 1980. doi: 10.1109/TAC.1980.1102457

[20] J. Moskwa and J. Hedrick, "Nonlinear algorithms for automotive engine control," *IEEE Control Systems Magazine*, vol. 10, no. 3, pp. 88–93, 1990. doi: 10.1109/37.55129

[21] M. Jung and K. Glover, "Calibratable linear parameter-varying control of a turbocharged diesel engine," *IEEE Transactions on Control Systems Technology*, vol. 14, no. 1, pp. 45–62, jan 2006. doi: 10.1109/TCST.2005.860513

[22] X. Wei and L. del Re, "Gain Scheduled Control for Air Path Systems of Diesel Engines Using LPV Techniques," *IEEE Transactions on Control Systems Technology*, vol. 15, no. 3, pp. 406–415, may 2007. doi: 10.1109/TCST.2007.894633

[23] Y.-Y. Wang, I. Haskara, and O. Yaniv, "Quantitative feedback design of air and boost pressure control system for turbocharged diesel engines,"

Control Engineering Practice, vol. 19, no. 6, pp. 626–637, jun 2011. doi: 10.1016/j.conengprac.2011.02.006

[24] M. Lee and M. Sunwoo, "Model-based control of a diesel engine variable geometry turbine and exhaust gas recirculation system using a linear parameter varying methodology," *Proceedings of the Institution of Mechanical Engineers, Part D: Journal of Automobile Engineering*, vol. 228, no. 14, pp. 1633–1643, 2014. doi: 10.1177/0954407012465069

[25] M. Postma and R. Nagamune, "Air-Fuel Ratio Control of Spark Ignition Engines Using a Switching LPV Controller," *IEEE Transactions on Control Systems Technology*, vol. 20, no. 5, pp. 1175–1187, sep 2012. doi: 10.1109/TCST.2011.2163937

[26] D. Cieslar, P. Dickinson, A. Darlington, K. Glover, and N. Collings, "Model based approach to closed loop control of 1-D engine simulation models," *Control Engineering Practice*, vol. 29, pp. 212–224, aug 2014. doi: 10.1016/j.conengprac.2014.01.021

[27] N. Giorgetti, G. Ripaccioli, A. Bemporad, I. Kolmanovsky, and D. Hrovat, "Hybrid Model Predictive Control of Direct Injection Stratified Charge Engines," *IEEE/ASME Transactions on Mechatronics*, vol. 11, no. 5, pp. 499–506, oct 2006. doi: 10.1109/TMECH.2006.882979

[28] P. Ortner and L. del Re, "Predictive Control of a Diesel Engine Air Path," *IEEE Transactions on Control Systems Technology*, vol. 15, no. 3, pp. 449–456, may 2007. doi: 10.1109/TCST.2007.894638

[29] F. Yan, J. Wang, and K. Huang, "Hybrid Electric Vehicle Model Predictive Control Torque-Split Strategy Incorporating Engine Transient Characteristics," *IEEE Transactions on Vehicular Technology*, vol. 61, no. 6, pp. 2458–2467, jul 2012. doi: 10.1109/TVT.2012.2197767

[30] J. Huber, H. Kopecek, and M. Hofbaur, “Nonlinear model predictive control of an internal combustion engine exposed to measured disturbances,” *Control Engineering Practice*, vol. 44, pp. 78–88, nov 2015. doi: 10.1016/j.conengprac.2015.06.007

[31] J. Larimore, S. Jade, E. Hellstrom, L. Jiang, and A. G. Stefanopoulou, “Adaptive Control of a Recompression Four-Cylinder HCCI Engine,” *IEEE Transactions on Control Systems Technology*, vol. 23, no. 6, pp. 2144–2154, nov 2015. doi: 10.1109/TCST.2015.2402235

[32] D. Pavkovic, J. Deur, and I. Kolmanovsky, “Adaptive Kalman Filter-Based Load Torque Compensator for Improved SI Engine Idle Speed Control,” *IEEE Transactions on Control Systems Technology*, vol. 17, no. 1, pp. 98–110, jan 2009. doi: 10.1109/TCST.2008.922556

[33] Y. Yildiz, A. M. Annaswamy, D. Yanakiev, and I. Kolmanovsky, “Spark-Ignition-Engine Idle Speed Control: An Adaptive Control Approach,” *IEEE Transactions on Control Systems Technology*, vol. 19, no. 5, pp. 990–1002, sep 2011. doi: 10.1109/TCST.2010.2078818

[34] K. Muske, J. Jones, and E. Franceschi, “Adaptive Analytical Model-Based Control for SI Engine AirâĂŞFuel Ratio,” *IEEE Transactions on Control Systems Technology*, vol. 16, no. 4, pp. 763–768, jul 2008. doi: 10.1109/TCST.2007.912243

[35] J. Ma, G. G. Zhu, and H. Schock, “Adaptive Control of a Pneumatic Valve Actuator for an Internal Combustion Engine,” *IEEE Transactions on Control Systems Technology*, vol. 19, no. 4, pp. 730–743, jul 2011. doi: 10.1109/TCST.2010.2054091

[36] T. Ba, X. Guan, and J. Zhang, “Vehicle predictive control based on the recursive subspace identification method,” *Proceedings of the Institution of Mechanical Engineers, Part D: Journal of Automobile Engineering*, vol. 229, no. 8, pp. 1094–1109, 2015. doi: 10.1177/0954407014555878

[37] A. K. Sood, A. A. Fahs, and N. A. Henein, "Engine Fault Analysis: Part II—Parameter Estimation Approach," *Industrial Electronics, IEEE Transactions on*, vol. IE-32, no. 4, pp. 301–307, 1985. doi: 10.1109/TIE.1985.350101

[38] M. Nyberg and T. Stutte, "Model based diagnosis of the air path of an automotive diesel engine," *Control Engineering Practice*, vol. 12, no. 5, pp. 513–525, may 2004. doi: 10.1016/S0967-0661(03)00120-5

[39] F. Kimmich, A. Schwarte, and R. Isermann, "Fault detection for modern Diesel engines using signal- and process model-based methods," *Control Engineering Practice*, vol. 13, no. 2, pp. 189–203, feb 2005. doi: 10.1016/j.conengprac.2004.03.002

[40] M. Desbazeille, R. Randall, F. Guillet, M. El Badaoui, and C. Hoisnard, "Model-based diagnosis of large diesel engines based on angular speed variations of the crankshaft," *Mechanical Systems and Signal Processing*, vol. 24, no. 5, pp. 1529–1541, jul 2010. doi: 10.1016/j.ymssp.2009.12.004

[41] J. Mohammadpour, K. Grigoriadis, M. Franchek, and B. J. Zwissler, "Real-Time Diagnosis of the Exhaust Recirculation in Diesel Engines Using Least-Squares Parameter Estimation," *Journal of Dynamic Systems, Measurement, and Control*, vol. 132, no. 1, p. 011009, jan 2010. doi: 10.1115/1.4000655

[42] Q. Ahmed, A. I. Bhatti, and M. Iqbal, "Virtual sensors for automotive engine sensors fault diagnosis in second-order sliding modes," *IEEE Sensors Journal*, vol. 11, no. 9, pp. 1832–1840, 2011. doi: 10.1109/JSEN.2011.2105471

[43] H. Lee, J. Lee, and M. Sunwoo, "Fault Diagnosis of Exhaust Gas Recirculation and Variable Geometry Turbocharger Systems in a Passenger Car Diesel Engine Based on a Sliding Mode Observer for Air System States Estimation," *Journal of Dynamic Systems, Measurement, and Control*, vol. 136, no. 3, p. 031016, feb 2014. doi: 10.1115/1.4026131

[44] C. M. Vong, P. K. Wong, and K. I. Wong, "Simultaneous-fault detection based on qualitative symptom descriptions for automotive engine diagnosis," *Applied Soft Computing*, vol. 22, pp. 238–248, sep 2014. doi: 10.1016/j.asoc.2014.05.014

[45] J. Chen and R. Bond Randall, "Improved automated diagnosis of misfire in internal combustion engines based on simulation models," *Mechanical Systems and Signal Processing*, vol. 64-65, pp. 58–83, dec 2015. doi: 10.1016/j.ymssp.2015.02.027

[46] G. P. Merker, C. Schwarz, and R. Teichmann, *Combustion Engines Development: Mixture Formation, Combustion, Emissions and Simulation*. Berlin Heidelberg: Springer-Verlag, 2011. ISBN 978-3-658-03980-6. doi: 10.1007/978-3-658-03981-3

[47] A. Chow and M. L. Wyszynski, "Thermodynamic modelling of complete engine systems, a review," *Proceedings of the Institution of Mechanical Engineers, Part D: Journal of Automobile Engineering*, vol. 213, no. 4, pp. 403–415, jan 1999. doi: 10.1243/0954407991526964

[48] R. S. Benson, *The Thermodynamic and Gas Dynamics of Internal Combustion Engines*. Oxford: Oxford University Press, 1982, vol. 1. ISBN 978-0198562122

[49] J. Heywood, *Internal Combustion Engine Fundamentals*. New York City: McGraw-Hill Education, 1988. ISBN 978-0070286375

[50] C. R. Ferguson, *Internal combustion engines, applied thermosciences*. New Jersey: Wiley, 1986. ISBN 9780471881292

[51] I. Arsie, C. Pianese, and G. Rizzo, "Models for the Prediction of Performance and Emissions in a Spark Ignition Engine - A Sequentially Structured Approach," 1998, SAE Technical Paper: 980779. doi: 10.4271/980779

[52] S. Karagiorgis, N. Collings, K. Glover, and T. Petridis, “Dynamic modeling of combustion and gas exchange processes for controlled auto-ignition engines,” in *American Control Conference*, 2006. doi: 10.1109/ACC.2006.1656494

[53] F. Salimi, A. H. Shamekhi, and A. M. Pourkhesalian, “Effects of Spark Advance, A/F Ratio and Valve Timing on Emission and Performance Characteristics of Hydrogen Internal Combustion Engine,” 2009, SAE Technical Paper: 2009-01-1424. doi: 10.4271/2009-01-1424

[54] R. Stone, *Introduction to Internal Combustion Engines*, 3rd ed. Troy, MI: Society of Automotive Engineers, 1999. ISBN 978-0768004953

[55] S. Verhelst and C. Sheppard, “Multi-zone thermodynamic modelling of spark-ignition engine combustion âĂŞ An overview,” *Energy Conversion and Management*, vol. 50, no. 5, pp. 1326–1335, may 2009. doi: 10.1016/j.enconman.2009.01.002

[56] M. Chiodi and M. Bargende, “Improvement of Engine Heat-Transfer Calculation in the Three-Dimensional Simulation Using a Phenomenological Heat-Transfer Model,” 2001, SAE Technical Paper: 2001-01-3601. doi: 10.4271/2001-01-3601

[57] G. Woschni, “A Universally Applicable Equation for the Instantaneous Heat Transfer Coefficient in the Internal Combustion Engine,” 1967, SAE Technical Paper: 670931. doi: 10.4271/670931

[58] S. Gordon and B. McBride, “Computer Program for Calculation of Complex Chemical Equilibrium Compositions, Rocket Performance, Incident and Reflected Shocks, and Chapman-Jouguet Detonations,” NASA SP-273. 1976.

[59] A. Pezouvanis, “Engine Modelling for Virtual Mapping,” PhD Thesis, University of Bradford, 2009.

[60] Y. H. Zweiri, J. F. Whidborne, and L. D. Seneviratne, “Dynamic simulation of a single-cylinder diesel engine including dynamometer modelling and friction,” *Proceedings of the Institution of Mechanical Engineers, Part D: Journal of Automobile Engineering*, vol. 213, no. 4, pp. 391–402, Apr. 1999. doi: 10.1243/0954407991526955

[61] J. A. Caton, “Use of a Cycle Simulation Incorporating the Second Law of Thermodynamics: Results for Spark-Ignition Engines Using Oxygen Enriched Combustion Air,” 2005, SAE Technical Paper: 2005-01-1130. doi: 10.4271/2005-01-1130

[62] A. Sobiesiak and S. Zhang, “The First and Second Law Analysis of Spark Ignition Engine Fuelled with Compressed Natural Gas,” 2003, SAE Technical Paper: 2003-01-3091. doi: 10.4271/2003-01-3091

[63] A. Chevalier, M. Müller, and E. Hendricks, “On the Validity of Mean Value Engine Models During Transient Operation,” no. 724, 2000, SAE Technical Paper: 2000-01-1261. doi: 10.4271/2000-01-1261

[64] I. Arsie, C. Pianese, and G. Rizzo, “An Integrated System of Models for Performance and Emissions in SI Engines: Development and Identification,” 2003, SAE Technical Paper: 2003-01-1052. doi: 10.4271/2003-01-1052

[65] M. Jung, R. G. Ford, K. Glover, N. Collings, U. Christen, and M. J. Watts, “Parameterization and Transient Validation of a Variable Geometry Turbocharger for Mean-Value Modeling at Low and Medium Speed-Load Points,” 2002, SAE Technical Paper: 2002-01-2729. doi: 10.4271/2002-01-2729

[66] P. Moraal and I. Kolmanovsky, “Turbocharger Modeling for Automotive Control Applications,” 1999, SAE Technical Paper: 1999-01-0908. doi: 10.4271/1999-01-0908

[67] A. Gambarotta and G. Lucchetti Ing, "Control-Oriented âĂIJCrank-AngleâĂİ Based Modeling of Automotive Engines," 2011, SAE Technical Paper: 2011-24-0144. doi: 10.4271/2011-24-0144

[68] P. Fiorani, A. Gambarotta, M. Tonetti, and E. Lanfranco, "A Real-Time Model for the Simulation of Transient Behaviour of Automotive Diesel Engines," 2006, SAE Technical Paper: 2006-01-3007. doi: 10.4271/2006-01-3007

[69] Y.-K. Chin and F. E. Coats, "Engine Dynamics: Time-Based Versus Crank-Angle Based," 1986, SAE Technical Paper: 860412. doi: 10.4271/860412

[70] G. Hubbard and K. Youcef-Toumi, "Modeling and simulation of a hybrid-electric vehicle drivetrain," in *American Control Conference*, 1997. doi: 10.1109/ACC.1997.611878

[71] A. J. Chaudhari, N. Sahoo, and V. Kulkarni, "Simulation Models for Spark Ignition Engine: A Comparative Performance Study," *Energy Procedia*, vol. 54, pp. 330–341, 2014. doi: 10.1016/j.egypro.2014.07.276

[72] J. H. Grau, J. M. García, J. P. García, A. V. Robles, and R. R. Pastor, "Modelling Methodology of a Spark-Ignition Engine and Experimental Validation: Part II: Gas Exchange Process," 2002, SAE Technical Paper: 2002-01-2194. doi: 10.4271/2002-01-2194

[73] J. H. Grau, J. M. García, J. P. García, A. V. Robles, and R. R. Pastor, "Modelling Methodology of a Spark-Ignition Engine and Experimental Validation: Part I: Single-Zone Combustion Model," 2002, SAE Technical Paper: 2002-01-2193. doi: 10.4271/2002-01-2193

[74] Y. H. Zweiri, J. F. Whidborne, and L. D. Seneviratne, "Instantaneous friction components model for transient engine operation," *Proceedings of the Institution of Mechanical Engineers, Part D: Journal of Automobile Engineering*, vol. 214, no. 7, pp. 809–824, Jul. 2000. doi: 10.1243/0954407001527664

[75] Y. H. Zweiri, J. F. Whidborne, and L. D. Seneviratne, "Detailed analytical model of a single-cylinder diesel engine in the crank angle domain," *Proceedings of the Institution of Mechanical Engineers, Part D: Journal of Automobile Engineering*, vol. 215, no. 11, pp. 1197–1216, Nov. 2001. doi: 10.1243/0954407011528734

[76] C. D. Rakopoulos and E. G. Giakoumis, "Review of Thermodynamic Diesel Engine Simulations under Transient Operating Conditions," 2006, SAE Technical Paper: 2006-01-0884. doi: 10.4271/2006-01-0884

[77] O. Grondin, R. Stobart, H. Chafouk, and J. Maquet, "Modelling the Compression Ignition Engine for Control: Review and Future Trends." 2004, SAE Technical Paper: 2004-01-0423. doi: 10.4271/2004-01-0423

[78] M. Cary, "A Model Based Engine Calibration Methodology for a Port Fuel Injection, Spark-Ignition Engine," PhD Thesis, Univeristy of Bradford, 2003.

[79] K. Röpke and C. von Essen, "DoE in engine development," *Quality and Reliability Engineering International*, vol. 24, no. 6, pp. 643–651, 2008. doi: 10.1002/qre.941

[80] J. J. Moskwa and J. Hedrick, "Automotive Engine Modeling for Real Time Control Application," in *American Control Conference*, 1987.

[81] K. J. Patton, R. G. Nitschke, and J. B. Heywood, "Development and Evaluation of a Performance and Efficiency Model for Spark-Ignition Engines," 1989, SAE Technical Paper: 890836. doi: 10.4271/890836

[82] D. Sandoval and J. B. Heywood, "An Improved Friction Model for Spark-Ignition Engines," 2003, SAE Technical Paper: 2003-01-0725. doi: 10.4271/2003-01-0725

[83] E. Hendricks and S. C. Sorenson, "Mean Value Modelling of Spark Ignition Engines," 1990, SAE Technical Paper: 900616. doi: 10.4271/900616

[84] E. Hendricks, A. Chevalier, M. Jensen, S. C. Sorenson, D. Trumpy, and J. Asik, "Modelling of the Intake Manifold Filling Dynamics," 1996, SAE Technical Paper: 960037. doi: 10.4271/960037

[85] M. Müller, E. Hendricks, and S. C. Sorenson, "Mean Value Modelling of Turbocharged Spark Ignition Engines," 1998, SAE Technical Paper: 980784. doi: 10.4271/980784

[86] E. Hendricks, "Isothermal vs. Adiabatic Mean Value SI Engine Models," in *Proceedings of the 3rd IFAC Workshop on Advances in Automotive Control*, 2001.

[87] A. Chevalier, C. W. Vigild, and E. Hendricks, "Predicting the Port Air Mass Flow of SI Engines in Air/Fuel Ratio Control Applications," 2000, SAE Technical Paper: 2000-01-0260. doi: 10.4271/2000-01-0260

[88] L. Eriksson, "Mean Value Models for Exhaust System Temperatures," 2002, SAE Technical Paper: 2002-01-0374. doi: 10.4271/2002-01-0374

[89] H. Melgaard, E. Hendricks, and H. Madsen, "Continuous Identification of a Four-Stroke SI Engine," in *American Control Conference*, 1990.

[90] K. Nikzadfar and A. H. Shamekhi, "Developing a state space model for a turbocharged diesel engine using the subspace identification method," *Proceedings of the Institution of Mechanical Engineers, Part D: Journal of Automobile Engineering*, vol. 225, no. 12, pp. 1692–1706, dec 2011. doi: 10.1177/0954407011413036

[91] J. V. Salcedo and M. Martínez, "LPV identification of a turbocharged diesel engine," *Applied Numerical Mathematics*, vol. 58, no. 10, pp. 1553–1571, oct 2008. doi: http://dx.doi.org/10.1016/j.apnum.2007.09.005

[92] G. C. Luh and G. Rizzoni, "Identification of a nonlinear MIMO IC engine model during I/M240 driving cycle for on-board diagnosis," in *American Control Conference*, 1994. doi: 10.1109/ACC.1994.752336

[93] N. Togun, S. Baysec, and T. Kara, “Nonlinear modeling and identification of a spark ignition engine torque,” *Mechanical Systems and Signal Processing*, vol. 26, pp. 294–304, jan 2012. doi: 10.1016/j.ymssp.2011.06.010

[94] V. M. Janakiraman, X. Nguyen, and D. Assanis, “Nonlinear identification of a gasoline HCCI engine using neural networks coupled with principal component analysis,” *Applied Soft Computing*, vol. 13, no. 5, pp. 2375–2389, may 2013. doi: http://dx.doi.org/10.1016/j.asoc.2013.01.006

[95] A. Stotsky, “Adaptive Estimation of the Engine Friction Torque,” in *Decision and Control, 2005 and 2005 European Control Conference. CDC-ECC ’05. 44th IEEE Conference on*, 2005. doi: 10.1109/CDC.2005.1583240

[96] J. C. Peyton Jones and K. R. Muske, “Automatic Calibration of 1 and 2-D Look-up Tables using Recursive Least-squares Identification Techniques,” 2007, SAE Technical Paper: 2007-01-1343. doi: 10.4271/2007-01-1343

[97] C. Guardiola, H. Climent, B. Pla, and D. Blanco-Rodriguez, “ECU-oriented models for NO x prediction. Part 2: adaptive estimation by using an NO x sensor,” *Proceedings of the Institution of Mechanical Engineers, Part D: Journal of Automobile Engineering*, vol. 229, no. 10, pp. 1345–1360, sep 2015. doi: 10.1177/0954407014561278

[98] S. Helm, M. Kozek, and S. Jakubek, “Combustion Torque Estimation and Misfire Detection for Calibration of Combustion Engines by Parametric Kalman Filtering,” *IEEE Transactions on Industrial Electronics*, vol. 59, no. 11, pp. 4326–4337, Nov. 2012. doi: 10.1109/TIE.2012.2193855

[99] A. Gangopadhyay and P. Meckl, “Modeling, validation and system identification of a natural gas engine,” in *American Control Conference*, 1997. doi: 10.1109/ACC.1997.611804

[100] A. Gangopadhyay and P. H. Meckl, “Extracting physical parameters from system identification of a natural gas engine,” *Control Systems Tech-*

nology, IEEE Transactions on, vol. 9, no. 3, pp. 425–434, 2001. doi: 10.1109/87.918896

[101] L. Eriksson, "Requirements for and a Systematic Method for Identifying Heat-Release Model Parameters." SAE International, 1998, SAE Technical Paper: 980626. doi: 10.4271/980626

[102] I. Brahma, M. C. Sharp, and T. R. Frazier, "Estimation of Engine Torque from a First Law Based Regression Model," 2008, SAE Technical Paper: 2008-01-1014. doi: 10.4271/2008-01-1014

[103] Y. Yeliana, C. Cooney, J. Worm, D. J. Michalek, and J. D. Naber, "Estimation of double-Wiebe function parameters using least square method for burn durations of ethanol-gasoline blends in spark ignition engine over variable compression ratios and EGR levels," *Applied Thermal Engineering*, vol. 31, no. 14âĂŞ15, pp. 2213–2220, oct 2011. doi: http://dx.doi.org/10.1016/j.applthermaleng.2011.01.040

[104] M. Cary, M. Ebrahimi, K. Ffrench, and R. Sbaschnig, "Throttle body: Modelling and identification," *Proceedings of the Institution of Mechanical Engineers, Part D: Journal of Automobile Engineering*, vol. 215, no. 7, pp. 813–825, jul 2001. doi: 10.1177/095440700121500707

[105] M. Neve, G. De Nicolao, G. Prodi, and C. Siviero, "Estimation of Engine Maps: A Regularized Basis-Function Networks Approach," *Control Systems Technology, IEEE Transactions on*, vol. 17, no. 3, pp. 716–722, 2009. doi: 10.1109/TCST.2008.2002040

[106] S. F. Rezeka and N. A. Henein, "A new approach to evaluate instantaneous friction and its components in internal combustion engines," 1984, SAE Technical Paper: 840179. doi: 10.4271/840179

[107] R. Constantinescu, “An Analysis of Three Model-Based Estimation Methods for Diesel Engine Condition Monitoring,” Master of Applied Science, The University of British Columbia, 1995.

[108] M. Mrosek, S. Zahn, and R. Isermann, “Parameter Estimation for Physical Based Air Path Models of Turbocharged Diesel Engines âĂŤ An Experience Based Guidance,” 2009, SAE Technical Paper: 2009-24-0134. doi: 10.4271/2009-24-0134

[109] F. Cruz-Peragón, J. M. Palomar, F. A. Díaz, and F. J. Jiménez-Espadafor, “Fast on-line identification of instantaneous mechanical losses in internal combustion engines,” *Mechanical Systems and Signal Processing*, vol. 24, no. 1, pp. 267–280, jan 2010. doi: http://dx.doi.org/10.1016/j.ymssp.2009.06.009

[110] A. A. Belaidi, H. Chafouk, and N. Langlois, “Detection and localization of faults based on parametric estimation applied to diesel engine,” in *Control & Automation (MED), 2010 18th Mediterranean Conference on*, 2010. doi: 10.1109/MED.2010.5547859

[111] N. Nickmehr, L. Eriksson, and J. Åslund, “Methodology for Modeling, Parameter Estimation, and Validation of Powertrain Torsional Vibration,” *SNE Simulation Notes Europe*, vol. 24, no. 3-4, 2014. doi: 10.11128/sne.24.tn.102261

[112] N. Nickmehr, “System Identification of an Engine-load Setup Using Grey-box Model,” Licentiate Thesis, Linköping University, 2015.

[113] A. Kebairi, M. Becherif, and M. El Bagdouri, “Modelling, simulation and identification of an engine air path electromechanical actuator,” *Control Engineering Practice*, vol. 34, pp. 88–97, jan 2015. doi: http://dx.doi.org/10.1016/j.conengprac.2014.07.009

[114] Yaojung Shiao and J. Moskwa, "Cylinder pressure and combustion heat release estimation for SI engine diagnostics using nonlinear sliding observers," *IEEE Transactions on Control Systems Technology*, vol. 3, no. 1, pp. 70–78, mar 1995. doi: 10.1109/87.370712

[115] I. Kolmanovsky, I. Sivergina, and J. Sun, "Simultaneous input and parameter estimation with input observers and set-membership parameter bounding: theory and an automotive application," *International Journal of Adaptive Control and Signal Processing*, vol. 20, no. 5, pp. 225–246, jun 2006. doi: 10.1002/acs.899

[116] K. Kar, S. Roberts, R. Stone, M. Oldfield, and B. French, "Instantaneous Exhaust Temperature Measurements Using Thermocouple Compensation Techniques," 2004, SAE Technical Paper: 2004-01-1418. doi: 10.4271/2004-01-1418

[117] P. Ortner, E. Gruenbacher, and L. del Re, "Model based nonlinear observers for torque estimation on a combustion engine test bench," in *2008 IEEE International Conference on Control Applications*, 2008. doi: 10.1109/CCA.2008.4629628

[118] D. Sengupta, S. Sengupta, and S. Mukhopadhyay, "Estimation of instantaneous states of an SI gasoline engine using EKF and UKF," in *2011 Annual IEEE India Conference*, 2011. doi: 10.1109/INDCON.2011.6139608

[119] K. Stricker, L. Kocher, E. Koeberlein, D. Van Alstine, and G. M. Shaver, "Estimation of effective compression ratio for engines utilizing flexible intake valve actuation," *Proceedings of the Institution of Mechanical Engineers, Part D: Journal of Automobile Engineering*, vol. 226, no. 8, pp. 1001–1015, aug 2012. doi: 10.1177/0954407012438024

[120] N. Daroogheh, N. Meskin, and K. Khorasani, "Particle filtering for state and parameter estimation in gas turbine engine fault diagnostics," in *American Control Conference*, 2013. doi: 10.1109/ACC.2013.6580508

[121] R. Baur, Q. Zhao, J. P. Blath, F. Kallage, M. Schultalbers, and C. Bohn, "Estimation of fuel properties in a common rail injection system by unscented kaiman filtering," in *Control Applications (CCA), 2014 IEEE Conference on*, 2014. doi: 10.1109/CCA.2014.6981603

[122] S. Hong, T. Smith, F. Borrelli, and J. K. Hedrick, "Vehicle inertial parameter identification using Extended and unscented Kalman Filters," in *Intelligent Transportation Systems - (ITSC), 2013 16th International IEEE Conference on*, 2013. doi: 10.1109/ITSC.2013.6728432

[123] M. Choi, J. J. Oh, and S. B. Choi, "Linearized Recursive Least Squares Methods for Real-Time Identification of Tire Road Friction Coefficient," *Vehicular Technology, IEEE Transactions on*, vol. 62, no. 7, pp. 2906–2918, 2013. doi: 10.1109/TVT.2013.2260190

[124] Christian Lundquist, "Sensor Fusion for Automotive Applications," PhD Thesis, Linköping University, Sweden, 2011.

[125] D. Eriksson, E. Frisk, and M. Krysander, "A method for quantitative fault diagnosability analysis of stochastic linear descriptor models," *Automatica*, vol. 49, no. 6, pp. 1591–1600, jun 2013. doi: http://dx.doi.org/10.1016/j.automatica.2013.02.045

[126] J. Huber, H. Kopecek, and M. Hofbaur, "Sensor selection for fault parameter identification applied to an internal combustion engine," in *Control Applications (CCA), 2014 IEEE Conference on*, 2014. doi: 10.1109/CCA.2014.6981334

[127] A. A. Sokolov and S. T. Glad, "Identifiability of Turbocharged IC Engine Models." SAE International, 1999. [Online]. Available: http://dx.doi.org/10.4271/1999-01-0216

[128] A. Alasty and A. Ramezani, “Genetic Algorithm Based Parameter Identification of a Nonlinear Full Vehicle Ride Model.” SAE International, 2002, SAE Technical Paper: 2002-01-1583. doi: 10.4271/2002-01-1583

[129] J. Angeles, *Dynamic Response of Linear Mechanical Systems: Modeling, Analysis and Simulation*, ser. Mechanical Engineering Series. Berlin Heidelberg: Springer-Verlag, 2011. ISBN 978-1-4614-2946-3. doi: 10.1007/978-1-4419-1027-1

[130] B. Mason, “Reconfigurable modelling of physically based systems,” PhD Thesis, University of Bradford, 2009.

[131] J. I. Ramos, *Internal Combustion Engine Modelling*. Abingdon: Taylor & Francis, 1989. ISBN 978-0891161578

[132] I. Souflas, A. Pezouvanis, B. Mason, and K. M. Ebrahimi, “CO2 Emissios Management through Ignition Timing Control: Theoretical and Experimental Analysis,” in *Controls, Measurements & Calibration Congress*, São Paulo, 2014.

[133] A. Medina, P. L. Curto-Risso, A. C. Hernández, L. Guzmán-Vargas, F. Angulo-Brown, and A. K. Sen, *Quasi-Dimensional Simulation of Spark Ignition Engines: From Thermodynamic Optimization to Cyclic Variability*. Berlin Heidelberg: Springer-Verlag, 2013. ISBN 978-1-4471-5288-0. doi: 10.1007/978-1-4471-5289-7

[134] Y. A. Çengel and M. A. Boles, *Thermodynamics: an engineering approach*. New York City: McGraw-Hill Higher Education, 2006. ISBN 9780072884951

[135] S. Karagiorgis, “Dynamic Modeling and Transient Control of Homogeneous Charge Compression Ignition Engines,” PhD Thesis, University of Cambridge, 2007.

[136] J. Deur, D. Hrovat, J. PetricÌĄ, and Z. SÌŇitum, “A Control-Oriented Polytropic Model of SI Engine Intake Manifold,” in *ASME 2003 Inter-*

national Mechanical Engineering Congress and Exposition, 2003. doi: 10.1115/IMECE2003-41086

[137] J. Deur, D. Hrovat, and J. Asgari, "Analysis of mean value engine model with emphasis on intake manifold thermal effects," in *Control Applications, 2003. CCA 2003. Proceedings of 2003 IEEE Conference on*, 2003. doi: 10.1109/CCA.2003.1223284

[138] J. Deur, S. W. Magner, M. Jankovic, and D. Hrovat, "Influence of Intake Manifold Heat Transfer Effects on Accuracy of SI Engine Air-Charge Prediction," in *ASME 2004 International Mechanical Engineering Congress and Exposition*, California, 2004. doi: 10.1115/IMECE2004-60376

[139] Y. H. Zweiri, "Nonlinear Modelling and Estimation for Diesel Engines," PhD Thesis, King's College London, 2002.

[140] J. J. Moskwa, "Automotive Engine Modeling for Real Time Control," PhD Thesis, Massachusetts Institute of Technology, 1988.

[141] C. D. Rakopoulos and E. G. Giakoumis, *Diesel Engine Transient Operation: Principles of Operation and Simulation Analysis*. Berlin Heidelberg: Springer-Verlag, 2009. ISBN 978-1-84882-374-7. doi: 10.1007/978-1-84882-375-4

[142] N. Mohan, *Electric Machines and Drives*. New Jersey: Wiley, 2012. ISBN 978-1118074817

[143] J. Bocker and S. Mathapati, "State of the Art of Induction Motor Control," in *Electric Machines & Drives Conference, 2007. IEMDC '07. IEEE International*, 2007. doi: 10.1109/IEMDC.2007.383643

[144] B. Amin, *Induction Motors: Analysis and Torque Control*, ser. Power Systems. Berlin Heidelberg: Springer-Verlag, 2001. ISBN 978-3-540-42374-4

[145] A. Veltman, D. W. J. Pulle, and R. W. de Doncker, *Fundamentals of Electrical Drives*. Berlin Heidelberg: Springer-Verlag, 2007. ISBN 978-1-4020-5503-4. doi: 10.1007/978-1-4020-5504-1

[146] N. Mohan, *Electric Drives: An Integrative Approach*. Minnesota: MNPERE, 2003. ISBN 978-0971529250

[147] R. H. Park, "Two-reaction theory of synchronous machines generalized method of analysis-Part I," in *American Institute of Electrical Engineers, Transactions of the*, vol. 48, no. 3, 1929. doi: 10.1109/T-AIEE.1929.5055275. ISBN 0096-3860 VO - 48 pp. 716–727.

[148] R. H. Park, "Two-reaction theory of synchronous machines- Part II," in *Electrical Engineering*, vol. 52, no. 1, 1933. doi: 10.1109/EE.1933.6430566. ISBN 0095-9197 VO - 52 pp. 44–45.

[149] S. Chapman, *Electric Machinery Fundamentals*, 4th ed. New York City: McGraw-Hill Higher Education, 2005. ISBN 978-0072465235

[150] N. Mohan, *Advanced Electric Drives: Analysis, Control, and Modeling Using MATLAB / Simulink*. New Jersey: Wiley, 2014. ISBN 978-1-118-48548-4

[151] B. K. Bose, *Modern Power Electronics and AC Drives*. London: Prentice Hall PTR, 2002. ISBN 978-0130167439

[152] C. Szabo, I. I. Incze, and M. Imecs, "Voltage-Hertz Control of the Synchronous Machine with Variable Excitation," in *Automation, Quality and Testing, Robotics, 2006 IEEE International Conference on*, 2006. doi: 10.1109/AQTR.2006.254546

[153] V. B. Koreboina, S. J. Magajikondi, and A. B. Raju, "Modeling, simulation and PC based implementation of a closed loop speed control of VSI fed induction motor drive," in *Power Electronics (IICPE), 2010 India International Conference on*, 2011. doi: 10.1109/IICPE.2011.5728065

[154] C. Versèle, O. Deblecker, and J. Lobry, "Implementation of Induction Motor Drive Control Schemes in MATLAB/Simulink/dSPACE Environment for Educational Purpose," in *MATLAB for Engineers - Applications in Control, Electrical Engineering, IT and Robotics*, K. Perutka, Ed. InTech, 2011, ch. Chapter 15. ISBN 978-953-307-914-1. doi: 10.5772/21142

[155] B. Wu, *High-Power Converters and AC Drives*. New York City: Wiley, 2006. ISBN 978-0-471-73171-9

[156] C. W. Vigild, A. M. R. Chevalier, and E. Hendricks, "Avoiding Signal Aliasing in Event Based Engine Control," 2000, SAE Technical Paper: 2000-01-0268. doi: 10.4271/2000-01-0268

[157] L. A. Zadeh, "On the Identification Problem," *Circuit Theory, IRE Transactions on*, vol. 3, no. 4, pp. 277–281, 1956. doi: 10.1109/TCT.1956.1086328

[158] L. Ljung, "Perspectives on system identification," *Annual Reviews in Control*, vol. 34, no. 1, pp. 1–12, Apr. 2010. doi: http://dx.doi.org/10.1016/j.arcontrol.2009.12.001

[159] R. Isermann and M. Münchhof, *Identification of Dynamic Systems: An Introduction with Applications*. Berlin Heidelberg: Springer-Verlag, 2010. ISBN 978-3-540-78878-2. doi: 10.1007/978-3-540-78879-9

[160] L. Ljung, *System Identification: Theory for the User*. New Jersey: Pearson Education, 1998. ISBN 978-0136566953

[161] O. Nelles, *Nonlinear System Identification: From Classical Approaches to Neural Networks and Fuzzy Models*. Berlin Heidelberg: Springer-Verlag, 2001. ISBN 978-3-540-67369-9. doi: 10.1007/978-3-662-04323-3

[162] K. J. Åström and P. Eykhoff, "System identification - A survey," *Automatica*, vol. 7, no. 2, pp. 123–162, Mar. 1971. doi: http://dx.doi.org/10.1016/0005-1098(71)90059-8

[163] P. H. Kvam and B. Vidakovic, *Nonparametric Statistics with Applications to Science and Engineering*. New York City: Wiley, 2007. ISBN 978-0-470-08147-1

[164] K. J. Keesman, *System Identification: An Introduction*. Berlin Heidelberg: Springer-Verlag, 2011. ISBN 978-0-85729-521-7. doi: 10.1007/978-0-85729-522-4

[165] Y. Huang, X. Chen, and W. B. Wu, "Recursive Nonparametric Estimation for Time Series," vol. 60, no. 2, pp. 1301–1312, 2014. doi: 10.1109/TIT.2013.2292813

[166] L. Ljung and T. Söderström, *Theory and Practice of Recursive Identification*. Massachusetts: MIT Press, 1983. ISBN 978-0262120951

[167] F. Cucker and S. Smale, "On the mathematical foundations of learning," *Bull. Amer. Math. Soc. 39 (2002), 1-49*, 2002. doi: http://dx.doi.org/10.1090/S0273-0979-01-00923-5

[168] L. Pronzato and A. Pázman, *Design of Experiments in Nonlinear Models: Asymptotic Normality, Optimality Criteria and Small-Sample Properties*. Berlin Heidelberg: Springer-Verlag, 2013. ISBN 978-1-4614-6362-7. doi: 10.1007/978-1-4614-6363-4

[169] R. Bellman and K. J. Åström, "On structural identifiability," *Mathematical Biosciences*, vol. 7, no. 3âĂŞ4, pp. 329–339, Apr. 1970. doi: http://dx.doi.org/10.1016/0025-5564(70)90132-X

[170] K. Glover and J. C. Willems, "Parametrizations of linear dynamical systems: Canonical forms and identifiability," *Automatic Control, IEEE Transactions on*, vol. 19, no. 6, pp. 640–646, 1974. doi: 10.1109/TAC.1974.1100711

[171] E. Walter, "Identifiability of State Space Models with applications to transformation systems." Berlin Heidelberg: Springer-Verlag, 1982. ISBN 978-3-540-11590-8

[172] E. Walter, K. Godfrey, and J. DiStefano, *Identifiability of Parametric Models*. Oxford: Pergamon, 1987. ISBN 978-0-08-034929-9

[173] O. Van Doren, Jorn F.M.; Douma, Sippe Geert; Van den Hof, Paul M.J.; Jansen, Jan Dirk; Bosgra, "Identifiability: From Qualitative Analysis to Model Structure Approximation," in *15th IFAC Symposium on System Identification*. IFAC, 2009. doi: 10.3182/20090706-3-FR-2004.00110

[174] A. Raue, J. Karlsson, M. P. Saccomani, M. Jirstrand, and J. Timmer, "Comparison of approaches for parameter identifiability analysis of biological systems," *Bioinformatics*, pp. 1–9, Jan. 2014. doi: 10.1093/bioinformatics/btu006

[175] O. T. Chis, J. R. Banga, and E. Balsa-Canto, "Structural Identifiability of Systems Biology Models: A Critical Comparison of Methods," *PLoS ONE*, vol. 6, no. 11, p. e27755, Nov. 2011. doi: 10.1371/journal.pone.0027755

[176] S. Srinath and R. Gunawan, "Parameter identifiability of power-law biochemical system models," *Journal of Biotechnology*, vol. 149, no. 3, pp. 132–140, Sep. 2010. doi: http://dx.doi.org/10.1016/j.jbiotec.2010.02.019

[177] S. Berthoumieux, M. Brilli, D. Kahn, H. de Jong, and E. Cinquemani, "On the identifiability of metabolic network models," *Journal of Mathematical Biology*, vol. 67, no. 6-7, pp. 1795–1832, 2013. doi: 10.1007/s00285-012-0614-x

[178] T. O. Lamberton, N. D. Condon, J. L. Stow, and N. A. Hamilton, "On linear models and parameter identifiability in experimental biological systems," *Journal of Theoretical Biology*, vol. 358, no. 0, pp. 102–121, Oct. 2014. doi: http://dx.doi.org/10.1016/j.jtbi.2014.05.028

[179] L. Ljung and T. Glad, "On global identifiability for arbitrary model parametrizations," *Automatica*, vol. 30, no. 2, pp. 265–276, 1994. doi: http://dx.doi.org/10.1016/0005-1098(94)90029-9

[180] F. Ollivier, “Inversibility of Rational Mappings and Structural Identifiability in Automatics,” in *Proceedings of ISSAC’89*, 1989.

[181] K. Z. Yao, B. M. Shaw, B. Kou, K. B. Mcauley, and D. W. Bacon, “Modeling Ethylene/Butene Copolymerization with Multi-site Catalysts: Parameter Estimability and Experiment Design,” *Polymer Reaction Engineering*, vol. 11, no. 3, pp. 563–588, 2003. doi: 10.1081/PRE-120024426

[182] S. Vajda, H. Rabitz, E. Walter, and Y. Lecourtier, “Qualitative and Quantitative Identifiability Analysis of Nonlinear Chemical Kinetic Models,” *Chemical Engineering Communications*, vol. 83, no. 1, pp. 191–219, 1989. doi: 10.1080/00986448908940662

[183] B. Kou, K. B. McAuley, J. C. C. Hsu, and D. W. Bacon, “Mathematical Model and Parameter Estimation for Gas-Phase Ethylene/Hexene Copolymerization With Metallocene Catalyst,” *Macromolecular Materials and Engineering*, vol. 290, no. 6, pp. 537–557, 2005. doi: 10.1002/mame.200400392

[184] D. E. Thompson, K. B. McAuley, and P. J. McLellan, “Parameter Estimation in a Simplified MWD Model for HDPE Produced by a Ziegler-Natta Catalyst,” *Macromolecular Reaction Engineering*, vol. 3, no. 4, pp. 160–177, 2009. doi: 10.1002/mren.200800052

[185] S. M. Baker, C. H. Poskar, and B. H. Junker, “Unscented Kalman filter with parameter identifiability analysis for the estimation of multiple parameters in kinetic models,” *EURASIP Journal on Bioinformatics and Systems Biology*, vol. 2011, no. 1, p. 7, Oct. 2011. doi: 10.1186/1687-4153-2011-7

[186] J. V. Beck and K. J. Arnold, *Parameter Estimation in Engineering and Science*. New York City: Wiley, 1977. ISBN 978-0471061182

[187] R. A. Fisher, *The Design of Experiments*, 8th ed. Edinburgh: Oliver and Boyd, 1960. ISBN 978-0028446905

[188] P. Goos and B. Jones, *Optimal Design of Experiments: A Case Study Approach*. New York City: Wiley, 2011. ISBN 978-0-470-74461-1

[189] P. C. Young, *Recursive Estimation and Time-Series Analysis: An Introduction for the Student and Practitioner*. Berlin Heidelberg: Springer-Verlag, 2011. ISBN 978-3-642-21980-1. doi: 10.1007/978-3-642-21981-8

[190] K. J. Åström and B. Wittenmark, *Adaptive Control*, 2nd ed. Mineola: Dover Publications, 2008. ISBN 978-0486462783

[191] Y. Boutalis, *System Identification and Adaptive Control: Theory and Applications of the Neurofuzzy and Fuzzy Cognitive Network Models*. Switzerland: Springer International Publishing, 2014. ISBN 978-3-319-06363-8. doi: 10.1007/978-3-319-06364-5

[192] L. Ljung, "Recursive identification algorithms," *Circuits, Systems and Signal Processing*, vol. 21, no. 1, pp. 57–68, 2002. doi: 10.1007/BF01211651

[193] C. R. Johnson, *Lectures on Adaptive Parameter Estimation*. New Jersey: Pearson Education, 1988. ISBN 9780135281260

[194] A. Vahidi, A. Stefanopoulou, and H. Peng, "Recursive least squares with forgetting for online estimation of vehicle mass and road grade: theory and experiments," *Vehicle System Dynamics*, vol. 43, no. 1, pp. 31–55, Jan. 2005. doi: 10.1080/00423110412331290446

[195] S. Bittanti, P. Bolzern, M. Campi, and E. Coletti, "Deterministic convergence analysis of RLS estimators with different forgetting factors," in *Decision and Control, 1988., Proceedings of the 27th IEEE Conference on*, 1988. doi: 10.1109/CDC.1988.194583

[196] S. Saelid and B. Foss, "Adaptive controllers with a vector variable forgetting factor," in *Decision and Control, 1983. The 22nd IEEE Conference on*, 1983. doi: 10.1109/CDC.1983.269785

[197] N. Yoshitani and A. Hasegawa, “Model-based control of strip temperature for the heating furnace in continuous annealing,” *Control Systems Technology, IEEE Transactions on*, vol. 6, no. 2, pp. 146–156, 1998. doi: 10.1109/87.664182

[198] P. Kaminski, A. E. Bryson, and S. Schmidt, “Discrete square root filtering: A survey of current techniques,” *Automatic Control, IEEE Transactions on*, vol. 16, no. 6, pp. 727–736, 1971. doi: 10.1109/TAC.1971.1099816

[199] T. S. Soderstrom and P. G. Stoica, *System Identification*. London: Prentice Hall, 1989. ISBN 9780138812362

[200] B. Friedlander, “A recursive maximum likelihood algorithm for ARMA spectral estimation,” vol. 28, no. 4, pp. 639–646, 1982. doi: 10.1109/TIT.1982.1056531

[201] B. L. Pence, H. K. Fathy, and J. L. Stein, “Recursive maximum likelihood parameter estimation for state space systems using polynomial chaos theory,” *Automatica*, vol. 47, no. 11, pp. 2420–2424, Nov. 2011. doi: http://dx.doi.org/10.1016/j.automatica.2011.08.014

[202] P. Navrátil and J. Ivanka, “Recursive Identification Algorithms,” in *17th International Conference on Process Control*, Strbske Pleso, Slovakia, 2009.

[203] M. S. Grewal and A. P. Andrews, *Kalman Filtering: Theory and Practice with MATLAB*, 4th ed. New York City: Wiley, 2015. ISBN 978-1-118-85121-0

[204] S. Haykin, *Kalman Filtering and Neural Networks*. New York: Wiley, 2001. ISBN 978-0-471-36998-1

[205] A. Solonen, J. Hakkarainen, A. Ilin, M. Abbas, and A. Bibov, “Estimating model error covariance matrix parameters in extended Kalman filtering,” *Nonlin. Processes Geophys.*, vol. 21, no. 5, pp. 919–927, Sep. 2014. doi: 10.5194/npg-21-919-2014

[206] T. D. Powell, “Automated Tuning of an Extended Kalman Filter Using the Downhill Simplex Algorithm,” *Journal of Guidance, Control, and Dynamics*, vol. 25, no. 5, pp. 901–908, Sep. 2002. doi: 10.2514/2.4983

[207] S. Julier, J. Uhlmann, and H. F. Durrant-Whyte, “A new method for the nonlinear transformation of means and covariances in filters and estimators,” *Automatic Control, IEEE Transactions on*, vol. 45, no. 3, pp. 477–482, mar 2000. doi: 10.1109/9.847726

[208] K. Halvorsen, T. Söderström, V. Stokes, and H. k. Lanshammar, “Using an Extended Kalman Filter for Rigid Body Pose Estimation,” *Journal of Biomechanical Engineering*, vol. 127, no. 3, pp. 475–483, Dec. 2004.

[209] A. Farina, B. Ristic, and D. Benvenuti, “Tracking a ballistic target: comparison of several nonlinear filters,” *Aerospace and Electronic Systems, IEEE Transactions on*, vol. 38, no. 3, pp. 854–867, 2002. doi: 10.1109/TAES.2002.1039404

[210] L. Ljung, “Asymptotic behavior of the extended Kalman filter as a parameter estimator for linear systems,” *Automatic Control, IEEE Transactions on*, vol. 24, no. 1, pp. 36–50, 1979. doi: 10.1109/TAC.1979.1101943

[211] Y. Wu, D. Hu, M. Wu, and X. Hu, “Unscented Kalman filtering for additive noise case: augmented vs. non-augmented,” in *American Control Conference*, 2005. doi: 10.1109/ACC.2005.1470611

[212] R. Van Der Merwe and E. A. Wan, “The square-root unscented Kalman filter for state and parameter-estimation,” in *Acoustics, Speech, and Signal Processing, 2001. Proceedings. (ICASSP ’01). 2001 IEEE International Conference on*, 2001. doi: 10.1109/ICASSP.2001.940586

[213] V. Yu, A. Headley, and D. Chen, “A Constrained Extended Kalman Filter for State-of-Charge Estimation of a Vanadium Redox Flow Battery With

Crossover Effects," *Journal of Dynamic Systems, Measurement, and Control*, vol. 136, no. 4, p. 41013, Apr. 2014.

[214] A. Martyr and M. A. Plint, *Engine Testing: Theory and Practice*, 3rd ed. Oxford: Butterworth-Heinemann, 2007. ISBN 9780080524726

[215] R. D. Atkins, *An Introduction to Engine Testing and Development*. Troy, MI: SAE International, 2009. ISBN 9780768020991

[216] Z. Kulesza, J. Sawicki, and A. L. Gyekenyesi, "Robust fault detection filter using linear matrix inequalities' approach for shaft crack diagnosis," *Journal of Vibration and Control*, pp. 1421–1440, May 2012. doi: 10.1177/1077546312447838

[217] R. Isermann, *Fault-Diagnosis Systems: An Introduction from Fault Detection to Fault Tolerance*. Berlin Heidelberg: Springer-Verlag, 2006. ISBN 978-3-540-24112-6. doi: 10.1007/3-540-30368-5

[218] J. Gertler, *Fault Detection and Diagnosis in Engineering Systems*. Abingdon: Taylor & Francis, 1998. ISBN 9780824794279

[219] S. Ding, *Model-Based Fault Diagnosis Techniques: Design Schemes, Algorithms and Tools*. Berlin Heidelberg: Springer-Verlag, 2012. ISBN 978-1-4471-4798-5. doi: 10.1007/978-1-4471-4799-2

[220] A. A. Tlaisi, A. Akinturk, A. S. Swamidas, and Mahmoud R. Haddara, "Crack Detection in Shaft Using Lateral and Torsional Vibration Measurements and Analyses," *Mechanical Engineering Research*, vol. 2, no. 2, p. 52, 2012. doi: 10.5539/mer.v2n2p52

[221] J. Xiang, Y. Zhong, X. Chen, and Z. He, "Crack detection in a shaft by combination of wavelet-based elements and genetic algorithm," *International Journal of Solids and Structures*, vol. 45, no. 17, pp. 4782–4795, Aug. 2008. doi: http://dx.doi.org/10.1016/j.ijsolstr.2008.04.014

[222] A. Muszynska, *Rotordynamics*. Abingdon: Taylor & Francis, 2005. ISBN 9781420027792

[223] A. Chaubey, H. Chelladurai, and S. S. Lamba, "Condition monitoring of rotating shaft using virtual instrumentation," in *5th International and 26th All India Manufacturing Technology, Design and Research Conference (AIMTDR 2014)*, IIT Guwahati, Assam, India, 2014.

[224] A. S. Sekhar, "Crack identification in a rotor system: a model-based approach," *Journal of Sound and Vibration*, vol. 270, no. 4âĂŞ5, pp. 887–902, Mar. 2004. doi: http://dx.doi.org/10.1016/S0022-460X(03)00637-0

[225] S. Seibold and K. Weinert, "A time domain method for the localization of cracks in rotors," *Journal of Sound and Vibration*, vol. 195, no. 1, pp. 57–73, Aug. 1996. doi: http://dx.doi.org/10.1006/jsvi.1996.0403

[226] B. S. Andersson, "Paper XVIII (iii) Company Perspectives in Vehicle Tribology - Volvo," in *Vehicle Tribology*, C. M. T. D. Dowson and M. G. B. T. T. Series, Eds. Elsevier, 1991, vol. Volume 18, pp. 503–506. ISBN 0167-8922. doi: http://dx.doi.org/10.1016/S0167-8922(08)70168-8

[227] E. Ciulli, "A Review of Internal Combustion Engine Losses Part 2: Studies for Global Evaluations," *Proceedings of the Institution of Mechanical Engineers, Part D: Journal of Automobile Engineering*, vol. 207, no. 3, pp. 229–240, Jul. 1993. doi: 10.1243/PIME_PROC_1993_207_184_02

[228] C. Sethu, M. E. Leustek, S. V. Bohac, Z. S. Filipi, and D. N. Assanis, "An Investigation in Measuring Crank Angle Resolved In-Cylinder Engine Friction Using Instantaneous IMEP Method," 2007, SAE Technical Paper: 2007-01-3989. doi: 10.4271/2007-01-3989

[229] M. Gore, M. Theaker, S. Howell-Smith, H. Rahnejat, and P. D. King, "Direct measurement of piston friction of internal-combustion engines using the floating-liner principle," *Proceedings of the Institution of Mechanical*

Engineers, Part D: Journal of Automobile Engineering, vol. 228, no. 3, pp. 344–354, Feb. 2014. doi: 10.1177/0954407013511795

[230] A. A. Stotsky, "Data-driven algorithms for engine friction estimation," *Proceedings of the Institution of Mechanical Engineers, Part D: Journal of Automobile Engineering*, vol. 221, no. 7, pp. 901–909, Jul. 2007. doi: 10.1243/09544070JAUTO230

[231] Y. Wakuri, M. Soejima, Y. Ejima, T. Hamatake, and E. Al, "Studies on Friction Characteristics of Reciprocating Engines," 1995, SAE Technical Paper: 952471. doi: 10.4271/952471

[232] A. A. Stotsky, "Method for estimating engine friction torque," May 2006, US Patent: US7054738.

[233] P. J. Shayler, D. K. W. Leong, and M. Murphy, "Contributions to engine friction during cold, low speed running and the dependence on oil viscosity," 2014, SAE Technical Paper: 2005-01-1654. doi: 10.4271/2005-01-1654

[234] S. Kounias and M. Chalikias, "Estimability of parameters in a linear model and related characterizations," *Statistics and Probability Letters*, vol. 78, no. 15, pp. 2437–2439, 2008. doi: 10.1016/j.spl.2008.02.019

[235] S. Larsson and I. Andersson, "Self-optimising control of an SI-engine using a torque sensor," *Control Engineering Practice*, vol. 16, no. 5, pp. 505–514, May 2008. doi: 10.1016/j.conengprac.2007.05.009

[236] M. Thor, B. Egardt, T. McKelvey, and I. Andersson, "Closed-loop diesel engine combustion phasing control based on crankshaft torque measurements," *Control Engineering Practice*, vol. 33, pp. 115–124, Dec. 2014. doi: 10.1016/j.conengprac.2014.08.011

[237] K. A. Gul and D. E. Adams, "Modeling and Torsional Vibration Analysis of Engine Cold-Test Stand Drivelines," in *ASME 2007 International Design*

Engineering Technical Conferences and Computers and Information in Engineering Conference, Jan. 2007. doi: 10.1115/DETC2007-35647. ISBN 0-7918-4802-7

[238] K. A. Gul and D. E. Adams, "Reducing Torsional Vibration in an Engine Cold-Test Cell for Improved Structural Reliability and Engine Assembly Defect Diagnostics," in *ASME 2009 Dynamic Systems and Control Conference*, Jan. 2009. doi: 10.1115/DSCC2009-2731

[239] K. A. Gul and D. E. Adams, "Modeling and Simulation of a Cold-Engine Test Stand Driveline With Experimental Comparisons," in *ASME 2006 International Mechanical Engineering Congress and Exposition*, Jan. 2006. doi: 10.1115/IMECE2006-15313

[240] K. A. Gul and D. E. Adams, "Modeling and Excitation Torque Estimation of an Engine Cold-Test Stand for Evaluating Driveline Design and Fault Diagnostics," in *ASME 2007 International Mechanical Engineering Congress and Exposition*, Jan. 2007. doi: 10.1115/IMECE2007-43255

[241] K. A. Gul, N. Bilal, and D. E. Adams, "Modeling and Torsional Vibration Analysis of an Engine Cold-Test Cell for Production Fault Diagnostics," in *ASME 2009 International Design Engineering Technical Conferences and Computers and Information in Engineering Conference*, Jan. 2009. doi: 10.1115/DETC2009-87020

[242] L. Wei, C. Xi, L. Jie, and X. Wen, "Modeling and simulation of system dynamics for cold test," in *Proceedings - 2008 2nd International Symposium on Intelligent Information Technology Application, IITA 2008*, 2008. doi: 10.1109/IITA.2008.507

[243] L. Wei, Z. Kun, X. Wen, and C. Xi, "The fault simulation of diesel engine in cold test," in *Proceedings - 2010 IEEE International Conference on Intelligent Computing and Intelligent Systems, ICIS 2010*, 2010. doi: 10.1109/ICICISYS.2010.5658468

[244] Y.-Y. Wang, V. Krishnaswami, and G. Rizzoni, "Event-based estimation of indicated torque for IC engines using sliding-mode observers," *Control Engineering Practice*, vol. 5, no. 8, pp. 1123–1129, Aug. 1997. doi: 10.1016/S0967-0661(97)00105-6

[245] Y. H. Zweiri, J. F. Whidbourne, and L. D. Seneviratne, "Numerical inversion of the dynamic model of a single-cylinder diesel engine," *Communications in Numerical Methods in Engineering*, vol. 16, no. 7, pp. 505–517, 2000. doi: 10.1002/1099-0887(200007)16:7<505::AID-CNM353>3.0.CO;2-K

[246] I. Souflas, A. Pezouvanis, B. Mason, and K. M. Ebrahimi, "Dynamic Modeling of a Transient Engine Test Cell for Cold Engine Testing Applications," in *ASME 2014 International Mechanical Engineering Congress and Exposition*, Nov. 2014. doi: 10.1115/IMECE2014-36286

Appendices

Appendix A

Publications

The novelty and originality of this work is supported with one journal and four conference peer reviewed publications. In this part of the thesis, the titles, abstracts and corresponding citation are submitted.

Parts of the publications were incorporated within the thesis. In particular, material from Paper 1 (Appendix A.1) was included in Chapter 8, Paper 2 (Appendix A.2) discusses the work that was presented in Chapter 6, whilst Papers 3 (Appendix A.3), 4 (Appendix A.4) and 5 (Appendix A.5) came out of Chapter 3.

A.1 Paper 1

Nonlinear Recursive Estimation with Estimability Analysis for Physical and Semi-Physical Engine Model Parameters

Abstract

A methodology for nonlinear recursive parameter estimation with parameter estimability analysis for physical and semi-physical engine models is presented. Orthogonal estimability analysis based on parameter sensitivity is employed with the purpose of evaluating a rank of estimable parameters given multiple sets of observation data that were acquired from a transient engine testing facility. The qualitative information gained from the estimability analysis is then used for estimating the estimable parameters by using two well-known nonlinear adaptive estimation algorithms known as Extended and Unscented Kalman Filters. The findings of this work contribute on understanding the real-world challenges which are involved in the effective implementation of system identification techniques suitable for online nonlinear estimation of parameters with physical interpretation.

Citation

I. Souflas, A. Pezouvanis, K. M. Ebrahimi, “Nonlinear Recursive Estimation with Estimability Analysis for Physical and Semi-Physical Engine Model Parameters", *ASME Journal of Dynanic Systems, Measurement, and Control*. Paper No: DS-15-1062. 2015.

A.2 Paper 2

Coupling Shaft Condition Monitoring System Using Recursive Identification Algorithms

Abstract

An online condition monitoring system for coupling shafts that can be found generally in testing facilities of rotating systems is proposed. For the application of the present framework the measurement of physical quantities such as shaft angular position, velocity and torque is required. Based on the measurements coupling shaftâĂŹs physical parameters are identified using three different recursive identification algorithms known as Recursive Least Squares with forgetting factor, Linear Kalman Filter and Discrete Square Root Filtering in covariance form. The information gained form the recursive identification of the parameters is then further used for detection of possible system faults and malfunctions. The functionality of the monitoring system is demonstrated with a particular application on the fault detection of an engine dynamometer coupling shaft. Both simulated results based on an overall system model and experimental results using an advanced transient engine testing facility are presented showing the capabilities of the proposed online condition monitoring system as well as the performance of the various recursive identification algorithms which were applied.

Citation

I. Souflas, A. Pezouvanis, K. M. Ebrahimi, “Coupling Shaft Condition Monitoring System Using Recursive Identification Algorithms", *24th International Conference on System Engineering*. Coventry University, Coventry, UK, 8-10 September, 2015.

A.3 Paper 3

Dynamic Modelling of a Transient Engine Test Cell for Cold Engine Testing Applications

Abstract

The increasing complexity in the development and manufacturing process of internal combustion engines leads to a higher demand for more effective testing and monitoring methods. Cold engine testing becomes progressively the main End-of-Line test which is used nowadays from automotive engine manufacturers with the purpose of determining the integrity of engine assembly. The present work is focused on the development of a detailed physics-based, lumped-parameter, dynamic model of a single cylinder internal combustion engine coupled with an alternating current transient dynamometer for cold engine testing applications. The overall transient engine test cell model is described based on a two-inertia system model consisting of the engine, the dynamometer and the coupling shaft. The internal combustion engine is modelled based on First Law of Thermodynamics and Second NewtonâĂŹs Law for rotational bodies. The transient dynamometer is actually an alternating current three-phase induction motor which is modelled according to direct-quadrature axis approach, and its drive unit which is responsible for controlling the speed of the motor using indirect field orientation scheme. The engine and dynamometer are connected through a coupling shaft which is modelled as a compliant member with damping. The model is validated against experimental measurements such as engine cylinder pressure, engine excitation torque and alternating currents of the induction motor. All of the experimental measurements were recorded from an identical single cylinder transient engine test cell using a highly advanced instrumentation system. The described model serves as an ideal platform for developing innovative model-based fault detec-

tion and diagnosis techniques for cold engine testing applications. In conclusion, this is presented successfully for two simulated fault cases, a process fault and a sensor fault, proving the functionality and usefulness of the model.

Citation

I. Souflas, A. Pezouvanis, B. Mason, K. M. Ebrahimi, “Dynamic Modelling of a Transient Engine Test Cell for Cold Engine Testing Applications", *ASME 2014 International Mechanical Engineering Congress & Exposition*. Paper No: IMECE2014-36286, Montreal, Canada, 14-20 November 2014.

A.4 Paper 4

Model-Based Hybrid Electric Vehicle Fuel Consumption, CO2 Emissions and Battery SOC Estimation

Abstract

This paper discusses a simple, fast and reliable model-based estimation approach of the fuel consumption, CO2 emissions and battery SOC quantities on the basis of a classical forward facing hybrid electric vehicle model. The model was developed with the minimum number of physical and experimental parameters while its structure and formulation was kept as simple as possible and as complex as necessary. Model global inputs are the desired vehicle speed, road gradient, initial battery SOC and initial fuel level in the tank while the main global outputs are the fuel consumptions, CO2 emission and battery SOC. The validity of the model was confirmed using experimental results obtained from a hybrid electric bus which was driven into three different arbitrary routes. Additionally, the limitations of this simplified approach are highlighted so that the reader will be informed not only about the advantages but also the disadvantages of the proposed method. The model can be used for understanding how the processes and the model parameters affect the overall vehicle performance and more particularly the fuel consumption, CO2 emission and battery SOC.

Citation

I. Souflas, A. Pezouvanis, B. Mason, K. M. Ebrahimi, “Model-Based Hybrid Electric Vehicle Fuel Consumption, CO2 Emissions and Battery SOC Estimation", *2nd Biennial Conference on Powertrain Mapping and Calibration*. University of Bradford, Bradford, UK, 10-11 September 2014.

A.5 Paper 5

CO2 Emissions Management through Ignition Timing Control: Theoretical and Experimental Analysis

Abstract

Carbon dioxide is an unavoidable combustion product which is proportional to the amount of fuel burned from the engine, however, experiments found in literature have shown that the combustion quality can affect the level of CO2 emissions emitted from an internal combustion engine. The current document presents a theoretical and experimental investigation on the effect of Ignition Timing (IT) on the CO2 emissions of a homogeneous charge Gasoline Direct Injection (GDI) engine. A thermodynamic-based two-zone engine combustion model is formulated and is used for the model-based prediction of the CO2 emissions. Simulation and experimental results are compared with the purpose of identifying the pattern which CO2 behaves when IT is changing. The results show that while maintaining all engine actuators fixed (particularly fuelling parameters) and varying only IT, the level of CO2 emissions is affected. More specifically, it is observed that CO2 emissions are increased when IT is retarded up to TDC.

Citation

I. Souflas, A. Pezouvanis, B. Mason, K. M. Ebrahimi, “CO2 Emissions Management through Ignition Timing Control: Theoretical and Experimental Analysis", *Controls, Measurements & Calibration Congress*. FEM-UNICAMP, São Paulo, Brazil, 13-14 March 2014.

Appendix B

MATLAB Codes & Simulink Block Diagrams

Some key MATLAB codes and Simulink block diagrams are presented here to support the discussions in the main part of the thesis.

More specifically in Appendix B.1 are provide the script for the model parameters and initial conditions, a function for the calculation of the thermodynamic properties of air, and figures with the major Simulink block diagram of the test cell dynamic model presented in Chapter 3. In Appendix B.2 is submitted the M-code for the evaluation of the rank of the friction parameters as discussed in Chapter 7. The M-code for the friction identifiability analysis that was presented in Chapter 7 can be found in Appendix B.3. And, the programme for evaluating the identifiability of the cyclic engine torque model parameters as described in Chapter 8 is provided in Appendix B.4.

The author is currently a *MathWorks Certified MATLAB Associate*.

B.1 Powertrain Dynamic Model MATLAB & Simulink

M-code: Model Parameters and Initial Conditions

```
% Model Parameters & Initial Conditions
% Created by I. Souflas - CERTIFIED MATLAB ASSOCIATE
% PhD Thesis - DECEMBER 2014
clear all;clc;
%% Solver parameters
% Crank angle step [deg;rad]
da=0.5;df=da*pi/180;
% Fixed solver parameters
N=1500; % Engine speed [RPM]
omega=(N*pi)/30;dt=df/omega; % Time step [s]
% Variable solver parameters
N_min=500;omega_min=(N_min*pi)/30;dt_max=df/omega_min;  % Max time step [s]
N_max=10000;omega_max=(N_max*pi)/30;dt_min=df/omega_max;% Min time step [s]
%% Coupling shaft parameters
% Default damper
B=0.95;                  % Damping coefficient [Nms/rad]
K=1252;                  % Stiffness coefficient [Nm/rad]
%% Dynamometer parameters
Rs=0.14;                % Stator resistance [Ohm]
Rr=0.15;                % Rotor resistance [Ohm]
Xls=0.31;               % Stator reactance [Ohm]
Xlr=0.49;               % Rotor reactance [Ohm]
Xm=13.1;                % Matual reactance [Ohm]
p=4;                    % Motor poles [-]
Jdy=0.13;               % Dynamometer inertia [kgm2]
% Calculation of Initial Conditions
%--------------------------------------------------------------------------
% Steady State Operating Condition
f=50; VLLrms= 400; s=0.023;% phase-a voltage is at its positive peak at t=0
Wsyn=2*pi*f;              % synchronous speed in electrical rad/s
Wm=(1-s)*Wsyn;            % rotor speed in electrical rad/s
% Phasor Calculations
Va = VLLrms * sqrt(2)/ sqrt(3);           % Va phasor
% Space Vectors at time t=0 with stator a-axis as the reference
Vs_0 = (3/2) * Va;                        % Vs(0) space vector
Theta_Vs_0 = angle(Vs_0);                 % angle of Vs(0) space vector
% We will assume that at t=0, d-axis is aligned to the stator a-axis.
% Therefore, Theta_da_0=0
Theta_da_0 = 0;
Vsd_0 = sqrt(2/3) * abs(Vs_0) * cos(Theta_Vs_0 - Theta_da_0);
Vsq_0 = sqrt(2/3) * abs(Vs_0) * sin(Theta_Vs_0 - Theta_da_0);
% Calculation of machine inductances
Ls = (Xls + Xm) / (2*pi*f);
Lm = Xm / (2*pi*f);
Lr = (Xlr + Xm) / (2*pi*f);
tau_r=Lr/Rr;
% Calculations of dq-winding currents
A = [Rs        -Wsyn*Ls       0         -Wsyn*Lm  ;...
     Wsyn*Ls    Rs            Wsyn*Lm    0        ;...
     0         -s*Wsyn*Lm     Rr        -s*Wsyn*Lr;...
     s*Wsyn*Lm  0             s*Wsyn*Lr  Rr];
Ainv = inv(A);
V_dq_0=[Vsd_0; Vsq_0; 0; 0];
I_dq_0=Ainv*V_dq_0; %#ok
Isd_0=I_dq_0(1);
Isq_0=I_dq_0(2);
Ird_0=I_dq_0(3);
Irq_0=I_dq_0(4);
% Inductance matrix M
M = [Ls 0  Lm 0 ;...
     0  Ls 0  Lm;...
     Lm 0  Lr 0 ;...
```

```
     0  Lm 0  Lr];
% dq winding Flux Linkages with the d-axis aligned with the stator a-axis
fl_dq_0 = M * [Isd_0; Isq_0; Ird_0; Irq_0];
fl_sd_0 = fl_dq_0(1);
fl_sq_0 = fl_dq_0(2);
fl_rd_0 = fl_dq_0(3);
fl_rq_0 = fl_dq_0(4);
[thetar, fl_r_dq_0]=cart2pol(fl_rd_0, fl_rq_0);
[thetas, fl_s_dq_0]=cart2pol(fl_sd_0, fl_sq_0);
[theta_Is_dq, Is_dq_0]=cart2pol(Isd_0, Isq_0);
[theta_Vs_dq, Vs_dq_0]=cart2pol(Vsd_0, Vsq_0);
% d-axis is now aligned with the rotor flux which
% results in the following new values:
fl_rd_0=fl_r_dq_0;
[fl_sd_0, fl_sq_0]=pol2cart(thetas-thetar, fl_s_dq_0);
[Isd_0, Isq_0]=pol2cart(theta_Is_dq-thetar, Is_dq_0);
[Vsd_0, Vsq_0]=pol2cart(theta_Vs_dq-thetar, Vs_dq_0);
% Controllers Settings
%--------------------------------------------------------------------------
% PI in flux loop
kpf=500;
kif=1000;
% PI in speed loop
ki=24.1;
kp=1.66;
% PI in current loop
kii=108.2;
kpi=0.47;
%% Engine parameters
% Intake Manifold Geometry - Characteristics
%--------------------------------------------------------------------------
Dth=0.025;            % throttle diameter [m]
Cd_th=0.65;           % throttle discharge coefficient [m]
Vima=0.00045;         % intake manifold volume [m3]
% Engine Geometry - Characteristics
%--------------------------------------------------------------------------
% Cylinder - Crankshaft mechanishm
b=0.055;              % cylinder bore [m]
S=0.0515;             % cylinder stroke [m]
L=0.088;              % connecting rod length [m]
a=0.0257;             % crankshaft arm [m]
Mrec=0.80;            % reciprocating mass [kg]
r=9.5;                % compression ratio [-]
d = 0;                % Piston pin offset [m]
% Valvetrain
%--------------------------------------------------------------------------
% Timing
IVO=320;              % inlet valve closing [deg]
IVC=616;              % inlet valve closing [deg]
EVO=102;              % exhaust valve opening [deg]
EVC=399;              % exhaust valve closing [deg]
% Inlet Valve
IV_lift = load('valveIn.mat');
IV_D=27.3;            % inlet valve diameter [mm]
IV_Di=25.3;           % inlet valve inner diameter [mm]
IV_SA=45;             % inlet valve seat angle [deg]
Cd_iv=0.65;           % inlet valve discharge coefficient [-]
% Exhaust Valve
EV_lift = load('valveIn.mat');
EV_D=23.3;            % exhaust valve diameter [mm]
EV_Di=20.3;           % exhaust valve inner diameter [mm]
EV_SA=45;             % exhaust valve seat angle [deg]
Cd_ev=0.65;           % exhaust valve discharge coefficient [-]
%--------------------------------------------------------------------------
% Initial Conditions - Characteristics
%--------------------------------------------------------------------------
% Atmospheric Conditons
```

```
Patm=100100;           % pressure [pa]
Tatm=293;              % temperature [K]
% Intake Maniflod Conditions
Pima=Patm;                          % pressure [pa]
Tima=Tatm;                          % temperature [K]
Rima=288;                           % universal gas constant (air)[J/kgK]
mima=((Pima*Vima)/(Rima*Tima));     % mass[kg]
% Cylinder Initial Conditions (TDC)
Pcyl=Patm*2;           % pressure [pa]
Tcyl=Tatm*2;           % temperature [K]
R=288;                 % universal gas constant (air)[J/kgK]
mcyl=((Pcyl*(((pi/4)*(b^2)*S)+(pi/4)*(b^2)*(S/(r-1))))/...
    (R*Tcyl));         % mass[kg]
% Exhaust Manifold Conditons
Pema=Patm;             % pressure [pa]
Tema=Tatm;             % temperature [K]
% Cylinder Wall Temperature
Tw=293;                % temperature [K]
% Oil Temperature
T_oil = 90; % temperature [C]
Tref = 90;  % temperature [C]
```

M-code: Thermodynamic Properties of Air

```
function [k, R, cp, cv, x]= Thermochemistry(T)
% Thermodynamic properties of pure air
% Created by I. Souflas - CERTIFIED MATLAB ASSOCIATE
% PhD Thesis - DECEMBER 2012
% References:
% -------------------------------------------------------------------------
% [1] S. Gordon and B. McBride, "Computer Program for Calculation of
%     Complex Chemical Equilibrium Compositions, Rocket Performance,
%     Incident and Refected Shocks, and Chapman-Jouguet Detonations",
%     NASA, Tech.Rep., 1976.
%% Thermodynamic properties
% Air data
% ********
%--------------------------------------------------------------------------
% 1. 300>=T<=1000K
Alo=[0.36255985E+01 -0.18782184E-02 0.70554544E-05 -0.67635137E-08 ...
0.21555993E-11 -0.10475226E+04 0.43052778E+01;   % O2
0.36748261E+01 -0.12081500E-02 0.23240102E-05 -0.63217559E-09 ...
-0.22577253E-12 -0.10611588E+04 0.23580424E+01]; % N2
% 2. 1000<T<5000K
Ahi=[ 0.36219535E+01 0.73618264E-03 -0.19652228E-06 0.36201558E-10 ...
-0.28945627E-14 -0.12019825E+04 0.36150960E+01;  % O2
0.28963194E+01 0.15154866E-02 -0.57235277E-06 0.99807393E-10 ...
-0.65223555E-14 -0.90586184E+03 0.61615148E+01]; % N2
%--------------------------------------------------------------------------
% INTAKE MANIFOLD THERMODYNAMIC PROPERTIES - COMPOSITION
% Chemistry-Mixture Composition (Air)
% ***********************************
%--------------------------------------------------------------------------
% mole
n_o2=1;                  % kmoles of oxygen
n_n2=79/21;              % kmoles of nitrogen
% Molar mass Kg/Kmol
M=[31.999; 28.013];  % [O2; N2]
% mass
m_o2=n_o2*M(1);          % kgrams of oxygen
m_n2=n_n2*M(2);          % kgrams of nitrogen
x_o2=m_o2/(m_o2+m_n2);   % mass fraction of oxygen for 1 kmol of oxygen
```

```
x_n2=m_n2/(m_o2+m_n2);    % mass fraction of nitrogen for 1 kmol of oxygen
x=[x_o2;x_n2]; % mixture composition (mass fraction)
%--------------------------------------------------------------------------
% Thermodynamic properties
% ************************
%--------------------------------------------------------------------------
% determine proper array between Alo & Ahi
Aair=zeros(1);if T<=1000;Aair=Alo;elseif T>1000;Aair=Ahi;end;
% Gas constant
Ru=8314.34;  % Universal gas constant J/kmolK
Ri=Ru./M;     % Gas constant of each individual
             % component [O2; N2] J/kmolK
% Calculation of cp, cv of each individual chemical component
% Specific heats
Tcp=zeros(1); %#ok
Tcp=[1 T T^2 T^3 T^4 0 0];% Temperature array
% at constant pressure cp J/kgK
cp_o2_m=sum(Tcp.*Aair(1,:)*Ri(1)); % O2
cp_n2_m=sum(Tcp.*Aair(2,:)*Ri(2)); % N2
% at constant volume cv J/kgK
cv_o2_m=cp_o2_m-Ri(1);                    % O2
cv_n2_m=cp_n2_m-Ri(2);                    % N2

% Calculation of cp, cv for air
% Specific heats
cp=(cp_o2_m*x_o2)+(cp_n2_m*x_n2); % @ constant pressure J/kgK
cv=(cv_o2_m*x_o2)+(cv_n2_m*x_n2); % @ constant volume J/kgK
k=cp/cv;              % @ ratio -
R=cp-cv;              % gas constant J/kgK
end
```

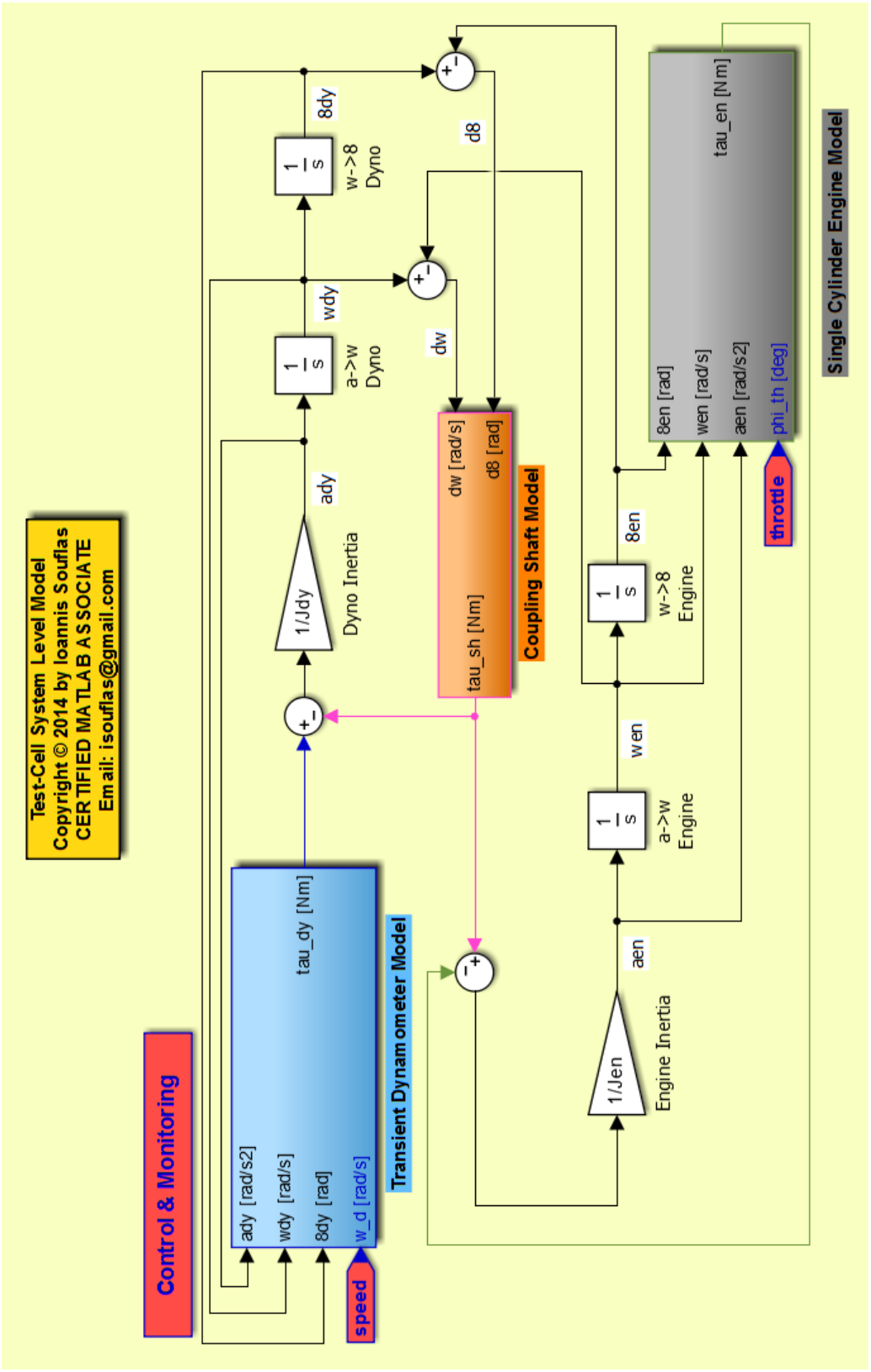

Figure B.1: Top level structure of the transient engine test cell model, Simulink block diagram.

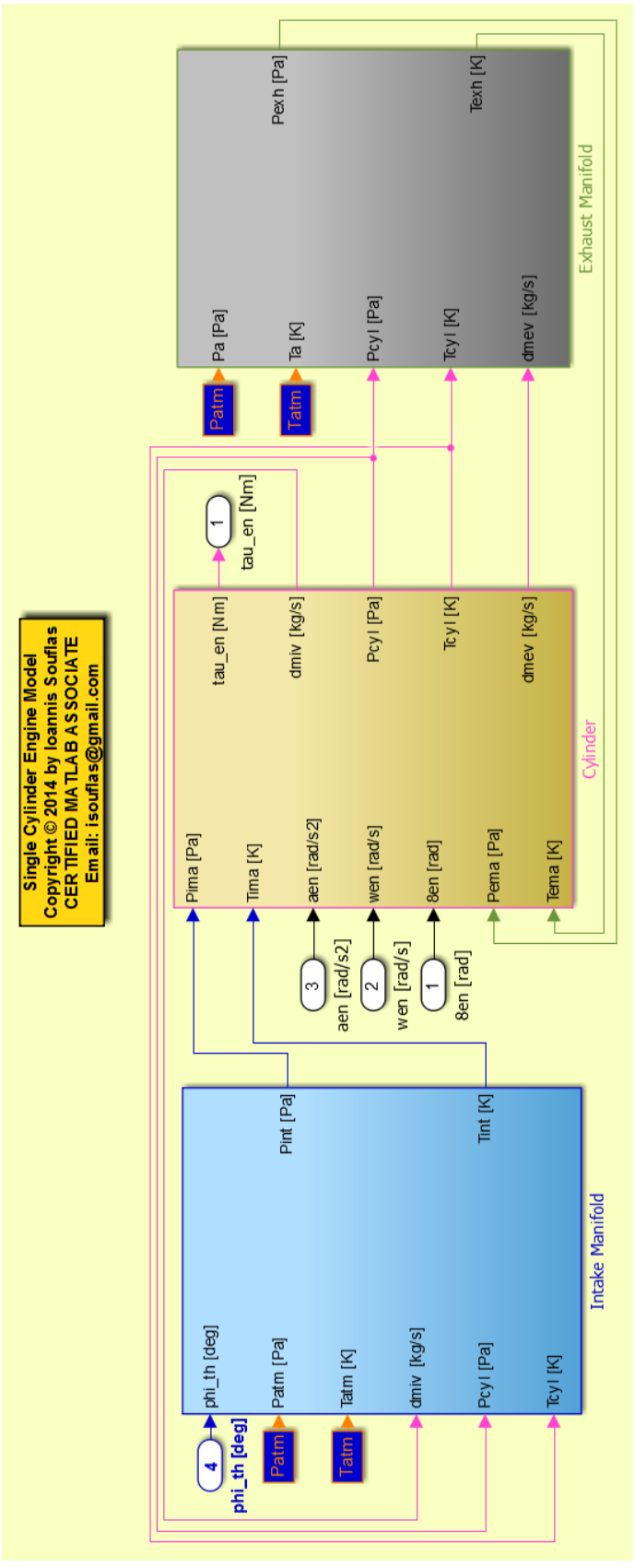

Figure B.2: Single cylinder engine model, Simulink block diagram.

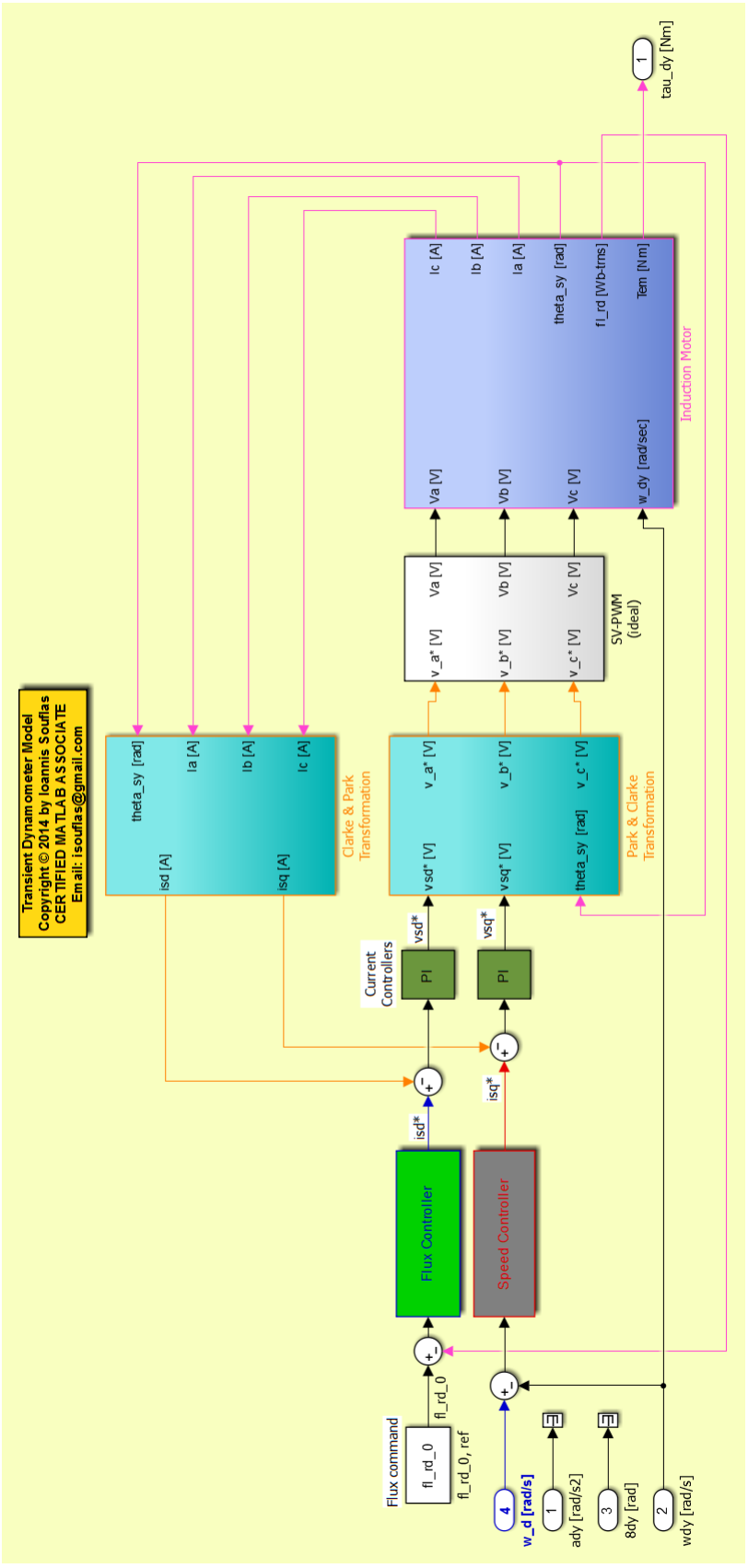

Figure B.3: Transient dynamometer model, Simulink block diagram.

B.2 Friction Parameters Ranking MATLAB Code

M-code: Engine Friction Parameters Ranking

```
% Engine Friction Parameters Ranking
% Created by I. Souflas - CERTIFIED MATLAB ASSOCIATE
% PhD Thesis - DECEMBER 2014
% References:
% D. Sandoval, J.B. Heywood, 'An Improved Friction Model for
% Spark-Ignition Engines', SAE Paper: 2003-01-0725
clear all;clc;
syms Tfri fmep N Toil Pi B S rc Di De Lv Db Lb r
%% Friction Model
% Physical Parameters
Tref=90;                % Reference oil temperature (Celsious)
OilGrade='0W40';        % Oil type
Valvetrain='SOHC_III'; % Valvetrain type
Ft_Fto=1;               % Piston ring tension factor
Cr=1;                   % Piston surface roughness
Pa=101;                 % Atmospheric pressure (kPa)
nc=1;                   % Number of cylinders
nv=2;                   % Number of valves
nb=2;                   % Number of bearings
% Constants
% Liner roughness factor
K=2.38*10^-2;
% APPENDIX A
switch OilGrade
    case '0W40';        k=0.01341;theta1=1986.4;theta2=189.7;u_uo=0.67;
    case '5W20';        k=0.04576;theta1=1224;theta2=134.1;u_uo=0.94;
    case '5W40';        k=0.15;theta1=1018.74;theta2=125.91;u_uo=0.8;
    case '10W30';       k=0.1403;theta1=869.72;theta2=104.4;u_uo=0.76;
    case '10W50A';      k=0.0352;theta1=1658.88;theta2=163.54;u_uo=0.49;
    case '10W50B';      k=0.0507;theta1=1362.4;theta2=129.8;u_uo=0.52;
    case '15W40A';      k=0.1223;theta1=933.46;theta2=103.89;u_uo=0.9;
    case '15W40B';      k=0.03435;theta1=1424.3;theta2=137.2;u_uo=0.79;
    case '20W50';       k=0.0639;theta1=1255.46;theta2=117.7;u_uo=0.84;
    case 'SAE10';       k=0.0258;theta1=1345.42;theta2=144.58;u_uo=1;
    case 'SAE30';       k=0.0246;theta1=1432.29;theta2=132.94;u_uo=1;
    case 'SAE50';       k=0.0384;theta1=1349.94;theta2=115.16;u_uo=1;
end
% Table 3
switch Valvetrain
    case 'SOHC_I';     Cff=600;Crf=0.0227;Coh=0.2;Com=42.8;
    case 'SOHC_II';    Cff=400;Crf=0.0151;Coh=0.5;Com=21.4;
    case 'SOHC_III';   Cff=200;Crf=0.0076;Coh=0.5;Com=10.7;
    case 'DOHC_I';     Cff=600;Crf=0.0227;Coh=0.2;Com=25.8;
    case 'DOHC_II';    Cff=133;Crf=0.0050;Coh=0.5;Com=10.7;
    case 'OHV';        Cff=400;Crf=0.0151;Coh=0.5;Com=32.1;
end
% Initial calculations
Sp=2*(S*10^-3)*(N/60); % mean piston speed (m/s)
ri=Di/B;               % intake valve diameter/bore
re=De/B;               % exhaust valve diameter/bore
% Lubricant viscosity
uo=k*exp(theta1/(theta2+Tref));                                  % Eq. (3)
u=k*exp(theta1/(theta2+Toil))*u_uo;                              % Eq. (4)
uscl=sqrt(u/uo);                                                 % Eq. (1)
% Crankshaft friction
cfmep=(1.22*(10^5))*(Db/((B^2)*S*nc))+(3.03*(10^-4))*uscl*...
    ((N*(Db^3)*Lb*nb)/((B^2)*S*nc))+(1.35*(10^-10))*(((Db^2)...
    *(N^2)*nb)/nc);                                              % Eq. (6)
% Reciprocating friction
rfmep=2.94*(10^2)*uscl*(Sp/B)+4.06*(10^4)*(Ft_Fto*Cr)*(1+...
    (500/N))*(1/(B^2))+3.03*(10^-4)*u_uo*((N*(Db^3)*Lb*nb)/...
    ((B^2)*S*nc));                                               % Eq. (9)
```

```
rfmep_gas=6.89*(Pi/Pa)*(0.088*uscl*rc+0.182*Ft_Fto*(rc^...
    (1.33-(2*K*Sp))));                                          % Eq. (10)
rfmep=rfmep+rfmep_gas;
% Valvetrain friction
vfmep=244*u_uo*((N*nb)/((B^2)*S*nc))+Cff*(1+(500/N))*(nv/(S*nc))...
    +Crf*((N*nv)/(S*nc))+Coh*u_uo*(((Lv^1.5)*(N^0.5)*nv)/(B*S*nc))...
    +Com*(1+(500/N))*((Lv*nv)/(S*nc));                          % Eq. (12)
% Auxiliary Losses
afmep=(8.32+1.86*(10^-3)*N+7.45*(10^-7)*(N^2));                 % Eq. (14)
% Pumping Losses
pmep_i=(Pa-Pi)+4.12*(10^-3)*((Pi/Pa)^2)*((Sp^2)/((nv^2)*...
    (ri^4)));                                                   % Eq. (15)
pmep_e=0.178*(((Pi/Pa)*Sp)^2)+4.12*(10^-3)*((Pi/Pa)^2)*...
    ((Sp^2)/((nv^2)*(re^4)));                                   % Eq. (16)
pmep=pmep_i+pmep_e;
% Total friction mean effective pressure
fmep=cfmep+rfmep+vfmep+afmep+pmep;
% Engine friction
Tfri = ((fmep*1e+3)/(2*pi))*((pi*((B/1000)^2))/4)*(r/1000);
%% Sensitivity Analysis
dB = diff(Tfri,B);          dB = matlabFunction(dB);        % 1
dS = diff(Tfri,S);          dS = matlabFunction(dS);        % 2
drc = diff(Tfri,rc);        drc = matlabFunction(drc);      % 3
dDi = diff(Tfri,Di);        dDi = matlabFunction(dDi);      % 4
dDe = diff(Tfri,De);        dDe = matlabFunction(dDe);      % 5
dLv = diff(Tfri,Lv);        dLv = matlabFunction(dLv);      % 6
dDb = diff(Tfri,Db);        dDb = matlabFunction(dDb);      % 7
dLb = diff(Tfri,Lb);        dLb = matlabFunction(dLb);      % 8
dr = diff(Tfri,r);          dr = matlabFunction(dr);        % 9
                            Tfri = matlabFunction(Tfri);
% Inputs
N=1000;             % Speed (RPM)
Pi=100;             % Intake manifold pressure (kPa)
Toil=90;            % Actual oil temperature
% Parameters
Db=52;              % Bearing diameter (mm)
B=54;               % Bore (mm)
S=51.5;             % Stoke (mm)
r = 25.7;           % Crank arm length (mm)
Lb=13;              % Bearing length (mm)
rc=12;              % Compression ratio
Lv=9;               % Maximum valve lift (mm)
Di=27;              % Intake valve diameter (mm)
De=23;              % Exhaust valve diameter (mm)
% Step 1: Scaling and calculation of sensitivity coefficients
Z(1,:) = dB(B,Db,De,Di,Lb,Lv,N,Pi,S,Toil,r,rc)*...
    (B/Tfri(B,Db,De,Di,Lb,Lv,N,Pi,S,Toil,r,rc));
Z(2,:) = dS(B,Db,De,Di,Lb,Lv,N,Pi,S,Toil,r,rc)*...
    (S/Tfri(B,Db,De,Di,Lb,Lv,N,Pi,S,Toil,r,rc));
Z(3,:) = drc(B,N,Pi,S,Toil,r,rc)*...
    (rc/Tfri(B,Db,De,Di,Lb,Lv,N,Pi,S,Toil,r,rc));
Z(4,:) = dDi(B,Di,N,Pi,S,r)*...
    (Di/Tfri(B,Db,De,Di,Lb,Lv,N,Pi,S,Toil,r,rc));
Z(5,:) = dDe(B,De,N,Pi,S,r)*...
    (De/Tfri(B,Db,De,Di,Lb,Lv,N,Pi,S,Toil,r,rc));
Z(6,:) = dLv(B,Lv,N,S,r)*...
    (Lv/Tfri(B,Db,De,Di,Lb,Lv,N,Pi,S,Toil,r,rc));
Z(7,:) = dDb(B,Db,Lb,N,S,Toil,r)*...
    (Db/Tfri(B,Db,De,Di,Lb,Lv,N,Pi,S,Toil,r,rc));
Z(8,:) = dLb(B,Db,N,S,Toil,r)*...
    (Lb/Tfri(B,Db,De,Di,Lb,Lv,N,Pi,S,Toil,r,rc));
Z(9,:) = dr(B,Db,De,Di,Lb,Lv,N,Pi,S,Toil,rc)*...
    (r/Tfri(B,Db,De,Di,Lb,Lv,N,Pi,S,Toil,r,rc));
% Step 2: Evaluation of sum of squares error
[s(1),~] = sumsqr(Z(1,:));[s(2),~] = sumsqr(Z(2,:));
[s(3),~] = sumsqr(Z(3,:));[s(4),~] = sumsqr(Z(4,:));
[s(5),~] = sumsqr(Z(5,:));[s(6),~] = sumsqr(Z(6,:));
```

```
[s(7),~] = sumsqr(Z(7,:));[s(8),~] = sumsqr(Z(8,:));
[s(9),~] = sumsqr(Z(9,:));
%% Visualise Results
[~,parameter_list] = sort(s,'descend');
ranking = {'B','S','rc','Di','De','Lv','Db','Lb','r'};
display(ranking(parameter_list))
%% Finalise Programm
clear;
```

B.3 Friction Identifiability Analysis MATLAB Code

M-code: Friction Regression Coefficients Identifiability Analysis

```
% Friction Regression Coefficients Identifiability Analysis
% Created by I. Souflas - CERTIFIED MATLAB ASSOCIATE
% PhD Thesis - DECEMBER 2014
% References:
% D. Sandoval, J.B. Heywood, 'An Improved Friction Model for
% Spark-Ignition Engines', SAE Paper: 2003-01-0725
clear all;clc;
syms T N Pi Pa Toil Tref c1 c2 c3 c4 c5 c6 c7 c8 c9 c10 c11 c12 c13...
    c14 c15 c16 c17 c18 c19 c20
%% Friction Model
% Physical Parameters
Tref=90;                % Reference oil temperature (Celsious)
OilGrade='0W40';        % Oil type
Valvetrain='SOHC_III'; % Valvetrain type
Ft_Fto=1;               % Piston ring tension factor
Cr=1;                   % Piston surface roughness
nc=1;                   % Number of cylinders
nv=2;                   % Number of valves
nb=2;                   % Number of bearings
B=54;                   % Bore (mm)
S=51.5;                 % Stoke (mm)
rc=12;                  % Compression ratio
Di=27;                  % Intake valve diameter (mm)
De=23;                  % Exhaust valve diameter (mm)
Lv=9;                   % Maximum valve lift (mm)
Db=52;                  % Bearing diameter (mm)
Lb=13;                  % Bearing length (mm)
r = 25.7;               % Crank arm length (mm)
G = (((r*1e-3)*((B*1e-3)^2))/8)*1e3;
% Constants
% Liner roughness factor
K=2.38*10^-2;
% APPENDIX A
% ----------
switch OilGrade
    case '0W40';        k=0.01341;theta1=1986.4;theta2=189.7;u_uo=0.67;
    case '5W20';        k=0.04576;theta1=1224;theta2=134.1;u_uo=0.94;
    case '5W40';        k=0.15;theta1=1018.74;theta2=125.91;u_uo=0.8;
    case '10W30';       k=0.1403;theta1=869.72;theta2=104.4;u_uo=0.76;
    case '10W50A';      k=0.0352;theta1=1658.88;theta2=163.54;u_uo=0.49;
    case '10W50B';      k=0.0507;theta1=1362.4;theta2=129.8;u_uo=0.52;
    case '15W40A';      k=0.1223;theta1=933.46;theta2=103.89;u_uo=0.9;
    case '15W40B';      k=0.03435;theta1=1424.3;theta2=137.2;u_uo=0.79;
    case '20W50';       k=0.0639;theta1=1255.46;theta2=117.7;u_uo=0.84;
    case 'SAE10';       k=0.0258;theta1=1345.42;theta2=144.58;u_uo=1;
    case 'SAE30';       k=0.0246;theta1=1432.29;theta2=132.94;u_uo=1;
    case 'SAE50';       k=0.0384;theta1=1349.94;theta2=115.16;u_uo=1;
```

```
end
% Table 3
% -------
switch Valvetrain
    case 'SOHC_I';        Cff=600;Crf=0.0227;Coh=0.2;Com=42.8;
    case 'SOHC_II';       Cff=400;Crf=0.0151;Coh=0.5;Com=21.4;
    case 'SOHC_III';      Cff=200;Crf=0.0076;Coh=0.5;Com=10.7;
    case 'DOHC_I';        Cff=600;Crf=0.0227;Coh=0.2;Com=25.8;
    case 'DOHC_II';       Cff=133;Crf=0.0050;Coh=0.5;Com=10.7;
    case 'OHV';           Cff=400;Crf=0.0151;Coh=0.5;Com=32.1;
end
% Initial calculations
Sp=2*(S*10^-3)*(N/60); % mean piston speed (m/s)
ri=Di/B;               % intake valve diameter/bore
re=De/B;               % exhaust valve diameter/bore
% Lubricant viscosity
uo=k*exp(theta1/(theta2+Tref));                                    % Eq. (3)
u=k*exp(theta1/(theta2+Toil))*u_uo;                                % Eq. (4)
uscl=sqrt(u/uo);                                                   % Eq. (1)
% Torque symbolic function
T =   (c1*(Db/((B^2)*S*nc))*G) ...
    + (c2*uscl*((N*(Db^3)*Lb*nb)/((B^2)*S*nc))*G)...
    + (c3*(((Db^2)*(N^2)*nb)/nc)*G)...
    + (c4*uscl*(Sp/B)*G)...
    + (c5*(Ft_Fto*Cr)*(1+(500/N))*(1/(B^2))*G)...
    + (c6*u_uo*((N*(Db^3)*Lb*nb)/((B^2)*S*nc))*G)...
    + (c7*(Pi/Pa)*(0.088*uscl*rc+0.182*Ft_Fto*(rc^(1.33-(2*K*Sp))))*G)...
    + (c8*G)...
    + (c9*u_uo*((N*nb)/((B^2)*S*nc))*G)...
    + (c10*(1+(500/N))*(nv/(S*nc))*G)...
    + (c11*((N*nv)/(S*nc))*G)...
    + (c12*u_uo*(((Lv^1.5)*(N^0.5)*nv)/(B*S*nc))*G)...
    + (c13*(1+(500/N))*((Lv*nv)/(S*nc))*G)...
    + (c14*G)...
    + (c15*N*G)...
    + (c16*(N^2)*G)...
    + (c17*(Pa-Pi)*G)...
    + (c18*((Pi/Pa)^2)*((Sp^2)/((nv^2)*(ri^4)))*G)...
    + (c19*(((Pi/Pa)*Sp)^2)*G)...
    + (c20*((Pi/Pa)^2)*((Sp^2)/((nv^2)*(re^4)))*G);
%% Orthogonal-based method for parameter estimability
% Use Symbolic Toolbox to find partial derivatives
dc1 = diff(T,c1); dc1 = matlabFunction(dc1);
dc2 = diff(T,c2); dc2 = matlabFunction(dc2);
dc3 = diff(T,c3); dc3 = matlabFunction(dc3);
dc4 = diff(T,c4); dc4 = matlabFunction(dc4);
dc5 = diff(T,c5); dc5 = matlabFunction(dc5);
dc6 = diff(T,c6); dc6 = matlabFunction(dc6);
dc7 = diff(T,c7); dc7 = matlabFunction(dc7);
dc8 = diff(T,c8); dc8 = matlabFunction(dc8);
dc9 = diff(T,c9); dc9 = matlabFunction(dc9);
dc10 = diff(T,c10); dc10 = matlabFunction(dc10);
dc11 = diff(T,c11); dc11 = matlabFunction(dc11);
dc12 = diff(T,c12); dc12 = matlabFunction(dc12);
dc13 = diff(T,c13); dc13 = matlabFunction(dc13);
dc14 = diff(T,c14); dc14 = matlabFunction(dc14);
dc15 = diff(T,c15); dc15 = matlabFunction(dc15);
dc16 = diff(T,c16); dc16 = matlabFunction(dc16);
dc17 = diff(T,c17); dc17 = matlabFunction(dc17);
dc18 = diff(T,c18); dc18 = matlabFunction(dc18);
dc19 = diff(T,c19); dc19 = matlabFunction(dc19);
dc20 = diff(T,c20); dc20 = matlabFunction(dc20);
                    Tf = matlabFunction(T);
% Inputs (Define based on DoE)
Pa=INPUT1;     % Atmospheric pressure (kPa)
Toil=INPUT2;   % Actual oil temperature
Pi=INPUT3;     % Intake manifold pressure (kPa)
```

```
N =INPUT4;     % Engine Speed (RPM)
% Paramters initilisation
c1 = 1.22*1e5;c2 = 3.03*1e-4;c3 = 1.35*1e-10;c4 = 2.94*1e2;c5 = 4.06*1e4;
c6 = 3.03*1e-4;c7 = 6.89;c8 = 4.12;c9 = 244;c10 = Cff;c11 = Crf;c12 = Coh;
c13 = Com;c14 = 8.3155;c15 = 1.86*1e-3;c16 = 7.45*1e-7;c17 = 1;
c18 = 4.12*1e-3;c19 = 0.178;c20 = 4.12*1e-3;
% Step 1 & 2
nop = 20;
Z = zeros(length(N),nop);
Z(:,1) = dc1().*...
    (c1./Tf(N,Pa,Pi,Toil,Tref,c1,c2,c3,c4,c5,c6,c7,c8,c9,c10,c11,c12,...
    c13,c14,c15,c16,c17,c18,c19,c20));
Z(:,2) = dc2(N,Toil,Tref).*...
    (c2./Tf(N,Pa,Pi,Toil,Tref,c1,c2,c3,c4,c5,c6,c7,c8,c9,c10,c11,c12,...
    c13,c14,c15,c16,c17,c18,c19,c20));
Z(:,3) = dc3(N).*...
    (c3./Tf(N,Pa,Pi,Toil,Tref,c1,c2,c3,c4,c5,c6,c7,c8,c9,c10,c11,c12,...
    c13,c14,c15,c16,c17,c18,c19,c20));
Z(:,4) = dc4(N,Toil,Tref).*...
    (c4./Tf(N,Pa,Pi,Toil,Tref,c1,c2,c3,c4,c5,c6,c7,c8,c9,c10,c11,c12,...
    c13,c14,c15,c16,c17,c18,c19,c20));
Z(:,5) = dc5(N).*...
    (c5./Tf(N,Pa,Pi,Toil,Tref,c1,c2,c3,c4,c5,c6,c7,c8,c9,c10,c11,c12,...
    c13,c14,c15,c16,c17,c18,c19,c20));
Z(:,6) = dc6(N).*...
    (c6./Tf(N,Pa,Pi,Toil,Tref,c1,c2,c3,c4,c5,c6,c7,c8,c9,c10,c11,c12,...
    c13,c14,c15,c16,c17,c18,c19,c20));
Z(:,7) = dc7(N,Pa,Pi,Toil,Tref).*...
    (c7./Tf(N,Pa,Pi,Toil,Tref,c1,c2,c3,c4,c5,c6,c7,c8,c9,c10,c11,c12,...
    c13,c14,c15,c16,c17,c18,c19,c20));
Z(:,8) = dc8().*...
    (c8./Tf(N,Pa,Pi,Toil,Tref,c1,c2,c3,c4,c5,c6,c7,c8,c9,c10,c11,c12,...
    c13,c14,c15,c16,c17,c18,c19,c20));
Z(:,9) = dc9(N).*...
    (c9./Tf(N,Pa,Pi,Toil,Tref,c1,c2,c3,c4,c5,c6,c7,c8,c9,c10,c11,c12,...
    c13,c14,c15,c16,c17,c18,c19,c20));
Z(:,10) = dc10(N).*...
    (c10./Tf(N,Pa,Pi,Toil,Tref,c1,c2,c3,c4,c5,c6,c7,c8,c9,c10,c11,c12,...
    c13,c14,c15,c16,c17,c18,c19,c20));
Z(:,11) = dc11(N).*...
    (c11./Tf(N,Pa,Pi,Toil,Tref,c1,c2,c3,c4,c5,c6,c7,c8,c9,c10,c11,c12,...
    c13,c14,c15,c16,c17,c18,c19,c20));
Z(:,12) = dc12(N).*...
    (c12./Tf(N,Pa,Pi,Toil,Tref,c1,c2,c3,c4,c5,c6,c7,c8,c9,c10,c11,c12,...
    c13,c14,c15,c16,c17,c18,c19,c20));
Z(:,13) = dc13(N).*...
    (c13./Tf(N,Pa,Pi,Toil,Tref,c1,c2,c3,c4,c5,c6,c7,c8,c9,c10,c11,c12,...
    c13,c14,c15,c16,c17,c18,c19,c20));
Z(:,14) = dc14().*...
    (c14./Tf(N,Pa,Pi,Toil,Tref,c1,c2,c3,c4,c5,c6,c7,c8,c9,c10,c11,c12,...
    c13,c14,c15,c16,c17,c18,c19,c20));
Z(:,15) = dc15(N).*...
    (c15./Tf(N,Pa,Pi,Toil,Tref,c1,c2,c3,c4,c5,c6,c7,c8,c9,c10,c11,c12,...
    c13,c14,c15,c16,c17,c18,c19,c20));
Z(:,16) = dc16(N).*...
    (c16./Tf(N,Pa,Pi,Toil,Tref,c1,c2,c3,c4,c5,c6,c7,c8,c9,c10,c11,c12,...
    c13,c14,c15,c16,c17,c18,c19,c20));
Z(:,17) = dc17(Pa,Pi).*...
    (c17./Tf(N,Pa,Pi,Toil,Tref,c1,c2,c3,c4,c5,c6,c7,c8,c9,c10,c11,c12,...
    c13,c14,c15,c16,c17,c18,c19,c20));
Z(:,18) = dc18(N,Pa,Pi).*...
    (c18./Tf(N,Pa,Pi,Toil,Tref,c1,c2,c3,c4,c5,c6,c7,c8,c9,c10,c11,c12,...
    c13,c14,c15,c16,c17,c18,c19,c20));
Z(:,19) = dc19(N,Pa,Pi).*...
    (c19./Tf(N,Pa,Pi,Toil,Tref,c1,c2,c3,c4,c5,c6,c7,c8,c9,c10,c11,c12,...
    c13,c14,c15,c16,c17,c18,c19,c20));
Z(:,20) = dc20(N,Pa,Pi).*...
```

```
    (c20./Tf(N,Pa,Pi,Toil,Tref,c1,c2,c3,c4,c5,c6,c7,c8,c9,c10,c11,c12,...
    c13,c14,c15,c16,c17,c18,c19,c20));
[s(1),~] = sumsqr(Z(:,1));[s(2),~] = sumsqr(Z(:,2));
[s(3),~] = sumsqr(Z(:,3));[s(4),~] = sumsqr(Z(:,4));
[s(5),~] = sumsqr(Z(:,5));[s(6),~] = sumsqr(Z(:,6));
[s(7),~] = sumsqr(Z(:,7));[s(8),~] = sumsqr(Z(:,8));
[s(9),~] = sumsqr(Z(:,9));[s(10),~] = sumsqr(Z(:,10));
[s(11),~] = sumsqr(Z(:,11));[s(12),~] = sumsqr(Z(:,12));
[s(13),~] = sumsqr(Z(:,13));[s(14),~] = sumsqr(Z(:,14));
[s(15),~] = sumsqr(Z(:,15));[s(16),~] = sumsqr(Z(:,16));
[s(17),~] = sumsqr(Z(:,17));[s(18),~] = sumsqr(Z(:,18));
[s(19),~] = sumsqr(Z(:,19));[s(20),~] = sumsqr(Z(:,20));
[mm,ind] = max(s);
%% Initialise while loop
kk = 0;
rr = 1;
Zr = zeros(length(N),nop);
while rr>=1e-20
    kk = kk + 1;
    X(:,kk) = Z(:,ind);  %#ok   % Step 3
    Zr = X*pinv(X'*X)*X'*Z;     % Step 4
    Zr(isnan(Zr)) = 0; % Correct numerical problems.
    R = Z - Zr;                 % Step 5
    [sr(1),~] = sumsqr(R(:,1));[sr(2),~] = sumsqr(R(:,2));
    [sr(3),~] = sumsqr(R(:,3));[sr(4),~] = sumsqr(R(:,4));
    [sr(5),~] = sumsqr(R(:,5));[sr(6),~] = sumsqr(R(:,6));
    [sr(7),~] = sumsqr(R(:,7));[sr(8),~] = sumsqr(R(:,8));
    [sr(9),~] = sumsqr(R(:,9));[sr(10),~] = sumsqr(R(:,10));
    [sr(11),~] = sumsqr(R(:,11));[sr(12),~] = sumsqr(R(:,12));
    [sr(13),~] = sumsqr(R(:,13));[sr(14),~] = sumsqr(R(:,14));
    [sr(15),~] = sumsqr(R(:,15));[sr(16),~] = sumsqr(R(:,16));
    [sr(17),~] = sumsqr(R(:,17));[sr(18),~] = sumsqr(R(:,18));
    [sr(19),~] = sumsqr(R(:,19));[sr(20),~] = sumsqr(R(:,20));
    [rr,ind] = max(sr);         % Step 6
    % ... Step 7 and 8
    % Show parameter rank
    pRank(kk) = ind;  %#ok
    if sum(any(~diff(pRank))) > 0;
        break;
    end; % Break when no more parameters can be identified.
end
%% Visualise & Finalise
disp('No more parameteres can be identified.')
parameters = {'c1','c2','c3','c4','c5','c6','c7','c8','c9','c10',...
    'c11','c12','c13','c14','c15','c16','c17','c18','c19','c20'};
Estimable_parameter = parameters(unique(pRank,'stable'));
display(Estimable_parameter)
%% Finalise Programm
clear;
```

B.4 Cyclic Torque Identifiability Analysis MATLAB Code

M-code: Identifiability of Cyclic Engine Torque Model Parameters

```
% Orthogonal Identifiability Analysis for Cyclic Engine Torque Model
% Physical and Semi-Physical Parameters
% Created by I. Souflas - CERTIFIED MATLAB ASSOCIATE
% PhD Thesis - DECEMBER 2014
% References:
% ------------------------------------------------------------------------
%[1] I. Souflas, A. Pezouvanis, B. Mason, K.M. Ebrahimi, "Dynamic Modeling
%    of a Transient Engine Test Cell for Cold Engine Testing Applications",
%    ASME 2014 International Mechanical Engineering Congress & Exposition,
%    ASME Paper: IMECE2014-36286, Montreal, Canada, 14-20 November 2014.
%
%[2] D. Sandoval, J.B. Heywood, 'An Improved Friction Model for Spark-
%    Ignition Engines', SAE Paper: 2003-01-0725.
clear all;clc;
syms Ten Tind Trec Tfri Toil Pcyl Patm theta omega alpha phi psi G G1 G2...
    M b L r d a0 a1 a2 a3 a4 a5 a6 a7 a8 a9
%% Cyclic Engine Torque Model
% General Constants and Functions
phi = asin(d/(r+L));% Geometric constant [Ref. 1, Eq. 12]
psi = 1-((d+(r*sin(theta-phi)))/L)^2;% Geometric func. [Ref. 1, Eq. 18]
G = sin(theta)+(sqrt((1-psi)/psi)...
    *cos(theta));% Geometric function [Ref. 1, Eq. 17]
G1 = r*(((cos(theta-phi))*(1+(((r/L)*cos(theta-phi))/(psi^...
    (3/2)))))-(sqrt((1-psi)/psi)...
    *sin(theta-phi)));% Geometric function [Ref. 1, Eq. 20]
G2=r*(sin(theta-phi)+((sqrt((1-psi)/psi))*...
    cos(theta-phi)));% Geometric function [Ref. 1, Eq. 21]
Tind = (Pcyl-Patm)*((pi*(b^2))/4)*r*G;% Indicated Torque [Ref. 1, Eq. 16]
Trec = M*r*G*((G1*(omega^2))+...
    (G2*alpha));% Reciprocating Torque [Ref. 1, Eq. 19]
Tfri = (a0 + (a1*((omega*30)/pi)) - (a2*Toil) + (a3*(((omega*30)/...
    pi)^2)) - (a4*((omega*30)/pi)*Toil) + (a5*(Toil^2)) - ...
    (a6*(((omega*30)/pi)^3)) + (a7*(((omega*30)/pi)^2)*Toil) + ...
    (a8*((omega*30)/pi)*(Toil^2)) - (a9*(Toil^3)))*((pi*(b^2)*...
    r)/4)*10^3;% Friction Torque [Ref. 1-2, Eq. 22-A11]
Ten = Tind - Trec - Tfri; % Engine Torque
%% Define Partial Derivatives
dM = diff(Ten,M);       dM = matlabFunction(dM);        %1
dL = diff(Ten,L);       dL = matlabFunction(dL);        %2
dr = diff(Ten,r);       dr = matlabFunction(dr);        %3
db = diff(Ten,b);       db = matlabFunction(db);        %4
dd = diff(Ten,d);       dd = matlabFunction(dd);        %5
da0 = diff(Ten,a0);     da0 = matlabFunction(da0);      %6
da1 = diff(Ten,a1);     da1 = matlabFunction(da1);      %7
da2 = diff(Ten,a2);     da2 = matlabFunction(da2);      %8
da3 = diff(Ten,a3);     da3 = matlabFunction(da3);      %9
da4 = diff(Ten,a4);     da4 = matlabFunction(da4);      %10
da5 = diff(Ten,a5);     da5 = matlabFunction(da5);      %11
da6 = diff(Ten,a6);     da6 = matlabFunction(da6);      %12
da7 = diff(Ten,a7);     da7 = matlabFunction(da7);      %13
da8 = diff(Ten,a8);     da8 = matlabFunction(da8);      %14
da9 = diff(Ten,a9);     da9 = matlabFunction(da9);      %15
                        Ten = matlabFunction(Ten);      %16
% Cleanup
clear Tind Trec Tfri Toil Pcyl Patm theta omega alpha phi psi G G1...
    G2 M b L r d a0 a1 a2 a3 a4 a5 a6 a7 a8 a9
%% Load Initial Conditions and Inputs
IC = load('Initial_Conditions.mat');% Intitial conditions
```

```
L = IC.p(1,1);M = IC.p(1,2);a0 = IC.p(1,6);a1 = IC.p(1,7);
a2 = IC.p(1,8);a3 = IC.p(1,9);a4 = IC.p(1,10);a5 = IC.p(1,11);
a6 = IC.p(1,12);a7 = IC.p(1,13);a8 = IC.p(1,14);a9 = IC.p(1,15);
b = IC.p(1,3);d = IC.p(1,4);r = IC.p(1,5);
IN = load('Inputs.mat');% Inputs
Case = 'T1';
switch Case
    case 'T1'
        Ten_a = IN.T1(:,2);theta = IN.T1(:,3);omega = IN.T1(:,4);
        alpha = IN.T1(:,5);Pcyl = IN.T1(:,6); IN.Patm = T1(:,7);
        Toil = IN.T1(:,8);
    case 'T2'
        Ten_a = IN.T2(:,2); theta = IN.T2(:,3);omega = IN.T2(:,4);
        alpha = IN.T2(:,5); Pcyl = IN.T2(:,6); Patm = IN.T2(:,7);
        Toil = IN.T2(:,8);
end
%% Orthogonal-based method for parameter identifiability
% Step 1
nop = 15; % Number of parameters
Z = zeros(length(Ten_a),nop);
Z(:,1) = dL(L,M,Patm,Pcyl,alpha,b,d,omega,r,theta).*(L./Ten(L,M,Patm,...
    Pcyl,Toil,a0,a1,a2,a3,a4,a5,a6,a7,a8,a9,alpha,b,d,omega,r,theta));
Z(:,2) = dM(L,alpha,d,omega,r,theta).*(M./Ten(L,M,Patm,Pcyl,Toil,a0,a1,...
    a2,a3,a4,a5,a6,a7,a8,a9,alpha,b,d,omega,r,theta));
Z(:,3) = da0(b,r).*(a0./Ten(L,M,Patm,Pcyl,Toil,a0,a1,a2,a3,a4,a5,a6,a7,...
    a8,a9,alpha,b,d,omega,r,theta));
Z(:,4) = da1(b,omega,r).*(a1./Ten(L,M,Patm,Pcyl,Toil,a0,a1,a2,a3,a4,a5,...
    a6,a7,a8,a9,alpha,b,d,omega,r,theta));
Z(:,5) = da2(Toil,b,r).*(a2./Ten(L,M,Patm,Pcyl,Toil,a0,a1,a2,a3,a4,a5,...
    a6,a7,a8,a9,alpha,b,d,omega,r,theta));
Z(:,6) = da3(b,omega,r).*(a3./Ten(L,M,Patm,Pcyl,Toil,a0,a1,a2,a3,a4,a5,...
    a6,a7,a8,a9,alpha,b,d,omega,r,theta));
Z(:,7) = da4(Toil,b,omega,r).*(a4./Ten(L,M,Patm,Pcyl,Toil,a0,a1,a2,a3,...
    a4,a5,a6,a7,a8,a9,alpha,b,d,omega,r,theta));
Z(:,8) = da5(Toil,b,r).*(a5./Ten(L,M,Patm,Pcyl,Toil,a0,a1,a2,a3,a4,a5,...
    a6,a7,a8,a9,alpha,b,d,omega,r,theta));
Z(:,9) = da6(b,omega,r).*(a6./Ten(L,M,Patm,Pcyl,Toil,a0,a1,a2,a3,a4,a5,...
    a6,a7,a8,a9,alpha,b,d,omega,r,theta));
Z(:,10) = da7(Toil,b,omega,r).*(a7./Ten(L,M,Patm,Pcyl,Toil,a0,a1,a2,a3,...
    a4,a5,a6,a7,a8,a9,alpha,b,d,omega,r,theta));
Z(:,11) = da8(Toil,b,omega,r).*(a8./Ten(L,M,Patm,Pcyl,Toil,a0,a1,a2,a3,...
    a4,a5,a6,a7,a8,a9,alpha,b,d,omega,r,theta));
Z(:,12) = da9(Toil,b,r).*(a9./Ten(L,M,Patm,Pcyl,Toil,a0,a1,a2,a3,a4,a5,...
    a6,a7,a8,a9,alpha,b,d,omega,r,theta));
Z(:,13) = db(L,Patm,Pcyl,Toil,a0,a1,a2,a3,a4,a5,a6,a7,a8,a9,b,d,omega,...
    r,theta).*(b./Ten(L,M,Patm,Pcyl,Toil,a0,a1,a2,a3,a4,a5,a6,a7,a8,...
    a9,alpha,b,d,omega,r,theta));
Z(:,14) = dd(L,M,Patm,Pcyl,alpha,b,d,omega,r,theta).*(d./Ten(L,M,Patm,...
    Pcyl,Toil,a0,a1,a2,a3,a4,a5,a6,a7,a8,a9,alpha,b,d,omega,r,theta));
Z(:,15) = dr(L,M,Patm,Pcyl,Toil,a0,a1,a2,a3,a4,a5,a6,a7,a8,a9,alpha,b,d,...
    omega,r,theta).*(r./Ten(L,M,Patm,Pcyl,Toil,a0,a1,a2,a3,a4,a5,a6,a7,...
    a8,a9,alpha,b,d,omega,r,theta));
Z(isnan(Z)) = 0;
% Step 2
[s(1),~] = sumsqr(Z(:,1));[s(2),~] = sumsqr(Z(:,2));
[s(3),~] = sumsqr(Z(:,3));[s(4),~] = sumsqr(Z(:,4));
[s(5),~] = sumsqr(Z(:,5));[s(6),~] = sumsqr(Z(:,6));
[s(7),~] = sumsqr(Z(:,7));[s(8),~] = sumsqr(Z(:,8));
[s(9),~] = sumsqr(Z(:,9));[s(10),~] = sumsqr(Z(:,10));
[s(11),~] = sumsqr(Z(:,11));[s(12),~] = sumsqr(Z(:,12));
[s(13),~] = sumsqr(Z(:,13));[s(14),~] = sumsqr(Z(:,14));
[s(15),~] = sumsqr(Z(:,15));[mm,ind] = max(s);
% Initialise while loop
kk = 0;
rr = 1;
Zr = zeros(length(Ten_a),nop);
while rr>=1e-3 % cutoff
```

```
    kk = kk + 1;
    fprintf('Estimable parameter %d out of %d\n',kk,nop)
    X(:,kk) = Z(:,ind);  %#ok    % Step 3
    Zr = X*pinv(X'*X)*X'*Z;      % Step 4
    Zr(isnan(Zr)) = 0; % Correct numerical problems.
    R = Z - Zr;                  % Step 5
    [sr(1),~] = sumsqr(R(:,1));    [sr(2),~] = sumsqr(R(:,2));
    [sr(3),~] = sumsqr(R(:,3));    [sr(4),~] = sumsqr(R(:,4));
    [sr(5),~] = sumsqr(R(:,5));    [sr(6),~] = sumsqr(R(:,6));
    [sr(7),~] = sumsqr(R(:,7));    [sr(8),~] = sumsqr(R(:,8));
    [sr(9),~] = sumsqr(R(:,9));    [sr(10),~] = sumsqr(R(:,10));
    [sr(11),~] = sumsqr(R(:,11));    [sr(12),~] = sumsqr(R(:,12));
    [sr(13),~] = sumsqr(R(:,13));    [sr(14),~] = sumsqr(R(:,14));
    [sr(15),~] = sumsqr(R(:,15));
    [rr,ind] = max(sr);          % Step 6
    % ... Step 7 and 8
    % Show parameter rank
    pRank(kk) = ind;  %#ok
    if sum(any(~diff(pRank))) > 0;
        break;
    end; % Break when no more parameters can be identified.
end
%% Visualise & Finalise
disp('No more parameteres can be identified.')
parameters = {'L' 'M' 'a0' 'a1' 'a2' 'a3' 'a4' 'a5' 'a6' 'a7' 'a8' 'a9'...
    'b' 'd' 'r'};
Estimable_parameter = parameters(unique(pRank,'stable'));
display(Estimable_parameter)
%% Finalise Program
clear;
```

Appendix C

Transient Cyclic Motoring Engine Test Cell

One of the most important, challenging and time consuming tasks of this research was the design and development of a suitable experimental apparatus for conducting collecting data, conducting experiments, and testing the efficacy of the identification algorithms.

In the following pages are provided some pictures of the hardware and software of the test-rig, in order to support the discussions in the main part of the thesis.

C.1 Hardware

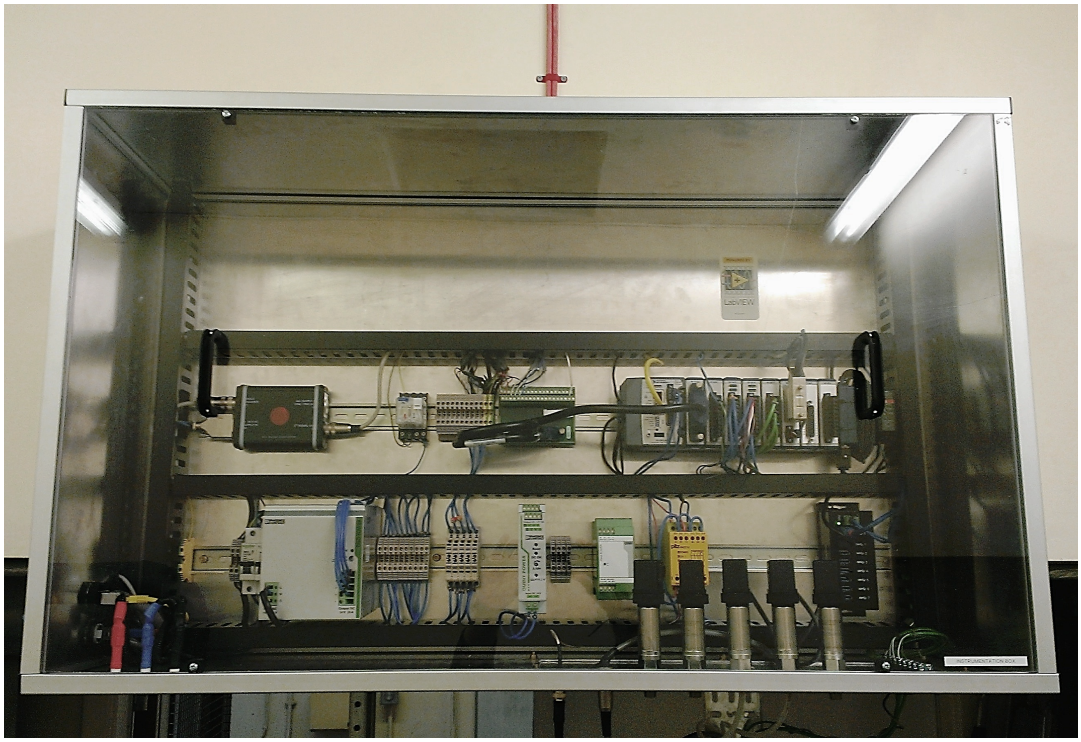

Figure C.1: Main instrumentation box.

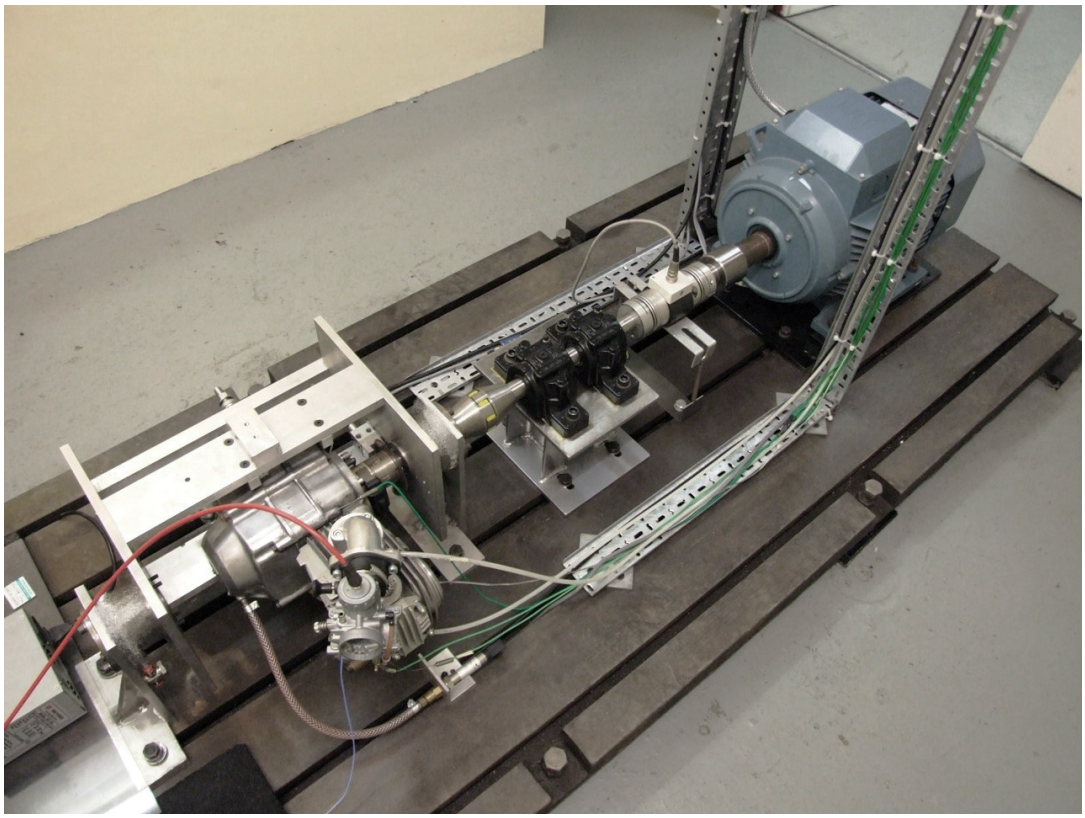

Figure C.2: Cyclic motoring single cylinder engine test bed.

C.2 Software

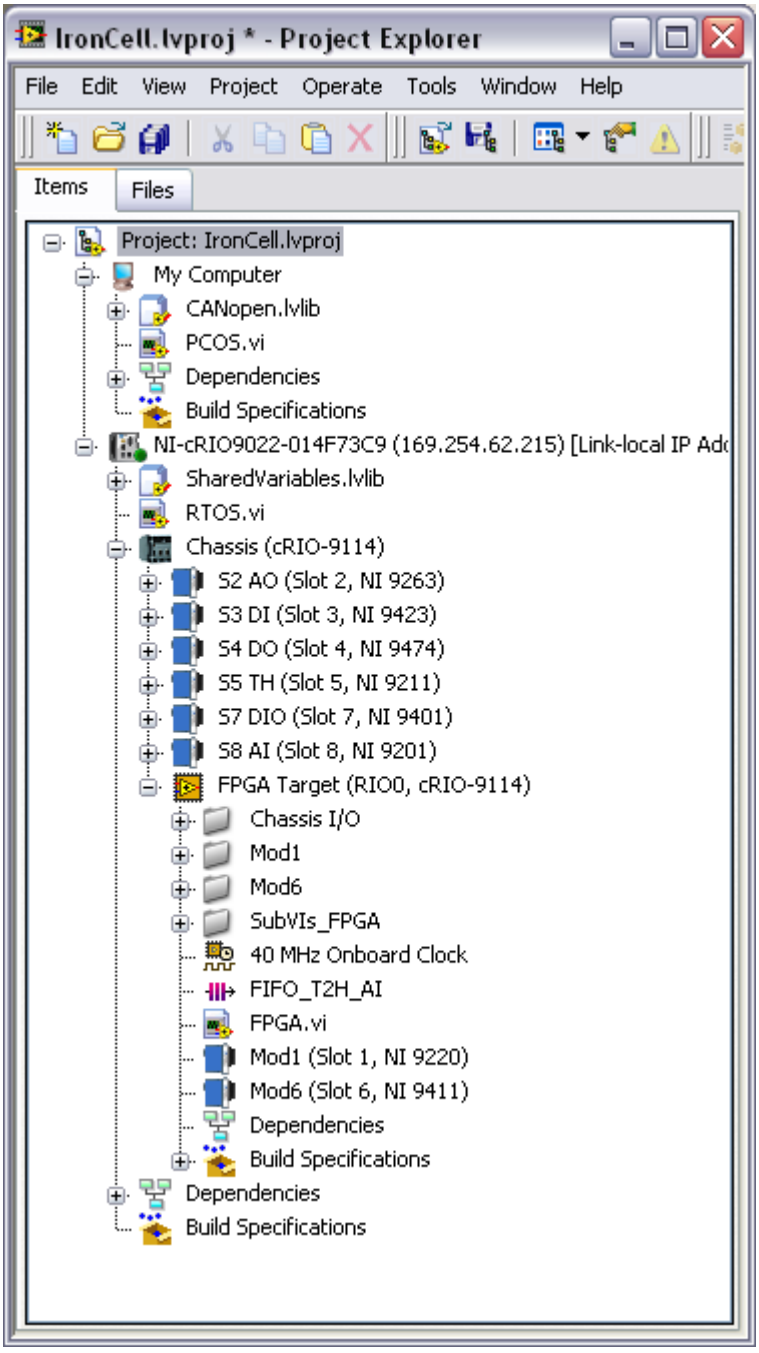

Figure C.3: Software architecture, LabVIEW Project Explorer.

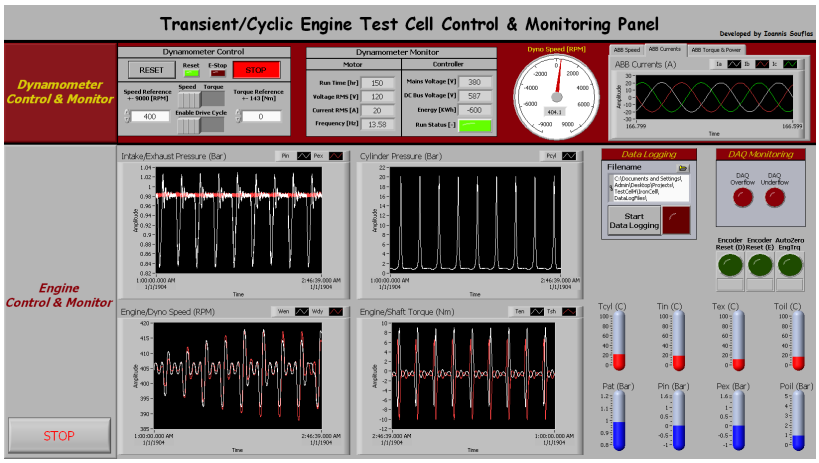

(a) Engine test cell control and monitoring panel user interface.

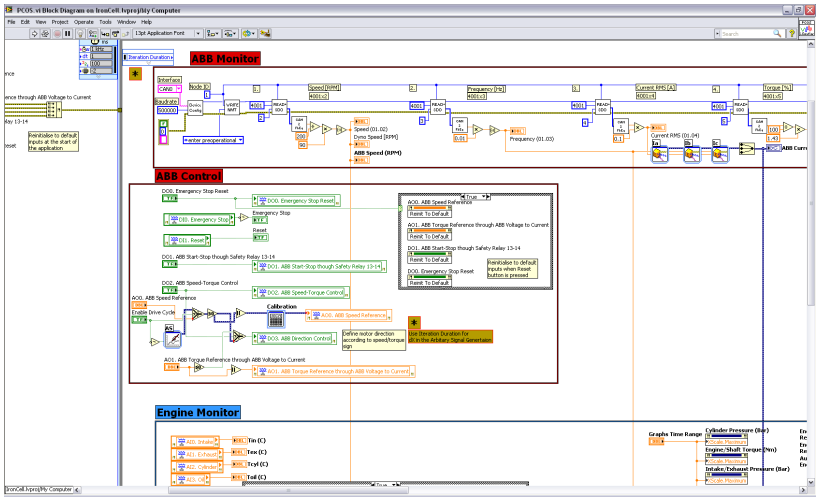

(b) Host Virtual Instrument Block Diagram, Section 1

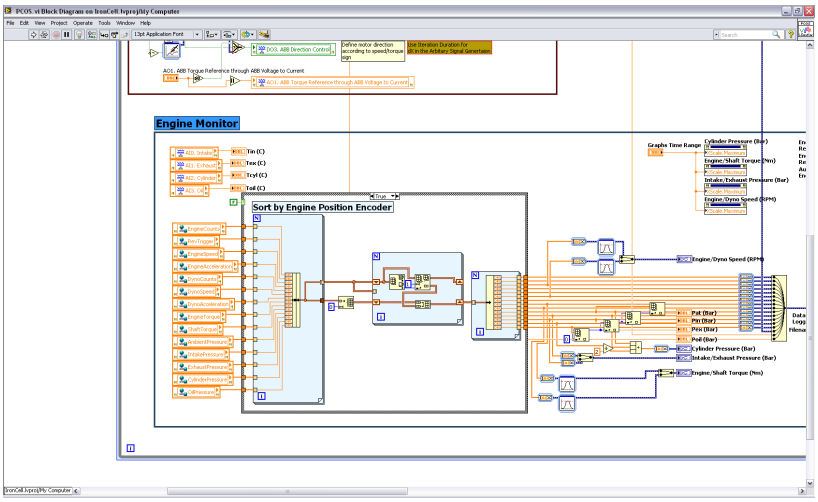

(c) Host Virtual Instrument Block Diagram, Section 2

Figure C.4: LabVIEW host Virtual Instrument.

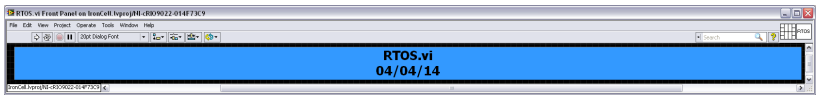

(a) Front Panel of the Real-Time Virtual Instrument

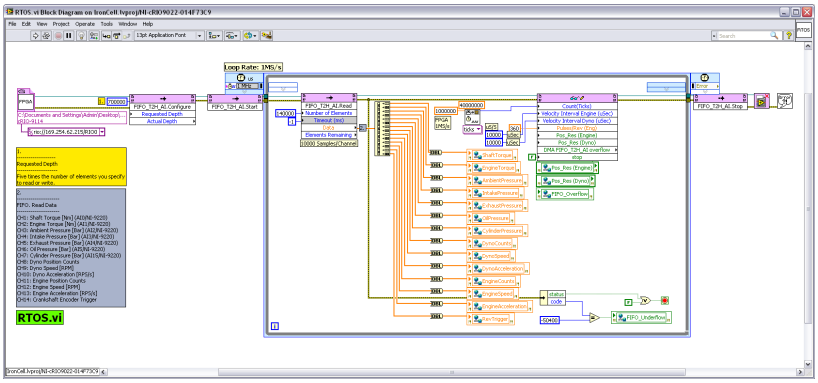

(b) Real-Time Block Diagram

Figure C.5: LabVIEW Real-Time Virtual Instrument.

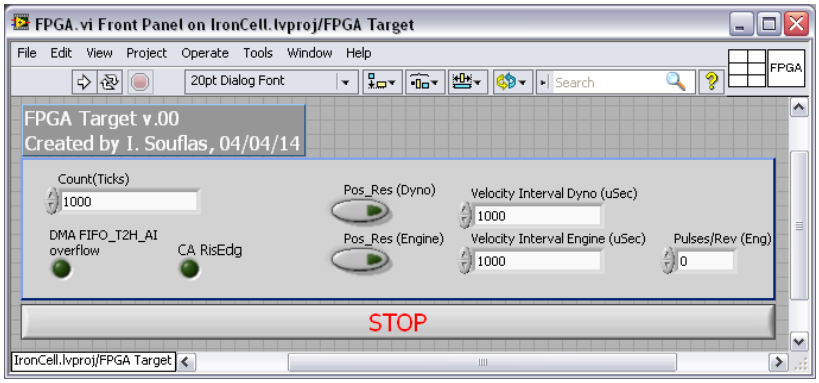

(a) Front Panel of the FPGA Virtual Instrument

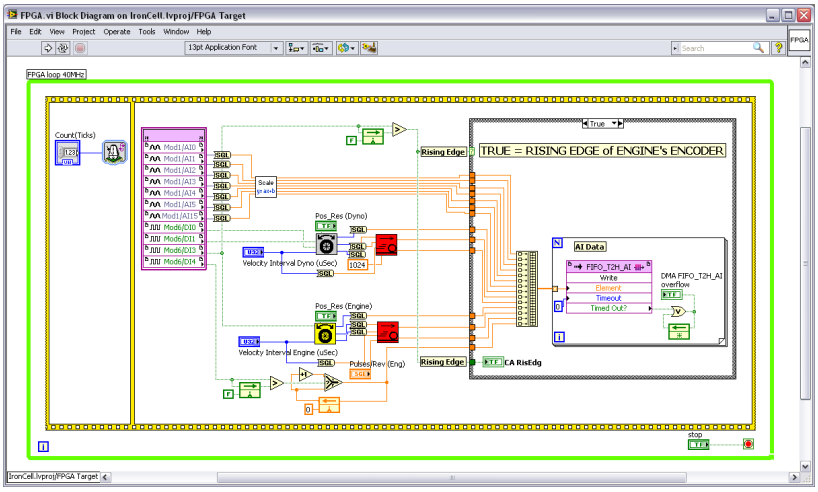

(b) FPGA Block Diagram

Figure C.6: LabVIEW FPGA Virtual Instrument.

This page intentionally left blank.